SEISMIC BEHAVIOR OF PILE-SUPPORTED BRIDGES

BY

WANCHALEARM KORNKASEM

DOUGLAS A. FOUTCH

JAMES H. LONG

University of Illinois at Urbana-Champaign, 2001

ABSTRACT

SEISMIC BEHAVIOR OF PILE-SUPPORTED BRIDGES

Wanchalearm Kornkasem, Ph.D.
Department of Civil and Environmental Engineering
University of Illinois at Urbana-Champaign, 2001
Professor Douglas A. Foutch, Advisor

An analytical technique of integrating a bridge structure and its soil-foundation system into the complete global model is proposed for seismic soil-structure interaction analysis of pile-supported bridges. A simple yet realistic model for single piles and grouped piles is developed based on dynamic beam-on-nonlinear-Winkler-foundation methods. Performance of the proposed single-pile and pile-foundation model in predicting static and dynamic response to vertical and lateral loads is validated through comparisons with both experimental results and analytical results from several other investigators. Performance of the integrated soil-foundation-structure model of the entire bridge is justified through comparisons with recorded responses of a road bridge in Japan. Parametric studies are also conducted to evaluate the sensitivity of the results to uncertainties in determining system parameters.

The presented modeling technique is applied for seismic analysis of an existing truss-arch bridge spanning across the Mississippi River in southern Illinois (the Cairo Bridge). The nonlinear time-history analysis is performed using input motions obtained from ground response analysis of bedrock motions artificially generated for the Cairo area. Comparison studies of dynamic characteristics and seismic response of the bridge obtained from the integrated model and those obtained from other foundation models (the fixed-base model, and the equivalent linear and nonlinear foundation spring models) are conducted. The results promote the use of the integrated model and emphasize the importance of the soil-structure interaction in seismic analysis of pile-supported bridges. The proposed model is applied to perform seismic performance evaluation of the Cairo Bridge for different excitation intensities and to identify an appropriate retrofit strategy for the bridge. Applications of the pile group model to investigate the behavior of retrofitted foundations and to develop a simple method of evaluating foundation characteristics are presented.

ACKNOWLEDGEMENTS

This work was supported in part by the Earthquake Engineering Research Center's program of the National Science Foundation under National Science Foundation Award Number EEC-9701785. Any opinions, findings and conclusions or recommendations expressed in this material are those of the author(s) and do not necessarily reflect those of the National Science Foundation.

TABLE OF CONTENTS

Chapter **Page**

Chapter **Page**

Chapter **Page**

Chapter **Page**

LIST OF TABLES

Table **Page**

LIST OF FIGURES

Figure **Page**

Figure **Page**

Figure **Page**

Figure **Page**

Figure **Page**

Figure **Page**

LIST OF SYMBOLS

A	=	loading type factor; 0.9 for cyclic loading and $3 - 0.8\ z/D_p \geq 0.9$ for static loading
A_d	=	dimensionless response amplitudes
a_0	=	dimensionless frequency, $w\, r_0/V_s$
C	=	damping coefficient of a single pile
C_L	=	damping coefficient of a pile in the lateral direction
C_V	=	damping coefficient of a pile in the vertical direction
C_S	=	damping coefficient of the far-field soil reactions
C_{SV}	=	damping coefficient of the far-field soil reactions in the vertical direction
C_{SL}	=	damping coefficient of the far-field soil reactions in the lateral direction
D_p	=	pile diameter
d	=	deformation
d	=	pile diameter
$\dot{d}$	=	deformation rate
E	=	Young's Modulus
E_s	=	Young's modulus of the subdivided soil layer
E_p	=	modulus of elasticity of pile material
exp	=	exponent greater than or equal to unity
$F(t)$	=	excitation force as a function of time
f	=	unit friction mobilized along a pile segment at displacement, z
$f_c^{\,1}$	=	compressive strength of concrete
f_{max}	=	maximum unit friction
G	=	small-strain shear modulus of the soil
G_s	=	shear modulus of the soil
Ig	=	gross moment of inertia
I_p	=	moment of inertia of pile section
$\overline{K}$	=	dynamic impedance of a pile ($\overline{K} = K + iw\, C$)
$\overline{K}_S$	=	complex stiffness of the far-field soil reactions ($\overline{K}_S = K_S + iw\, C_S$)
K	=	stiffness of an isolated pile

K_L	=	lateral stiffness of a pile
K_S	=	stiffness coefficients of the far-field soil reactions
K_{SV}	=	stiffness coefficient of the far-field soil reactions in the vertical direction
K_{SL}	=	stiffness coefficient of the far-field soil reactions in the vertical direction
K_V	=	vertical stiffness of a pile
K_{VG}	=	vertical stiffness of a pile group
k	=	elastic spring constant
k_{con}	=	constant modulus of subgrade reaction (F/L^2)
k_s	=	coefficient of initial modulus of subgrade reaction (F/L^3)
k_{sec}	=	coefficient of secant modulus of subgrade reaction (F/L^3)
L	=	length of the pile
$m_e e$	=	excitation intensities
m_x, m_y, m_z	=	unit acceleration loads in X, Y and Z directions
M_x, M_y, M_z	=	total unrestrained masses acting in X, Y and Z directions
N	=	blow counts for standard penetration test
$(N_1)_{60}$	=	energy corrected and stress corrected standard penetration test value
p	=	lateral resistance (F/L^2) mobilized at any value of $y < 8y_{50}$
$PSPI$	=	pile soil pile interaction
p_u	=	ultimate soil resistance per unit depth (F/L^2)
q	=	tip resistance mobilized at any value of $z < z_{cq}$
q_{max}	=	maximum tip resistance
$ratio$	=	specified ratio of the post yield stiffness to elastic stiffness
R	=	relative stiffness factor
R_d	=	displacement amplification ratio
r_d	=	$1-e^{1.5(E_s/E_p)(L/d)^{-2}}$
r_1	=	size of cylindrical soil mass having a diameter of multiple pile diameters
r_j	=	participation mass ratios for any mode j
r_0	=	pile radius
s	=	spacing between piles in a group
S_{u1}	=	dimensionless factor for real lateral stiffness
S_{u2}	=	dimensionless factor for complex lateral stiffness (damping)
S_{w1}	=	dimensionless factor for real stiffness

S_{w2}	=	dimensionless factor for complex stiffness (damping)
T	=	period of vibration
T	=	relative stiffness factor
t_{max}	=	ultimate soil resistance
u	=	measured vertical displacement
u_0,, $(u_{st})_0$	=	dynamic and static displacements at the same loading amplitude
U_x, U_y, U_z	=	deformation in X, Y and Z directions
V_p	=	compression-extension wave velocity
V_s	=	shear wave velocity of the soil
V_{La}	=	average of the shear wave velocity over the depth of soil layer; $V_{La} = 3.4V_s/\pi(1-n_s)$
y	=	lateral pile deflection
y_{50}	=	deflection at one-half the ultimate soil resistance
yield	=	yield force
z	=	movement of the pile in the vertical direction
z_{cf}	=	critical displacement of the pile at which f_{max} is fully mobilized
z_{cq}	=	critical displacement of the pile at which q_{max} is fully mobilized
z_d	=	depth below ground surface
z_i	=	internal hysteretic variable
a	=	interaction factor
a_L	=	lateral interaction factor
a_{RL}	=	cross-coupling lateral and rotational interaction factor
a_{RR}	=	rotational interaction factor
a_V	=	vertical interaction factor
a_{Vij}	=	vertical interaction factor between pile *i* and pile *j*
b	=	damping of the soil
h	=	pile shape factor; $h = 1.0$ for circular piles
n_s	=	Poisson's ratio of the soil
w	=	frequency of input excitation
j_i^T	=	transpose of the mode shape *j*
r_s	=	soil density
w_n	=	resonant frequency
w_s	=	$(\pi/2)V_s/H$: H = soil layer thickness

x	=	modal damping ratio

CHAPTER 1

INTRODUCTION

1.1 Introduction

Of particular interest in this study is the case of pile-supported bridges whose behavior is highly sensitive to soil-foundation-structure interaction (SFSI) effects. When a pile-supported bridge is located in an earthquake-prone area, the seismic performance evaluation of the bridge including the SFSI effects should be included in the analysis. Piles and pile foundations have been used to provide supports to structures for thousands of years. There is evidence that the Neolithic inhabitants of Switzerland used wooden poles driven into soft soil deposits to support their homes 12,000 years ago [Sowers (1979)]. Up to date, pile foundations have provided an expedient means for transferring the loads through soft, compressible soils onto stiffer, less compressible soils or onto rock. Not only have pile foundations been used to transfer vertical loads to more suitable materials at greater depth, but they have been extensively used to resist horizontal or uplift loads also. In case of providing supports to specific types of structures such as retaining walls, offshore structures and bridges, pile foundations are designed to resist combinations of vertical and horizontal loads.

The seismic response of bridges including the SFSI effects has been the subject of considerable attention in recent years, especially after failures of a number of pile-supported bridges during recent earthquakes such as the 1994 Northridge earthquake in California and the 1996 Hyogo-Ken Nanbu earthquake in Japan [Badoni and Makris (1997)]. Several attempts have been made to analyze the SFSI effects on seismic response of pile-supported bridges. A variety of numerical and analytical modeling methods to simulate the SFSI have been developed. Among these methods is the Winkler method which has received considerable attention, because of its simplicity and its ability to account for nonlinear behavior of the soils. Therefore, the emphasis herein is placed on an application of the Winkler method in seismic performance evaluation of pile-supported bridges.

1.2 Research Motivation

The Winkler method is used in practice to evaluate foundation characteristics in the forms of nonlinear springs or linear stiffness matrix, for response analysis of the bridge superstructure. After completion of the bridge superstructure and substructure response analysis, which is mostly done by structural engineers, the computed seismic demand forces (e.g., axial force, shears and moments) at the base of the piers are then used in a performance evaluation of the bridge foundations, which is commonly performed by geotechnical engineers. These bridge superstructure and foundation response analyses are usually performed using different computer programs and by different engineering divisions. A plausible explanation for these back and forth procedures, as noted by Reese and Isenhower (1999), is the lack of adequate integration between structural and geotechnical engineering.

Among other probable explanations is that the computer program that is capable of integrating the structure model and foundation model into the complete global model and performing a complete analysis has not been feasible from the standpoint of computer time and cost. However, the development of computer capacity and programming has grown rapidly in the past few years. The modeling and analysis techniques that might not be attainable in the past may even be performed on personal computers at present. With an application of the more powerful computers, the complete analysis of the entire bridge system now becomes more viable. Attempts are made consequently to incorporate the concept of integrating a bridge superstructure and its foundation system into a complete global model to be used in seismic soil-structure interaction analyses of pile-supported bridges.

In view of practicality, the computer program should not only be capable of incorporating the bridge superstructure model and its foundation model into the complete model for the SFSI analysis, but should also be versatile and easy to use. Developing a new computer program with these capabilities is, although achievable, certainly not an easy task. An alternative is to utilize an existing program with justifiable modifications. Fortunately, a commercial computer program whose applications meet all of the requirements is the SAP2000 program. In addition to its friendly graphical user interface, this program offers many features such as linear and nonlinear time history analyses as well as nonlinear link and spring elements. By properly utilizing all these applications, it is believed that the realistic seismic response of the entire bridge system including the SFSI effects can be obtained. The SAP2000 program is therefore used to provide an analysis tool for the proposed modeling method for seismic performance evaluation of pile-supported bridges.

1.3 Objectives and Scope of the Study

The main objective of this study is to investigate seismic behavior of pile-supported bridges using the presented analytical technique of integrating the bridge structure and its soil-foundation system into the complete global model. This integration will allow the response of the entire bridge system including its foundation to be concurrently obtained in one analysis. The analytical results obtained from this integrated soil-pile-foundation-structure model will serve in examining the seismic performance of a river-crossing, pile-supported bridge, and in identifying appropriate retrofit measures for the bridge. The pile foundation model, which is developed in a process of implementing the integrating technique, will also be applied to develop a simple method of evaluating the foundation characteristics to be readily used in preliminary design and analysis of pile-supported bridges in practice. To achieve these objectives, completion of the following tasks are required:

1. Extensive study of existing publications on modeling of the pile-soil system to account for soil-pile-foundation-structure interaction effects in seismic response analysis of bridges.
2. Development of the pile-soil model for single piles that complies with applications provided in the SAP2000 program.
3. Investigation of the capability of the proposed pile-soil model in estimating static and dynamic response of single piles subjected to vertical and horizontal loads through comparisons with experimental results from field tests.
4. Incorporation of the pile-soil model for an individual pile into the pile group model with probable modifications to account for the pile-soil-pile interaction effects.
5. Verification of the pile group model in predicting the static and dynamic response of pile group foundations to vertical and horizontal loads by comparing the analytical results obtained using the proposed model with experimental and analytical results.
6. Integration of the proposed pile foundation model and the bridge superstructure model into the complete global model whose capability in predicting the seismic response of the entire bridge including its foundation is assessed through parametric and comparison studies with the recorded responses of the Ohba-Ohashi Bridge, Japan.
7. Application of the detailed pile foundation model to establish a simplified foundation model in forms of nonlinear springs for representing foundations characteristics for seismic performance evaluation of pile-supported bridges including the SFSI effects.

8. Application of both detailed and simplified pile foundation models integral with the superstructure model in nonlinear time-history analysis for evaluating the seismic response of an existing major river-crossing bridge, the bridge carrying F.A.I. Route 57 over the Mississippi River at Cairo, Illinois (the Cairo Bridge).
9. Investigation of the effects of different foundation models including a fixed-base model as well as linear static and dynamic spring models, which are often used in practice.
10. Application of the proposed pile-soil model for investigating the behavior of retrofitted foundations and for developing a simple method of evaluating the foundation characteristics in the form of equivalent linear springs.

1.4 Organization of the Report

This report consists of eight chapters. An outline of the contents of each chapter is presented below.

Chapter 1 provides a background, motivation, an overview of the objectives, and organization of this report.

Chapter 2 provides a comprehensive discussion on criteria used in developing the pile-soil model for response analysis of single piles. The validation of the proposed model is assessed through comparisons with experimental results of actual field tests. In addition, comparison and parametric studies are performed to substantiate assumptions and evaluate the applicability of the SAP2000 program in performing required analyses. The parametric study is also conducted to evaluate the sensitivity of the results of the SPSI analysis to uncertainties in identifying model parameters.

In Chapter 3, the proposed pile-soil model for single piles is integrated into the pile group model with justifiable modifications for the pile-soil-pile interaction or group effects. A number of numerical and experimental approaches to account for the PSPI effects in response analysis of pile group foundations are extensively reviewed. Among all these approaches, the one, which is simple and probable, is adopted in the proposed pile group model. Details of the incorporation of the single pile model into the pile group model including modeling of pile to pile-cap connections are thoroughly discussed. The performance of the proposed pile group model is evaluated through comparisons with both experimental and analytical results from other investigators.

In Chapter 4, the capability of the proposed pile group model for simulating the soil-pile-foundation-structure interaction (SPFSI) effects in seismic response analysis of bridges is investigated through comparisons with recorded response of an existing bridge including its foundation during earthquakes. The recorded responses of the Ohba-Ohashi Bridge are used in a case history study. The complete global model including the bridge superstructure and its foundation is used in the nonlinear time-history analysis.

Chapter 5 provides details on descriptions, modeling, and dynamic analysis of the Cairo Bridge. Details of the bridge models with various foundation models for soil-foundation-structure interaction analysis including the proposed integrated model are presented. Also presented in Chapter 5 are details of site response analyses performed to obtain the input motions for nonlinear time-history analyses from the rock outcrop motions, which are artificially generated for the New Madrid seismic zone.

In Chapter 6, the nonlinear time-history analyses are performed for all bridge models as discussed in Chapter 5. Extensive comparison studies are conducted to investigate the sensitivity of the seismic response and dynamic characteristics of the Cairo Bridge to uncertainties in defining system parameters such as foundation properties. The proposed model is applied to perform seismic performance evaluation of the Cairo Bridge for different intensity levels of input ground motions, and to identify an appropriate retrofit strategy for the bridge.

In Chapter 7, the proposed pile-foundation model is applied to evaluate the behavior of the retrofitted foundation and to develop a simple alternative to account for the pile-soil-pile interaction effects for large pile groups. To be of more practical use, the pile-foundation model is also applied to establish ready-to-use charts from which the pile group stiffness can be evaluated as a function of group configurations, pile properties and soil properties.

Chapter 8 presents a summary and concluding remarks of this research study.

CHAPTER 2

SINGLE PILE MODEL

2.1 Introduction

Considerable research has been conducted on static and dynamic response of a single pile based on the Winkler's hypothesis [Matlock (1970), Matlock and Reese (1960), Novak and Sheta (1980), Nogami and Konagai (1987, 1988), Makris and Gazetas (1992), El-Naggar and Novak (1996). Among these proposed analytical models, the one adopted in this study was based on Nogami and Konagai's work. who developed a dynamic soil-pile interaction model in which the soil response is divided into two components: near-field and far-field soil components. The concept of using two soil components to represent the soil response was originated by Novak and Sheta (1980) and adopted in recent works by El-Naggar and Novak (1996). Based on these works, the pile-soil model for single piles is modified to be applicable for nonlinear analysis in the time domain and complied with the modeling features available in the SAP2000 program. The performance of the single pile model is evaluated through comparison studies with results from a number of experiments conducted on static and dynamic pile responses.

2.2 Proposed Single Pile Model

In the pile-soil model for single piles, the pile is modeled using a series of linear or nonlinear frame elements, and the soil is modeled using a series of linear or nonlinear springs and dashpots attached to each node along the length of the pile as shown in Figure 2.1. Details of modeling the pile and its surrounding soil are discussed as follows.

2.2.1 Pile Model

In general, it is believed that the number of elements used in pile modeling has an effect on the accuracy of analytical results. The greater the number of elements used, the more accurate the results. Using a large number of pile elements is however not computationally efficient if, in fact, a smaller number of pile elements can be used and yield the same degree of accuracy. The number of pile elements should be selected in such a way that accurate results are obtained with a minimum of computational effort. El-Sharnouby and Novak (1985) found that good accuracy in static and low frequency response of piles could be obtained by using 12 pile elements increasing in length

with depth with the top elements ¼ of the average element length. El-Naggar and Novak (1996) also found that using 20 pile elements increasing in length with depth gave accurate results for dynamic analysis. These findings however may not be applicable for long piles or for soil profiles consisting of layers of different soil properties.

The number of pile elements to be used to achieve accurate results not only depends on the length of the pile but also depends on the layering nature of soil deposits. Since the highly distinct soil layers are not present in any of the soil profiles used in this study, the effects of different soil layers are not considered in a sensitivity study on the number of pile elements. However, it is well to note that in case the soil profile consists of layers of highly distinct soil properties, large number of pile elements should be used to accurately model the discontinuity between layers. The sensitivity study is conducted herein to determine the number of pile elements to be efficiently and accurately used. Typically, only a top portion of 5-10 pile diameters is influential to the response of long piles to lateral loading; therefore the pile elements are divided in such a way that at least 5 elements are used for the top 10 pile diameters of the entire length of the piles.

In the case of using linear frame elements to model the pile, the following properties of the pile are required: area, diameter, width, depth, moment of inertia, torsional constant, and Young's modulus. In case a nonlinear pile model is required, the pile can be modeled using nonlinear elements or a combination of linear and nonlinear elements (i.e., the nonlinear elements are only used in a region where the nonlinearity is expected). The nonlinear load-deformation characteristics are required for each nonlinear pile element. In case of batter piles, the batter slope can be specified as angles from three axes of reference.

2.2.2 Soil Model

Various methods have been developed for modeling of soils surrounding a pile to be applicable in the Beam on Nonlinear Winkler Foundation method of analysis [Matlock (1970), Matlock and Reese (1970), Nogami (1983), Makris and Gazetas (1992), Badoni and Makris (1995) and El-Naggar and Novak (1996)]. Among these soil-modeling methods, two of which are briefly reviewed herein.

Matlock, Foo and Bryant (1978) employed the Winkler model to develop a dynamic beam-column computer program, namely Seismic Pile Analysis with Support Motion (SPASM), for seismic response analysis of a single pile. In this program, a series of discrete linear or nonlinear springs and dashpots is used to model the pile and its surrounding soils. Kagawa and Kraft (1980a, 1980b) further extended this analysis method by including a viscous damper in parallel with a

hysteretic soil model to simulate the effects of radiation damping (Figure 2.2(a)). Since the hysteretic and viscous components of damping are in parallel, this method of modeling the radiation damping is referred to as "parallel radiation damping" soil-modeling method. This method has been employed in recent work by Badoni and Makris (1996).

Novak and Sheta (1980) proposed a different method of soil modeling in which the soil around the pile is divided into two different zones: a near-field zone where strong soil nonlinearity is expected, and a far-field zone where the soil behavior is primarily linear elastic. The near-field soil reaction which is modeled by a linear or nonlinear spring is placed in series with the far-field soil reaction which is modeled by a set of a linear spring and dashpot. Since the viscous damper that is used to account for radiation damping effects is placed in series with the hysteretic soil model as shown in Figure 2.2(b), this method is so called "series radiation damping" soil modeling method. Such a method has been adopted by Nogami and Konagai (1987, 1988) and more recently by El-Naggar and Novak (1996).

The capability of these two soil modeling methods in predicting the seismic response of a single pile was studied by Wang et al. (1998). In their study, the verification of these methods was assessed through a comparison study in which the measured response of a pile from a centrifuge model test was used. It was shown in the comparison study that the capability of the "series radiation damping" soil-modeling method in predicting the seismic pile response is superior to that of the "parallel radiation damping" soil-modeling method. The results also suggested that the "parallel radiation damping" method could produce unrealistically large damping forces in case the soils undergo a certain degree of nonlinearity. A rational explanation is that the soil nonlinearity introduces additional material (hysteretic) damping, but it reduces the energy radiation to infinity (radiation damping). Placing the radiation damping element in parallel with the hysteretic damping element cannot account for the reduction of the radiation damping force due to soil nonlinearity and thus results in unrealistically large damping forces as the nonlinearity developed in the soils. This error introduced by the use of the "parallel radiation damping" soil-modeling method has also been recognized by several researchers such as Nogami et al. (1992) and Badoni and Makris (1996). As a result, the "series radiation damping" soil-modeling method is adopted in this study.

The soil surrounding the pile is divided into a number of layers. In each subdivided layer, the soil is further divided into two soil resistance characteristics; vertical and horizontal soil resistance. These two soil resistance characteristics are assumed to be independent of one another. The assumption of uncoupled lateral and vertical soil resistance is warranted because a significant lateral soil resisting zone is usually confined to a depth of 5 to 10 pile diameters from the ground

surface whereas the vertical soil resistance is mobilized along the entire length of the pile, with higher resistance at greater depth.

The assumption of uncoupled resisting components of the soil permits the use of the Winkler hypothesis stating that each subdivided soil layer can be represented by a series of independent, discrete springs in the vertical and lateral direction. Each vertical and lateral resisting component of the soil model is further divided into two parts; (1) a near-field model representing the nonlinear behavior of the soil in the immediate vicinity of a pile (2) a far-field model representing the elastic behavior of the soil outside the region of strong nonlinearity as shown in Figure 2.1. More details of modeling of the near-field and far-field soil resistance in the vertical and lateral directions are discussed as follows.

2.2.2.1 Modeling of Near-Field Soil Reactions

The near-field soil reactions are modeled using nonlinear springs to account for local nonlinearities at the pile-soil interface. The nonlinear behavior of the soil is described by load-transfer characteristics for both vertical and lateral soil reactions. Some other types of local nonlinearities such as slippage and gapping may occur at near-surface, soil-pile interface. The slippage and gapping can be simulated using gap elements available in the SAP2000 program. To develop an insight into the modeling of the pile-soil discontinuity conditions, the concept of using gap elements is discussed in brief here. The gap elements are used at both sides of a pile. The element is attached to the pile in one direction and its resistance is activated if the deformation exceeds a specified gap characteristic. The element will be detached as the pile moves away. The resistance of the element is activated again only when the pile returns to the point where it previously left. The amount of the reduced resistance due to the gapping effect is controlled by program users by specifying how many of the sub-elements are gap elements.

In case the slippage and gapping effects at the near-surface, soil-pile interface is expected, a set of a gap element and near-field and far-field soil model is used at each side of the pile in the lateral direction. In the vertical direction, the pile-soil discontinuity may be modeled by excluding the vertical components of the soil resistance over a portion of the pile along which the gap forms from the pile-soil system.

Employed in the proposed model, the nonlinear load-deformation curves of the near-field soil reactions for both vertical and lateral directions must be adjusted to comply with the available nonlinear models provided in the SAP2000 program. To begin developing an insight into the modeling of the nonlinear soil behavior, the nonlinear model available in the SAP2000 program is

briefly discussed. The nonlinear model is based on the hysteretic behavior proposed by Wen (1976). The proposed load-deformation characteristic is exponentially defined. The load-deformation relationship is given by:

[2.1] $$f = (ratio.k)d + (1 - ratio)yield.z_i ,$$

where

d = deformation,

k = elastic spring constant,

$ratio$ = specified ratio of the post yield stiffness to elastic stiffness,

$yield$ = yield force,

z_i = internal hysteretic variable defined below.

The initial value of z is zero, and it evolves according to the differential equation:

[2.2] $$\dot{z}_i = \frac{k}{yield}\begin{cases} \dot{d}\left(1 - |z_i|^{\exp}\right) & if \quad \dot{d}.z_i > 0 \\ \dot{d} & otherwise \end{cases},$$

where

$\dot{d}$ = deformation rate.

exp = exponent greater than or equal to unity,

Larger values of the exponent, exp, increase the sharpness of yielding as shown in Figure 2.3. In case exp = 1 and exp = 2, the load-deformation relationships respectively become:

[2.3] $$f = yield\left\{1 - e^{-\left(\frac{kd}{yield}\right)}\right\},$$

[2.4] $$f = yield\left\{\tanh\left(\frac{kd}{yield}\right)\right\}.$$

Vertical soil reactions

To model the nonlinear behavior of the near-field soil reactions in the vertical direction, the axial load-transfer characteristics (t-z and q-z curves) are used. The t-z curves refer to the relationship between the side-friction resistance of the soil along the side of a pile and its pile deflection. The q-z curves refer to the relationship between the end-bearing resistance of the soil at the pile tip and its deflection. The concept of using the load transfer characteristics to predict the axial soil movement of a pile under vertical loads was originated by Seed and Reese (1957) and

extended by Coyle and Reese (1966). This concept provides an efficient means of simulating nonlinear behavior and layering nature of the soil deposit. Nonetheless, the accuracy of this load-transfer method depends on development of realistic load-transfer characteristics of the soil and success in developing realistic load-displacement characteristics depends on the accuracy in determining the following parameters.

1. Ultimate side-friction capacity along the length of the pile
2. Ultimate end-bearing capacity at the pile tip
3. Displacement characteristic of the soil during load transfer (shape of the load-transfer curves)

Empirical and theoretical procedures are available to generate the load-transfer curves. The empirical procedures based on field test data for both cohesive and cohesionless soils were proposed by several researchers such as Coyle and Reese (1966), Vijayvergiya (1969), Aschenbrener (1984), Mosher (1984), Lam and Martin (1986), Reese and O'Neill (1988, 1989), and Heydinger (1989). Additionally, the theoretical formulation of the load-transfer curves suggested by Randolph and Wroth (1979) and modified by Kraft et al. (1981) has been widely used among researchers.

Although some of these procedures for generating load-transfer curves, especially the empirical ones, have been widely used in practice, none of them is accepted universally. However, among all previously mentioned procedures, the one presented in "Seismic design of highway bridge foundations, Vol. II: Design procedures and guidelines" by Lam and Martin (1986) has been used by many designers. The suggested criteria were originally proposed by Vijayvergiya (1969). Such criteria for constructing the load-transfer curves are adopted for modeling the near-field soil behavior in vertical direction in the subsequent study. The adopted load-transfer relationships for both side-friction and end bearing soil resistance are given below.

For side friction,

[2.5] $$f = f_{\max}\left(2\sqrt{(z/z_{cf})} - z/z_{cf}\right),$$

where

f = unit friction mobilized along a pile segment at displacement, z,

f_{max} = maximum unit friction,

z_{cf} = critical displacement of the pile segment at which f_{max} is fully mobilized. A z_{cf} value of 5 mm (0.2 in) is recommended for all soil types.

For end bearing,

[2.6] $$q = \left(\frac{z}{z_{cq}} \right)^{1/3} q_{\max} ,$$

where

q = tip resistance mobilized at any value of $z < z_{cq}$,

q_{max} = maximum tip resistance,

z_{cq} = critical displacement corresponding to q_{max}. A z_{cq} value of 0.05 of the pile diameter is recommended for all soil types.

The assumption of using the same load-displacement relationship for all soil types is somewhat essential. However, results of several field tests have indicated a fairly similar shape of the load-transfer curves for both cohesive and cohesionless soils. In addition, the realistic load-transfer curves are dependent not only on the shape but also on the accuracy in the determination of ultimate soil capacities. The latter appears to be more influential to the results than the former as concluded from the parametric study conducted herein and by other investigators.

A number of methods have been proposed to predict the ultimate side-friction and end-bearing soil capacities to be used in the formation of *t-z* and *q-z* curves. They can be grouped as follows:

1. Empirical methods based on correlation of shear strength of soil and pile load test data.
2. In situ testing method based on field measurement data (e.g., the Standard Penetration Test (SPT) and Cone Penetration Test (CPT).
3. Direct application of site-specific static pile load test data.

The load-transfer curves as suggested by Lam and Martin need to be adjusted in order to be compatible with the available nonlinear model in the SAP2000 program and to be capable of approximately representing the complete curves over a possible range of loading. To obtain the adjusted curves best fit to the axial load-transfer curves suggested by Lam and Martin, the elastic stiffness parameter (k) may be empirically specified as the secant stiffness at $z = 0.06z_c$ and $z = 0.08z_c$ of the originally suggested *t-z* and *q-z* curves, respectively. Figures 2.4(a) and 2.4(b) show the normalized *t-z* and *q-z* curves used in SAP2000 as well as the actual curves.

Lateral soil reactions

Similar to the modeling of the near-field soil reactions in the vertical direction, the nonlinear load-transfer characteristics, so called *p-y* curves, are used for modeling the near-field soil reactions in lateral direction. However, in the lateral soil model, the soil reactions at each side of the pile are

sometimes modeled separately as shown in Figure 2.1 to account for the pile-soil discontinuity that may occur for some specific soil types (e.g. stiff fissured clay). This discontinuity conditions usually occur at the near-surface, soil-pile interface as the load direction changes. Below the level at which the gap disappears, the lateral soil reactions can be modeled using only one set of the near-field and far-field soil model attached to one side of the pile. In case the pile-soil discontinuity is not expected, the gap elements are not required and only one set of lateral soil model at each pile node is needed.

The technique of handling the nonlinear behavior of the soil in lateral direction using the nonlinear spring (*p-y* curves) was first proposed by McClelland and Focht (1956). This technique has been initially adopted by the American Petroleum Institute (API) in predicting static and cyclic response of offshore pile foundations to wave and earthquake loading. Because of its simplicity, the analysis approach with *p-y* curves has become widely accepted to be used for other types of structures and loading applications. A large amount of research has been dedicated toward verification on the application of the *p-y* curve approach to dynamic or seismic pile response analysis. Nogami is one of many investigators to examine its application to dynamic loading. It was concluded in his work that the nonlinear soil behavior could be sufficiently modeled by the *p-y* curves that could also be applied for predicting the dynamic response of piles and pile foundations. The *p-y* curves as recommended by the API (1991) are therefore used to describe the nonlinear near-field soil reactions in lateral direction.

For soft clay, the *p-y* criteria proposed by Matlock (1970) was adopted and given as:

[2.7] $$\frac{p}{p_u} = 0.5\left(\frac{y}{y_{50}}\right)^{1/3}$$

where

p = lateral resistance (F/L^2) mobilized at any value of $y < 8y_{50}$,

p_u = ultimate soil resistance per unit depth (F/L^2).

y = deflection,

y_{50} = deflection at one-half the ultimate soil resistance,

For stiff clay above the water table, the *p-y* criteria proposed by Reese and Welch (1975) are adopted and given as:

[2.8] $$\frac{p}{p_u} = 0.5\left(\frac{y}{y_{50}}\right)^{1/4}$$

The stiffness parameter (k) is taken as the secant stiffness at $y = 0.8y_{50}$ for soft clay and $y = 1.2y_{50}$ for stiff clay above water table. The actual and adjusted curves for soft clay and stiff clay above water table are shown in normalized scale in Figure 2.5. Reese and Cox (1975) also proposed the *p-y* criteria for stiff clay below the water table. The parameter (k) can be specified to be the same value as the tangent stiffness k_s as recommended.

For sand, the *p-y* criteria proposed by O' Neill and Murchinson (1983) are adopted and given as:

[2.9] $$p = h.A.p_u \tanh\left[\left(\frac{k_s.z_d}{Ah.p_u}\right).y\right]$$

where

A = loading factor; 0.9 for cyclic loading, and $3-0.8z/D_p \geq 0.9$ for static loading,

D_p = pile diameter,

k_s = coefficient of initial modulus of subgrade reaction (F/L^3) of the soils,

z_d = depth below ground surface,

h = a factor used to describe pile shape; $h = 1.0$ for circular piles.

This proposed *p-y* curve for sand can be completely described in the SAP2000 with the elastic stiffness (k) taken equal to $k_s.z/Ah$, the parameter *exp* = 2, and *yield* = $Ah\ p_u$. For other types of soils, the adjusted *p-y* criteria should be evaluated on a case-by-case basis.

2.2.2.2 Modeling of Far-Field Soil Reactions

The far-field soil reactions in each subdivided layer are modeled by a set of springs and dashpots representing the dynamic stiffness and radiation damping properties of the soil. The evaluation of coefficients for these springs and dashpots has been a subject of considerable attention for years. Several researchers have proposed a solution for this problem both in theoretical and empirical forms. Some of these solutions are discussed herein.

Berger et al. (1977) proposed 1-D radiation damping model which utilized a fundamental concept of the dynamic response of any 1-D wave propagating through a viscous dashpot. In this model, two primary assumptions have been made. The first assumption is that a dashpot fully absorbs the energy of the wave traveling with velocity, V, along a cylinder (Figure 2.6(a)). The second one is that a horizontally-moving pile only generates 1-D compression and extension waves (P-waves) traveling in the direction of shaking and 1-D shear waves (S-waves) traveling in the perpendicular direction as shown in Figure 2.6(b). This 1-D model, although very simple to use,

has one important drawback that the computed soil reactions (spring and dashpot) are not frequency-dependent, as they should be in reality. Its simplicity and versatility in approximately modeling the dynamic soil behavior, however, render a simple solution for calculating the far-field soil parameters.

Gazetas and Dobry (1984) presented an analytical approach based on a plane strain model to define the soil reactions to harmonic oscillations of a vertically embedded rigid, infinitely long cylindrical body in an infinite linear viscoelastic soil medium as shown in Figure 2.6(c). The soil reactions in form of complex soil stiffness (coefficients for soil stiffness and radiation damping) obtained from this solution are frequency-dependent. This approach for determining the dynamic soil reactions has been adopted by several researchers and recently by El-Naggar and Novak (1996).

Roesset (1980) used a three-dimensional finite element formulation to establish the relationship between soil reactions and the corresponding pile displacements. The soil reactions comparable to those of the plane-strain case were then obtained by properly averaging the results. Kagawa and Kraft (1980a, 1980b) also used a 3-D finite element analysis with a somewhat different averaging procedure to derive the soil reactions comparable to the plane-strain case. However, they eventually decided to adopt simpler expressions derived from a one-dimensional, plane-strain model proposed by Berger et al. (1977) in their study.

Gazetas and Dobry (1984) employed a simple approximate plane-strain model to derive frequency-dependent soil reactions. In this model, it is assumed that energies are radiated away from the pile in orthogonal directions as shown in Figure 2.6(d). The compression-extension waves (P-wave) propagate with velocity, V_p, in two quarter planes parallel to the direction of shaking and at right angles, the shear waves (S-wave) propagate with velocity, V_s, in the other two-quarter planes. Their study showed a very good agreement between their results and the results obtained from more rigorous analysis by Novak and Roesset.

All aforementioned models for determining the frequency-dependent coefficients for springs and dashpots except the 3-D finite element formulation by Roesset (1980) were used in the comparison and sensitivity studies. The stiffness and radiation damping properties of the soil deposit are inherently frequency-dependent. However, in the time-domain dynamic analysis provided in SAP2000, only frequency- or time-independent stiffness and damping parameters can be used. These parameters are, therefore, chosen according to the properties of the soil layer and the dominant frequency of the input motion.

Vertical soil reactions

In each subdivided layer, the far-field soil reactions in vertical direction are modeled by using a linear spring and viscous damper (dashpot) for stiffness and radiation damping properties of the soil deposit, respectively. A significant amount of research has been conducted on determination of the dynamic soil properties in terms of springs and dashpots. Among these proposed methods, two methods were chosen for the parametric study. The first one was proposed by Novak et al. (1978) using a plane-strain solution. An explicit solution of the soil complex stiffness for vertical vibration ($\overline{K}_{SV} = K_{SV} + iw\, C_{SV}$) of a unit length of a cylinder embedded in a linear viscoelastic medium is given in brief by:

[2.10] $$K_{SV} = G.S_{w1}(n_s, a_0)$$

[2.11] $$C_{SV} = \frac{Gr_0}{a_0 V_s} S_{w2}(n_s, a_0)$$

where

a_0 = dimensionless frequency, $w\, r_0/V_s$,
G = small-strain shear modulus of the subdivided layer,
r_0 = pile radius,
S_{w1} = dimensionless factor for real vertical stiffness,
S_{w2} = dimensionless factor for complex vertical stiffness (damping).
V_s = shear wave velocity of the soil,
w = frequency of input excitation,
n_s = Poisson's ratio of the soil layer,

Figure 2.7(a) shows the variation of S_{w1} and S_{w2} with the dimensionless frequency a_0 and n. Since only frequency-independent stiffness and damping parameters can be specified in the time-domain analysis provided in the SAP2000 program, the values of frequency-independent S_{w1} and S_{w2} are chosen according to the Poisson's ratio and the dominant dimensionless frequency, a_0. The typical value of the dimensionless frequency for seismic loading or other loading applications varies between 0.05 and 0.5.

The second method was proposed by Gazetas and Makris (1991) using a simpler plane-strain model. The expressions for dynamic stiffness and radiation damping of soil surrounding a pile are given by:

[2.12] $$K_{SV} = 0.6E_s\left(1 + 0.71\sqrt{a_0}\right)$$

[2.13] $$C_{SV} \approx 5.28 a_0^{-1/4} r_0 \, r_s V_s$$

where

E_s = Young's modulus of the subdivided soil layer,

r_s = soil density.

These spring and dashpot coefficients are also frequency-dependent. The dominant a_0 must be evaluated beforehand and used in calculation of the frequency-independent soil parameters.

The aforementioned methods have been used by other researchers and engineers. They both have been verified to be satisfactory for estimating the dynamic soil reaction to vertical vibrations for most cases. These methods are, therefore, chosen to be used in modeling of the far-field soil reaction in the vertical direction.

Lateral soil reactions

In the proposed far-field soil model in the lateral direction, three different methods proposed by Berger et al. (1977), Novak et al. (1978), and Gazetas and Dobry (1984) were used to compute the coefficients of linear springs and dashpots. The first two methods were derived from the same concept as those for vertical soil reaction. Novak's expressions for complex soil stiffness are given below. The variation of S_{u1} and S_{u2} is shown in Figure 2.7(b).

[2.14] $$K_{SL} = G.S_{u1}(n_s, a_0),$$

[2.15] $$C_{SL} = \frac{Gr_0}{a_0 V_s} S_{u2}(n_s, a_0).$$

where

S_{u1} = dimensionless factor for real lateral stiffness,

S_{u2} = dimensionless factor for complex lateral stiffness (damping).

Simpler expressions for coefficients of soil stiffness and radiation damping by Gazetas and Dobry (1984) are as follows:

[2.16] $$K_{SL} \approx 1.2 E_s$$

[2.17] $$C_{SL} \approx 10 a_0^{-1/4} r_0 \, r_s V_s$$

The coefficients obtained from the above expressions are frequency dependent. Similar to the determination of the vertical far-field soil reactions, the frequency-independent soil reactions are obtained according to the dominant dimensionless frequency, a_0.

Unlike the first two methods, the expression proposed by Berger et al. (1977) for computing radiation-damping coefficient is frequency-independent. It is given as:

[2.18] $$C_{SL} \approx 4 r_0 \, r_s V_s \left[1 + \frac{V_p}{V_s} \right]$$

where

V_p = dilatational wave velocity,

V_s = shear wave velocity.

It is shown by Gazetas and Dobry (1984) that the variation of the spring coefficient with a_0 as obtained from dynamic finite element analysis is fairly steady. The dynamic spring coefficient of far-field soil reaction can be rationally assumed equal to the static spring coefficient.

All of these different expressions or procedures for modeling the near-field and far-field soil reactions in both vertical and lateral directions are used in the following studies. The comparison and sensitivity studies were performed to evaluate the accuracy of applying these expressions in the proposed pile-soil model for predicting the single pile response to vertical and lateral loading.

2.3 Performance of the Proposed Single Pile Model

The SAP2000 program was used to model the pile and the nonlinear soil behavior to examine the capability of the proposed pile-soil model in predicting the static and dynamic response of the single piles subjected to vertical and lateral loading. Results obtained from the SAP2000 program are compared with results obtained from the computer programs such as AXPILL [Long (1996)] for vertical response and COM624 [Reese and Sullivan (1980)] for lateral response. The performance of the proposed pile-soil model is further assessed through comparisons with experimental results of actual field tests. The parametric study is then conducted to evaluate the sensitivity of the analytical results to uncertainties in determining model parameters. These procedures are applied in performance evaluation of the proposed model for both vertical and lateral loading.

2.3.1 Vertical Loading

The capability of the proposed model in predicting the static and dynamic pile response to vertical loading is evaluated through comparison with the results of field tests. Three experimental results of static and dynamic load tests on piles were used for this purpose. The studies on the performance of the proposed model are divided into three case studies accordingly. The first two case studies are to verify the capability of the proposed model in predicting the response of a single

pile subjected to static vertical loading. The third case study is intended for verification of the proposed model in predicting the pile response to dynamic vertical loading. In addition, parametric studies are performed in each case study to evaluate the effects of model parameters on the analytical results.

2.3.1.1 Case Study 1: Response of a Friction Pile to Static Vertical Loads

A full-scale test on a single pile under static vertical loads was conducted by Southern Earth Sciences at south Mobile County, Alabama. A 36.3-m steel "H" pile (12-H-74) was axially loaded to failure. The results of this test including details of site conditions and test description were reported by Laier (1989). The details of soil profile and results of the Standard Penetration Test and Cone Penetration Test are given in Figure 2.8. As shown from the given field exploration results, the soils at the test site were predominantly sands varying from silty to very dense sands. The ground water level was located at about 0.6 m below existing ground surface. Based on the results from the Standard Penetration Tests, an empirical method proposed by Meyerhof (1976) to evaluate the ultimate side-friction and end-bearing capacity of the soil was used. The theoretical method was also used as a comparison. It was found that the ultimate soil resistance obtained from both methods was fairly similar.

Comparison study between the adjusted and actual load-transfer curves

To justify the use of the adjusted nonlinear load-transfer characteristics (*t-z* and *q-z* curves) in SAP2000, the comparison study between the results of the SAP2000 program and those of the AXPILL program [Long (1996)] in which the actual load-transfer curves as suggested by Lam and Martin can be completely specified was done. To eliminate the effects of other system parameters (i.e., the far-field soil reaction) only the near-field soil reactions were used. The results in form of load-settlement relationship at the pile head from both programs as shown in Figure 2.9(a) are highly comparable. The predicted load-settlement curves, although slightly stiffer, also agree reasonably well with the measured response. This good agreement among the computed and measured pile responses justifies the use of adjusted load-transfer curves in the SAP2000 program.

Sensitivity study on the number of pile elements

Since it is generally believed that the accuracy of the results is dependent on the number of pile elements (i.e., the greater the number of pile elements, the more accurate the results), a sensitivity study on the number of elements was performed for a static-vertical-loading case. Three different numbers of pile elements (50, 15 and 10) were used herein. The load-settlement curves computed

from the pile model with different numbers of pile elements are shown in Figure 2.9(b). It can be seen from this figure that the curves lie mostly on top of one another. Therefore, the number of pile elements equal to or greater than 10 increasing in length with depth and with at least 5 elements for the top 10 pile diameters of the pile length can be adequately used to predict the response of the pile to static vertical load.

2.3.1.2 Case Study 2: Response of an End-Bearing Pile to Static Vertical Loads

Another full-scale test of a single pile subjected to static axial loads was used in justifying the adjusted *t-z* and *q-z* curves. Unlike the previous case study, most of the pile resistance is derived from the end-bearing capacity of the soil at the pile tip (so called end-bearing-type pile). A pile-testing program was conducted at the west bank of the Mississippi River, about one mile from the existing Locks and Dam No. 26, Missouri by Stevens et al. (1979). A brief summary of the load testing procedures and soil profile was given as follows.

Untreated green Douglas-fir piles were used in this test. The 12.2-m-long pile having diameter varying along the length of approximately between 0.35 and 0.22 m was driven through a deposit of sand to a final penetration of approximately 10.6 m and tested to failure in the vertical direction. The assumed soil profile obtained from 25 exploratory borings and the range of standard penetration blow count as well as cone penetration values are shown in Figure 2.10. From the exploratory results, the soil condition was predominantly sand varying from medium to dense sand. The ground water level was maintained between 0.3-0.6 m (1-2 ft) below the ground line.

Similar to the Case Study 1, both theoretical and empirical methods were used to calculate the ultimate soil resistances (t_{max} and q_{max}) and the differences between the results of these two methods were found to be insignificant. Since the in-situ soil properties were given in range, the upper- and lower-bound ultimate soil resistances obtained from the empirical method were used in the following study. The results from the AXPILL program were also used for comparison. Figure 2.11 shows a comparison of the measured and computed load-settlement curves. Agreement between the curves obtained from AXPILL and SAP2000 is favorable.

In addition, the measured load-settlement data are mostly within the upper- and lower-bound computed curves. It can be observed from Figure 2.11 that the ultimate soil capacities (t_{max} and q_{max}) strongly affect the load-settlement curves. The determination of correct values of ultimate soil capacity is of great influence in constructing realistic load-transfer curves, and thus in accurately predicting the static pile-response to vertical loading.

2.3.1.3 Case Study 3: Response of a Model Pile to Dynamic Vertical Loads

El-Marsafawi, Han and Novak (1992) reported results of dynamic experiments on two pile group foundations; one at prototype scale and one at model scale which is considered here. In this series of testing programs a single model-scale pile was tested under harmonic loading in the vertical direction and free vibration in the horizontal direction. Only vertical response of the steel single pile under vertical excitation is considered herein. The model pile was a hollow pipe having an outside diameter of 101.6 mm and a wall thickness of 6.4 mm with conical plug at the tip. The pile was driven hydraulically to a depth of 2.75 m below the ground surface with a free length of 0.30 m. The tests were conducted on the campus of University of Western Ontario. The soil profile consists of a layered noncohesive stratum of silty fine sand with a gravel seam resting on dense silty till at the pile tip level. The soil profile and results of the shear wave velocity measurements using the cross-hole technique and the steady state vibration technique are shown in Figure 2.12.

The system was harmonically excited by a mechanical oscillator. The load amplitude was quadratically proportional to the square of the excitation frequency (w) varying from 62 Hz to 6 Hz at a constant speed. The excitation force as a function of time, *F(t)*, for different intensities is given by:

[2.19] $$F(t) = (m_e e) w^2 \cos wt \, .$$

Three excitation intensities ($m_e e$) of 2.45, 4.92 and 9.84 kg.mm were applied to the system. The measured displacement amplitudes under vertical excitation are then normalized as:

[2.20] $$A_d = \left(\frac{m}{m_e e} \right) u$$

where

A_d = dimensionless response amplitudes,

u = measured vertical displacement,

m = mass (941 kg) attached to a steel mounting flange to simulate the inertial effect of the pile cap and static load above the ground.

The maximum vertical displacement amplitude was measured to be 0.07 mm corresponding to a normalized displacement of 0.00069 pile diameter for the single pile. This amplitude is indeed very small. Special attention must be drawn to modeling of the near-field soil reactions, especially the initial range of the load-transfer curves in which the soil response is expected to concentrate.

The load-transfer curves are thus adjusted in such a way that the initial part (0-0.5 mm) is most accurately defined. Additionally, since only the results of the shear wave velocity measurements are available, the ultimate soil capacities were estimated using the theoretical method. Other soil properties, which were not given, were empirically obtained based on the soil descriptions.

In modeling of the far-field soil reactions, the required soil properties such as shear modulus and Young's modulus were directly calculated from the measured shear wave velocity. The plane-strain solutions derived by Novak, Gazetas and their colleagues were used to calculate the coefficients for springs and dashpots. The damping ratio of the system (pile-material and soil-material damping) is assumed to be 2.5% similar to that used by El-Marsafawi et al. The effects of loading sequences (i.e., the static self-weight and weight of the mass (m = 941 kg) which was resisted by the soil prior to the application of dynamic loads) were also considered in the analysis. The displacement amplitudes taken from the analysis results are the difference between the total displacement and the static-mass-induced displacement.

Parametric and comparison studies were performed to substantiate the modeling assumptions and to evaluate the effects of uncertainties in the model parameters on the results of dynamic pile response analysis. The effects of distribution of soil reaction, soil mass, material damping ratio of the system, radiation damping properties of the soil, and level of excitation intensities on the results are evaluated through parametric studies. The pile response calculated from the proposed soil model having two different sets of far-field soil coefficients is also compared to investigate the sensitivity of the pile response to uncertainties in identifying the far-field characteristics.

Sensitivity study on the number of pile elements

A sensitivity study on the number of elements was performed for this dynamic-vertical-loading case. Three different numbers of pile elements (50, 15 and 10) were used. The dynamic response curves computed from the pile-soil models for the excitation intensity of 9.84 kg.mm and systematic damping ratio of 2.5% are shown in Figure 2.13(a). The difference among the response curves obtained from the pile models with different numbers of pile elements is nearly invisible. From this comparison, it can be concluded that the dynamic response of a single pile subjected to vertical vibration is not affected by the distribution of soil reactions. As previously concluded from the sensitivity study for a static-vertical-loading case, the effect of numbers of pile elements or distribution of soil reaction used in the analysis is insignificant. In consideration of accurately predicting the static and dynamic response of a single pile to vertical loading, the number of pile elements of greater than 10 elements with at least 5 elements for the top portion of 10 pile diameters of the pile length is therefore recommended.

However the efficient number of pile elements to be used in seismic analysis is dependent not only on the accuracy in predicting the static and dynamic pile response to vertical load but also on the accuracy in predicting the static and dynamic pile response to lateral load. In order to attain the number of pile elements to be used efficiently in the analysis, a sensitivity study was subsequently conducted for a case of a single pile subjected to static and dynamic lateral loads.

Effects of soil mass for near-field soil model

The effects of soil mass on the dynamic pile response to vertical vibration are examined. Four different sizes of cylindrical soil mass (r_1 = $1.0r_0$ (no mass), $1.5r_0$, $2.0r_0$ and $3.0r_0$: r_0 = pile diameter) are considered in the near-field soil model. Figure 2.13(b) shows the measured and computed dynamic response curves for different sizes of soil mass. These response curves are obtained from the pile-soil models in which only near-field soil model is used and computed for the excitation intensity of 9.84 kg.mm and systematic damping ratio of 2.5%. The difference among the results computed for various values r_1 is quite small.

The resonant frequency as shown in Figure 2.13(b) decreases by approximately 3% as the size of the soil mass increases from $r_1 = 1.0r_0$ (no mass) to $r_1 = 3.0r_0$. The cause of such reduction in resonant frequency or natural frequency of the system is from the inclusion of the soil mass in the pile-soil system. The natural frequency is an inverse function of the square root of the mass and thus the higher the mass in the system, the smaller the natural frequency of that system. It is also observed that the difference among the displacement amplitudes of all response curves is small until a point at which the smallest resonant frequency (the $r_1 = 3.0r_0$ model) occurs. After this point, the difference is quite noticeable.

This circumstance can be explained through the fundamental basis of dynamic analysis of a structure with an assumption that the pile-soil system can be treated as a single-degree-of-freedom system. As the forcing frequency (w) is greater than the resonant frequency (w_n), the w/w_n ratio is greater than unity. In case that the w/w_n ratio is greater than unity, at the same forcing frequency, the larger value of the w/w_n ratio results in the smaller the displacement amplification ratio (R_d = $u_0/(u_{st})_0$ where u_0, $(u_{st})_0$ = dynamic and static displacements at the same loading amplitude), which is given as follows.

For an undamped case (x = 0),

[2.21] $$R_d = \frac{u_0}{(u_{st})_0} = \frac{1}{1-\left(\frac{w}{w_n}\right)^2}.$$

For a damped case ($x \neq 0$),

[2.22] $$R_d = \frac{u_0}{(u_{st})_0} = \frac{1}{\sqrt{\left[1-\left(\frac{w}{w_n}\right)^2\right]^2 + \left[2x\left(\frac{w}{w_n}\right)\right]^2}}.$$

Consequently, at the same forcing frequency greater than the resonant frequency, the w/w_n ratio of the $r_1 = 3.0r_0$ model is greater than that of other models resulting in the smaller the displacement amplitudes. This explains the descending trend of displacement amplitudes for the forcing frequency of greater than the resonant frequency as the total mass of the system increases. It can be concluded from this comparison that the effects of soil mass on the response of a single pile to static lateral load is not quite significant and the size of the cylindrical soil mass equal to $r_1 = 2.0r_0$ is thus used in the following study.

Effects of modal damping ratio (pile- and soil- material damping)

The response curves obtained for the excitation intensity of 9.84 kg.mm and for different modal damping ratio (x = 1%, 2.5% and 5%) plotted against the measured response are shown in Figure 2.14(a). The resonant displacement amplitude increases by roughly 50% as the damping ratio decreases from 5% to 1% (the higher the modal damping ratio, the smaller the resonant amplitude); however, the resonant frequencies are similar for all cases. This circumstance is in fact expected according to the theoretical basis of a dynamic analysis of structures. The damping ratio of the pile-soil system was set equal to 2.5% in this study. This value, similar to that used by El-Marsawafi et al. (1992), appears to give comparable displacement amplitudes to the measured amplitudes.

Effects of different modeling for far-field soil reactions

In calculation of spring and dashpot coefficients for far-field soil reactions, the determination of a dimensionless frequency a_0 is required. It was found that the dimensionless frequency (a_0) varies between 0.01-0.46 for possible range of variation of the soil profile and input frequency excitations. As a_0 varies between 0.01-0.46, Novak's expressions for dynamic soil parameters become $K_{SV} = 0.77E_s$ and C_{SV} = (7.61 to 70)($r_0 r_s V_s$) for $n_s = 0.3$ which is a typical value for sand. Gatezas' expressions become K_{SV} = (0.64 to 0.89)E_s and C_{SV} = (6.42 to 17)($r_0 r_s V_s$) for the spring stiffness and radiation damping coefficient, respectively. It should be noted that the spring

coefficients derived from both methods are quite similar. The radiation-damping coefficients derived from both methods, although somewhat different at very low frequency, appear to agree well with increasing a_0.

Figure 2.14(b) shows a comparison between the normalized response curves computed from two different sets of far-field soil parameters for the excitation intensity of 9.84 kg.mm and the system damping of 2.5%. The difference between the computed curves is insignificant as can be expected from slight difference of the soil parameters obtained from both methods. Since the expressions for the far-field soil parameters derived by Gazetas and his colleagues do not require a chart-reading task and are simpler to use, they are adopted in modeling the far-field soil reactions in the following comparison studies.

Effects of far-field soil reactions

The effects of far-field soil reactions or radiation damping properties of the soil on the dynamic pile response are evaluated through a comparison study. The normalized response curves computed from the pile-soil model with and without the far-field soil model for the excitation intensity of 9.84 kg.mm and modal damping ratio of 2.5% are compared with the measured response in Figure 2.14(c). The far-field soil model appears to play quite an important role in predicting the resonant frequency and amplitude. It can be observed that by including the far-field soil model, the soil-pile system becomes more flexible as evidenced by a descending shift of the resonant frequency by approximately 5%. As the far-field soil model is included, the stiffness of the system decreases, thus resulting in a reduction of the natural frequency and resonant frequency.

In addition, the resonant displacement amplitude obtained from the model in which only the near-field soil model is used decreases approximately 24% as the far-field soil model is included. This reduction is mostly due to the radiation damping effect as modeled by viscous dampers in the far-field soil model. Besides the radiation damping effects, the reduction of the natural frequency of the system itself also contributes to the reduction of the displacement amplitude for the range at which the forcing frequencies are greater than the resonant frequency. At forcing frequencies less than the resonant frequency, the dynamic displacement amplitudes of the NF+FF model are slightly greater than that of the NF model. This phenomenon is in fact expected and can be explained with a similar fundamental concept of dynamic of structures as given previously in the study on the effect of soil mass on the pile response.

As a result of this comparison, it can be concluded that the dynamic pile response (e.g. resonant frequency and amplitude) is influenced by the far-field soil model. The accurate model of

far-field soil reactions (stiffness and radiation damping) is therefore required in the dynamic pile response analysis for high-frequency loading ranges. However, it should be noted that the applied forcing frequency range (6 to 62 Hz) is very much higher that the frequency range typical for earthquake loading (0.1 to 10 Hz). For the frequency range that is of interest for seismic analysis, the effects of far-field soil model on the dynamic pile response are observed to be insignificant.

Effects of level of excitation intensities

If the pile and the soil deposits were a linear viscoelastic, homogeneous material, the vibration amplitudes would be independent of the level of excitation intensities. This is obviously not the case of soil material which is nonhomogeneous and behaves nonlinearly and inelastically. From the measured response of different excitation intensities, it can be observed that the effect of nonlinear behavior of the soil, although not strongly pronounced, causes a reduction of resonant frequency. The resonant frequency of the excitation intensity ($m_e e$) of 2.45, 4.92 and 9.84 kg.mm is approximately 50 Hz, 47 Hz and 46 Hz, respectively. As shown in Figure 2.14(d), the computed response curves of different excitation intensities show a similar descending trend.

It can also be observed that the computed displacement amplitudes decrease as the level of excitation intensity increases. This reduction in the displacement amplitudes with increasing level of excitation intensity can be explained by the nonlinear behavior of near-field soil. In SAP2000, the energy dissipation in the nonlinear elements (near-field soil reactions) is directly and automatically accounted for by recognizing the inelastic force-deformation relationship in the nonlinear time history analysis. The higher degree of nonlinearity implies that greater energy is dissipated through hysteretic behavior of the material (hysteretic or material damping) leading to smaller resonant displacement amplitudes.

From these studies, the proposed model for a single pile has been verified to be capable of predicting the static and dynamic pile response to vertical loading. The assumptions made in soil modeling have been substantiated. One of many advantages of the proposed model for single piles is its flexibility for allowing users to define different load-transfer characteristics and far-field soil parameters. However, the studies show that the near-field load-transfer characteristics as suggested by Lam and Martin (1986) and the far-field soil parameters as proposed by Gazetas et al. (1991) are satisfactory in modeling the soil deposits. The adjustment that was made in characterizing the load-transfer curves based on Lam and Martin's (1986) recommendation to comply with the criteria of nonlinear model provided in the SAP2000 was also justified.

2.3.2 Lateral Loading

To further examine the capability of the proposed model in predicting static and dynamic pile response to lateral loading, the same procedures used for vertical loading were repeated. First, the adjusted nonlinear load-deformation characteristics (*p-y* curves) for the near-field soil model were validated through correlations with results of a static lateral load test on piles. The Mustang Island tests reported by Cox et al. (1974) were used in the first investigation. The proposed pile-soil model was then assessed for its capability of predicting the dynamic pile response to lateral vibration. This assessment was done through comparisons with experimental results of dynamic lateral load test on a single pile reported by Blaney and O'Neill (1985). Parametric studies were also performed to evaluate the effect of the uncertainties of the model parameters on the results.

2.3.2.1 Case Study 4: Response of a Single Pile to Static Lateral Loads

The Mustang Island tests on a single pile subjected to static and cyclic loading were chosen in this study. The complete report on these tests was presented by Cox et al. (1974). Only brief descriptions of the testing procedure and soil profile are discussed herein. Two steel-pipe piles (21 m long) were driven open-ended at the test site on Mustang Island near Corpus Christi, Texas. The piles were identical in design and properties. They both had the same outside diameter of 0.61 m and wall thickness of 9.2 mm. The soil at the site was uniformly graded fine sands having a friction angle of 39 degrees estimated from correlation with penetration tests. The submerged unit weight was found to be 10.4 kN/m^3. The water table was maintained above the ground surface throughout the test program. The test setup and soil profile for the test site is given in Figure 2.15.

Two types of loadings were applied, static and cyclic. For each loading type, the bending moment along the pile length was measured. In addition to the measurement of the bending moment profile, the loads at ground line, the pile-head deflections and pile-head rotations were measured. In the following study, the test results of the bending moment profile and the lateral load-deflection relationship at the pile-head for the static-loading case are presented for comparison.

Due to the limited capability of the SAP2000 program in applying the nonlinear model, the load-deformation relationships (*p-y* curves) need to be adjusted. To justify the use of adjusted *p-y* curves in SAP2000, a comparison study between the results from the SAP2000 and COM624 programs in which the *p-y* curves can be completely characterized as recommended by API was conducted. A sensitivity study on the number of pile elements to be properly used in modeling the

pile was also performed. In addition, a parametric study on the effects of soil mass included in near-field soil model and effects of including the far-field soil model on the results were done.

Comparison study between the adjusted and actual p-y curves

The verification of the adjusted *p-y* curves is conducted through comparisons of the results from the SAP2000 and those from the COM624 as well as field test data. In these comparisons, the far-field soil model is excluded from the proposed soil model so that its effects on the static pile response are eliminated. The measured and computed values of the lateral load versus the deflection at the ground surface and the lateral load versus the maximum moment for static test are shown in Figures 2.16(a) and 2.16(b). The computed and measured moment distributions and deflections along the length of the pile are also shown for the maximum load in Figures 2.17(a) and 2.17(b). The predicted pile response is in a good agreement with the measured response, and the computed responses from the SAP2000 and COM624 are also highly comparable, indicating that the adjusted *p-y* curves are valid to be used for modeling the near-field soil reactions.

Sensitivity study on the number of pile elements

In addition to realistic soil modeling, the accuracy of the results is dependent on the distribution of soil reactions. Since the soil spring is attached at each node along the length of the pile, the number of pile elements indicates the number of distributed soil springs which affect the accuracy of the results. A sensitivity study on the number of pile elements to be accurately and efficiently used in modeling a pile was performed. Three different numbers of pile elements (50, 15 and 10) which increase in length with depth and with at least 5 elements for the top 10 pile diameters of the pile length were used in this study.

The load-deflection curves and moment profiles computed from the model with 50, 15 and 10 pile elements are shown in Figures 2.18(a) and 2.18(b). The pile response from three models appears to be comparable. The difference between the responses of the 50-pile-element model and those of the 15-pile-element model is not evident. The responses of 10-pile-element model somewhat deviate from those of other models. In other words, the responses converge rapidly as the number of pile elements is greater than 10. Therefore, the number of elements of greater than 10 elements with at least 5 elements for the top 10 pile diameters of the pile length is recommended to be efficiently and accurately used in modeling of the pile for predicting static pile responses to lateral loads. This conclusion also conforms to that of several researchers [El-Sharnouby and Novak (1985) and El-Naggar and Novak (1996)]. Nonetheless, a sensitivity study on the effect of

the number of pile elements on the pile response to lateral vibration is still required and will be performed subsequently.

Effects of far-field soil reactions

The effect of the far-field soil model on the static pile response is evaluated. A number of different proposed expressions for evaluating the far-field soil parameters were considered in this parametric study. It should be noted however that the results obtained from these expressions are somewhat similar. The measured and computed load-deflection curves at the ground surface and the moment profiles obtained from the model with and without the far-field soil models are shown in Figures 2.19(a) and 2.19(b).

The pile-soil system including the far-field soil model appears to be slightly more flexible. Such slight decrease in the stiffness of the pile-soil system is indeed expected because the overall stiffness of the soil system decreases as the far-field soil model is included, and because the spring stiffness of the far-field soil model is usually much larger than that of the near-field soil model. Therefore, the behavior of the system is mainly governed by the less stiff springs or the near-field soil springs with a minor reduction in stiffness due to the effects of including the far-field soil models.

2.3.2.2 Case Study 5: Response of a Single Pile to Dynamic Lateral Loads

For further examination of the proposed model in predicting the dynamic response of single piles to lateral vibration, the results of full-scale dynamic field tests are used. The results of dynamic lateral load tests conducted by Blaney and O'Neill (1986) were chosen. The dynamic lateral load tests were performed on an instrumented steel pipe pile driven into a deposit of clay. Details of the test set-up and soil profile information are given in brief in Figure 2.20.

These tests were conducted on the campus of the University of Houston, Texas. The soil was characterized as a stiff to very stiff desiccated, overconsolidated clay with undrained shear strength and small-strain shear modulus summarized in Figure 2.20. The pile had a 0.273-m outer diameter and 9.27-mm wall thickness and penetrated 13.4 m into the clay deposits. A concrete and steel cap mass was attached to the top of the pile to simulate the effects of a superstructure on the response of the pile-soil system. The system was subjected to a sinusoidal excitation at various frequencies produced by a vibrator rigidly attached to the extension of the pile above the ground surface. The frequency of each sweep load varies from 15 Hz to 1 Hz at a constant rate. The load amplitude was maintained approximately constant during each sweep. The sinusoidal excitation having the load

amplitude of 890 N was first applied and next increased to 2.67 kN, then reduced to 890 N for the final test.

The horizontal frequency response functions were measured at the pile cap. The dynamic displacements along the length of the pile at resonance were also measured. The measured pile responses for the load amplitude of 2.67 kN will be compared with the pile responses computed from the proposed model. Also used for comparison was the static displacement profile measured from a static pile-head load test that was performed after the dynamic tests were finished. The similar steps in performance evaluation of the proposed model in predicting the static pile response were repeated.

Sensitivity study on the number of pile elements

A sensitivity study on the number of pile elements was also performed for the dynamic loading case. Three different numbers of pile elements (50, 15, and 10) increasing in length with depth were again used. The horizontal frequency response and the dynamic deflection profile at resonance are shown in Figures 2.21(a) and 2.21(b), respectively. These response curves were computed for load amplitude of 2.67 kN and systematic damping ratio of 5%. As can be observed from Figure 2.21(a), the dynamic pile response obtained from the 15-pile-element model and that obtained from the 50-pile-element model lie very closely together. The response obtained from the 10-pile-element model slightly deviates from that obtained from other models.

From Figure 2.21(b), the difference among the deflection profiles determined from these three models is almost invisible. Based on these comparisons, the same conclusion as that obtained for static loading case has been reached. Using 10 or more pile elements increasing in length with depth and with at least 5 elements for the top 10 pile diameters of the pile length gives accurate results for both static and dynamic analysis of single piles. The number of elements equal to or greater than 10 is therefore recommended and used for modeling a single pile under both static and dynamic lateral loading.

Effects of soil mass for near-field soil model

The pile-soil model including both near-field and far-field soil models is then used in evaluating the effects of soil mass on the dynamic response of a single pile to lateral vibration. Similar to the preceding study, four sizes of cylindrical soil mass surrounding the pile ($r_1 = 1.0r_0$ (no mass), $1.5r_0$, $2.0r_0$ and $3.0r_0$) were considered for the near-field soil model.

Figures 2.22(a) and 2.22(b) show the measured and computed horizontal frequency response at the pile cap as well as deflection profile at resonance for various sizes of soil mass. Observed from this figure is a descending trend of the resonant frequency. The resonant frequency decreases by approximately 3% as the size of soil mass increases from $r_1 = 1.0r_0$ (no mass) to $r_1 = 3.0r_0$. The differences among these curves are relatively small and the computed responses also agree reasonably well with the measured responses. The comparison of horizontal frequency response of the load amplitude of 890 N, although not presented herein, reveals the same comparable agreement. To maintain consistency throughout this study, the size of cylindrical soil mass equal to $r_1 = 2.0r_0$ is used in the following parametric study.

Effects of modal damping ratio (pile- and soil- material damping)

The response curves in the previous study were obtained for a modal damping ratio of 5% for all modes, which is usually assumed for most structural systems. To investigate the effect of modal damping ratio on the pile response to lateral vibration, three different values of damping ratio (x = 1%, 2.5% and 5%) are used. The pile response computed for different damping ratios are plotted against the measured response is shown in Figure 2.23(a). It can be observed that the resonant displacement amplitude increases by approximately 10% as the damping ratio decreases from 5% to 1% but the resonant frequency for all cases are fairly similar. This trend is similar to that observed for a case study in which the pile is subjected to vertical vibration. However, in this case study, the results of a full-scale test were used: therefore, the modal damping ratio (5%) used in this case is expected to be higher than that (2.5%) used in the previous case in which the test results of a model-pile were used.

Effects of different modeling for far-field soil reactions

The effects of the far-field soil reactions on the dynamic pile response to lateral vibration are evaluated. Three different methods proposed by Berger et al. (1977), Novak et al. (1978), and Gazetas and Dobry (1984) for calculating the coefficients for springs and dashpots were considered. The procedures used in calculation of far-field soil reactions in vertical direction were repeated for calculating of lateral far-field soil parameters.

From all possible variations of the soil profile and frequency of excitations, the dimensionless frequency, a_0, varies between 0.02-0.09. With this variation of a_0, Novak's expressions for dynamic soil parameters become $K_{SL} = 1.15E_s$ for stiffness coefficient and C_{SL} = (500 to 28)($r_0 r_s V_s$) for radiation damping coefficient. These coefficients are based on Poisson's ratio of 0.4. Gatezas'

expressions become K_{SL} = 1.2E_s and C_{SL} = (47 to 18)($r_0 r_s V_s$) for soil stiffness and radiation damping coefficients, respectively. Berger's expression for radiation damping coefficient becomes C_{SL} = 13.8($r_0 r_s V_s$) for clay (n_s = 0.4). Note that the spring coefficients derived from the expressions proposed by Novak and Gazetas are very similar. The radiation damping coefficients tend to be more agreeable as a_0 increases. Although the differences between these radiation damping coefficients is quite large at very low frequency, such differences should not be of great influence on the analytical results because the results of dynamic analysis at very low frequency is approximately similar to those of static analysis in which the damping part of the equation of motion is not significant.

The measured and computed horizontal frequency responses at the pile cap for different sets of far-field soil parameters are shown in Figure 2.23(b). They all appear to be in a very good agreement. Since the effects of different methods used in modeling the far-field soil reactions seem negligible, the method proposed by Gazetas and Dobry was chosen to be consistent with the far-field soil model in the vertical direction.

Effects of far-field soil reactions

The dynamic response curves computed from the pile-soil model with and without the far-field soil model for the load amplitude of 2.79 kN are compared with the measured response in Figure 2.23(c). The resonant frequency of the pile-soil system decreases by approximately 3% as the far-field soil model in included. The difference between the computed curves is relatively small as compared to the previous case study for vertical vibration. Besides the relatively low frequency loading range, the effect of soil nonlinearity is believed to be responsible for this difference. The soil nonlinearity, although it introduces an additional material (hysteretic) damping, reduces the radiation damping. The higher the degree of soil nonlinearity, the greater the energy dissipated through hysteretic behavior of the material (material damping), but the less the energy dissipated through the radiation damping.

In the previous case study, the maximum displacement (settlement) is so small that soil nonlinearity is not strongly pronounced; consequently, the effect of including the far-field soil model is somewhat significant. In this case study; however, the soil nonlinearity is strongly pronounced and therefore whether or not the far-field soil model is included does not affect the overall behavior of the pile-soil system. From this comparison study, it can be concluded that the proposed pile-soil model is able to realistically capture the effect of radiation damping in case of small amplitude loading as well as the effect of soil nonlinearity in case of large amplitude loading.

Effects of soil-pile discontinuity

The formation of a permanent elliptical soil-pile discontinuity of approximately 13 mm at the ground surface was observed during the test. It was seen that the pile-soil discontinuity extended to greater than 0.25 m below the ground surface. The effects of the gap on the dynamic pile response were examined through comparison between the pile-soil model with and without the gap model. The modeling of the soil-pile discontinuity was made possible by using the gap element available in SAP2000. Figure 2.23(d) shows a comparison of the measured and computed frequency response. By accounting for the effects of gap in the model, the resonant frequency decreases by 4% and the resonant amplitude increases by 10%. As a result of the formation of the gap, the pile-soil system becomes more flexible. A note is made of the fact that the difference of the response from both models is relatively small, however.

2.4 Concluding Remarks

The results of these studies demonstrate that the proposed model is capable of predicting the static and dynamic pile response to both vertical and lateral loading. Additionally, the load-transfer characteristics, as suggested by Lam and Martin (1981) for vertical loading and by the API (1991) for lateral loading, appear to be satisfactory for modeling the near-field soil reactions. The effect of the distribution of soil reaction interpreted in form of the number of pile elements was also evaluated though sensitivity studies. Based on these studies, it can be concluded that the number of pile elements of greater than 10 elements with at least 5 elements for the top 10 pile diameters of the entire length of the pile can be efficiently and accurately used in modeling the pile for static and dynamic response analysis of single piles subjected to both vertical and lateral load.

In addition, the comparison study shows that the effect of different sizes of soil mass on the dynamic pile response is small, and so is the effect of different modeling of far-field soil properties. The dynamic pile response is also found to be insensitive to the far-field soil model for the frequency range typical for earthquake loading (0.1-10 Hz). In conclusion, the capability of the proposed pile-soil model in predicting the static and dynamic pile response to both vertical and lateral loading has been verified through comparison studies with several experimental results. Once the proposed pile-soil model is found satisfactory for estimating the static and dynamic response of single piles, the next step is to incorporate the single pile model into a pile group foundation model.

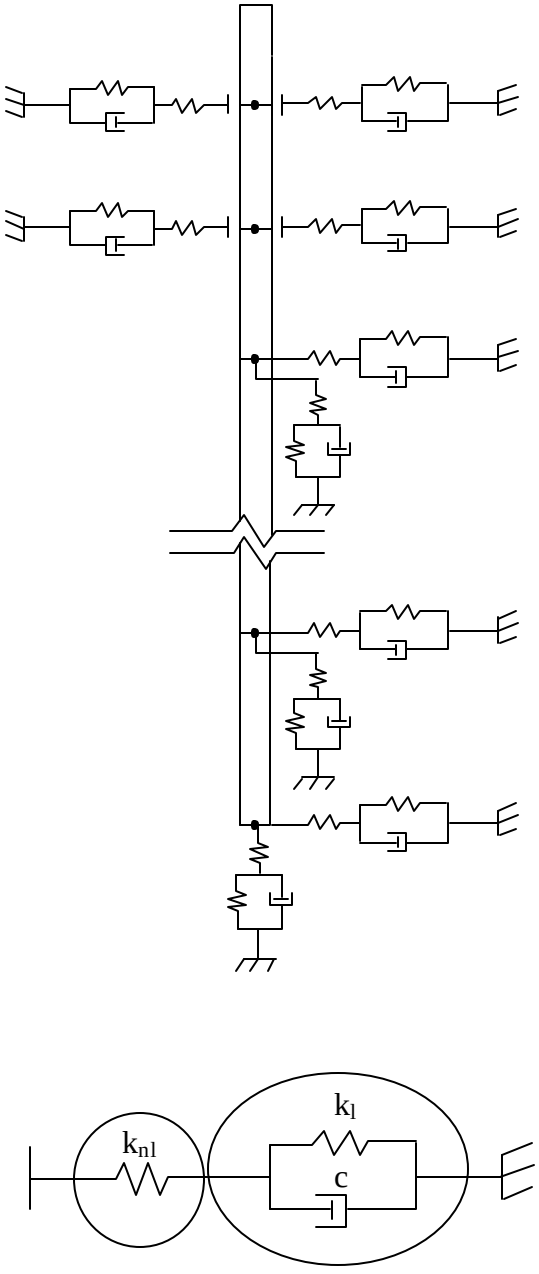

Figure 2.1. Proposed Pile-Soil Model for Single Piles.

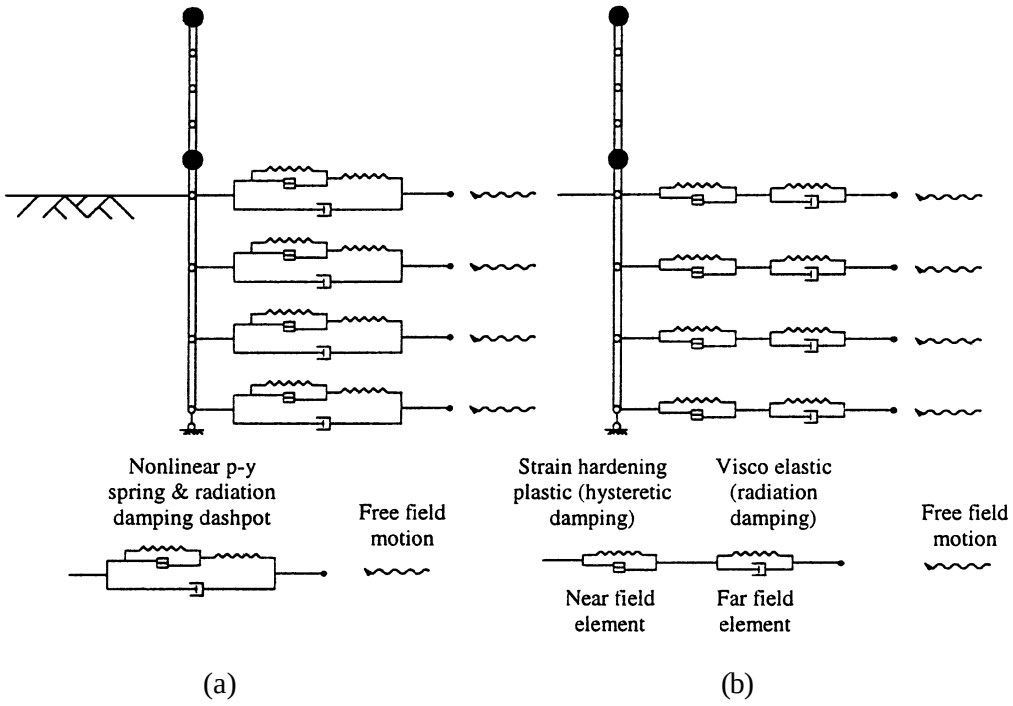

Figure 2.2. Soil-Modeling Methods for Single Piles [after Wang et al. (1998)].

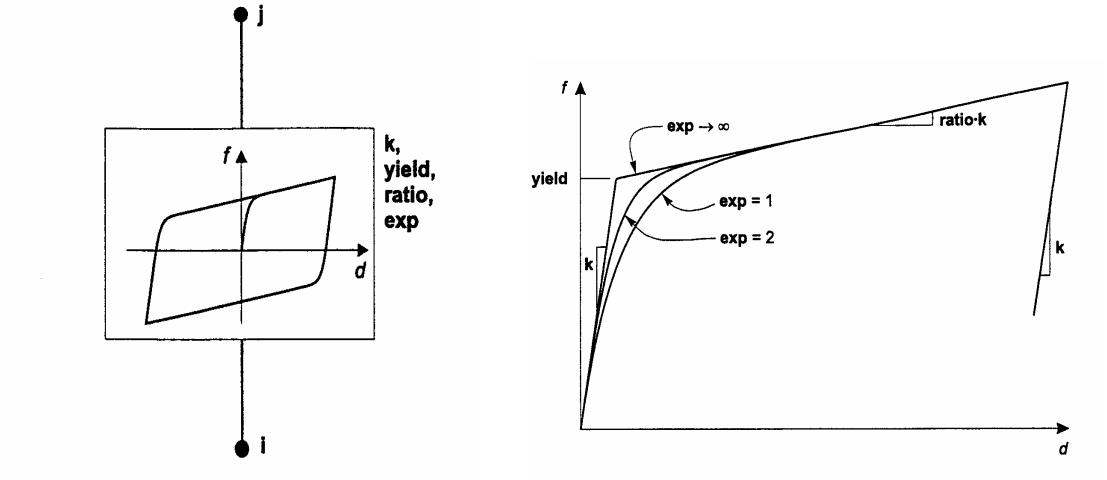

Figure 2.3. Nonlinear Load-Deformation Model for Uniaxial Deformation (from SAP2000 Analysis Reference, Volume I).

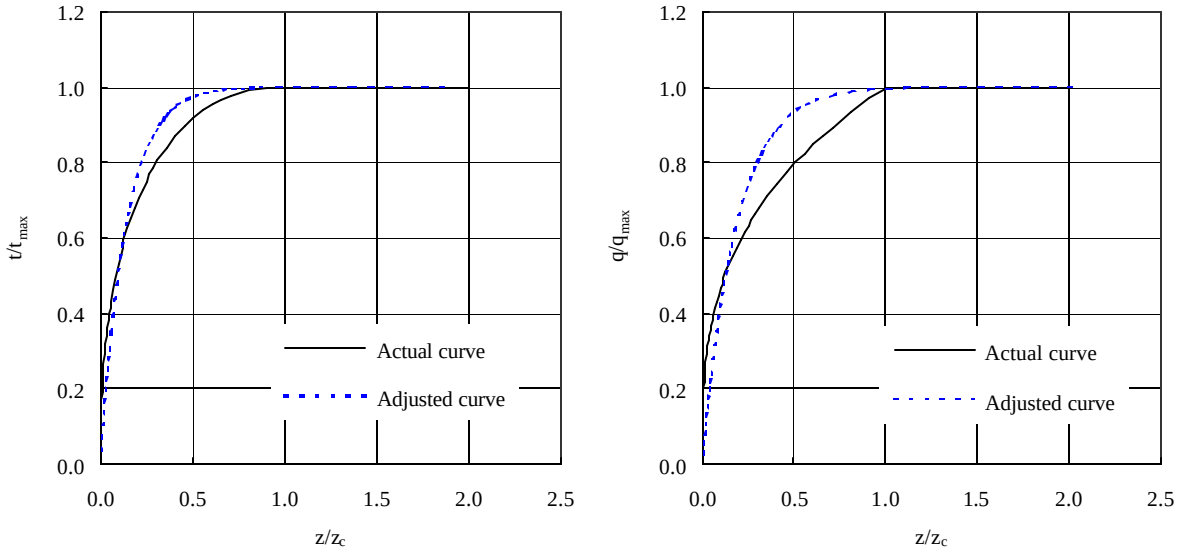

(a) *t-z* Curves (b) *q-z* Curves

Figure 2.4. Actual and Adjusted Load-Transfer Curves: (a) *t-z* Curves, and (b) *q-z* Curves in Normalized Unit.

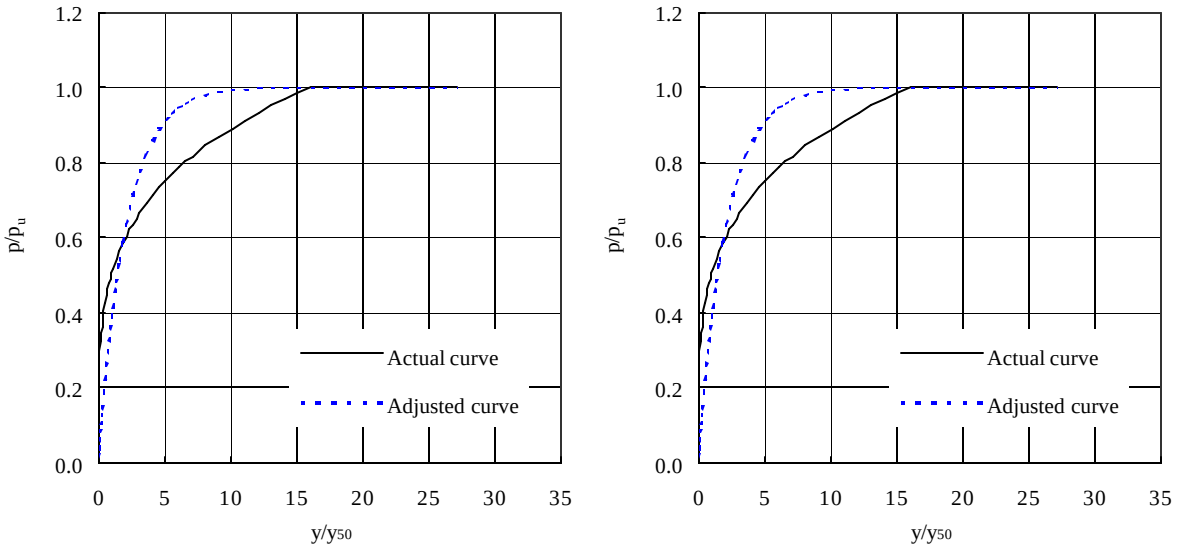

(a) Soft Clay (b) Stiff Clay

Figure 2.5. Actual and Adjusted *p-y* Curves for a Pile in (a) Soft Clay, and (b) Stiff Clay in Normalized Unit.

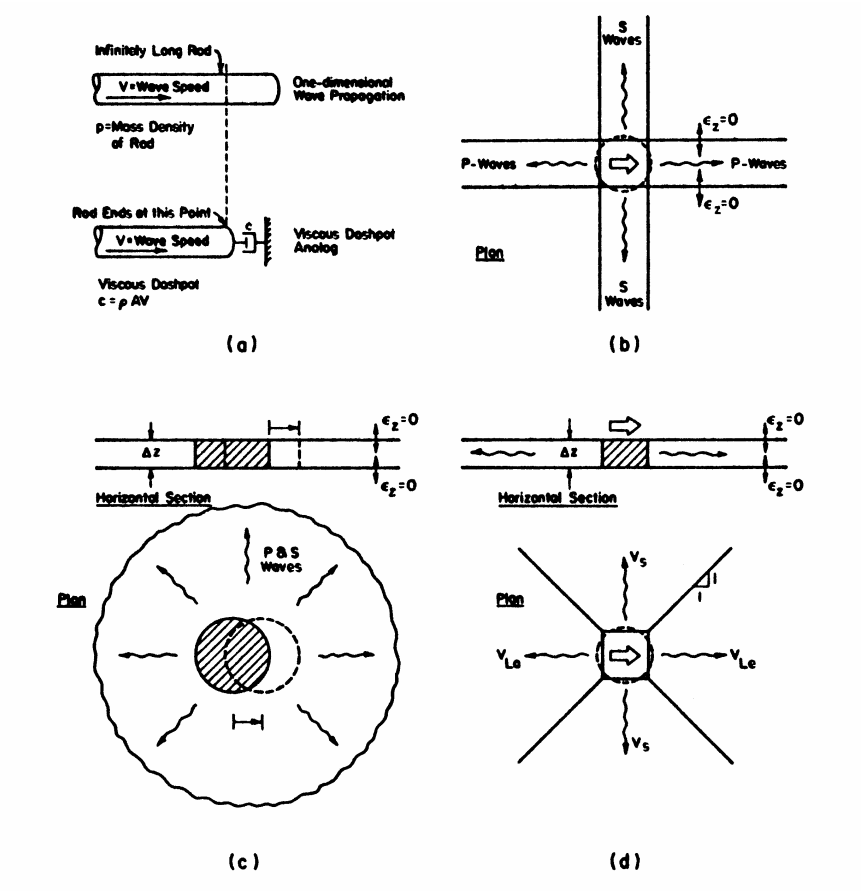

Figure 2.6. 1-D and 2-D Radiation Damping Models [after Gazetas and Dobry (1984)].

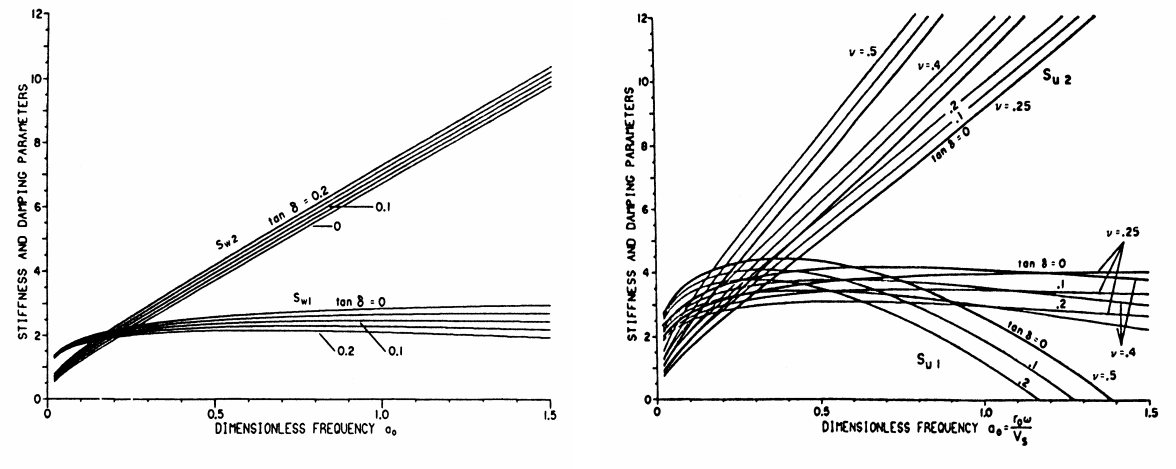

(a) S_{w1} and S_{w2} (b) S_{u1} and S_{u2}

Figure 2.7. Variation of (a) S_{w1} and S_{w2} , and (b) S_{u1} and S_{u2} with a_0 [after Novak et al. (1978)].

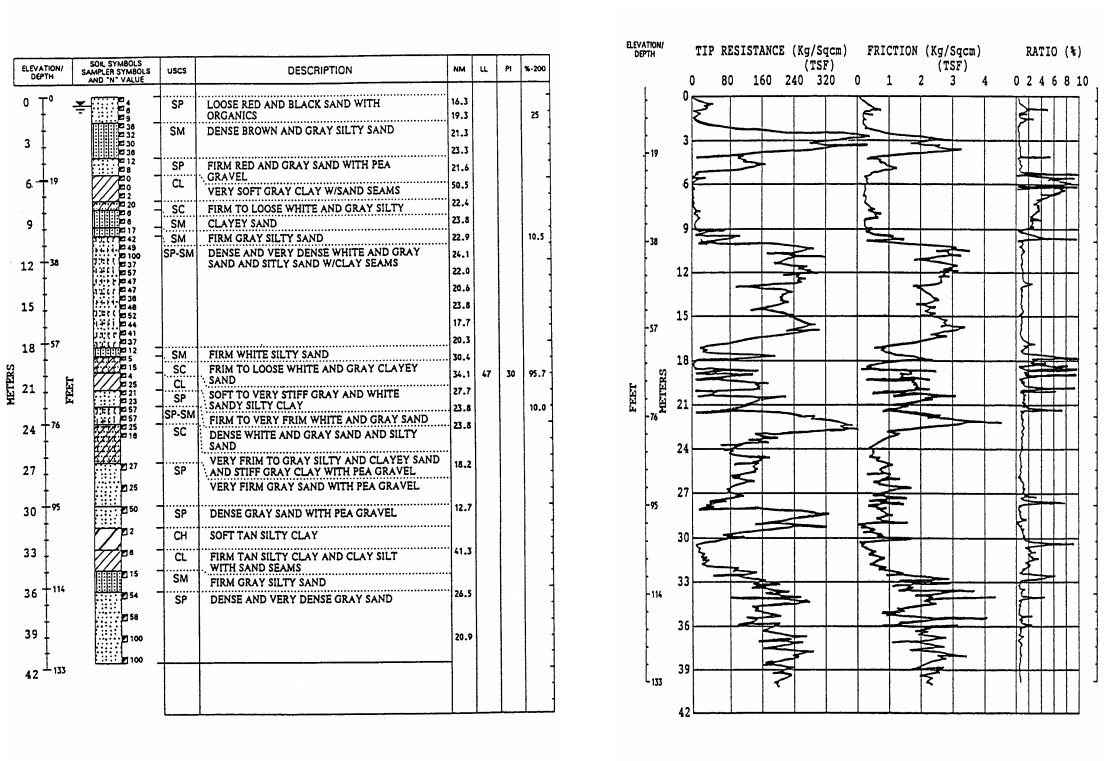

Figure 2.8. Soil Profile and SPT and CPT Results for Case Study 1 [after Laier (1989)].

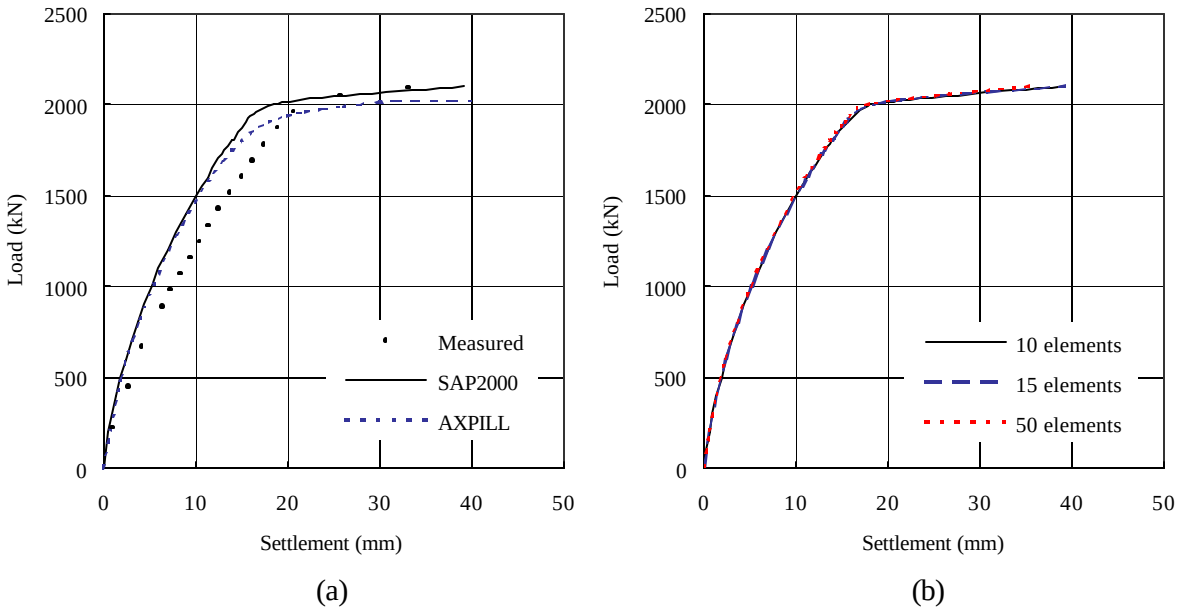

Figure 2.9. Load-Settlement Curves Obtained from (a) Different Computer Programs, and (b) Pile Models with Different Numbers of Pile Elements.

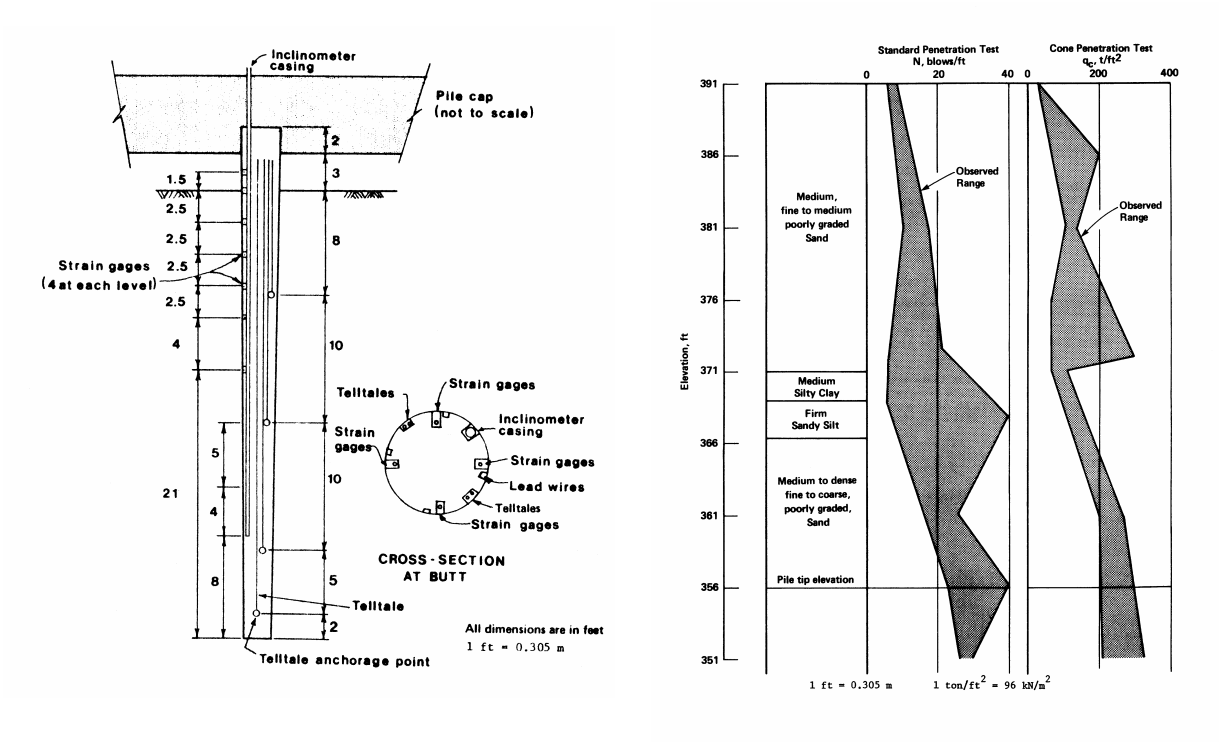

Figure 2.10. Pile Instrumentation, Soil Profile and Penetration Test Data for Case Study 2 [after Stevens et al. (1979)].

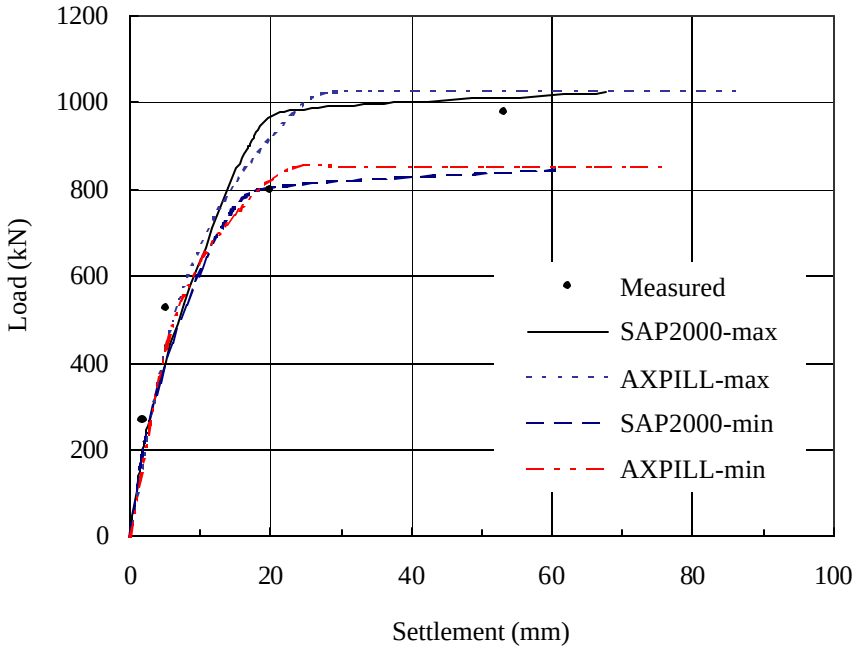

Figure 2.11. Load-Settlement Curves Obtained from SAP2000 and AXPILL.

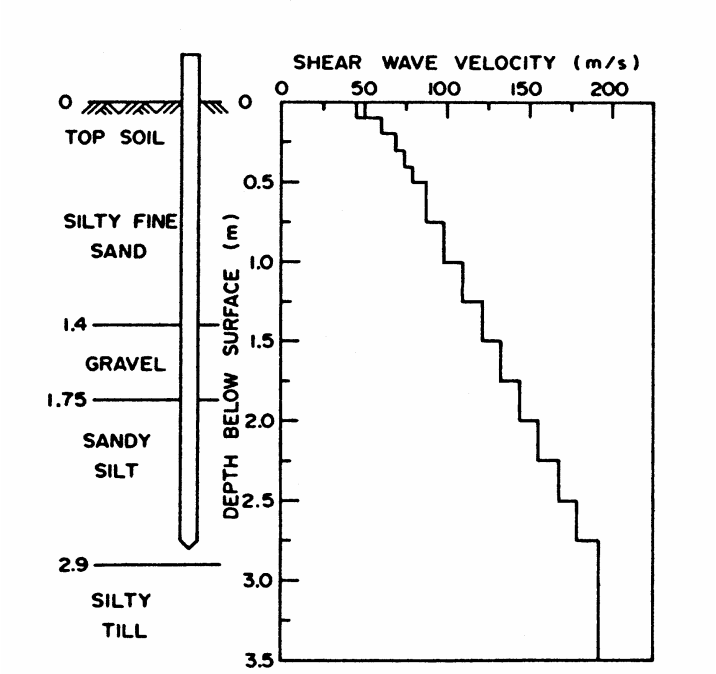

Figure 2.12. Soil Profile and Shear Wave Velocity Measurement for Case Study 3 [after El-Marsafawi et al. (1992)].

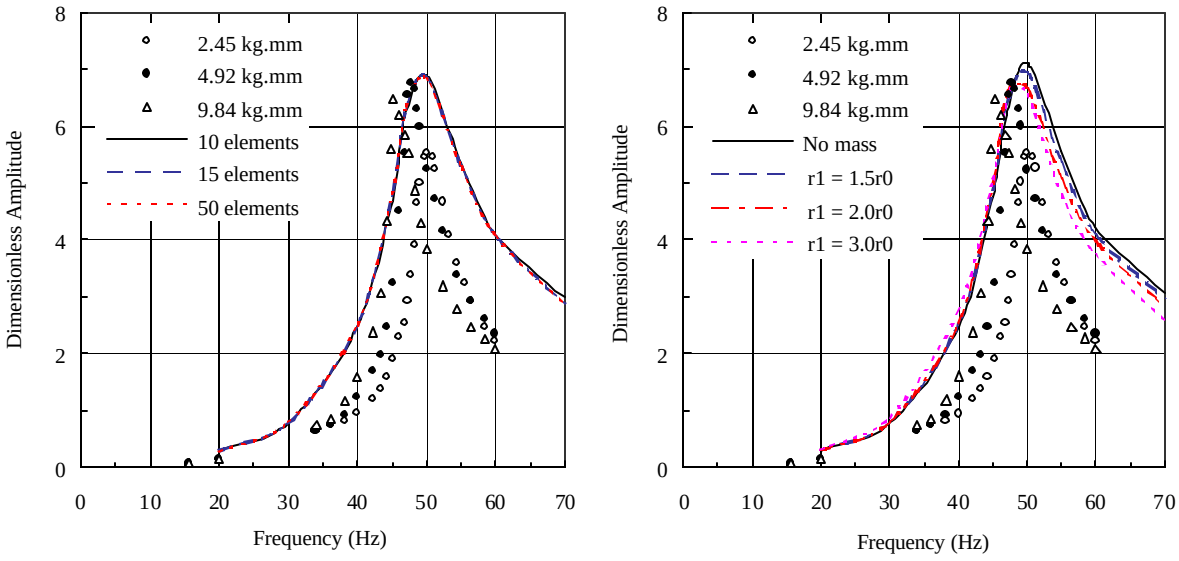

(a) (b)

Figure 2.13. Dynamic Response Curves from Pile Models with (a) Different Numbers of Pile Elements, and (b) Different Sizes of Soil Mass.

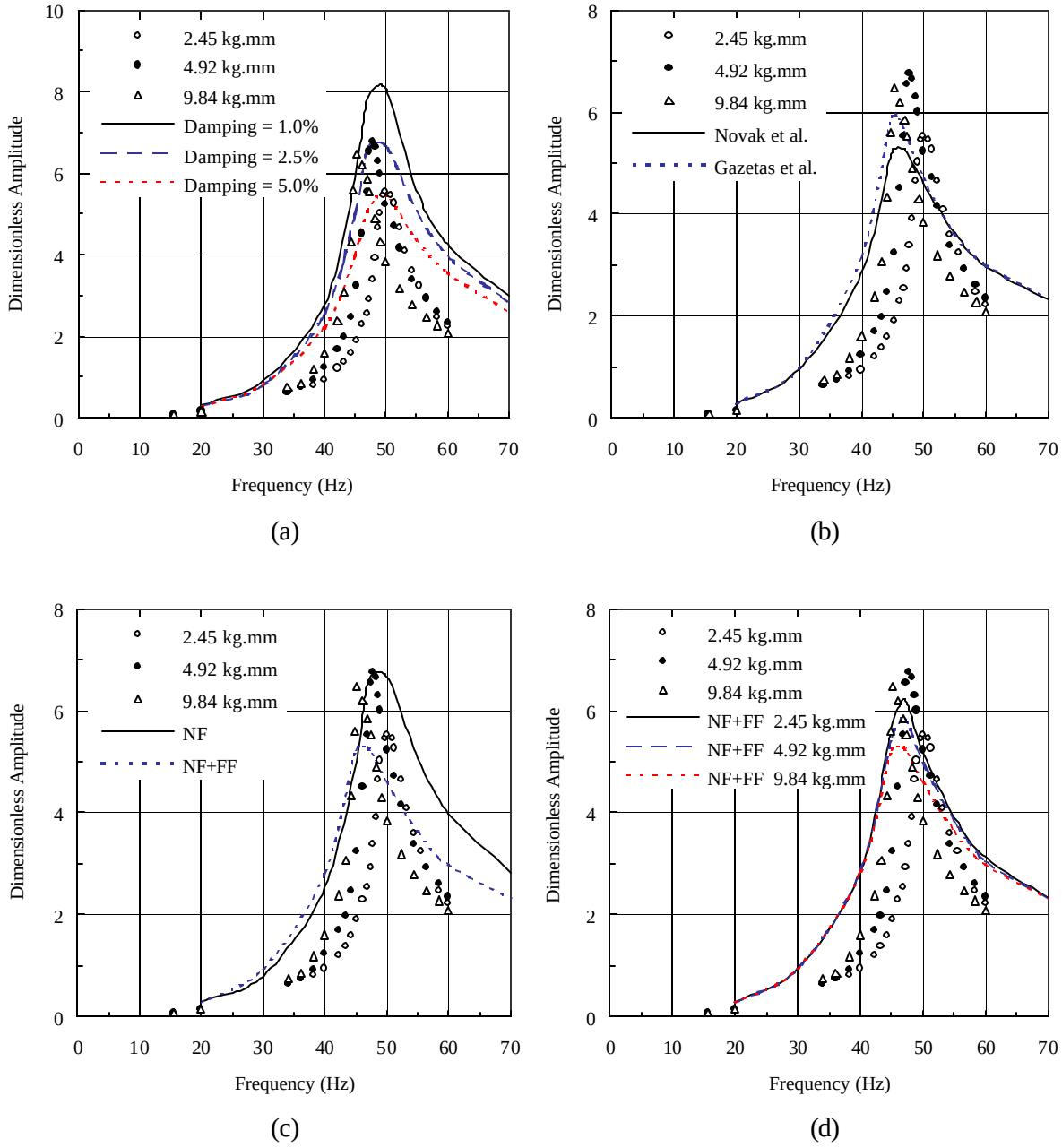

Figure 2.14. Dynamic Response Curves for (a) Different Modal Damping Ratios, (b) Different Modeling of Far-Field Soil Reactions, (c) Different Soil Modeling Concepts, and (d) Different Levels of Excitation Intensity.

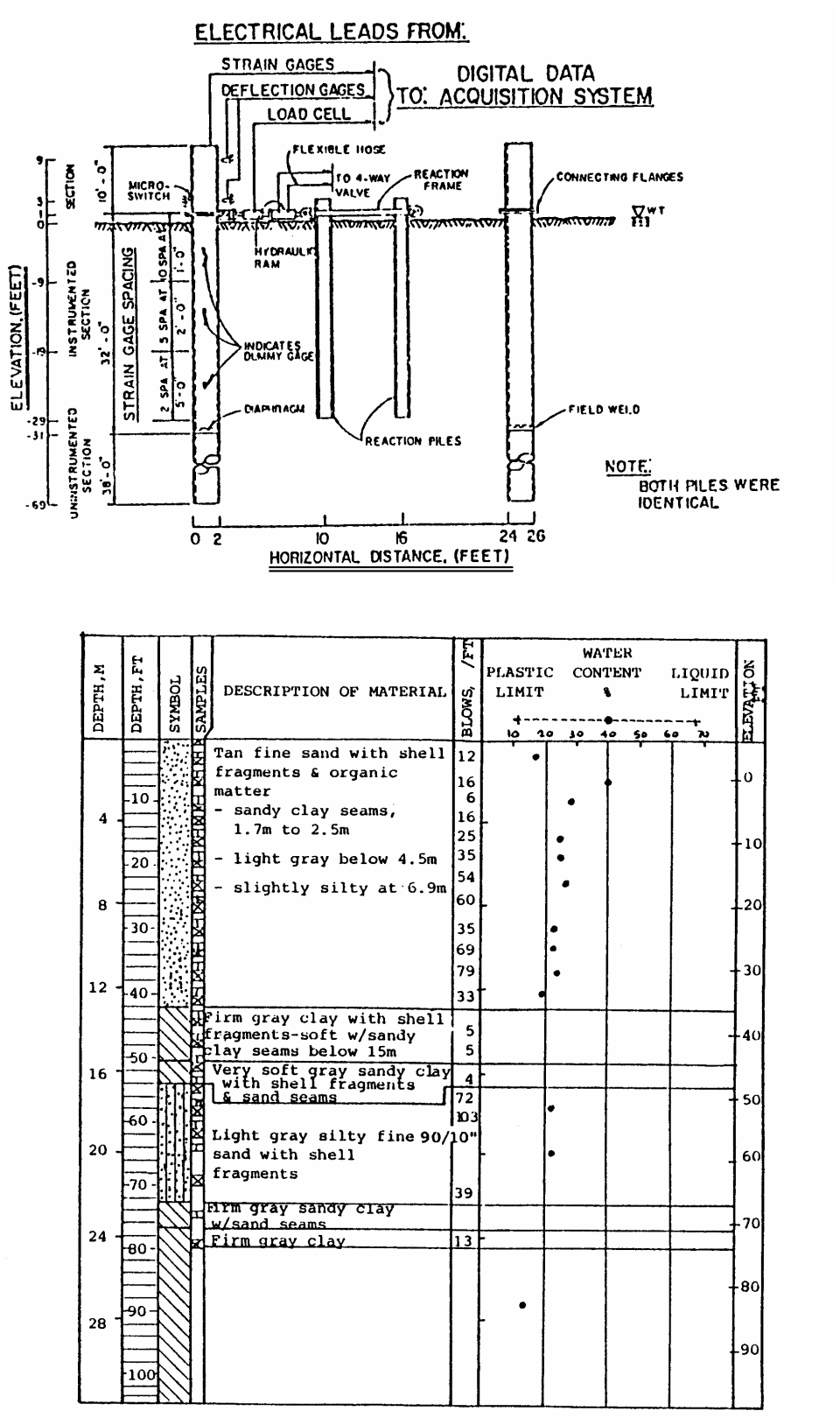

Figure 2.15. Test Setup and Soil Profile for Case Study 4 [after Reese et al. (1974)].

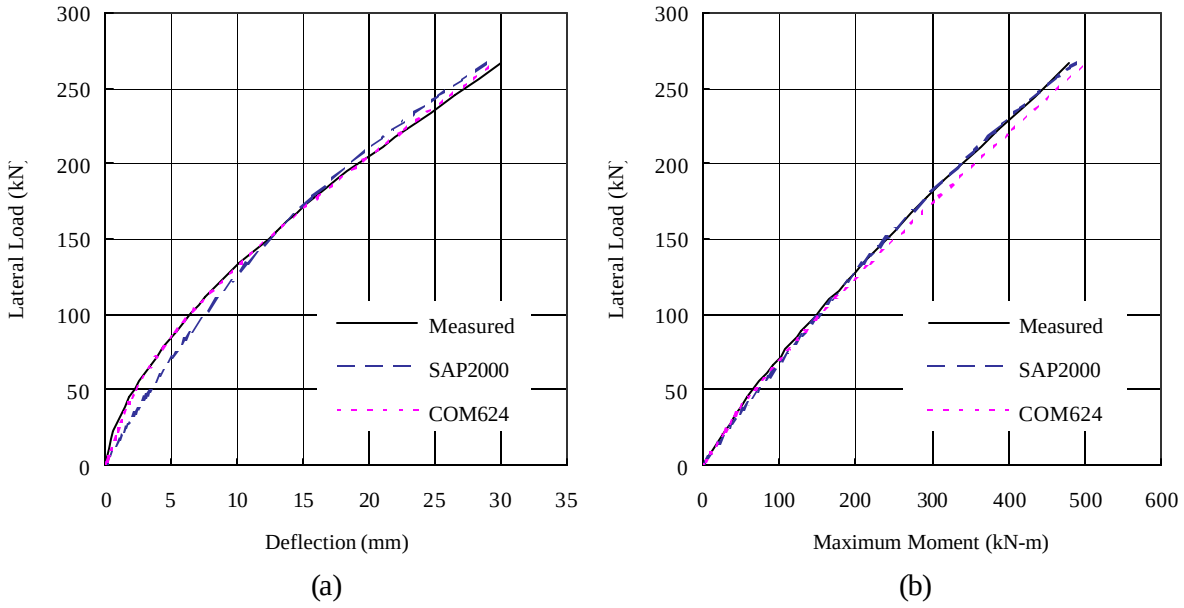

Figure 2.16. Response Curves: (a) Lateral Load versus Deflection at Ground Surface, and (b) Lateral Load versus Maximum Moment.

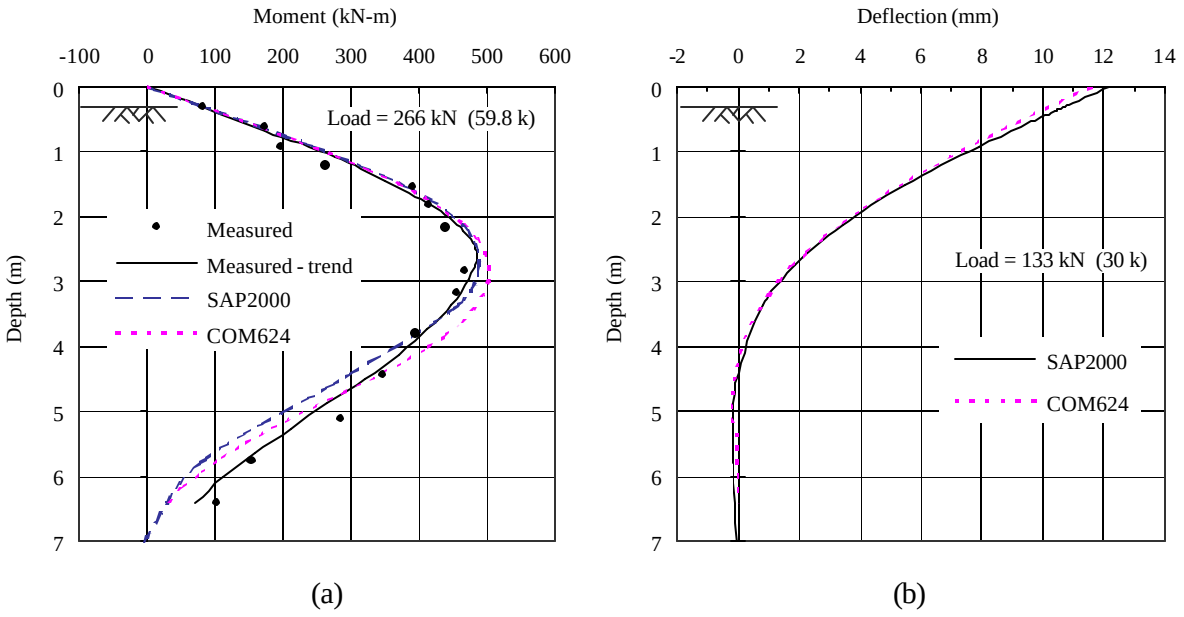

Figure 2.17. Moment Profiles (a) and Deflection Profiles (b) for the Mustang Island Pile Test.

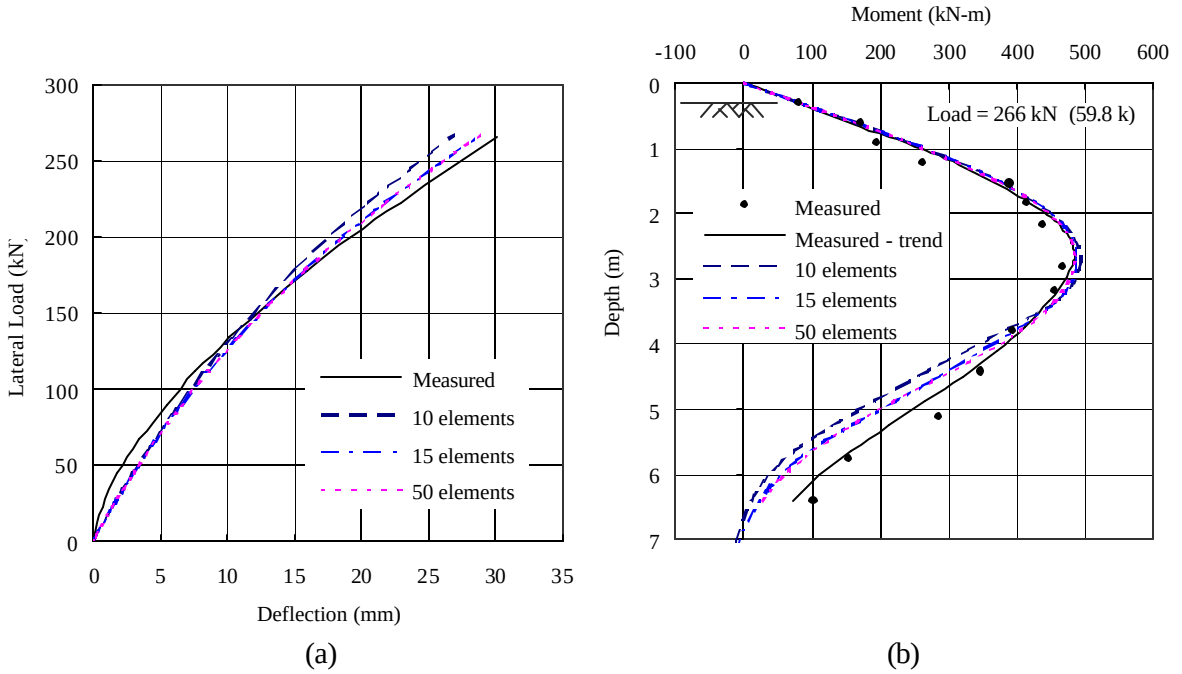

Figure 2.18. Load-Deflection Curves (a) and Moment Profiles (b) for Different Numbers of Pile Elements.

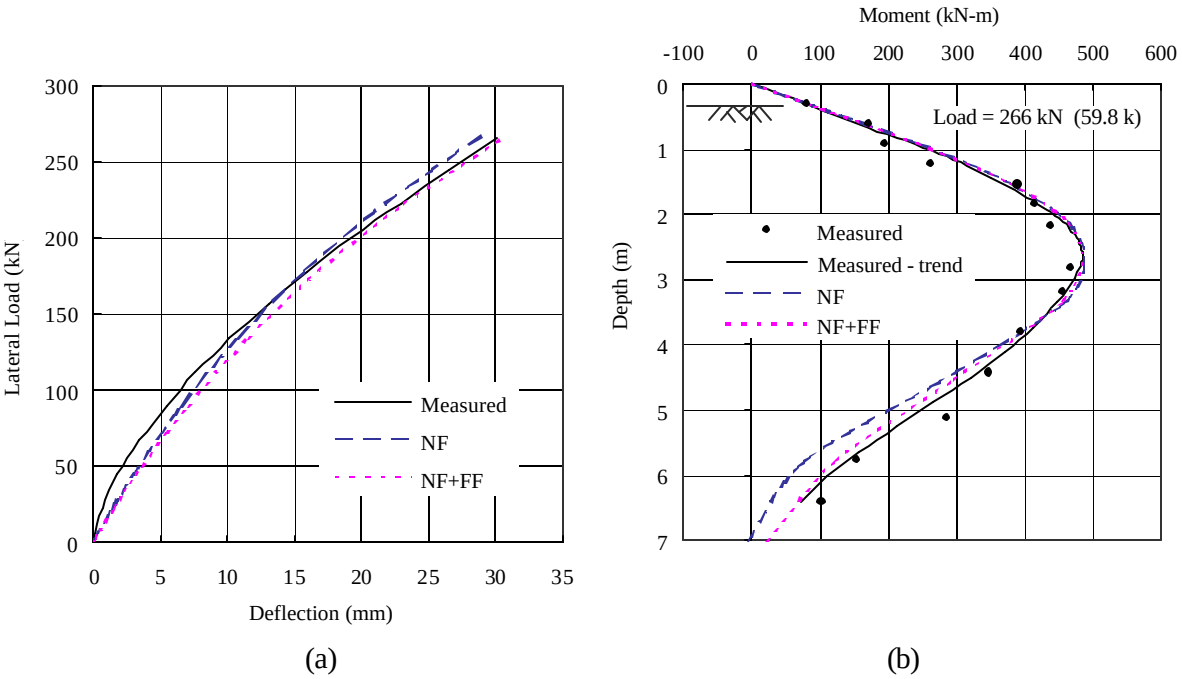

Figure 2.19. Response Curves: (a) Lateral Load versus Deflection at Ground Surface, and (b) Lateral Load versus Maximum Moment for Models with and without Far-Field Soil Models.

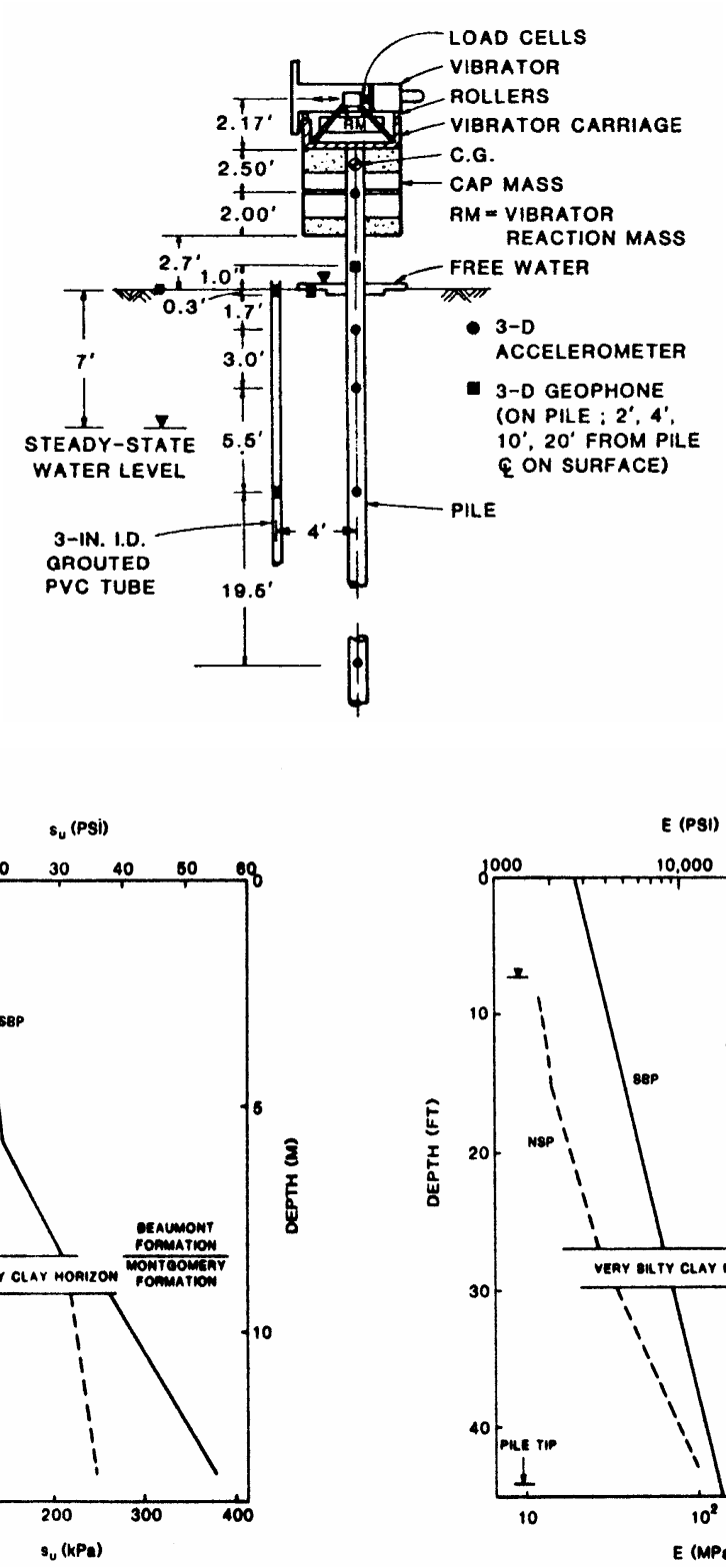

Figure 2.20. Pile Instrumentation, Soil Profile and Exploratory Results for Case Study 5 [after Blaney and O'Neill (1985)].

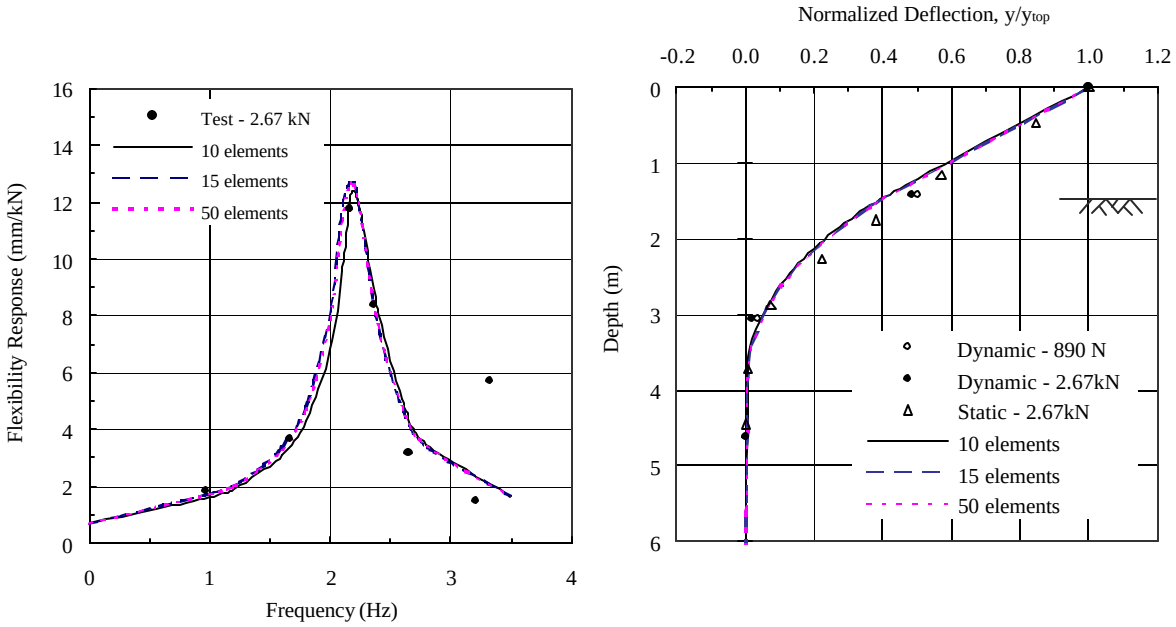

Figure 2.21. Response Curves: (a) Horizontal Frequency Responses, and (b) Dynamic Deflection Profiles at Resonance for Different Numbers of Pile Elements.

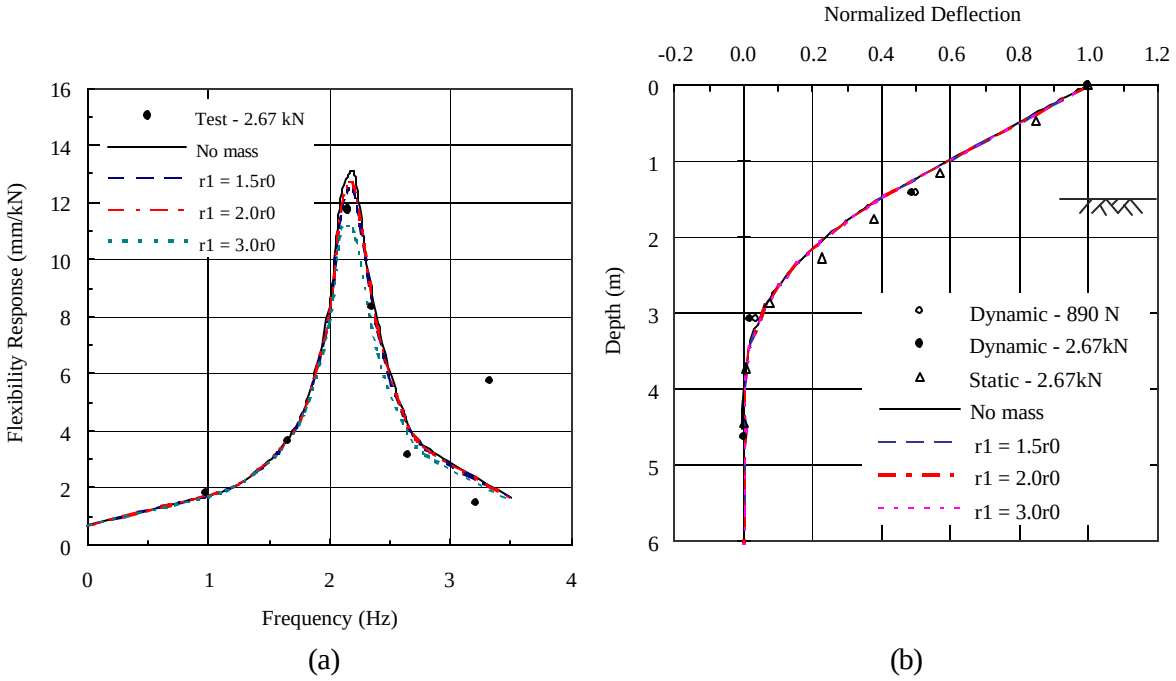

Figure 2.22. Response Curves: (a) Horizontal Frequency Responses, and (b) Dynamic Deflection Profiles at Resonance for Different Sizes of Soil Mass.

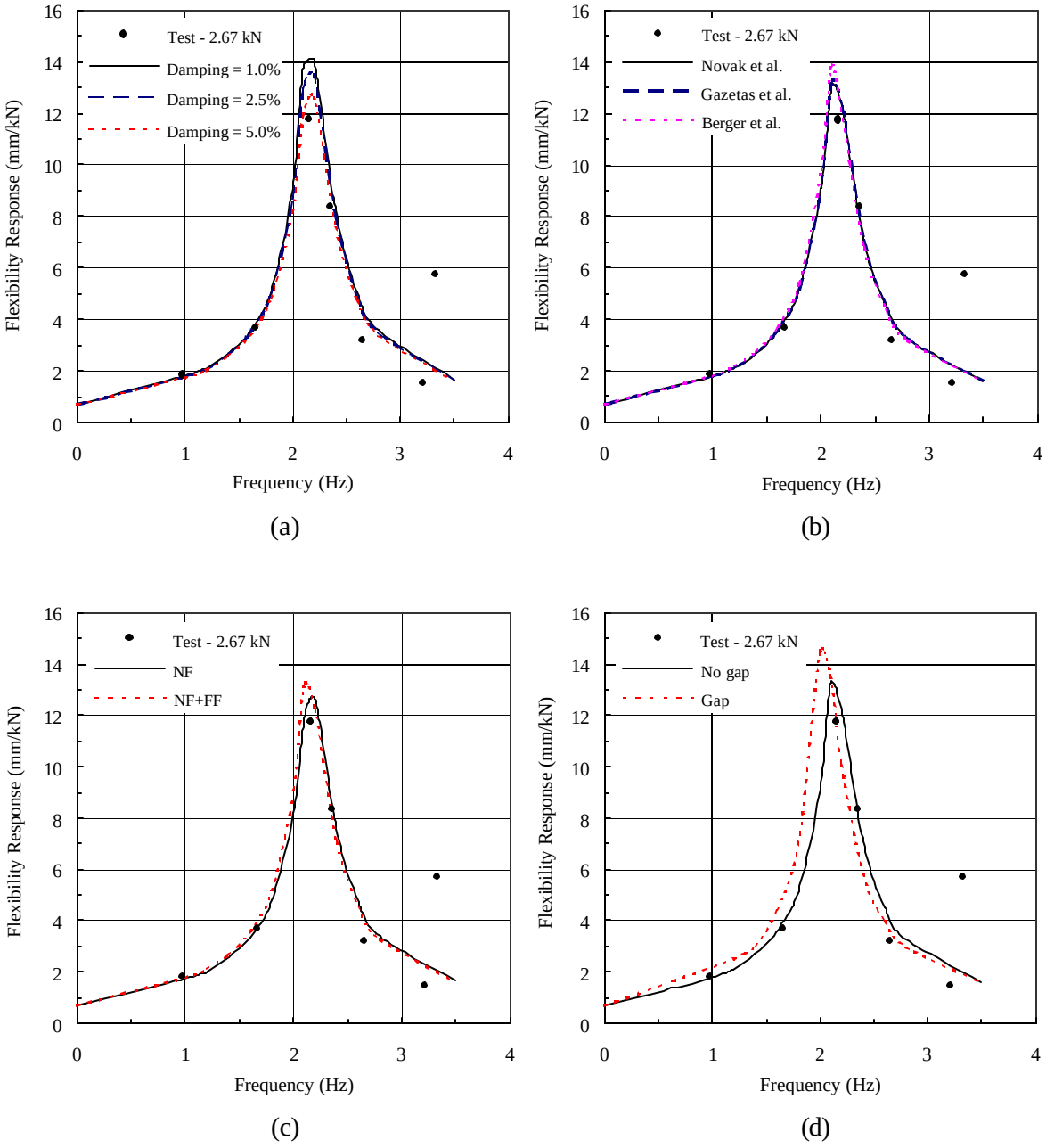

Figure 2.23. Horizontal Frequency Responses (a) for Different Sizes of Soil Mass, (b) for Different Modeling of Far-Field Soil Reactions, (c) for Different Soil Modeling Concepts, and (d) for Pile Models with and without Modeling of Pile-Soil Discontinuity.

CHAPTER 3

PILE FOUNDATION MODEL

3.1 Introduction

To attain an analytical model for pile group foundations, the pile-soil model of each individual pile is integrated. In a process of integrating the pile-soil model of single piles into the pile group model, the effects of the pile-soil-pile interaction (PSPI) need to be properly considered. A number of numerical and experimental methods have been proposed to account for the PSPI effects in static and dynamic response analysis of pile group foundations. Among these methods is the empirical multiplier-factor method in which the load-transfer curves are adjusted to account for the PSPI effects by stretching and reducing the ultimate capacity of the curves. This multiplier-factor method is adopted in the following study. Experimental data of several static and dynamic load tests on pile groups as well as on an existing pile foundation supporting a two-span bridge are used in a process of investigating the performance of the proposed pile group model in predicting the response of pile group foundations. The analytical results presented by other investigators are also used for comparison.

3.2 Proposed Pile Foundation Model

Similar to the proposed single pile model, each pile in a pile group foundation is modeled using a series of linear or nonlinear frame elements. Although the soil models for single piles need to be adjusted to account for the PSPI effects to be appropriate for the pile group model, a similar concept of using a series of linear and nonlinear springs and dashpot in modeling the soil reactions is still applicable for the pile group model. The pile cap can be modeled using shell or solid elements. The idealized pile-soil model for pile group foundations is shown in Figure 3.1.

3.2.1 Pile and Pile Cap Model

From the performance evaluation study of the single pile model, it was found that accurate results of static and dynamic analysis could be obtained with the pile model having a minimum of 10 pile elements increasing in length with depth and with at least 5 elements for the top 10 pile

diameters of the pile length. The number of elements greater than 10 elements is thus used for modeling each pile in a group.

3.2.1.1 Pile-to-Pile-Cap Connection

In general, the pile-group response, especially to lateral loading, is significantly affected by the fixity conditions between pile heads and pile cap. The pile-to-pile-cap connections are typically assumed in practice to be either pinned-head or fixed-head conditions as illustrated in Figure 3.2. Although the fixed or pinned conditions are often assumed for design purpose, the degree of fixity at the pile head, in reality, is neither infinite (fixed-head) nor zero (pinned-head) but falls between these conditions. More details on the subject of idealization of the pile-to-pile-cap connection can be found in several publications such as Khan, N. M. (1993) and Chaemmangkang (2001).

As an alternative to a theoretical or numerical method, the empirical criteria for determining the fixity of a pile-to-pile-cap connection suggested by McVay et al. (1996) and Castilla et al. (1984) can be used. Castilla et al. (1984) concluded based on the analytical results that the pile embedment length equal to or greater than twice the pile depth or diameter is required to develop a full fixity condition. It was also found that the 0.3-m (1-ft) embedment length of the piles into the concrete pile cap, which is considered in practice to be a pinned condition, developed 61 to 83 percent of the moments for a 1.2-m (4-ft) embedment length therefore should be considered as a partially fixed condition.

Once the fixity conditions of the pile-to-pile-cap connections are determined, they can be modeled in the SAP2000 by specifying equivalent linear or nonlinear uniaxial and rotational springs. The difficult task is generally not the modeling task but the determination-of-the-degree-of-fixity-condition task which requires an engineering judgment in an idealization of structural or as-built construction details. In the subsequent study, the fixity conditions of the pile-to-pile-cap connection is accounted for in an approximate manner by carefully considering the as-built construction details and modeling them accordingly.

3.2.1.2 Pile Cap Model

The pile cap may be modeled using solid or shell elements. It is generally believed that using solid elements to model a relatively thick reinforced concrete pile cap is more realistic than using shell elements, which are typically used for modeling a thin structural members (i.e., the length to

thickness ratio of between 10 and 100). However, using the solid elements requires more computational effort and may not be appropriate from the practicality standpoint. Alternatively, several researchers have used shell elements for modeling the pile cap. Using shell elements certainly requires less computational effort. Nonetheless, in order to provide a complete confidence in applying the proposed model, the following study is devoted to evaluate the applicability and accuracy of shell elements in modeling the pile cap.

Shell elements versus solid elements

A comparison study of the responses computed from the model of 3 steel pipe piles jointed by the reinforced concrete pile cap (1.37-m thick) is conducted first. The pile cap is modeled by the equivalent 2-D shell elements (frame elements) for modeling Case 1 and equivalent 2-D solid elements (plane-strain elements) for modeling Case 2. The schematic models are illustrated in Figure 3.3. The piles are rigidly capped with the massive concrete pile cap; therefore, the rigid elements are used to simulate the effect of piles embedding into the pile cap (the rigid end-zone effects). To eliminate the effects of other system parameters, all modeling parameters besides the pile cap model are the same for both models. The PSPI effects are not considered here.

The 13.4-m long pipe piles having an outside diameter of 0.273 m and a wall thickness of 9.4 mm are used in the study. The spacing between each pile is 0.82 m (i.e., the spacing and diameter (s/d) ratio is equal to 3). The soil conditions are predominantly clay. This pile group is actually one of the case studies that will be subsequently discussed in detail. Therefore, the pile group layout and geotechnical conditions that can be obtained later in this chapter are not presented here.

These two pile-group models are loaded in both vertical and lateral directions. The vertical load (800 kN/pile) is applied at the top of the center pile and the lateral load (200 kN/pile) is applied at the center of the pile cap as shown in Figure 3.3. For the vertical loading case, the axial forces and deformations calculated at the pile-to-pile-cap interface for each pile from both modeling cases are compared in Table 3.1. For the lateral loading case, the shear forces and lateral deformations at the pile-to-pile-cap interface for each pile are compared in Table 3.2.

It is observed that the difference is minuscule (less than 0.7% for all comparisons). The deformed shapes of these two models for both loading cases, although not shown here, are quite similar. For both vertical and lateral loading cases, the pile cap modeled using the 2-D solid elements is slightly more flexible than that using the shell elements. This is because the effects of

shear deformation are not included in the plate bending behavior of the shell elements. The bending stiffness of the thick shell elements is derived solely from the plate bending behavior and thus resulting in the stiffer elements than the solid elements which can intrinsically account for the effects of shear deformation.

Based on these above comparisons, the effects of shear deformation, which were first believed to be influential for such a thick pile cap, appear to be insignificant. The difference of the results obtained from these two pile cap models is very small. This is possibly because the pile cap is relatively stiff compared to other structural elements (e.g., piles and surrounding soil). The applied load is transferred to the weak part of the structural system which is the soil springs in this case. Since most of the applied force is transferred to the soil, the pile cap behaves like the rigid body and thus the difference of modeling the pile cap using shell and solid elements is inconsequential. Consequently, the shell elements can be efficiently used to model the pile cap.

Table 3.1. Comparison of Vertical Pile Responses for Different Modeling of Pile Cap.

	Pile 1	Pile 2	Pile 3
(a) Axial Force (kN)			
Shell Element	798.39	803.22	798.39
Solid Element	797.10	805.80	797.10
(b) Deformation (mm)			
Shell Element	6.00	6.09	6.00
Solid Element	5.97	6.14	5.97

Table 3.2. Comparison of Lateral Pile Responses for Different Modeling of Pile Cap.

	Pile 1	Pile 2	Pile 3
(a) Lateral Force (kN)			
Shell Element	199.94	200.26	199.77
Solid Element	198.79	201.13	200.08
(b) Deformation (mm)			
Shell Element	35.58	35.58	35.54
Solid Element	35.62	35.70	35.64

Effects of different patterns of finite element mesh

In general, it is often believed that the finer the finite element mesh, the more accurate the results; however, using a very fine FE mesh is certainly not computationally efficient. The following study is therefore devoted to evaluation of the effects of FE mesh refinement on the results and determination of the appropriate FE mesh to yield reasonable results with acceptable tolerance and with minimum computational efforts. Three patterns of FE mesh (2x2, 4x4 and 6x6) as shown in Figure 3-4 are used. The loading conditions for this parametric study are similar to those used previously except that the loads are now applied at the central row of the pile group.

A similar procedure to that employed in the previous comparison study is repeated for this study. For the vertical loading case, due to the symmetry of geometry and loading, there are only three different pile forces; the force carried by the corner piles (labeled V-1), that by the mid-side piles (V-2) and that by the center pile (V-3) as shown in Figure 3-4. The responses obtained from different patterns of FE mesh are compared in Table 3-3. For lateral loading case, the loading is anti-symmetrical; therefore, the lateral force carried by each pile is different. In this comparison study, the responses of only three piles (labeled L-1, L-2 and L-3 in Figure 3-4) are presented in Table 3-4.

The difference of the pile response obtained from different patterns of FE mesh is relatively small (less than 0.5% for all comparisons). The comparisons of the response of other piles, although not shown here, also show a similar trend. The effects of FE mesh refinement on the results are negligible. The 2x2 FE mesh of 4-node shell elements can be efficiently used to model the pile cap and to yield reasonable pile response with minimum computational effort. In conclusion, it is recommended that the pile cap be modeled using the 4-node shell elements. Each node represents one individual pile in a group.

Table 3.3. Comparison of Vertical Pile Responses for Different Patterns of FE Mesh.

	Pile V-1	Pile V-2	Pile V-3
(a) Axial force (kN)			
2x2	798.73	800.48	803.16
4x4	798.58	800.62	803.20
6x6	798.54	800.66	803.20

(b) Deformation (mm)			
2x2	6.004	6.035	6.085
4x4	6.001	6.038	6.086
6x6	6.000	6.039	6.086

Table 3.4. Comparison of Lateral Pile Responses for Different Patterns of FE Mesh.

	Pile L-1	Pile L-2	Pile L-3
(a) Horizontal force (kN)			
2x2	200.46	200.26	200.14
4x4	200.41	200.45	200.05
6x6	200.51	200.53	200.11
(b) Deformation (mm)			
2x2	28.93	28.87	28.85
4x4	28.99	28.94	28.91
6x6	29.02	28.96	28.92

3.2.2 Soil Model

The soil model for pile groups is somewhat different from that for single piles because of the effect of pile-soil-pile interaction. As a result of the fact that the soil inside a pile group foundation is well confined by the presence of the piles, the far-field soil reactions are not expected to be significant. Only the near-field soil model is therefore used to represent the behavior of the soil inside the pile group. Since the soil surrounding the peripheral piles is connected to the free-field soil, it is represented by both near-field and far-field soil models. An example of the soil model for 3x3 pile group foundation is depicted in Figure 3.1. As shown in this figure, two patterns of soil models are used; (1) the inner soil among the piles in the group idealized by a near-field soil model and (2) the peripheral soil idealized by both near-field and far-field soil models. The near-field soil model shall be properly adjusted for the PSPI effects.

In a pile group foundation, the response of an individual pile which is situated closely enough to one another (i.e., less than 3 pile diameters for driven piles and 5 pile diameters for drilled shafts) is

likely to be influenced by the response and geometry of neighboring piles. The piles in a group interact with one another through the surrounding soil, resulting in so-called pile-soil-pile interaction or group effects (Sayed and Bakeer, 1992). Due to the pile-soil-pile interaction (PSPI) effects, the load-transfer characteristics that are used to model the near-field soil reactions for single pile models may not be directly applicable for modeling of soil reactions for pile group models. The PSPI effects are accounted for by using multiplier factors applied to the load-transfer curves of the individual piles. These multipliers effectively increase and decrease the stiffness (*z*- and *y*-multipliers) and strength (*t*- and *p*-multipliers) of the soil to which they are applied. The multiplier-factor method for modeling the PSPI effects in vertical and lateral soil reactions is discussed in brief here.

3.2.2.1 Vertical Soil Reactions on Piles

The PSPI effects may be divided into two components: (1) the installation effects and (2) the loading effects [O'Neill (1983)]. The installation effects tend to increase the stiffness and ultimate loading capacity of a pile group as compared to the summation of the stiffness and loading capacity of each individual pile in the group. However, the loading effects always reduce the stiffness and ultimate loading capacity of a pile group. A large amount of research has been contributed to evaluating and incorporating both components of the PSPI effects into modeling of the static and dynamic vertical soil reactions.

Several models (O'neill, et al., 1983; Poulos, 1980) have been developed for the analysis of pile foundations including the PSPI effects by using elastic half-space theory (the Mindlin theory [Mindlin (1936)]). These models have several shortcomings. For instance, they do not account for soil disturbance from pile installation effects or reinforcing effects of the existence of piles within the soil mass. They also do not realistically account for many aspects of the PSPI effects (e.g., pile-soil discontinuity effects and shadowing effects: the alteration of failure zone around an individual pile by the failure zones of neighboring piles). All these aspects cannot be easily or directly accounted for in theoretical methods of analysis. They can be however indirectly handled in semi-empirical or empirical manners based on field test data.

O'Neill, Ghazzaly and Ha (1977) have proposed an iterative "hybrid" method in which the individual pile response is modeled using load-transfer characteristics (*t-z* and *q-z* curves) and the PSPI effects are simulated using the Mindlin's solutions. The load-transfer curves for pile group

foundations adjusted to account for the PSPI effects can be obtained by properly stretching the load-transfer curves for single piles. The stretching procedure consists of (1) calculating elastic soil displacements at the depth of each *t-z* curve on each pile due to loading from every other pile in the group using the Mindlin's solutions, (2) adding these displacements to displacement (z value) on the load-transfer curve at the appropriate level of stress, and (3) multiplying the ratio of the resultant sum to the original z values to all z values on the load-transfer curves. Due to the fact that incorporating this concept is a laborious task and provided that there are several other uncertainties involved, this concept may not be suitable in practice.

In addition to the concept of using the iterative hybrid method, several analytical methods have been proposed to relate the behavior of a pile group to that of each individual pile in the group using the concept of efficiency of the pile group which is defined as the ratio of the actual capacity of the group to summation of the capacities of the individual piles in the group when considered as single piles. A number of vertical load tests on pile groups have been conducted to evaluate the efficiency factor of pile groups. Some of the experimental results are discussed as follows.

O'Neill (1983) reported that experimental results of field load tests on piles in loose sand indicating that efficiency of the pile group in compression usually exceeds unity with the highest values occurring at a spacing-to-diameter (s/d) ratio of 2. In dense sand, the efficiency may be however either greater or less than unity although the trend is toward greater than unity. The explanation of this phenomenon is that when the initial relative density of the sand is low (loose and medium sand), the sands surrounding the piles become compacted during driving (Broms, 1981), leading to the pile group efficiency of greater than unity. This pile installation effect rarely occurs for the case of pile groups driven in dense sand or clay.

Brand et al. (1972) conducted full-scale load tests on pile groups in Bangkok clay with different s/d ratios. The group efficiencies were reported to be slightly greater than unity for all cases (1.03-1.08). Barden and Monckton (1970) also conducted small-scale load tests on piles in square groups of 3x3 and 5x5 in clay. The piles were driven in soft and stiff clay. The results of their tests showed that the pile groups in the stiff clay were measured to be less than unity. For the 5x5 pile groups with s/d ratio of 2, the efficiency of the pile group was measured as 0.89 in the stiff clay and 0.69 in the soft clay.

Conventional practice for the analysis of pile groups in sand suggests the efficiency of pile groups of 1.0 for driven piles and 0.67 for bored piles (Coduto, 2001; Meyerhose, 1976). For pile

groups in clay, current practice suggests a value of pile group efficiency of 1.0 provided that block failure does not occur and sufficient time has elapsed between installation and the first application of loading to permit excess pore pressure to dissipate [Sayed and Bakeer (1992)].

Several efficiency formulae have been proposed by relating the group efficiency to the spacing between the piles using an elastic continuum soil model. They usually yield efficiency values of less than unity regardless of the pile-soil conditions. These formulae have been found to be deficient in many cases. As reported by many researchers, the values of group efficiency are usually greater than unity. The efficiency factor as much as 2.0 has been measured [Vesic (1975)].

Although there have been a large number of proposals for determination of the group efficiency, there has been none that is universally accepted. The incorporation of the PSPI effects especially the pile installation effects in response analysis of pile groups has not yet been made possible for all soil types or pile configurations.

In view of the above uncertainties, and until the analytical method in which the PSPI effects (especially pile installation effects) can be realistically accounted for is developed, the value of group efficiency as recommended by AASHTO will be used in subsequent studies. A group efficiency value of 1.0 is recommended for driven friction piles for all pile configurations and soil types except in cohesive soil. An efficiency factor of 0.7 is recommended for driven, friction piles in cohesive soil with s/d ratios less than 3. For drilled shafts in cohesive soils, the efficiency factor of 0.67 should be used for s/d ratio of 3, and 1.0 should be used for s/d ratio of 6. For drilled shafts in cohesionless soils, the efficiency factor of 0.67 should be used for s/d ratio of 3, and 1.0 should be used for s/d ratio of 8. The efficiency factor may be approximated by linear interpolation between these values.

The group efficiency factor actually serves as the *t*-multiplier factor to be applied to the *t-z* curves to account for the PSPI effects on the frictional resistance at the pile-soil interface along the pile. For the end-bearing resistance at the pile tip, the PSPI effect is less pronounced; therefore, the *q-z* curve at pile tip for a single pile model may be appropriately used for pile-group model. Not only does the *t*-multiplier factor reduce the ultimate soil resistances (t_{max}) but it also softens the stiffness of the load-transfer curves of each individual pile in a group.

3.2.2.2 Lateral Soil Reactions on Piles

Similar to the determination of vertical soil reactions for pile group models, the PSPI effects on lateral soil reactions have been estimated from theoretical methods using an elastic half-space theory. As previously discussed, these methods, however, do not consider many aspects of the PSPI such as the pile installation effects. Additionally, the linear elastic continuum methods cannot realistically account for the nonlinear behavior of the soil in the group. The PSPI effects are therefore usually overpredicted by using these elastic continuum solutions.

The subject of pile group effects for typical and extremely larger pile groups was extensively discussed by Lam and Kapuskar (1998). Several aspects of the PSPI summarized from a number of experimental studies have been presented by Brown et al. (1987, 1988), McVay et al. (1995), Rollin et al. (1997), and Ruesta and Townsend (1997). Some notable conclusions are briefly presented as follows:

1. The Reese and Matlock *p-y* criteria have been verified to provide reasonable solutions for response analysis of single piles.
2. It was concluded from reported full-scale or centrifuge model experiments that the PSPI effects cannot be accounted for by only softening the elastic stiffness of the *p-y* curves (i.e., applying only y-multipliers on *p-y* curves).
3. It was recommended by several researchers that the *p-y* curves for single piles should be modified by adjusting the resistance values using p-multipliers.

Due to the shadowing effects (i.e., leading piles are loaded more heavily than trailing piles when all are loaded to the same direction), the back-calculated values of p-multipliers for the front row piles were found to be higher than those for the trailing row piles. For cyclic loading conditions, the leading row piles will become the trailing row piles and vice versa when loading is reversed and thus the p-multipliers have to be adjusted accordingly. These changes of p-multipliers may be simplified using a uniform average multiplier to represent an average condition to fit the overall group effects.

Brown (1985) suggested the overall p-multiplier factor to be equal to 1.0 at a large pile spacing (s/d ratio > 8) and reduced to 0.5 for s/d ratio of 3. In addition, from back-fitting analyses of several experiment data, the uniform p-multiplier factor of approximately 0.5 is recommended for representing the overall behavior of typical pile groups (s/d ratio of 3). Furthermore, the results of more recent full-scale vibratory pile load tests reported by Lam and Cheang (1995) for submerged sands and by Crouse et al. (1993) for peat corroborated the implementation of a uniform average p-

multiplier of 0.5 to be applied on the standard static *p-y* curves for response analysis of typical pile group foundations.

The preceding discussion was mainly emphasized on the PSPI effects for typical pile group foundations consisting of 9-25 piles in a group. For extremely large pile groups which are usually used to support major river-crossing bridges, the pile-soil system resembles a reinforced soil mass and behaves dfferently from the typical pile groups. Lam and Law (1994) utilized a periodic boundary condition to solve for the pile response for an infinite repeating pile pattern. They found that for large pile groups having pile spacing to diameter ratio (s/d ratio) of less than 3, it is necessary to soften the elastic branch of the *p-y* curves by using a y-multiplier larger than unity in conjunction with the p-multiplier of 0.5. As observed from their study, the y-multiplier can be as large as 4 for the s/d ratio of 3. However, there exists no clear explanation on how the PSPI effects especially the pile installation effects are accounted for. In addition to the PSPI effects, for large pile group foundations, the scattering wave effects on the input motions (kinematic interaction effects) can also be more significant than typical pile group foundations. The kinematic interaction effect will be discussed in following studies.

3.2.2.3 Vertical and Lateral Soil Reactions on Pile Caps

In addition to a rational model of a component of soil resistance acting on a pile, a component of the soil resistance acting on a pile cap also needs to be properly modeled. Various research studies have been conducted to evaluate the component of soil resistance associated with the pile cap. Lam and Kapuskar (1998) summarized major conclusions and findings from several research programs and recommended procedures for incorporating the pile cap stiffness into the pile group. Such recommendations adopted in this study for modeling of pile group foundations are briefly reviewed.

The lateral soil resistance characteristics of the pile cap are derived from various components: (1) passive pressure acting on the front face, (2) side shears acting on two vertical side surfaces, and (3) base shear acting on the bottom face of the pile cap. Based on experimental results, it is found that most of the total resistance is contributed from the passive pressure acting on the front face of the pile cap. Since the component of the passive pressure soil resistance is most significant and since there is a potential interaction effect (e.g., soil-pile-cap discontinuity), it is recommended to ignore other components of soil resistance.

Although the passive pressure soil resistance acting on the pile cap should be regarded as a force capacity rather than stiffness, it can be used, with proper justification, to construct an elasto-perfectly-plastic load-deflection characteristic of the soil. The ultimate passive pressure capacity can be calculated using the classical earth pressure theories and the secant stiffness of the load-deformation curve can be estimated by the ratio of the ultimate capacity and the pile cap deflection at which the ultimate capacity is reached (approximately 1 to 2 inches based on centrifugal tests).

Several research studies have been devoted to determination of the value of the pile cap deflection at ultimate. Among these is the study conducted by Gadre (1997) showing that the deflection at ultimate is in the vicinity of 0.03-0.05 times the embedment depth. The embedment depth refers to the thickness of the pile cap that is embedded below the ground surface. However, the pile cap deflection at ultimate of about 0.02 times the embedment depth is recommended to be consistent with data from other wall-soil interaction experiments. The vertical soil resistance in this case is neglected from the assumption that all the vertical resistance is derived solely from the frictional resistance at the pile-soil interface and the end-bearing resistance at the pile tip.

3.3 Performance of the Proposed Pile Foundation Model for Small Pile Groups

The procedures used in examining the capability of the proposed pile-group model are quite similar to those used for the single pile model. The pile-group model will be tested for its capability to predict pile-group response to static and dynamic loading in both vertical and lateral directions through comparisons with experimental results from field tests in several case studies. Through these case studies, the static and dynamic PSPI effects on pile group response are closely examined. The parametric studies are performed in each case study to evaluate the effects of uncertainties of determining input parameters on response of pile group foundations.

To examine the effectiveness of the pile-group model in predicting the response of pile foundations to static and dynamic vertical load, experimental results of static and dynamic load tests on a 3x3 full-scale pile group conducted by Blaney et al. (1987) are used in Case Study 1. In investigating the performance of the proposed pile-group model in estimating the static and dynamic response of pile groups to lateral loading, experimental results from two load tests on pile groups (one static and one dynamic loading) are used. Results of static lateral load tests on a 3x4 pile group foundation conducted by Stevens et al. (1979) are used in Case Study 2. The dynamic test on

a full-scale 3x3 pile group subjected to harmonic lateral loading conducted by Blaney and O'Neill (1986, 1989) is used in Case Study 3.

3.3.1 Case Study 1: Response of a Full-Scale 3x3 Pile Group to Static and Dynamic Vertical Loads

Blaney et al. (1987) conducted a vertical vibration test of a full-scale group of nine steel pipe piles and an isolated pile driven into overconsolidated clay. Prior to the dynamic test, this pile group was tested statically to failure by O'Neill et al. (1982). The test setup and pile layout are shown in Figure 3.5(a) for the isolated pile and in Figure 3.5(b) for the pile group. The pile group consisted of nine steel pipe piles arranged in form of a square 3x3 matrix with the s/d ratio of 3. Each pile has an outside diameter of 0.273 m and a wall thickness of 9.4 mm. The piles were driven closed-ended to a penetration of 13.1 m and tested statically to failure in compression. Following the static test and prior to the dynamic tests, the piles were redriven to a final penetration of 13.4 m in order to reestablish the stress conditions in the soil that would have existed had the piles not been tested statically. Geotechnical descriptions of this site soils are given in Case Study 2 for a single pile subjected to dynamic lateral loads.

The 9-pile group and the isolated pile were rigidly capped with massive concrete caps whose bases were approximately 0.81 m above the ground surface as shown in Figure 3.5. The weight of the group cap and isolated-pile cap was 249.4 kN and 55.3 kN, respectively. There occurred 0.10-m-deep visible gaps around the piles resulting from pile installation. The ground surface used in the analytical model is thus taken at 0.10 m below the actual ground surface. The pile group was dynamically loaded by consecutive 30-second downsweeps from 95 Hz to 50 Hz and from 50 Hz to 5 Hz. The amplitude of the applied load was maintained constant equal to 71.2 kN over the full range of frequencies during each sweep. The isolated pile was subjected to a 30-second downsweep for 50 Hz to 5 Hz with the loading amplitude of 17.8 kN. The Fourier transform techniques were used to interpret the system response.

The response analysis of the isolated pile subjected to static and dynamic loads was first performed and followed by the response analysis of the pile group to investigate the effects of soil mass included in the near-field soil model, the far-field soil reaction model as well as the PSPI effects. The PSPI effects are accounted for by using the *t*-multiplier of 0.7 as recommended by AASHTO for driven piles in cohesive soil with the s/d ratio of 3.

Effects of far-field soil reactions

A comparison study is conducted to evaluate the effects of far-field soil reactions or radiation damping on the dynamic response of both the isolated pile and pile group. Plotted against the measured curves in Figures 3.6(a) and 3.6(b) are the dynamic response of the isolated pile and the pile group computed from the model with and without the far-field soil model. It can be observed that the measured frequency response curve of the pile group contains two resonant peaks (10 Hz and 68 Hz). The first resonant frequency is associated with a rocking mode due to irregularities in the geometry of the piles and in the location of the vibrator. The second peak is primarily associated with the vertical mode of vibration. The irregularities are not considered in the analytical model, thus only one resonant peak is obtained; 43 Hz and 50 Hz associated with the vertical mode of vibration from the model with and without the far-field soil model, respectively.

The difference between the computed response from the model with and without the far-field soil model is observed to be more significant for the pile group than for the isolated pile. The effect of including the far-field soil model is evidently much more pronounced for the response of the pile group. This is mainly because the loading amplitude is much smaller; therefore, the soil nonlinearity is expected to be insignificant, and the effects of radiation damping become highly influential to the response of the pile group. In addition, the loading frequency of the pile group (the resonant frequency at about 43 Hz and 50 Hz) is so high that the effects of the radiation damping or far-field soil models are believed to be of great consequence, and thus larger discrepancies between the responses computed from the model with and without the far-field soil model is anticipated for the pile group than for the isolated pile.

A significant difference between the measured response and the computed response for the model without the far-field soil model is noted. The effects of far-field soil models or radiation damping properties of the soil appear to play an important role in predicting the pile group response. It is observed that, by including the far-field soil model, the predicted response is in better agreement with the measured response. In addition to the effects of far-field soil models, the large difference may be attributed to the irregularities that existed during the test and were not accounted for in the analytical model. Furthermore, it is important to note that this pile group was tested full scaled under in-situ conditions and under such a high-frequency and low-amplitude loading condition. This testing and loading condition should be clearly kept in mind when comparing predictions with the measurements.

Although the difference between the measured and computed response of the pile group is notable, the predicted response over the range of frequency between 0.1 to 10 Hz, which is a typical range for earthquake loading, seems reasonable and representative. The computed responses agree better with the measured response at lower frequency (less than 25 Hz). It is also shown that the responses computed from the model with and without the far-field soil model over such frequency range are comparable. Therefore, for the range of frequency that is of interest in this study (less than 10 Hz), the presented pile group model can be used.

Effects of soil mass for near-field soil model

The effects of soil mass on the dynamic response of the pile and pile group foundation to vertical vibration are investigated. Three different sizes of cylindrical soil mass $r_1 = 1.0r_0$ (no mass), $2.0r_0$ and $3.0r_0$: r_0 = pile diameter) are considered. The computed dynamic response of the pile group for different sizes of soil mass are shown in Figure 3.7. These responses are computed for the modal damping of 5% and only the near-field soil model is used for this comparison. Similar to the conclusion obtained from the previous study on the response of the single piles, the effect of soil mass on the dynamic response of pile groups is insignificant. The comparison of dynamic response of the isolated pile, although not presented herein, leads to a similar conclusion. The size of cylindrical soil mass is set equal to $r_1 = 2.0r_0$ in the following study.

Effects of pile-soil-pile interaction

The PSPI effects are also investigated through a comparison study. The static and dynamic responses of the pile group to vertical loading are computed from the model with and without the modification for the PSPI effects are compared with the measured response as shown in Figure 3.8. The *t*-multiplier of 0.7 for the cohesive soil condition and the s/d ratio equal to 3 is used to account for the PSPI effects. It is observed from Figure 3.8(a) that the ultimate pile capacity reduces about 30%, which is anticipated from applying the *t*-multiplier of 0.7. For the dynamic loading case (Figure 3.8(b)) the PSPI is not as significant. In fact, the resonant frequency remains roughly the same and the resonant amplitude increases only by 5% as the PSPI effect is considered.

A small increase in the resonant amplitude is expected from a slight decrease in the initial stiffness of the load-transfer curves due to the application of *t*-multiplier. In addition, since the loading amplitude is so small that the soil nonlinearity is insignificant, the effect of hysteretic

damping is inconsequential. Therefore, the PSPI effects in this case study tend to increase the resonant amplitude due to the stiffness-softening effects rather than decrease it due to the hysteretic damping effects.

3.3.2 Case Study 2: Response of a 3x4 Pile Group to Static Lateral Loads

As a part of an extensive pile-testing program, Stevens et al. (1979) conducted static lateral load tests on a 12-pile group in addition to a static load test on a single timber pile which was used previously in the case study in Chapter 2. The load testing procedures and site characteristics were presented in Case Study 2 for a single pile subjected to static vertical loading. Only additional information to that previously presented is given in brief here. The load test setup and pile group configurations are shown in Figure 3.9.

A center-to-center pile spacing of 0.915 m (s/d ratio of 3) was used. After the piles were driven to a depth of about 10.68 m. They were cut off leaving 1.50 m extending above the ground. A 1.83-m-thick reinforced concrete cap was then cast 0.915 m off the ground, embedding the piles 0.61 m into the concrete. This embedding length of the piles into the cap is quite sufficient to develop a full fixity condition for the pile-to-pile-cap connection. The purpose of the ground clearance was intended to eliminate the soil-cap interaction effects and to facilitate load-transfer interpretation; all loads applied to the cap were resisted by the piles only.

The lateral load capacity of the 12-pile group was measured under combined axial and lateral loads. In the combined load tests, an axial load of 267 kN/pile was first applied to the pile groups and maintained constant during the test. The lateral load was then applied in increments at the center of the pile cap until failure occurred. The PSPI effect is accounted for by applying p-multiplier of 0.5 to the lateral load-transfer of the single pile.

Effects of pile-soil-pile interaction

The PSPI effects on the static response of the pile group are evaluated. In addition to the uniform average p-multiplier of 0.5, the varying p-multipliers according to the location of the piles due to the shadowing effects are used. Table 3.5 summarizes some of the back-calculated p-multiplier values from experiments conducted on 3x3 pile groups having the s/d ratio of 3. Additionally, Ruesta and Townsend (1997) reported experimental results of a full-scale test of a 4x4 pile group in loose sand. The concrete piles having a 0.762-m (30-in) square cross section were

rigidly clamped into the reinforced concrete pile cap. From back-fitting analyses, the p-multipliers of 0.8, 0.7, 0.3 and 0.3 are obtained for row 1 (front row) to row 4 (trailing row), respectively. These p-multipliers are adopted in the comparison study and they are applied to the pile group as shown in Figure 3.10.

Table 3.5. Back-Calculated p-Multipliers from Various Experiments [after Lam and Kapuskar (1998)].

Pile test, soil description and reference	p-multiplier on *p-y* curve of a single pile		
	Front row	Middle row	Back row
Free-head, medium dense sand, D_r = 50% Brown et al. (1988)	0.8	0.4	0.3
Fixed-head, medium dense sand, D_r = 55% McVay Centrifuge (1995)	0.8	0.45	0.3
Fixed-head, medium dense sand, D_r = 33% McVay Centrifuge (1995)	0.65	0.45	0.35
Free-head, soft to medium clays and silts Rollins et al. (1997)	0.6	0.38	0.43

The computed load-displacement curves are plotted against the measured curve in Figure 3.11(a). It is observed that the static behavior of the pile group to lateral load is fairly different from that of the vertical load. The ultimate vertical capacity of the piles pile groups is governed mainly by the ultimate soil resistance (i.e., the pile moves as a rigid body) whereas the ultimate lateral capacity is governed by the soil capacity for short piles and the pile capacity for long piles. Adopted herein is the criteria suggested by Broms (1964) stating that to be considered as a long pile, the pile length must be greater or equal to 4 times the relative stiffness factor (*T* or *R*) defined below.

For subgrade modulus increasing with depth,

$$T = \left(\frac{E_p I_p}{k_{\text{sec}}} \right)^{0.20} . \qquad [3.1]$$

For subgrade modulus constant with depth,

[3.1] $$R = \left(\frac{E_p I_p}{k_{con}} \right)^{0.25} .$$

where

E_p = modulus of elasticity of pile material,

I_p = moment of inertia of pile section,

k_{sec} = coefficient of secant subgrade reaction (F/L^3),

k_{con} = constant subgrade reaction (F/L^2),

The piles used in this test can be specified as long piles, and it can be shown that the ultimate lateral capacity of the pile group (Figure 3.11(a)) is controlled by the moment capacity of the piles. Consequently, for the static response of the pile group to lateral load, the PSPI effects are to primarily soften the stiffness rather than reduce the ultimate capacity (i.e., the ultimate load capacity decreases by less than 15% in spite of the fact that the ultimate soil reaction has been reduced by 50% due to the application of the p-multiplier value of 0.5). On the contrary, for the response of the pile group to vertical load, the PSPI effects tend to not only soften the stiffness but also reduce the ultimate capacity. Note that the difference between the load-deflection curve obtained from the model having the uniform p-multiplier and that from the model having varying *p*-multipliers is nearly invisible.

The ultimate load capacity of the pile group is defined as the load at which the bending moment capacity of the pile is reached. In this case study, the bending moment capacity of the pile is approximately equal to 213 kN-m corresponding to the compressive strength of 48.3 MPa for wooden piles having a diameter of 0.356 m. In consideration of the strength of the material, the ultimate load capacity of the pile group is equal to 1,600 kN and 1,800 kN for the model with and without the PSPI effect, respectively. In consideration of the serviceability or differential displacement that may cause failure to adjacent structural members, the displacement criterion of about 40-50 mm (1.5-2 in) is typically used to define the maximum load capacity. For this studied pile group, the displacement criterion is reached first and therefore, the maximum load capacity is approximately 850 kN and 1100 kN for the model with and without the PSPI, respectively.

To be consistent for all comparisons, the bending moment profiles of four center piles (one for each row) computed at the load amplitude of 1500 kN are plotted in Figures 3.11(b), 3.11(c) and 3.11(d). It is observed from Figures 3.11(b) and 3.11(c) that the moment profiles for all center piles

of each row are virtually identical. In case of the varying-*p*-multiplier model, the moment profile varies corresponding to the *p*-multiplier. The maximum bending moment occurs at the pile in the front row to which the *p*-multiplier value of 0.8 is applied. It is evident from Figure 3.12 that the moment profile of each pile obtained from the model having a uniform *p*-multiplier is somewhat comparable to that from the model having varying *p*-multiplier. The difference between the maximum moments at the pile-to-pile-cap interface is smaller than 15% for all cases.

Not only was the effect of varying *p*-multipliers found insignificant on the load-displacement relationship of the pile group, but also it was not highly influential to the moment distribution along the pile. The uniform *p*-multiplier of 0.5 was demonstrated to give a reasonable overall pile group response as well as a satisfactory response of each individual pile in the group. The *p*-multiplier of 0.5 is therefore adopted to be applied to all piles in a group.

3.3.3 Case Study 3: Response of a Full-Scale 3x3 Pile Group to Dynamic Lateral Loads

A series of vertical and lateral, static and dynamic load tests were conducted on a full-scale 3x3 pile group by O'Neill and his colleagues. In this pile-testing program, the piles were first driven closed-ended to a depth of 13.1 m into a layered deposit of overconsolidated clay and were statically tested to failure in vertical direction [O'Neill et al. (1982)]. The same group of piles was redriven to a penetration of 13.4 and tested dynamically in vertical direction as described in Case Study 1 for dynamic response of a pile group to vertical loading [Blaney, Mahar and O'Neill (1987)]. About 2 years later, the very same pile group was driven to a depth of 13.7 m. and tested dynamically in the lateral direction (Figure 3.13). The results of this full-scale dynamic field tests conducted on the group of 9 instrumented steel pipe piles rigidly clamped into the concrete mass were reported by Blaney and O'Neill (1989).

The geotechnical conditions and pile test setup are basically identical to the previous case study and are not repeated. Details of the loading procedures are discussed in brief here. Vibratory loads were applied to the pile cap at several load levels (17.79 kN, 35.58 kN and 1.78 kN) to determine the horizontal fundamental frequency, the dynamic stiffness of the system and the distribution of horizontal pile-soil relative motion with depth. Harmonic downsweep loads having 30 seconds in duration were applied to the pile groups. The frequency of each sweep load varies from 50 Hz to 2 Hz at a constant rate of frequency change. Such loading frequencies were in the range of frequencies of interest for seismic or machine loading. The load amplitude remained nearly

constant during each sweep. A downsweep of approximately 17.79-kN load amplitude was first applied and the load amplitude was next increased to 35.58 kN, then reduced to 1.78 kN for the final test.

The horizontal response amplitudes per unit horizontal force input were obtained at the centerline of the pile cap, 1.50 m above the ground surface for nominal load amplitudes of 1.78 kN, 17.79 kN and 35.58 kN. The peak amplitude of the frequency response function varies roughly from 0.103 mm/kN to 0.107 mm/kN as the load amplitude was decreased from 35.58 kN to 1.78 kN. The maximum horizontal displacement amplitude of about 3.8 mm is observed for the largest load amplitude test (35.6 kN).

Effects of soil mass for near-field soil model

The effects of soil mass on the dynamic response of the pile group to lateral vibration are investigated. The dynamic responses of the pile group computed from the model with different sizes of cylindrical soil mass ($r_1 = 1.0r_0$ (no mass), $2.0r_0$ and $3.0r_0$: r_0 = pile diameter) are plotted against the measured response in Figure 3.14. This comparison indicates that the effect of different sizes of soil mass is inconsequential to the dynamic response of the pile group. The size of cylindrical soil mass is set equal to $r_1 = 2.0r_0$ in the following study.

Effects of far-field soil reactions

Figures 3.15(a) and 3.15(b) show the comparison between the measured and computed dynamic response and computed moment profile from the model with and without the far-field soil model. The responses are evaluated for the modal damping ratio of 5% and for the highest load amplitude of 35.58 kN. The overall behavior of the pile group (resonant frequency and amplitude) is captured by the proposed model quite adequately. The radiation damping evidently has little influence on the resonant amplitude. The radiation damping effect for this loading case is much less significant than that for the vertical-dynamic loading case. This is basically because the frequency range of loading is lower and because the loading amplitude is quite large for this test. The soil nonlinearity associated with this high amplitude of loading has apparently lessened the effects of radiation damping.

The difference between the moment profiles computed from both models is small, the maximum bending moment computed from the model with far-field soil model appears to be slightly less than that computed from the model without the far-field soil model. This can be explained by the effects

of both of the radiation damping and hysteretic damping due to the soil nonlinearity. The smaller resonant amplitude or displacement leads to the smaller maximum moment.

Effects of pile-soil-pile interaction

The PSPI effects on the dynamic response of the pile group to lateral vibration are also evaluated. The dynamic response and the moment profiles at resonance computed from the model with and without the incorporation of the PSPI effects are plotted in Figure 3.16. The difference between the response curves is evident. The resonant frequency remains pretty much the same but the resonant amplitude decreases by approximately 20% due to the PSPI effects. The comparison of the moment profiles also reveals that the maximum positive and negative moments are reduced by about 20% for the model in which the PSPI effect is considered.

These comparison results are contrary to the previous findings on the PSPI effects on the pile group response to static loading (i.e., the PSPI effects result in larger displacements and maximum moment experienced by the piles at the same load level.). An engineering instinct would first suggest that there must be something suspicious about the pile group model. After a due consideration of all parameters affecting the dynamic behavior of the structure, it is concluded that the computed dynamic response of the pile group is indeed reasonable. A rational explanation for such behavior is due to the effects of hysteretic damping. The soil nonlinearity is more significant for the PSPI model thus resulting in the higher hysteretic (material) damping and smaller displacement amplitude and maximum moment.

In contrast of the general belief, the PSPI effects are likely to be positive rather than negative to the response of the studied pile group to the dynamic loads. However, this conclusion may not be valid for a pile foundation supporting a heavy structure because the stiffness-softening and ultimate-capacity-reduction effects due to the PSPI may become significant and may actually govern the overall response of the system.

3.4 Performance of the Proposed Pile Foundation Model for an Existing Pile Group

The preceding work has been devoted to the performance evaluation of the proposed pile group model in predicting the static and dynamic response of the pile groups consisting of 12 piles or fewer. These pile groups qualify to be categorized as the small pile group foundations. The capability of the proposed model in estimating the response of the typical 25-pile group is also

investigated in the following study. The pile foundation of an existing two-span bridge is used in this investigation. The results computed from the proposed model are compared with the experimental results as well as the analytical results presented by other researchers.

3.4.1 Case Study 4: Response of the pile foundation of the Meloland Road Overcrossing

The Meloland Road Overcrossing (MRO) is a continuous two-span (each 31.7 m long) reinforced concrete box girder bridge located within 400 m of the Imperial Fault near EI Centro, California. The bridge elevation is shown in Figure 3.17. This bridge was instrumented in November 1978. Since then, the MRO bridge has been subjected to several earthquakes, one of which is the 1979 Imperial Valley earthquake having magnitude of 6.8 and peak acceleration of 0.3g in the far-field and 0.5g on the deck. The bridge was however undamaged during this earthquake. A number of system identification studies have been performed using these recorded motions. Among these studies were a series of studies performed by Werner et al. (1993) to identify the model parameters such as the abutment spring stiffness, the embankment stiffness and the foundation stiffness at the base of central pier.

In addition to the recorded motions of the MRO bridge during earthquakes, the recorded response during a full-scale, quick-release static and dynamic field tests of the MRO bridge conducted by Douglas et al. in 1988 was also used in the system identification study. Complete details of the test procedures and test results are provided by Douglas et al. (1990). The system identification study using the field test response was conducted and reported by Douglas et al. (1991). In their study, the finite element model of the bridge was used to identify the structural parameters (e.g., modal period and damping ratio) as well as the spring stiffness at the abutments and the central pier foundation. More recently, Crouse (1992) also performed the system identification study based on the field test results.

Additionally, an analytical finite element model of the foundation of the central pier was developed by Maragakis et al. (1994) to determine the vertical, lateral and rotational foundation stiffness. The equivalent linear iterative procedure was employed in the FE method of analysis to simulate the nonlinear behavior of the material. Besides the FE modeling approach, the beam-on-elastic-foundation (*p-y* curves) approach was applied to determine the lateral and rotational stiffness

of the foundation by Norris (1987). The foundation stiffness values predicted by all these investigators are compared with those predicted using the proposed pile group model.

Descriptions of the foundation and geotechnical conditions

The foundation supporting the central pier of the MRO bridge consists of 25 tapered timber piles having a diameter equal to 0.32 m at the pile cap and 0.20 m at the pile tip. The piles are equally spaced as a square grid at 0.92 m center-to-center (i.e., the s/d ratio equals to 3). The piles were driven to a final penetration of 12.5 m below the reinforced concrete pile cap which is embedded 0.60 m below the ground surface. The piles are embedded into the pile cap for only 0.075 m. This small embedment length qualifies the pile-to-pile-cap connection to be treated as the pinned connection. The modulus of elasticity of the timber piles is equal to 12,410 MPa (1.8×10^6 psi). The soil conditions at the MRO site are predominantly a medium-stiff to stiff clay with a trace of silt and sand. The soil profile and the exploratory test results are shown in Figure 3.18, which was taken from the soil description given by Norris (1987). The *t*-multiple is set equal to 0.7 and the *p*-multiplier is set to 0.5 to account for the PSPI effects.

Comparison study

The responses of the pile group to vertical, lateral and moment loading (as shown in Figure 3.19(a)) are plotted in Figures 3.19(b), 3.19(c) and 3.19(d). These responses are computed from the model with and without the multipliers for the PSPI effects. The initial tangent stiffness and the secant stiffness at ultimate of each response curve are listed in Column 1 of Table 3-6. The values in parenthesis are calculated from the response curves obtained from the model with the PSPI effects. Also presented in Table 3-6 are the foundation spring stiffness values for the central pier predicted by other investigators. The stiffness coefficients obtained from the study by Maragakis et al. (1994) in which the finite element approach is used are listed in Column 2. Column 3 lists the stiffness coefficients predicted by Douglas et al. (1991) based on the system identification study using results from the full-scale, quick-release tests. The response data of the quick release tests were also analyzed by Crouse et al. (1987) and Crouse (1992) to estimate the pile foundation stiffness. The results are listed in Column 4. Norris and his colleagues (1986-1989) also computed the lateral and rotational stiffness of this foundation under liquefied soil condition using an equivalent linear procedure based on beam-on-elastic-foundation (*p*-*y* curve) approach. These values are presented in Column 5.

Table 3.6. Stiffness Coefficients of the Foundation Supporting the Central Pier of the MRO Bridge.

Spring	Stiffness Coefficients				
	(1) Present	(2) Maragakis	(3) Douglas	(4) Crouse	(5) Norris
$K_{vertical}$ (kN/m) x10^6	1.431-3.897 (1.081-3.867)	1.458	1.896	2.625-2.917	-
$K_{lateral}$ (kN/m) x10^6	0.210-1.125 (0.189-1.122)	1.006	0.875	0.613-1.356	0.904
$K_{rotational}$ (kN-m) x10^6	4.658-5.828 (4.431-5.821)	5.698	6.512	3.934-12.21	0.373-1.695

The foundation stiffness coefficients predicted using the proposed pile-group model agree reasonably well with those predicted by other researches. For the vertical loading case, the ultimate load capacity, which is defined as the load at which the displacement criterion of 10 mm (0.4 in) is reached, is approximately equal to 12,000 kN and 15,000 kN for the model with and without the PSPI, respectively. For the lateral loading case, the ultimate load capacity, which is defined as the load at which the bending moment capacity of the piles is reached, is equal to 8,500 kN for the PSPI model and 10,000 kN for the no-PSPI model. The ultimate moment capacity of the pile group is defined as the moment at which either the ultimate vertical load capacity of an individual pile or the ultimate bending moment capacity of the pile is reached. In this case the ultimate vertical load capacity of the pile is reached first, thus resulting in the ultimate moment capacity roughly equal to 15,000 kN-m for both models.

3.5 Concluding Remarks

Through all these case studies, the capability of the proposed pile-group model in predicting the overall response of the pile group foundation as well as the response of each individual pile in a group is verified to be satisfactory. The proposed model is able to capture the response of the pile group reasonably well, especially for the static loading case. For the dynamic loading case, the effectiveness of the proposed model in predicting the response of the pile group to both vertical and

lateral vibration is also found to be acceptable especially for a low-frequency loading range of between 0.1 to 10 Hz. This is actually the range of frequencies for earthquake loading, which is of particular interest in this study.

The results of parametric study indicate that, for the range of loading frequency that is of interest, the dynamic response of the pile group is insensitive to the far-field soil model. In other words, whether or not the far-field soil model is included in the pile group model does not significantly affect the dynamic response of the pile group to earthquake loading. Therefore, the overall characteristics of the soils surrounding the piles can be sufficiently represented using only the near-field soil model.

The effects of applying the uniform *p*-multiplier to account for the PSPI effects on the pile group response to lateral loads are also investigated through the comparison study. The study reveals a slight difference between the pile group responses obtained from the model having the uniform *p*-multiplier and those from the model having varying *p*-multipliers. The load-deformation curve of the pile group is found to be insensitive to whether the uniform or varying *p*-multiplier is used. The responses of each individual pile in forms of the moment distribution along the pile obtained from those two models appear to be fairly comparable as well. Therefore, the uniform *p*-multiplier can be properly used to simulate the PSPI in modeling of the pile group foundations.

In conclusion, the capability of the proposed pile group model in capturing the behavior of the pile foundations subjected to both static and dynamic loading is justified. As a result, this proposed model shall be used in modeling the pile foundations to be attached to the superstructure model of the bridge. The seismic performance evaluation of the entire pile-supported bridge can then be performed and the response of the bridge superstructure as well as its pile foundations can be obtained all in one analysis.

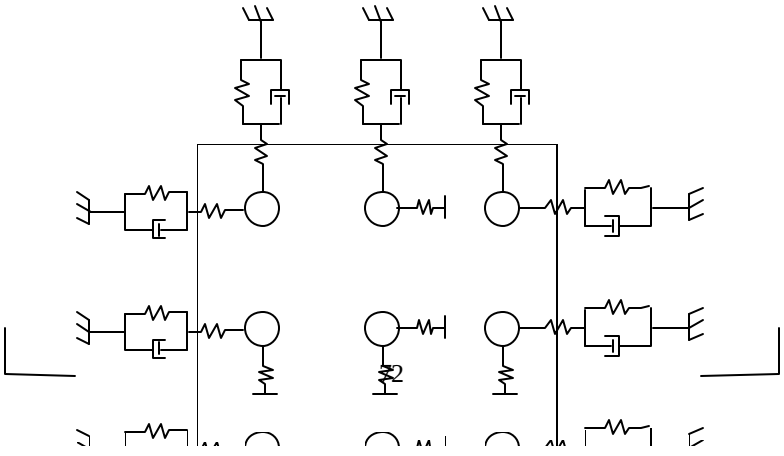

Figure 3.1. Proposed Pile Foundation Model.

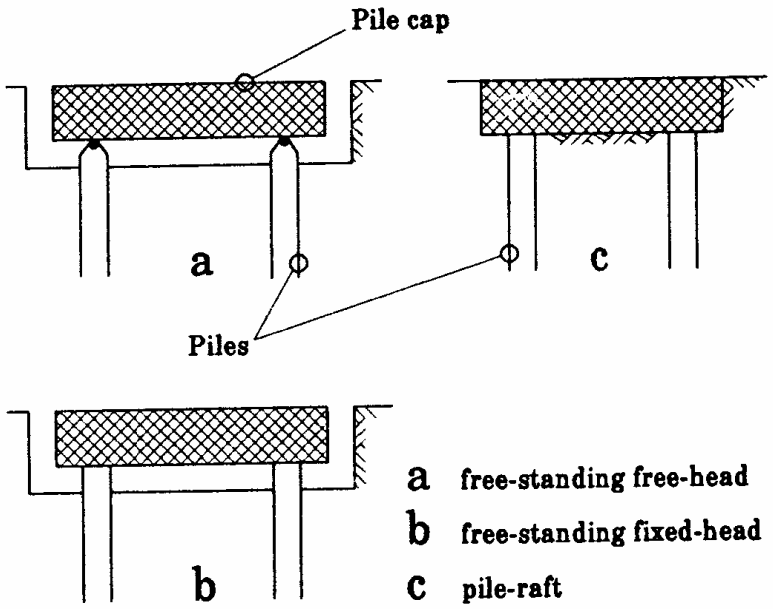

Figure 3.2. Various Pile Group Configurations [after Pender (1993)].

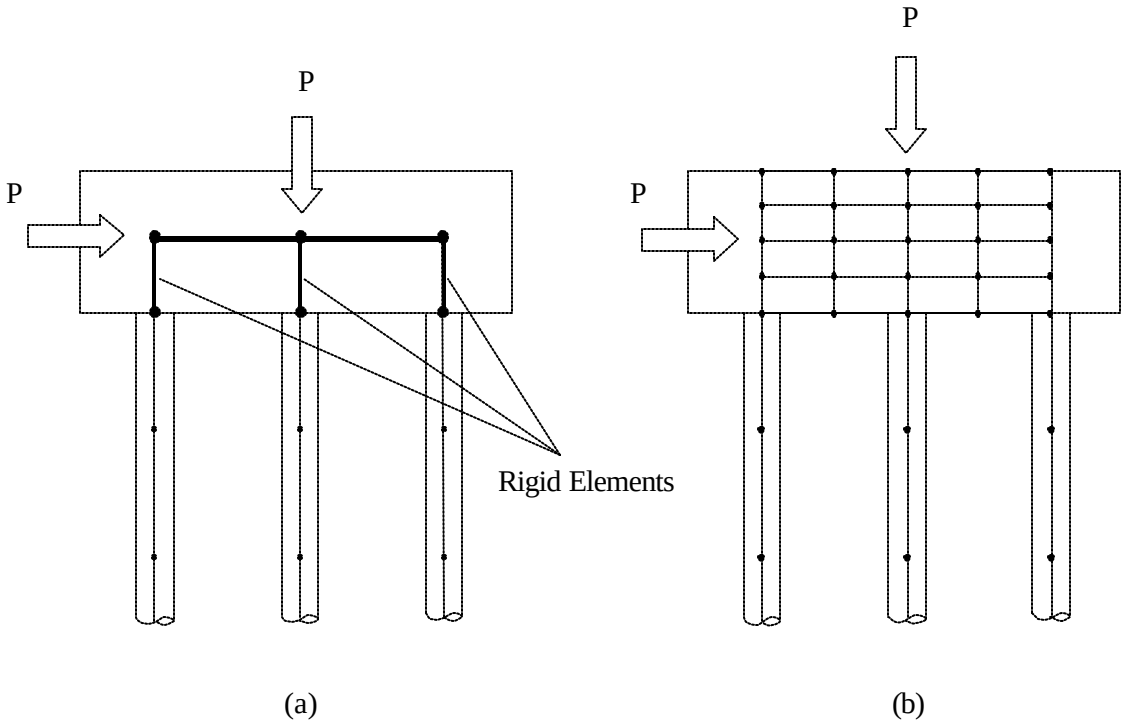

Figure 3.3. Different Schematic Models of Pile Cap: (a) 2-D Shell Elements, and (b) 2-D Solid Elements.

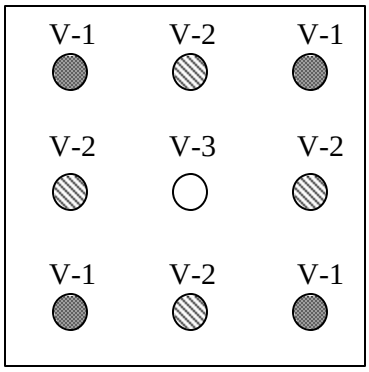

(a) Vertical Layout

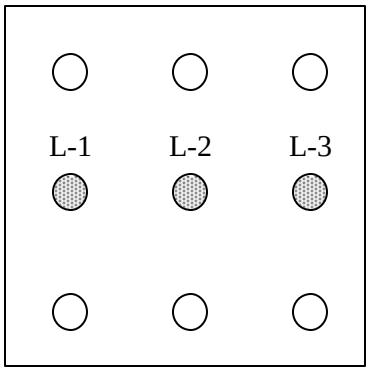

(b) Lateral Layout

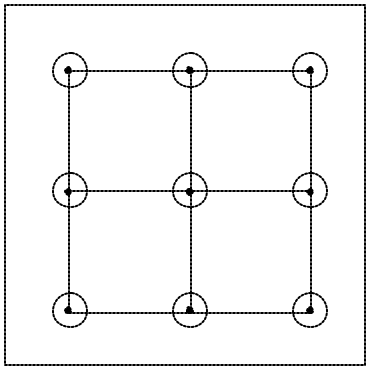

(c) 2x2 FE Mesh

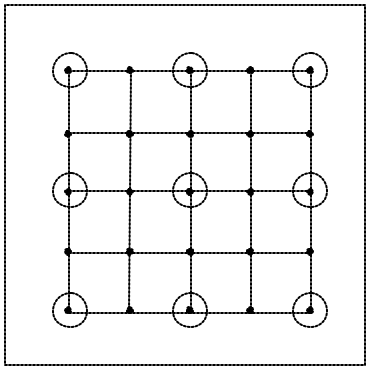

(d) 4x4 FE Mesh

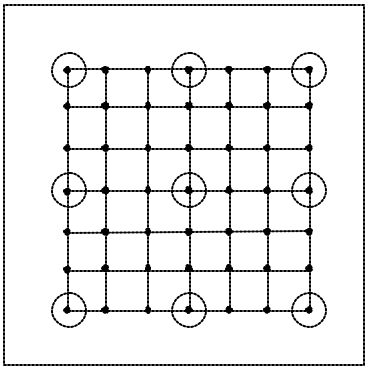

(e) 6x6 FE Mesh

Figure 3.4. Different Patterns of Finite Element Mesh.

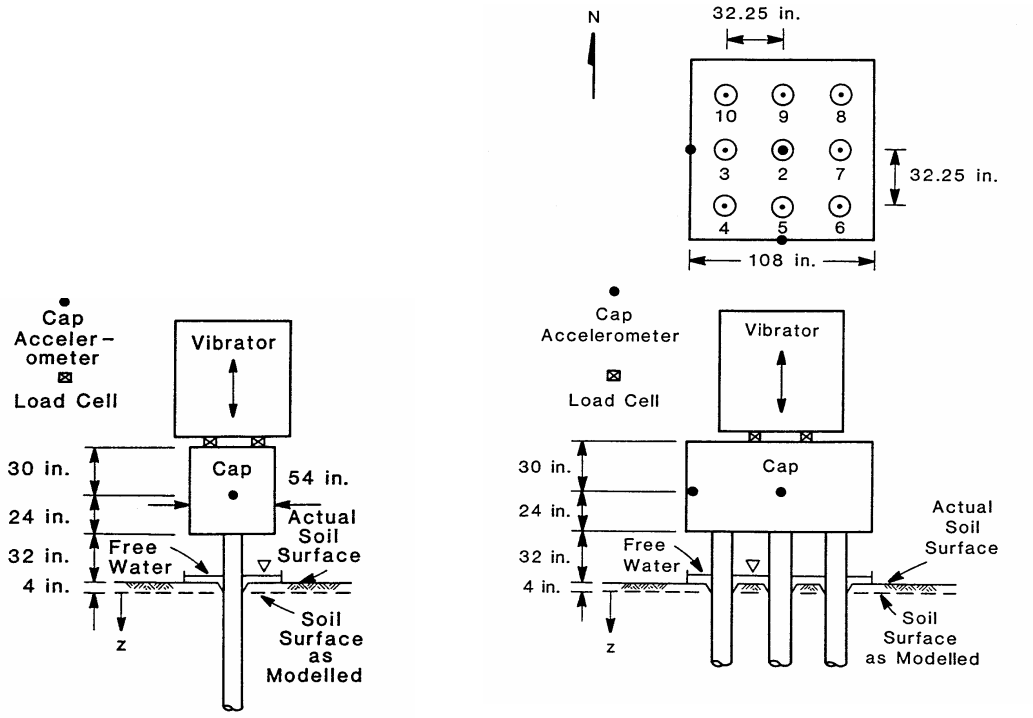

(a) Isolated Pile (b) Pile Group

Figure 3.5. Test Setup and Pile Layout for (a) Isolated Pile and (b) Pile Group for Case Study 1 [after Blaney et al. (1987)].

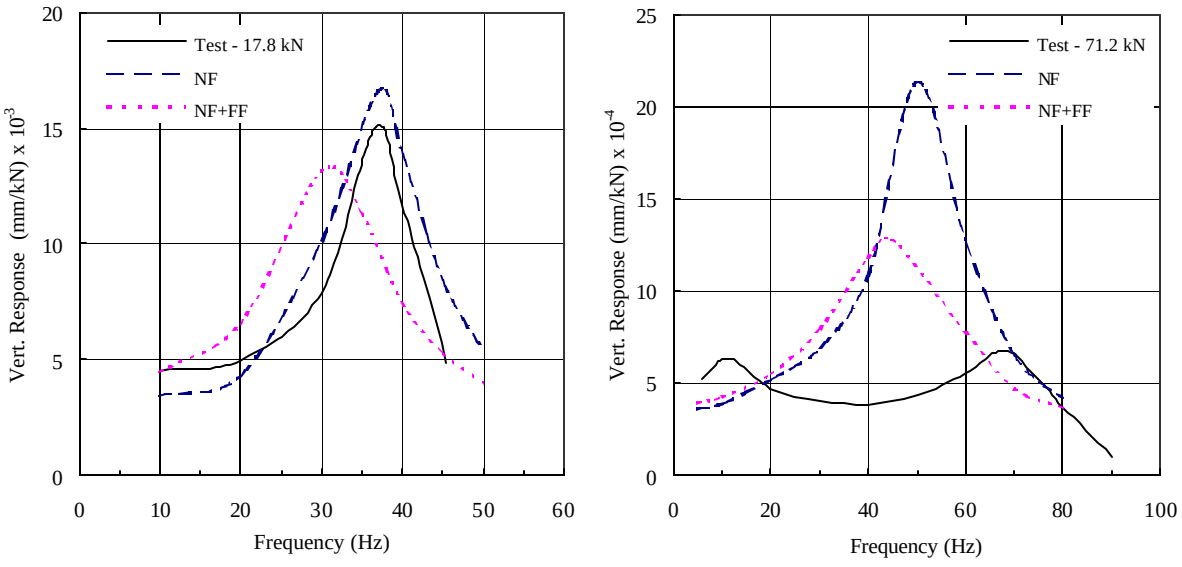

(a) Isolated Pile (b) Pile Group

Figure 3.6. Dynamic Response Curves of (a) Isolated Pile, and (b) Pile Group Computed from Models with and without Far-Field Soil Models.

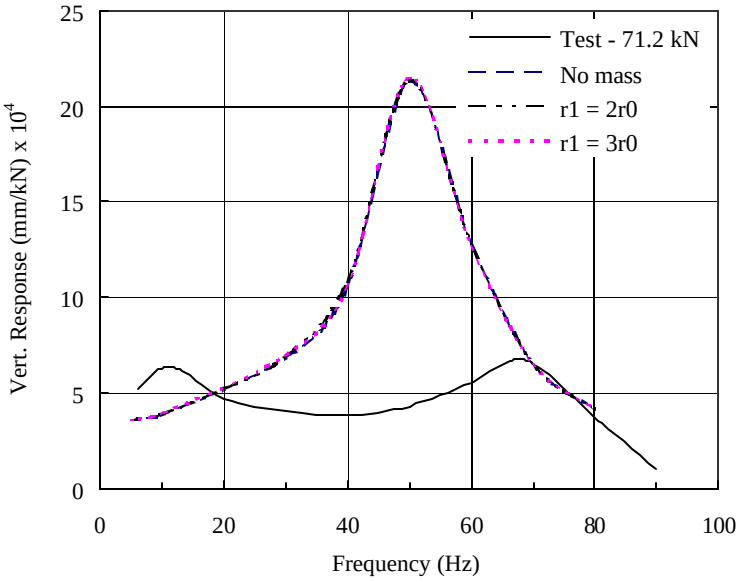

Figure 3.7. Dynamic Response Curves for Different Sizes of Soil Mass.

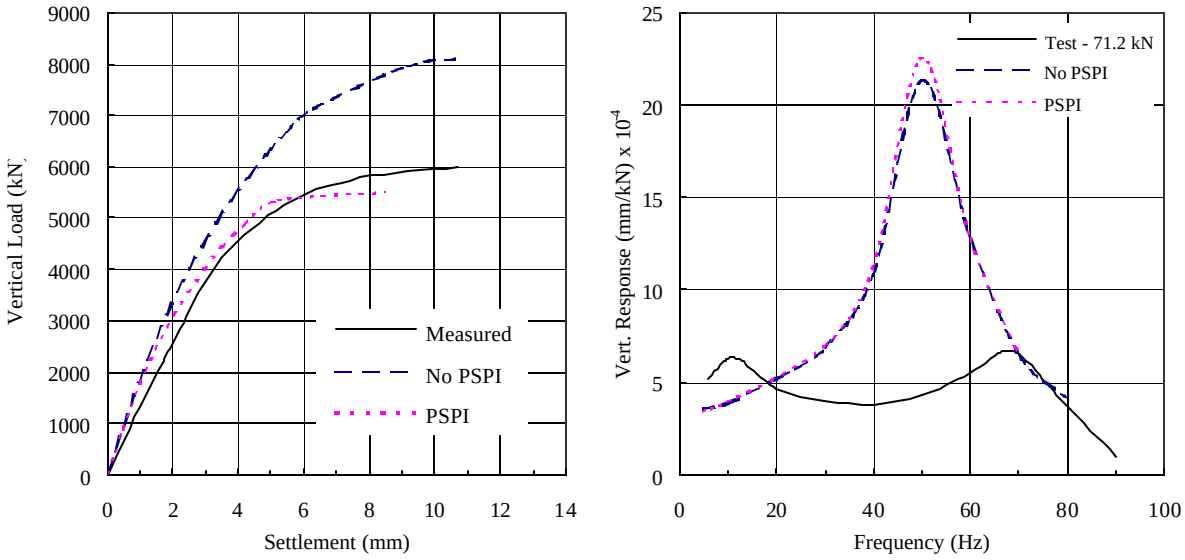

(a) Static response (b) Dynamic response

Figure 3.8. Effects of PSPI on (a) Static and (b) Dynamic Response Curves of the Pile Group.

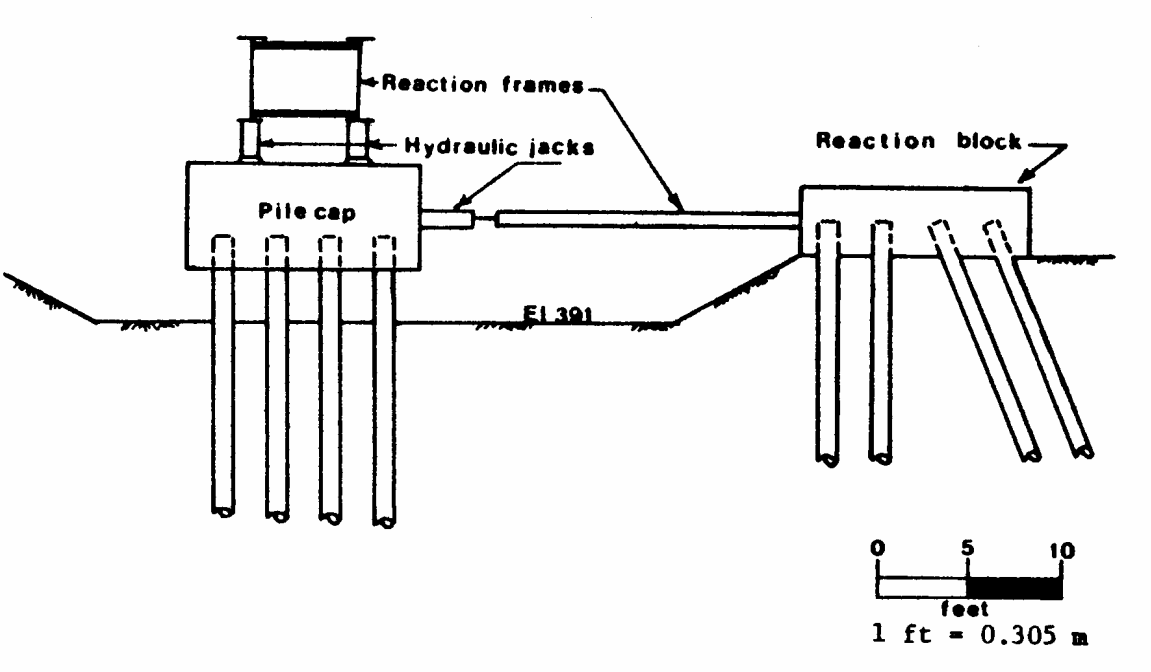

Figure 3.9. Load Test Setup for Case Study 2 [after Stevens et al. (1979)].

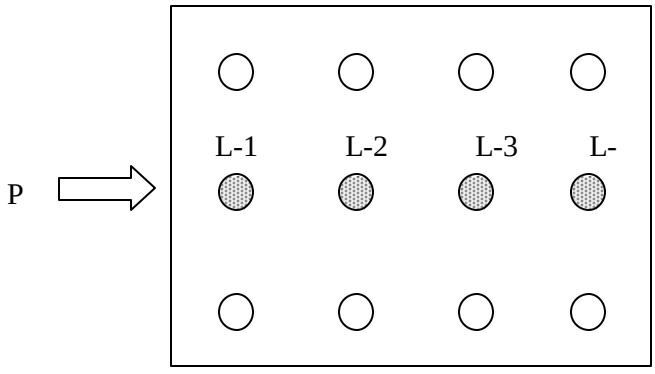

p-Multipliers	0.3	0.3	0.7	0.8

Trailing Row ---------- Front Row

Figure 3.10. Pile Layout and Definition of *p*-Multipliers.

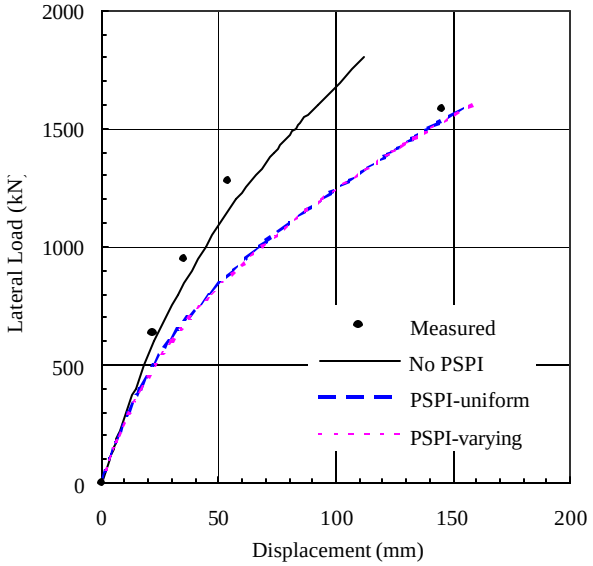

(a) Load-Deflection Response

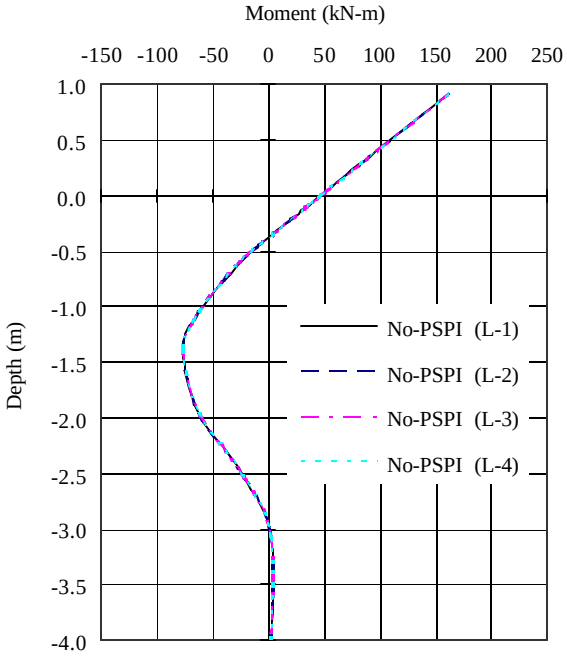

(b) PSPI-Uniform

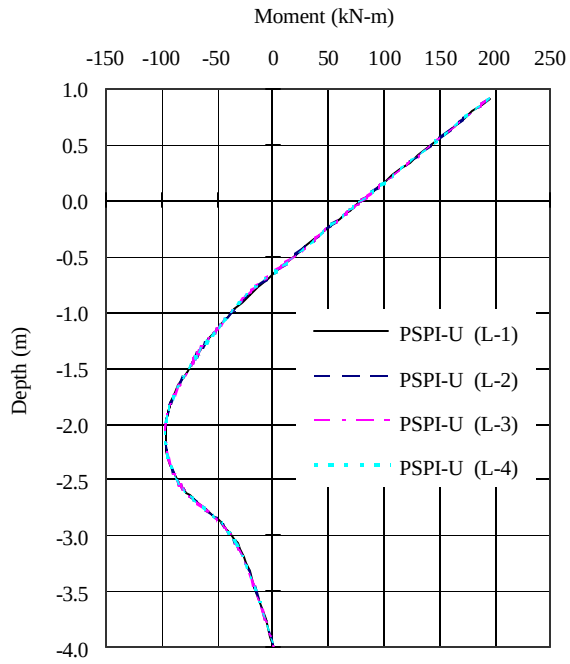

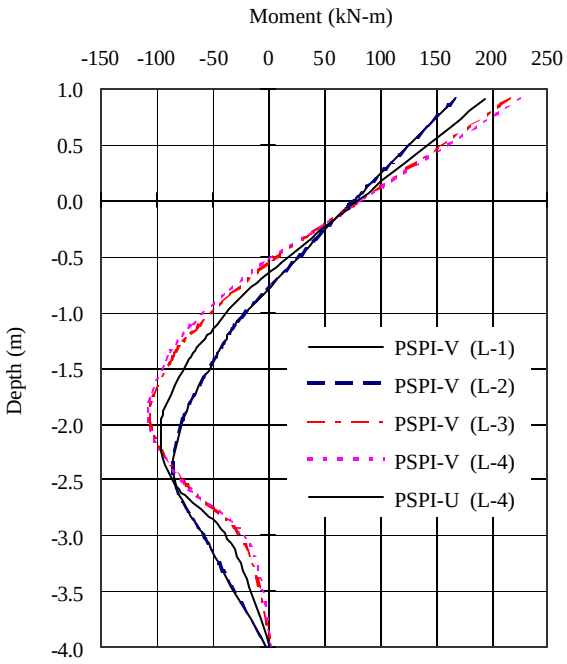

(c) PSPI-Uniform (d) PSPI-Varying

Figure 3.11. Load-Deflection Response and Moment Profiles for Different Modeling of the PSPI.

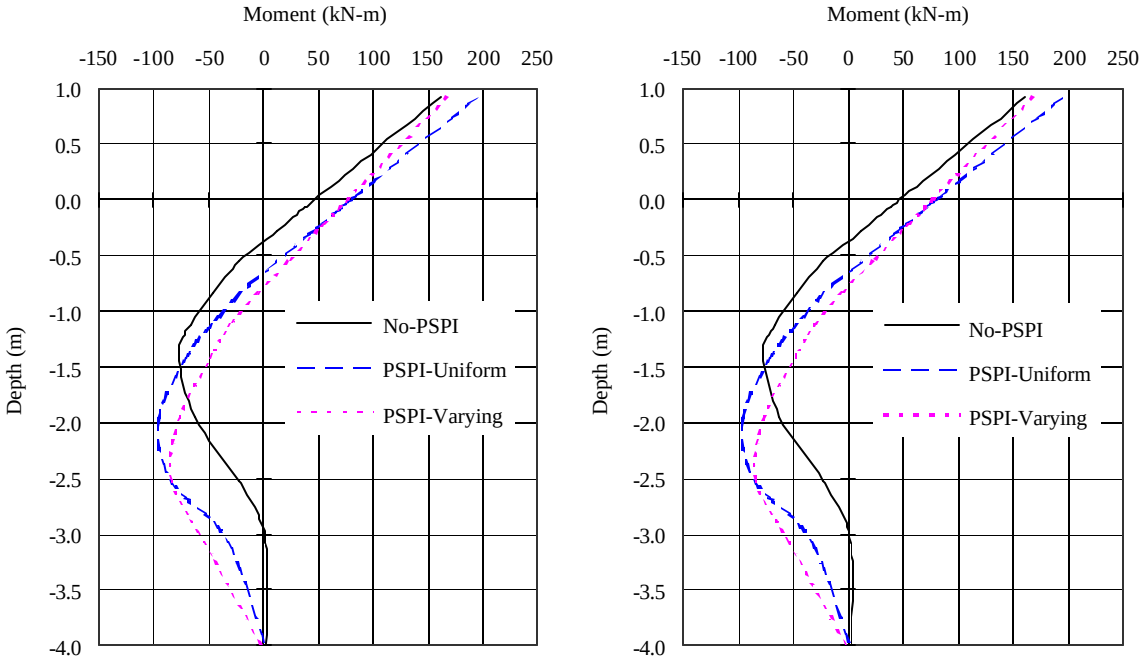

(a) Pile L-1 (b) Pile L-2

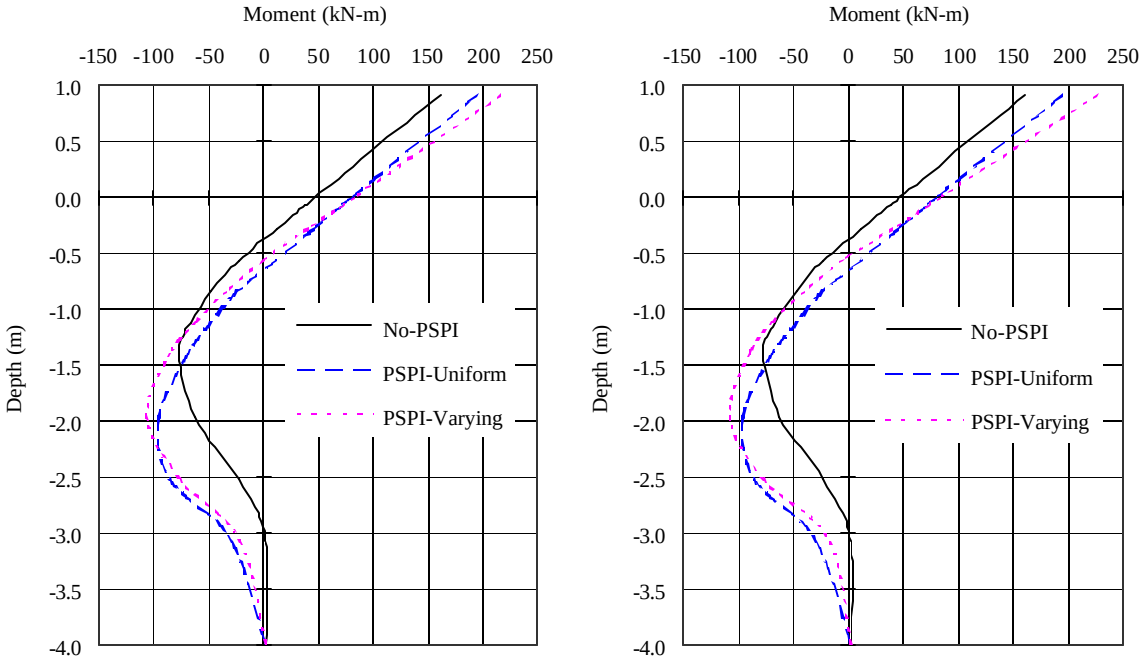

(c) Pile L-3 (d) Pile L-4

Figure 3.12. Moment Profiles of the Center Pile of Each Row.

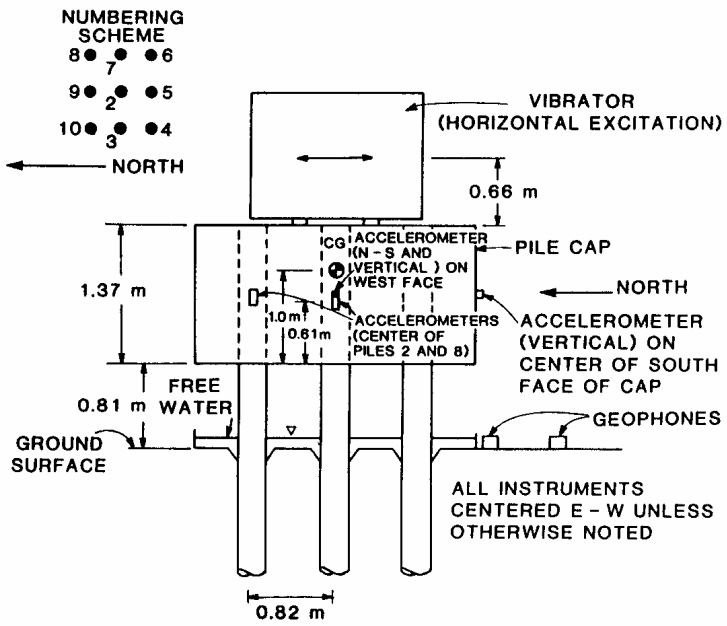

Figure 3.13. Load Test Setup for Case Study 3 [after Blaney and O'Neill (1989)].

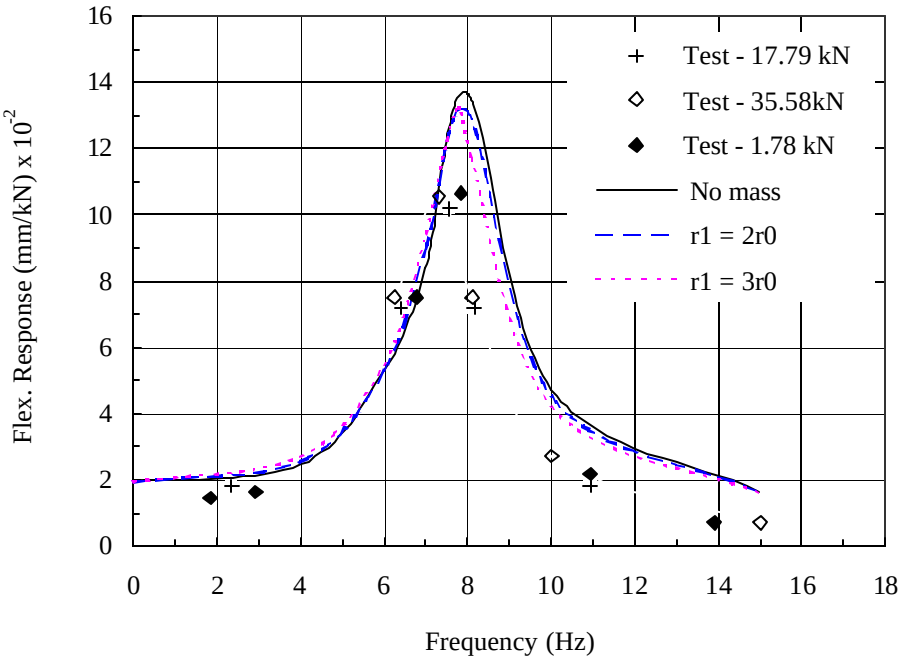

Figure 3.14. Dynamic Response Curves for Different Sizes of Soil Mass.

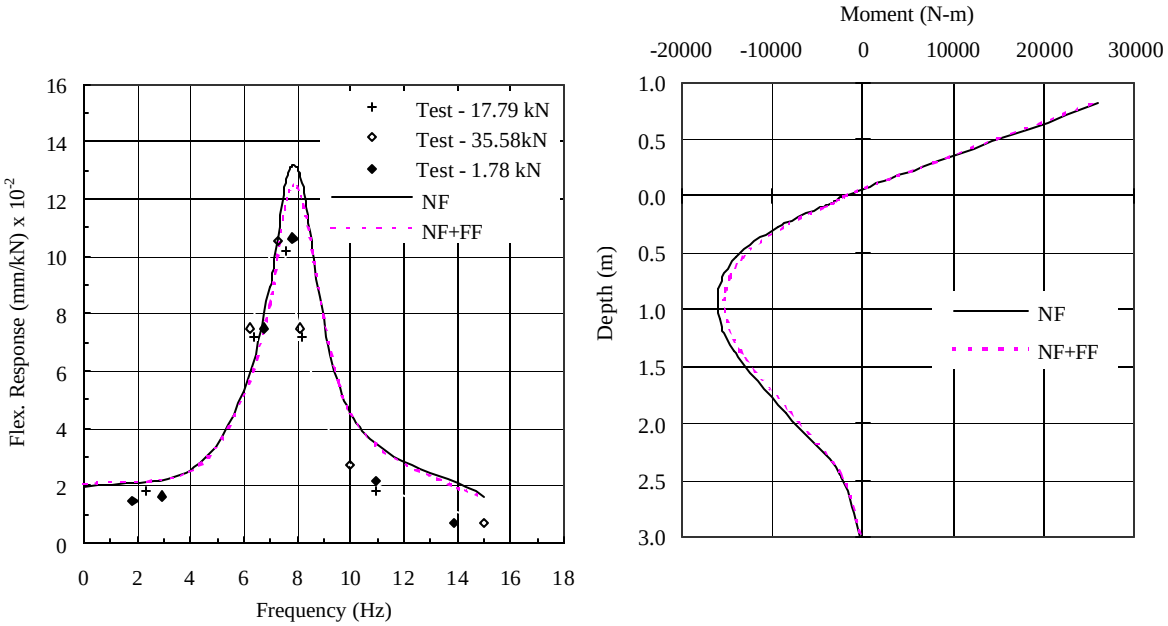

(a) (b)

Figure 3.15. Dynamic Response Curves (a), and Moment Profiles of the Central Pile (b) for Different Soil Modeling.

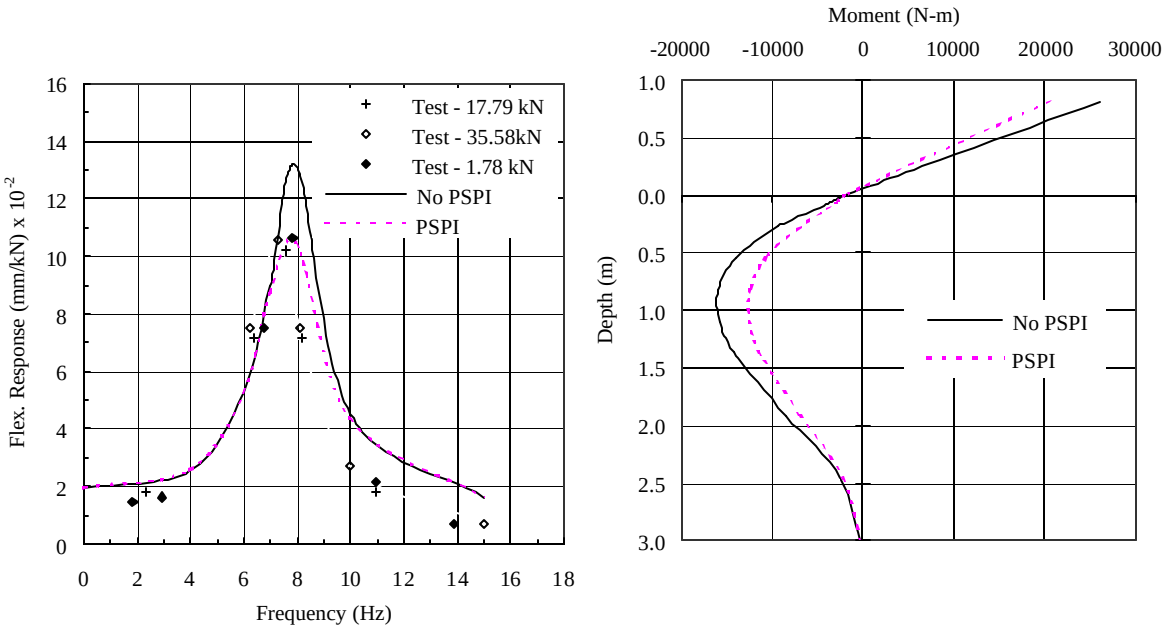

(a) (b)

Figure 3.16. Effects of the PSPI on Dynamic Response Curves (a), and Moment Profiles of the Central Pile (b).

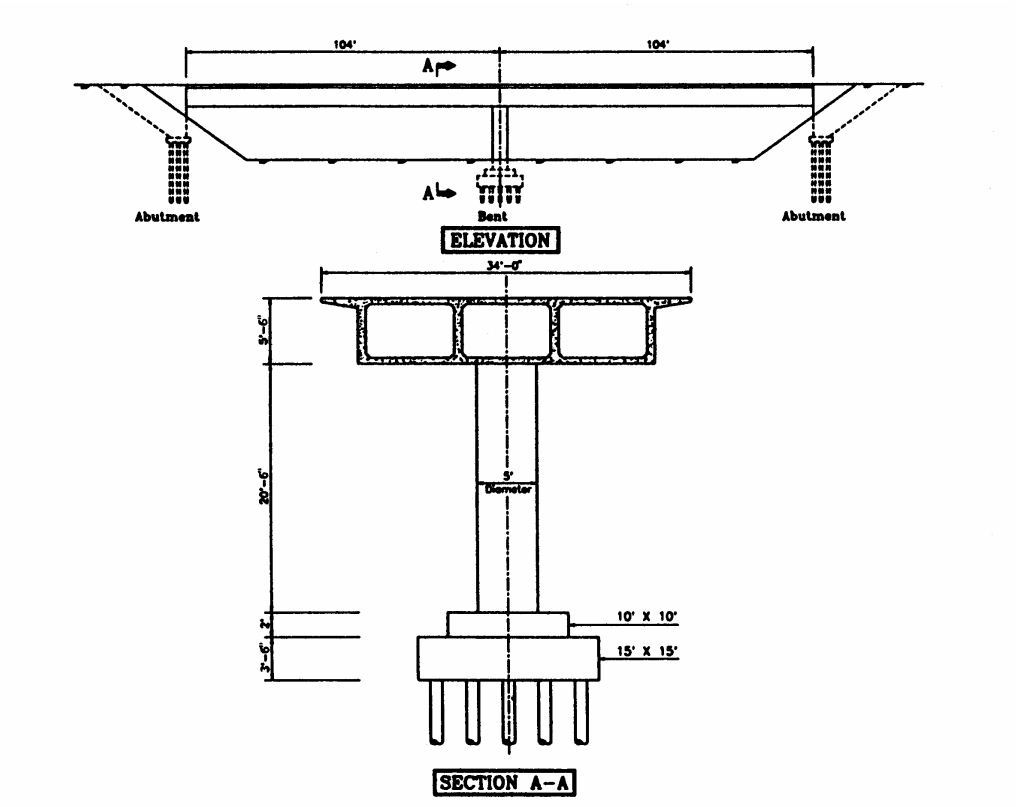

Figure 3.17. Elevation and Section of the Meloland Road Overpass [after Maragakis et al. (1994)].

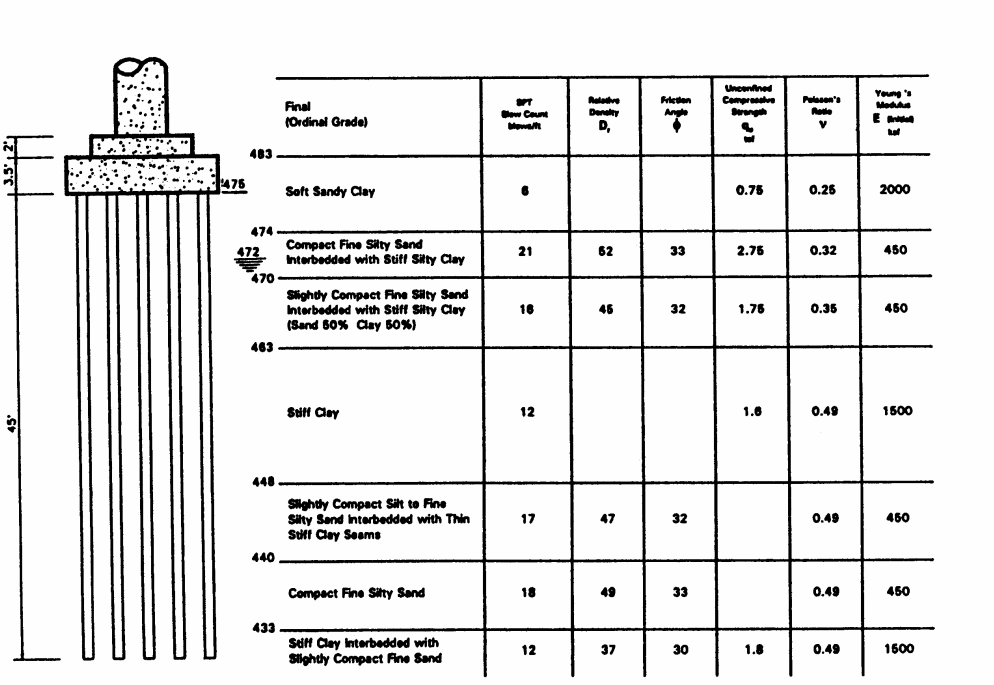

Final (Ordinal Grade)	SPT Blow Count blows/ft	Relative Density D_r	Friction Angle ϕ	Unconfined Compressive Strength q_u tsf	Poisson's Ratio ν	Young's Modulus E tsf
Soft Sandy Clay	6			0.75	0.25	2000
Compact Fine Silty Sand Interbedded with Stiff Silty Clay	21	52	33	2.75	0.32	450
Slightly Compact Fine Silty Sand Interbedded with Stiff Silty Clay (Sand 50% Clay 50%)	18	45	32	1.75	0.35	450
Stiff Clay	12			1.8	0.49	1500
Slightly Compact Silt to Fine Silty Sand Interbedded with Thin Stiff Clay Seams	17	47	32		0.49	450
Compact Fine Silty Sand	18	49	33		0.49	450
Stiff Clay Interbedded with Slightly Compact Fine Sand	12	37	30	1.8	0.49	1500

Figure 3.18. Soil Profile at the Foundation of the Central Pier of the MRO [after Noris and Sack (1986)].

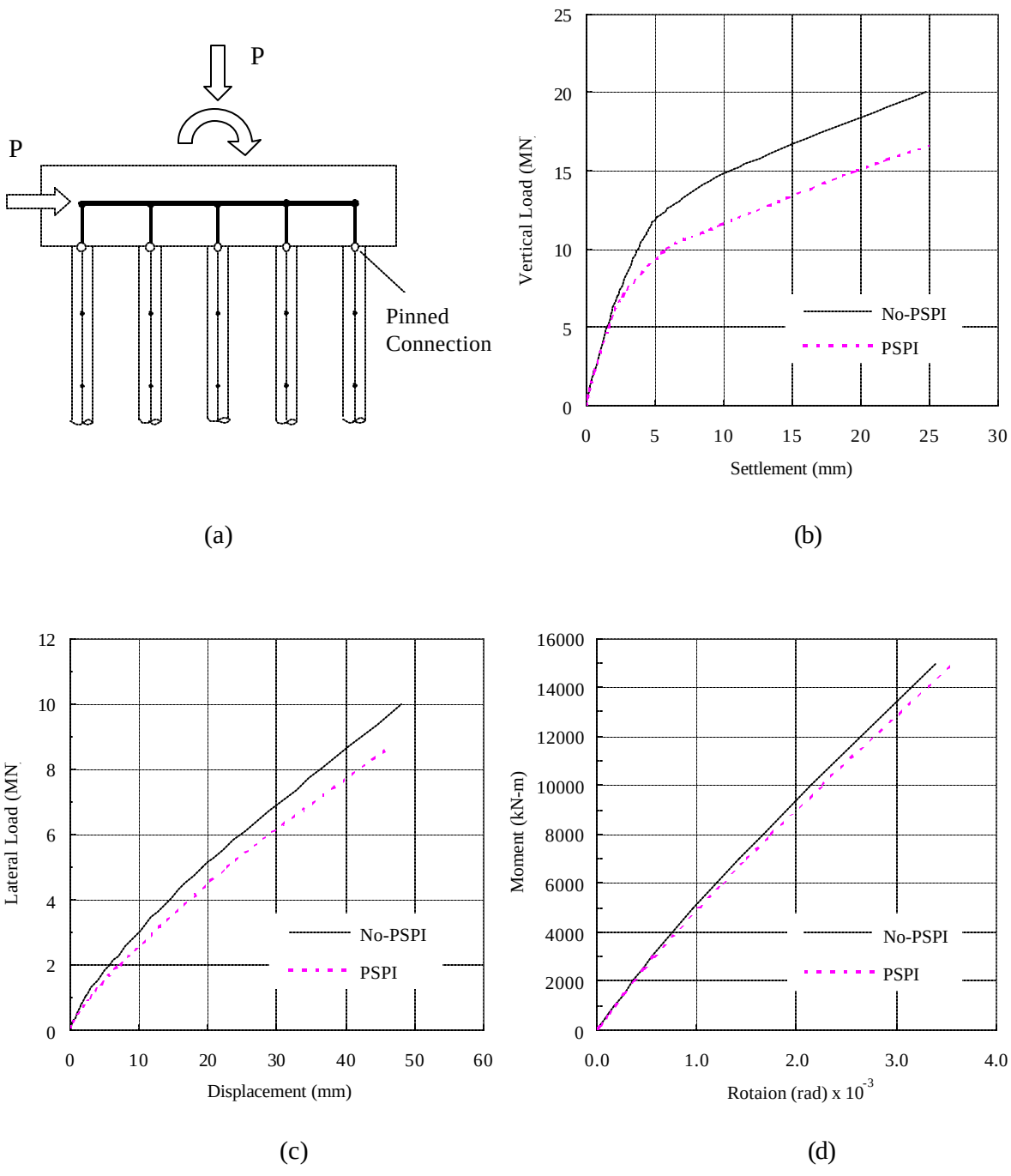

Figure 3.19. Loading of the Foundation Model (a), Vertical Load-Settlement Responses (b), Lateral Load-Displacement Responses (c), and Moment-Rotation Responses (d) of the Pile Group.

CHAPTER 4

CASE HISTORY STUDY: THE OHBA OHASHI BRIDGE

4.1 Introduction

The pile-soil-structure interaction is essentially caused by 2 phenomena: (1) the differences between the motions of the foundation or the soil adjacent to the structure and the free-field motions (kinematic interaction), (2) the effects of the dynamic response of the structure-foundation system on the movement of the foundation and supporting soil (inertial interaction). The kinematic interaction or the reinforcing effect of the presence of piles in the soil medium can induce additional modes of deformation (rocking and torsion modes), which cannot be simulated by the typically used fixed-base model. The inertial interaction occurs because of the forces transmitted to the foundation system by the dynamic response of the superstructure, which can also induce foundation movements that would not occur in a fixed-base structure model.

The inertial interaction may be simulated by an application of loads at the pile head or pile cap. This loading application is what this report has focused on thus far. The proposed model has been verified for its capability in predicting the static and dynamic response of pile foundations to vertical and lateral loads applied at the pile cap. In other words, the proposed soil-pile-foundation model is able to adequately capture the inertial interaction effects. Although several researchers have reached a corroborating conclusion that the effects of the inertial interaction are more pronounced than those of the kinematic interaction, the pile-cap loading condition is certainly different from the seismic loading condition. The kinematic interaction effects on the bridge response are therefore investigated for complete confidence in applying the proposed foundation model in the following study.

4.2 Site Characteristics and Earthquake Observations

The Ohba-Ohashi Bridge is located in Fujisawa City, Kanagawa Prefecture near Tokyo. The bridge is 484.8 m long and 10.75 m wide. The entire bridge elevation and soil condition are shown in Figure 4.1. The construction joints divide the bridge into three sections. Of interest in this study is the second section where accelerations and strain gauges were installed. The bridge section

being considered consists of three continuous spans of steel plate girders between Pier 5 and Pier 8 (48.4 m, 55.0 m and 44.8 m). The movable bearings were used at Piers 5, 7 and 8 and the fixed bearing was used at Pier 6. Figure 4.2 shows the plan and elevation view of the considered bridge section and the location of the instrumentation devices.

The soil conditions obtained near Pier 6 are shown in Figure 4.1. The top layer of the soil profile consists of extremely soft alluvial strata of humus and silt. The results from the Standard Penetration Test indicated very small blow count (SPT(N) value about 10 and the results from the down-hole test indicated that the shear wave velocity was in the range of 50 m/s to 100 m/s. Much stiffer is the underlying substratum of diluvial deposits of stiff clay and fine sand. The test results indicated that the shear wave velocity was about 400 m/s and the SPT(N) values were over 50. The ground water table was one meter below the ground surface. The water content of the top layers was greater than 100% and even reached 250%. The pile group foundation is of end-bearing type.

Eleven accelerometers were installed at various locations along the bridge section: 3 units at the superstructure (BR1-BR3), 3 units at the pile caps (BS1 and BS2 at Pier 6 and BS3 at Pier 8), 1 unit at 1.0 m below ground surface near Pier 6 (GS1) and 4 units at the base of the valley (GB1-GB4). Eight strain gauges were installed at four depths along one vertical and one batter pile at the foundation under Pier 6. The cross section at Pier 6 and the configuration of the pile foundation including a setup of strain gauges on the piles are shown in Figure 4.3. Among 14 earthquakes that have struck the Ohba-Ohashi Bridge, the recorded accelerations of an earthquake having the largest peak horizontal ground acceleration are selected. A part of the observed records from this earthquake is shown in Figure 4.4.

4.3 Literature Review

Some findings and conclusions obtained from other investigators on the bridge response are reviewed first. The observations of the seismic response of the Ohba-Ohashi Bridge were first presented by Ohira et al. (1984). A few years later, several investigators such as Tazoh et al. (1988) and Fan (1992) utilized the recorded seismic response of the bridge foundation for comparison with the response predicted from their proposed analytical method for soil-foundation-structure interaction. The review of literature and reports given by the above-mentioned investigators is presented below.

Taken from the report by Ohira et al. (1984) is Figure 4.5 comparing the Fourier amplitude spectra ratios of recorded motions at the ground surface (GS1) and those at the top of the pile cap (BS1) to the recorded motion at the base of the valley (GB1) in both the longitudinal and transverse directions. It can be observed that the periodic characteristics of the motions at both locations are somewhat similar although the amplitudes of accelerations recorded at the ground surface are about 2 times larger than those recorded at the top of the pile foundation for periods up to about 5 seconds. The smaller amplitude of the motions recorded at the pile cap may result from the reinforcing effect of the pile foundation (i.e., the presence of the piles in the soil medium).

Tazoh et al. (1988) used a seismic response method for pile-foundation structures proposed by Tajimi (1969) to evaluate the dynamic behavior of this bridge. Tajimi's analytical method was based on three-dimensional elastic wave propagation theory. It is evident from the Fourier spectra for axial and bending strains that the shapes of the spectra remain practically unchanged throughout the length of the pile even though the amplitudes of the spectra decrease with increasing depth. The strain histories at the location of the strain gauge labeled SA1 are shown in Figure 4.4. It was concluded that both axial and bending strains among the piles induced by the excitations have approximately similar periodic characteristics, implying that the wave scattering effects (kinematic interaction effects) on periodic characteristics of the excitations are insignificant. This observation very well conforms to the observation of the recorded response reported by Ohira et al. (1984).

Fan (1992) applied the substructure method to perform seismic soil-foundation-structure interaction analyses. Also conducted in his study was the site response analysis in which the 1-dimensional wave propagation analytical method was adopted. It was reported that the 1-D wave propagation analysis failed to reproduce the free-field motions at ground surface (GS1) from the input motion (GB1) at the base of the valley. The discrepancies between the computed and recorded group motions are believed to be attributed mainly to the valley effects or geometry effects which are of 2- or 3-dimensional-type problems and cannot be simulated using 1-D wave propagation concept. The valley effects are also believed to be responsible for disagreements between the recorded response and computed response from the soil-structure interaction analysis conducted in his study.

4.4 Modeling of the Bridge Structure

The accelerometers and strain gauges were installed along the bridge section spanning between Pier 5 and Pier 8. Therefore, only this section of the bridge is modeled in the following study. The concept of modeling only the interested section taken out of the entire bridge is justifiable since there observed no visible damage due to pounding between two adjacent sections of the bridge at Pier 5 and Pier 8 during the selected earthquake.

4.4.1 Superstructure Model

Details regarding the quantitative member sizes and material properties of the superstructure and the piers are unfortunately not available. All these quantitative values however can be approximately obtained from preliminary bridge design based on the bridge configuration (span length and width of the bridge). From the available information (bridge drawings and pictures taken during construction), the number and shape of steel plate girders and configuration of the bridge piers and foundations are obtained. The bridge superstructure consists of 3 continuous spans of 5 steel plate girders supporting the reinforced concrete deck. The superstructure system is modeled using 3-D frame elements connected transversely by rigid frame elements forming a grid system. To account for the cracking of concrete, the flexural stiffness of the reinforced concrete members is reduced to 50% of the gross flexural stiffness (EI_g: E = Young's modulus of concrete and I_g = moment of inertia of the reinforced concrete member) as recommended by ATC-32 (1996). The shear and torsional stiffness remained unchanged.

4.4.2 Foundation Model

Although details of the configuration and material properties of the pile foundations are not available except for the pile foundation supporting Pier 6, they can be roughly measured from the elevation view of the bridge as given in Figure 4.2. The number of piles used at each foundation can also be estimated based on the available bridge pictures and the preliminary calculation for the number of piles required to support the factored design loads. The pile foundation supporting all piers except Pier 6 is represented by a 6x6 equivalent linear stiffness matrix. A computer code was written to compute the stiffness of the pile foundation according to a recommendation of the American Association of State Highway and Transportation Officials (AASHTO).

The 6x6 equivalent linear stiffness matrix of each pile is calculated based on an estimated soil modulus according to an assumed level of shaking or loading, which shall be checked against values obtained from the bridge response analysis for verification. An iterative procedure will be used until

the assumed level of loading is close to the computed level of loading. The stiffness matrix of every single pile is then statically condensed to develop a 6x6 stiffness matrix of the pile group foundation which will be attached to the base of the pier column.

Of interest in this study is the pile foundation supporting Pier 6 which consists of 8x8 = 64 concrete filled steel pipe piles (32 batter and 32 vertical piles) as shown in Figure 4.3. The piles are equally spaced at 1.5 m in both directions throughout the group leading to a spacing-to-diameter (s/d) ratio of 2.5. The 22-m-long steel pipe piles have an outside diameter of 0.60 m and a wall thickness of 9 mm for vertical piles and 12 mm for batter piles. The piles are modeled using 10 frame elements increasing in length with depth as previously demonstrated to be satisfactory for capturing both static and dynamic pile responses. The reinforced concrete pile cap has a varying thickness of about 1.5 at the perimeter to 2.0 m at the center. The pile cap is modeled using shell elements. The embedded length of the steel pipe piles into the concrete cap of about 0.5 m is sufficient for the pile-to-pile-cap connection to be considered as a partially fixed connection. The rigid end zone factor of 0.85 is used to represent such connection.

Two patterns of soil models are used. The behavior of the soil inside the group is modeled using a near-field soil model and the soil surrounding the peripheral piles is modeled using both near-field and far-field soil models. More details on soil modeling can be obtained in Chapter 3.

4.5 Dynamic Analysis and Summary of the Bridge Models

The nonlinear time-history analyses of the Ohba-Ohashi Bridge are performed using the SAP2000 program. Implemented in this program is the Fast Nonlinear Analysis (FNA) method developed by Wilson [Ibrahimbegovic and Wilson (1989)]. This FNA method is well suited for the analyses conducted in this study since it is designed to be accurately used for structural systems which are primarily linear elastic with a limited number of nonlinear elements. The basic concepts of the FNA method and steps that are taken to ensure the accuracy of the results are discussed in Chapter 5.

4.5.1 Specification of Input Motions and Damping

The differences in amplitudes and phases of the excitation at each foundation or multiple support excitations due to the effects of traveling wave are not considered. The presumption is based on the fact that the total length of the bridge section being considered is only 143.8 m. In

addition, the recorded motions that are of interest and used in the following comparison study are obtained in the vicinity of Pier 6. It is therefore rational to use the recorded motions at the base of the valley near Pier 6 (GB1-H1, GB1-H2 and GB1-V) as the input motions to the soil-foundation-structure model in the nonlinear time-history analysis. The input motions in all three directions are shown in Figure 4.6. As recommended by several seismic guidelines for highway bridges, the 5% damping ratio is used to characterize an overall damping of the system and it is applied to all vibration modes of the bridge.

4.5.2 Summary of the Bridge Models

The bridge models with three different soil-modeling assumptions are used in this study. In the first soil model, both the near-field (NF) and far-field (FF) soil models are used to represent the soil surrounding the peripheral piles and stiffness and radiation damping properties of the far-field soil model are computed using the expressions derived by Novak et al. (1978). The second soil model is similar to the first model except that the coefficients for stiffness and radiation damping of the far-field soil model are obtained based on the closed-form expressions given by Gazetas and Dobry (1984), and Gazetas and Makris (1991). In the third soil model, only the near-field soil model is used to represent the nonlinear behavior of the soil surrounding the pile regardless of its location in the group. These three different soil-modeling assumptions are incorporated into the full 3-D bridge model (Figure 4.7) to evaluate the sensitivity of the bridge response to different soil modeling concepts and uncertainties in characterizing the soil properties. The descriptions and numbering system of the three modeling cases are summarized in Table 4.1. The results obtained from the nonlinear time-history analysis of the bridge with these various models are compared with the recorded responses in the following study.

Table 4.1. Cases Considered in Seismic Response Analysis of the Ohba-Ohashi Bridge.

Case	Descriptions of bridge models
A	Both NF and FF soil models are used & FF soil properties by Novak et al. (1978).
B	Both NF and FF soil models are used & FF soil properties by Gazetas et al. (1984).
C	Only NF soil model is used.

4.6 Comparison Studies

The following comparison studies are dedicated to investigation of the effects of different soil modeling concepts on the bridge response and its dynamic characteristics. First, the periods of the bridge obtained from all modeling cases are compared in Table 4.2. The effects of soil modeling assumptions on the bridge responses are then examined through comparison of the computed responses from different soil models. A parametric study is also conducted to evaluate the effects of far-field soil model on the bridge response for stiff soil conditions. Furthermore, the computed motions at several locations on the bridge are also compared with the recorded motions.

4.6.1 Dynamic Characteristics of the Bridge

Dynamic characteristics of the bridge in the form of modal periods for various models are listed in Table 4.2. The characters in the parentheses denote the vibration mode corresponding to the given period. The modal periods of the bridge computed from different soil models are nearly identical. In fact, the difference among the periods for each mode is less than 5%. The mode shapes are also found to be similar. Therefore, it is concluded that the effects of soil modeling have only a small effect on the dynamic characteristics of the bridge.

Table 4.2. First 10 Modal Periods of the Ohba-Ohashi Bridge for All Cases.

Mode	Case A	Case B	Case C
1	1.370 (T)	1.369 (T)	1.385 (T)
2	0.995 (L)	0.995 (L)	0.997 (L)
3	0.728 (T)	0.727 (T)	0.725 (T)
4	0.470 (L+V)	0.470 (L+V)	0.476 (L+V)
5	0.435 (T+V)	0.434 (T+V)	0.432 (T+V)
6	0.371 (Tor)	0.371 (Tor)	0.356 (Tor)
7	0.203 (NL)	0.203 (NL)	0.266 (T)
8	0.203 (NL)	0.203 (NL)	0.215 (L)
9	0.203 (NL)	0.203 (NL)	0.201 (NL)
10	0.200 (NL)	0.200 (NL)	0.200 (NL)

Notes:

1. L, T, V and T denote longitudinal, transverse, vertical and torsional vibration mode of the structure, respectively.
2. NL denotes the vibration mode corresponding to the nonlinear soil elements.

4.6.2 Effects of Soil Modeling Assumptions on the Bridge Response

To examine the effects of soil modeling assumptions on the bridge response, the computed absolute acceleration responses at the bent cap and at the top of the foundation of Pier 6 for Cases A, B and C are compared in Figure 4.8. The relative displacement responses at the bent cap and the foundation at Pier 6 for are shown in Figure 4.9. The member forces (axial force and bending moments about x and y axis) experienced in the vertical pile at 1 m and at 7 m below the bottom of the pile cap (location of the installed strain gauge labeled SA1 and SA2) computed from different soil modeling cases are compared in Figure 4.10.

It can be observed that the differences among the computed acceleration and displacement responses at different locations of the bridge from all modeling cases are very small. The difference among the computed member forces in the pile obtained from different soil models is also trivial. The small difference between Cases A and B indicate that the bridge responses are not sensitive to the uncertainty in characterizing the far-field soil properties (soil stiffness and damping properties). Not only that, it is observed from these figures that the effect of the far-field soil model on the bridge responses is small.

It is observed that the forces and moments at along the length of the pile (Figure 4.10) and among the piles (not shown) have relatively similar periodic characteristics, implying that the wave scattering effects (kinematic interaction effects) are not important. This observation conforms to that made by Ohira et al. (1984) based on the recorded response and that made by Tazoh et al. (1988) based on the three-dimensional elastic wave propagation theory previously discussed in Section 4.3.

The force-displacement histories (hysteresis responses) at different locations are shown in Figure 4.11. The member forces at the base of the pier versus the displacements at the bent cap are plotted in Figure 4.11(a) and the soil reaction histories at 1 m below ground surface for all three

principal directions are also plotted in Figure 4.11(b). These figures are intended for developing an insight on the level of forces and displacements induced by the input motions. The displacement amplitudes for all three translational degrees of freedom are fairly small. The analytical results reveal that there occur minor excursions into nonlinear behavior of the top layer soil. At greater depth from which most of the pile resistance is derived, the soil behaves essentially in elastic range.

The soil nonlinearity was found in the previous study to have a significant effect on the contribution of the radiation damping effects. The more strongly pronounced the soil nonlinearity, the less significant the radiation damping effects. In this case study, the soil-pile interaction is primarily elastic; therefore, the radiation damping effects would not be diminished by the soil nonlinearity if there occurred any. The analytical results however demonstrate that the effects of radiation damping or far-field soil model on the overall bridge response are found insignificant. Therefore, the far-field soil model may be disregarded in modeling the soil surrounding the piles for the soil condition at the Cairo Bridge site (soft alluvial soils).

4.6.3 Parametric Study on Effects of Far-Field Soil Model for Stiff Soil Conditions

For other soil types such as stiff soils, a parametric study is also conducted to evaluate the effects of far-field soil model on the bridge response. The soil properties used in modeling the near-field and far-field soil reactions are to be classified as site class C according to NEHRP Guidelines for Seismic Rehabilitation of Buildings (FEMA 273). The site class C is specified for very dense soil and soft rock with the shear wave velocity in a range of 366 to 763 m/sec (1,200 to 2,500 ft/sec) or with SPT(N) value greater than 50 or undrained shear strength greater than 95.8 kPa (2,000 psf). The soil reactions are modeled in such a way that the soil properties at the pile head represent the lower bound values and the soil properties at the pile tip represent the upper bound values. The linear variation is assumed for the soil properties in between.

The absolute acceleration and relative displacement responses at the bent cap and the top of the foundation from different soil modeling concepts for stiff soil condition are shown in Figures 4.12 and 4.13, respectively. It is evident from these figures that the effects of the far-field soil model on the bridge response for stiff soils are insignificant. Since the behavior of the structural system is observed to be essentially in elastic range, the effects of far-field soil model or radiation damping (if there are any) are not expected to be lessened by the soil nonlinearity and since the difference of the computed responses from Cases A, B and C is insignificant, it can be concluded that the far-

field soil model can be neglected in modeling the soils surrounding the piles for stiff soil conditions. As a result of this parametric study and previous studies, it can be concluded that the far-field soil model can be neglected for static response as well as dynamic response over the frequency range that is of interest for earthquake loading.

4.6.4 Comparison Study of the Predicted and Recorded Motions

Since the computed responses from different soil modeling cases are similar, the acceleration histories from Case C are chosen for comparison with the recorded responses. The predicted and recorded absolute acceleration responses at the bent cap and the foundation are computed in Figure 4.14. The predicted responses compare reasonably well with the recorded responses, especially in the vertical direction. The overall maximum amplitudes and periodic characteristics of the accelerations at both locations are captured reasonably well by the analytical models except for the transverse motion at the bent cap and longitudinal at the foundation.

For a more successful prediction of the seismic bridge response, the system parameters such as the damping property of the structure may be varied. However, no attempt is made to do so since there are uncertainties that involves in identifying the structural properties (member section and material properties) as well as in identifying the foundation and soil properties, which should be kept in mind when comparing the predictions with the measurements. Despite all these uncertainties, the predicted response from the proposed pile-foundation model in combination with the global bridge model compares reasonably well with the recorded response.

4.7 Concluding Remarks

The performance of the proposed pile-foundation model in predicting the bridge response to seismic loading is investigated through a comparison study. A number of different bridge models are used in this study to evaluate the sensitivity of the bridge response to different soil modeling concepts and uncertainties in characterizing the soil properties. The parametric study is also performed to examine the effects of the far-field soil models for different soil types (soft and stiff soils). Based on the comparison and parametric studies, the effects of the far-field soil model on the bridge response and its dynamic characteristics are found to be insignificant and therefore may be neglected in modeling the soil surrounding the piles. The comparison study also shows that the predicted responses are in reasonable agreement with the recorded responses.

In conclusion, it is recommended that the proposed pile-foundation model be used in combination with the global bridge model in seismic response analysis of pile-supported bridges. It is well to emphasize once again that the effects of far-field soil models on the bridge response to seismic loads is insignificant and may be disregarded in modeling of the soils in the pile-foundation model. In addition, the previous study concluded that the far-field soil model can be neglected for static and dynamic response at the range of frequency between 0.1-10 Hz, which is a typical range for earthquake loading. Consequently, the near-field soil model alone is capable of adequately representing the soil behavior and thus will be used in modeling the soil component of the proposed pile-foundation model in the subsequent study.

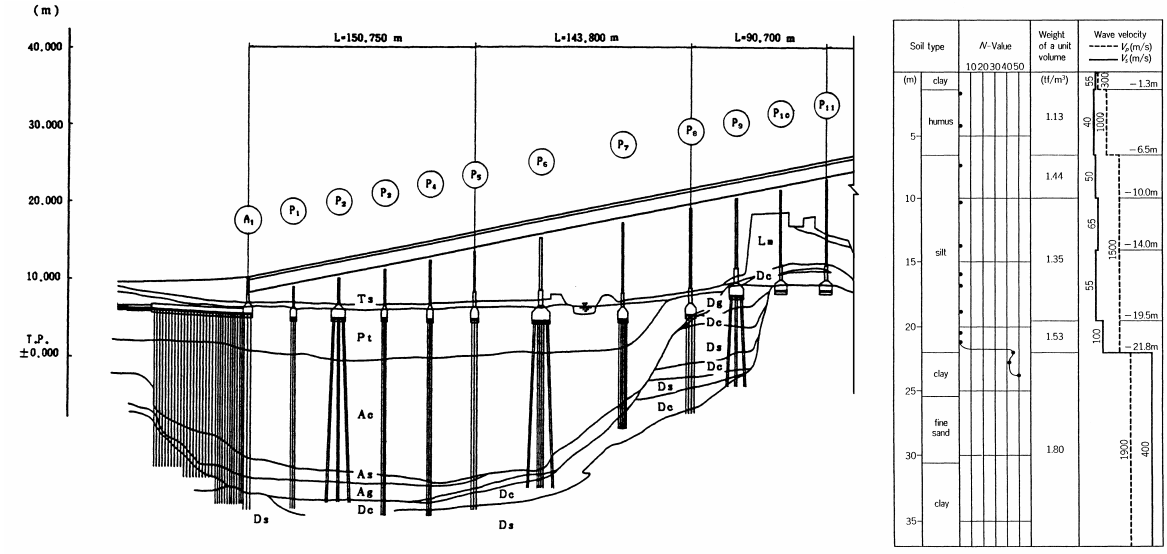

Figure 4.1. Bridge Elevation and Soil Conditions [after Ohira et al. (1984)].

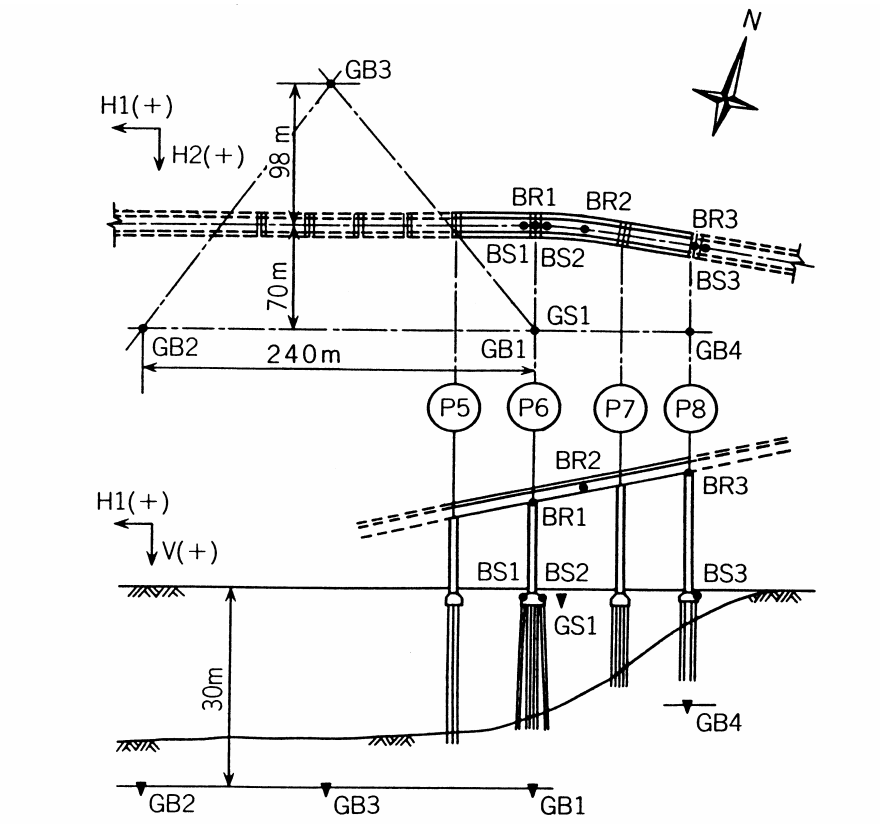

Figure 4.2. Plan and Elevation View of the Considered Bridge Section and Installation of Accelerometers [after Ohira et al. (1984)].

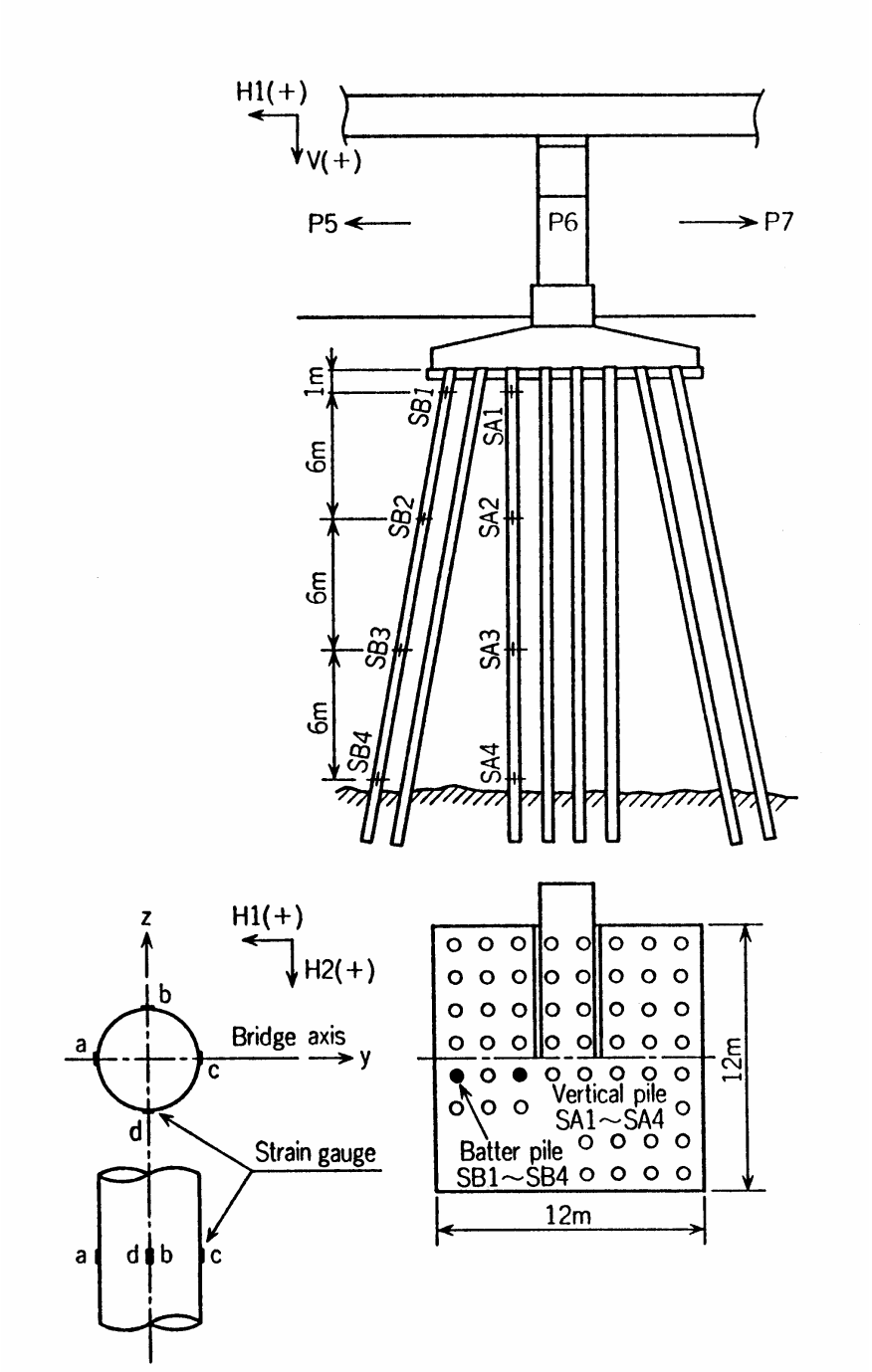

Figure 4.3. Configuration of the Pile Foundation at Pier 6 and Locations of Strain Gauges [after Ohira et al. (1984)].

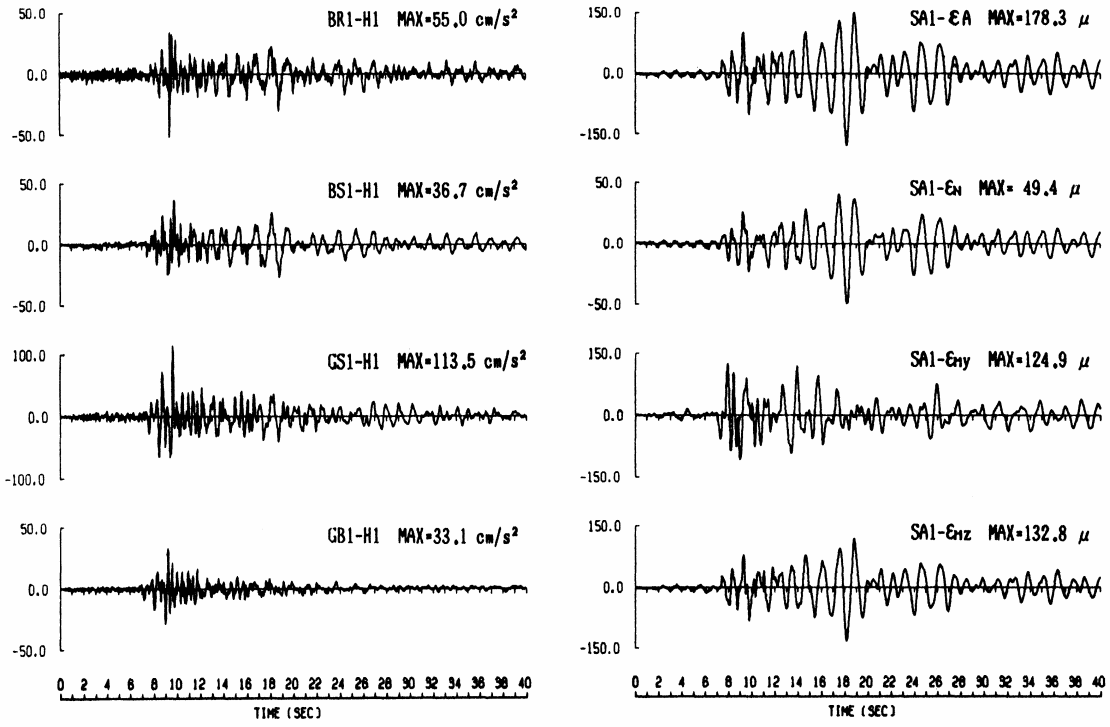

Figure 4.4. Samples of the Observed Records [after Ohira et al. (1984)].

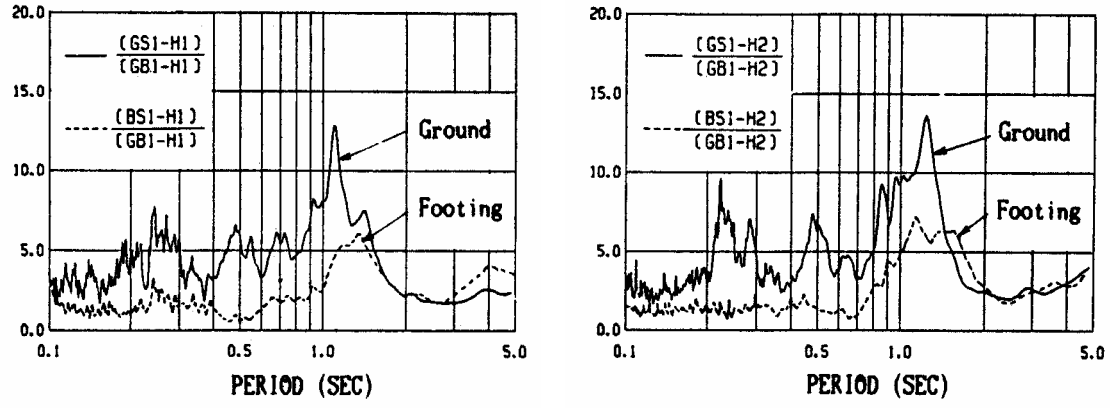

Figure 4.5. Fourier Amplitude Spectral Ratios for Horizontal Motions at Foundation and Ground Surface with Respect to Motions at Base of the Valley [after Ohira et al. (1984)].

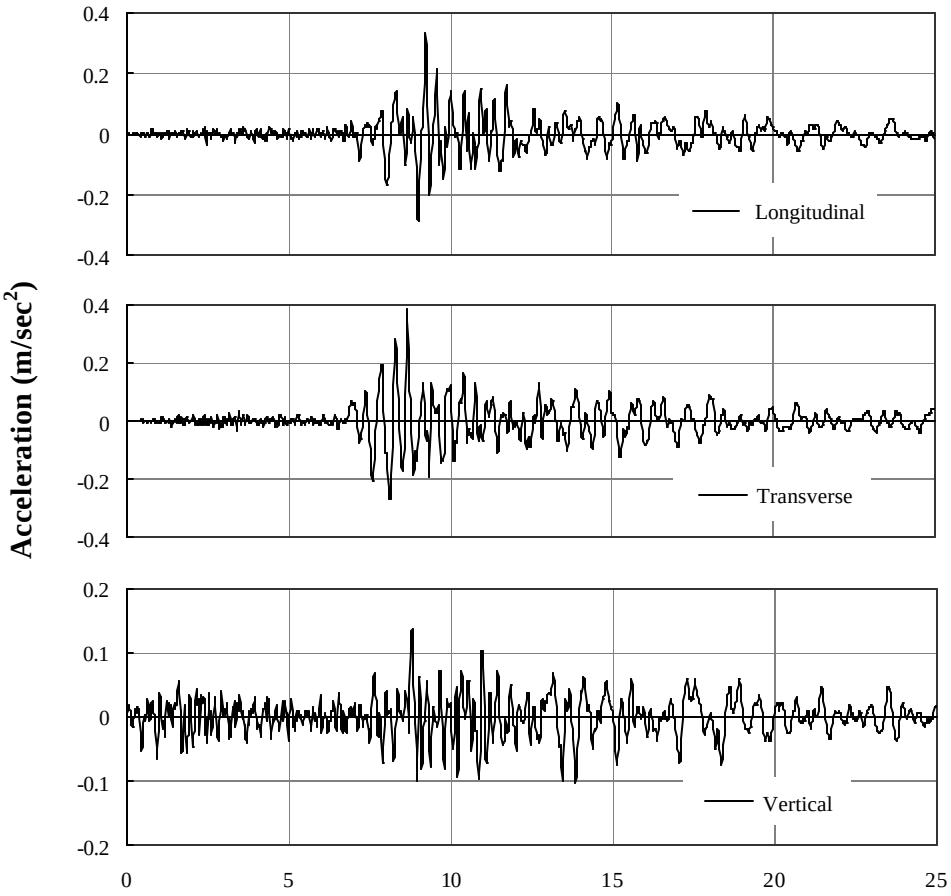

Figure 4.6. Input Motions (GB1) for Nonlinear Time History Analyses.

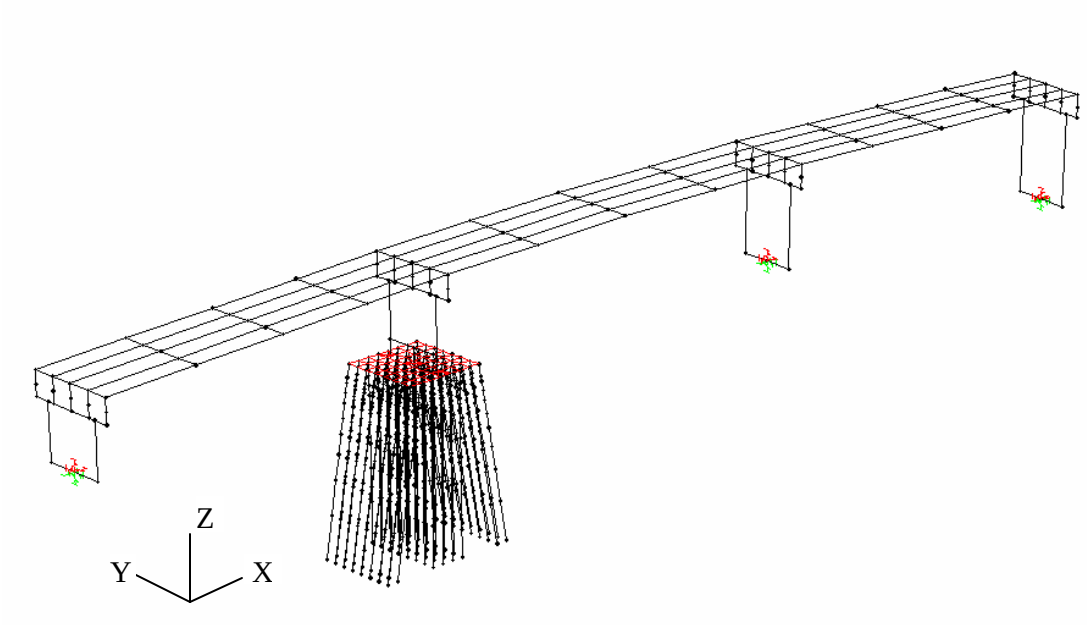

Figure 4.7. Schematic View of the Entire Bridge Section Model.

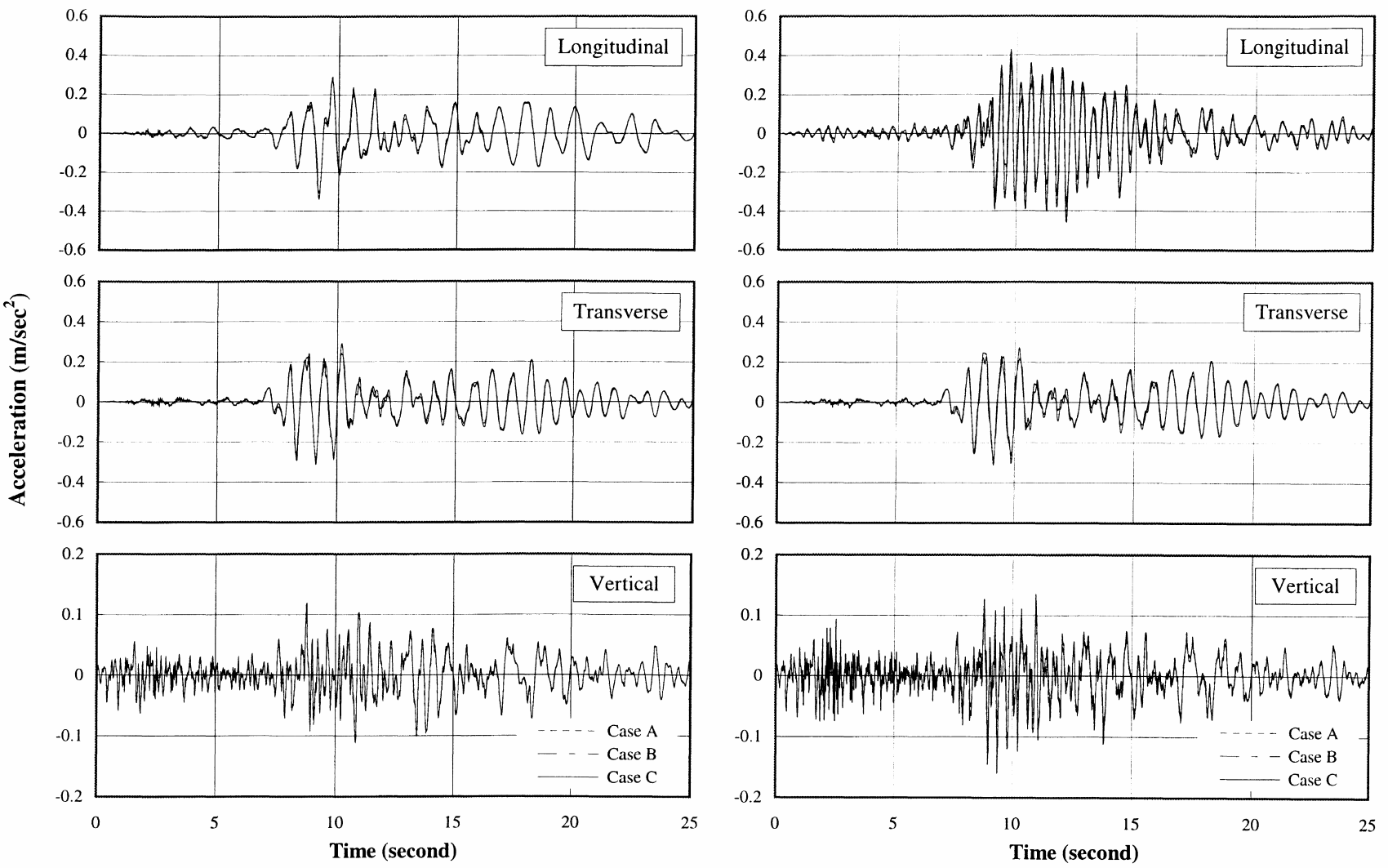

Figure 4.8. Computed Accelerations at (a) Bent Cap, and (b) Foundation of Pier 6 for Different Soil Models.

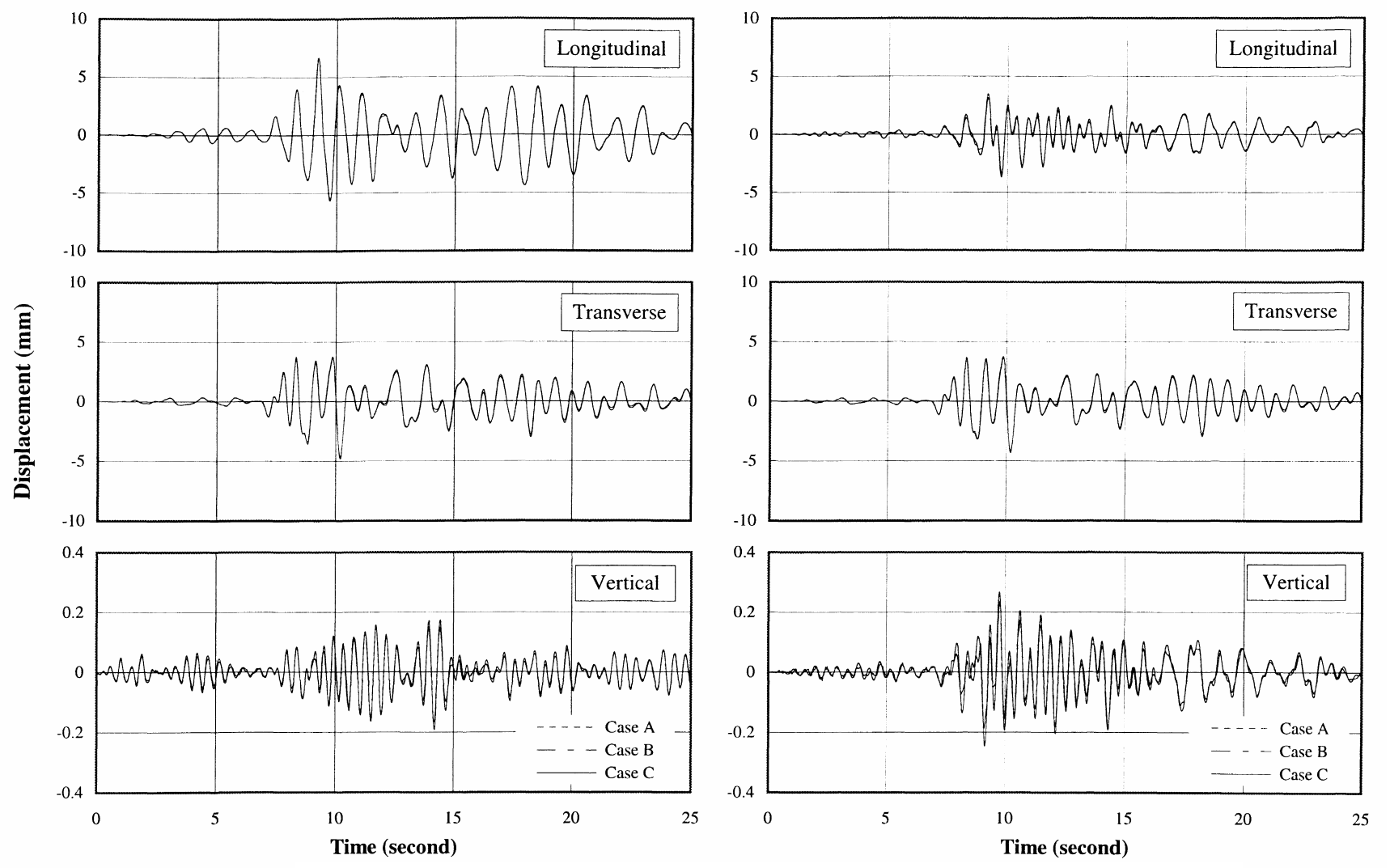

Figure 4.9. Computed Displacement Responses at (a) Bent Cap, and (b) Foundation of Pier 6 for Different Soil Models.

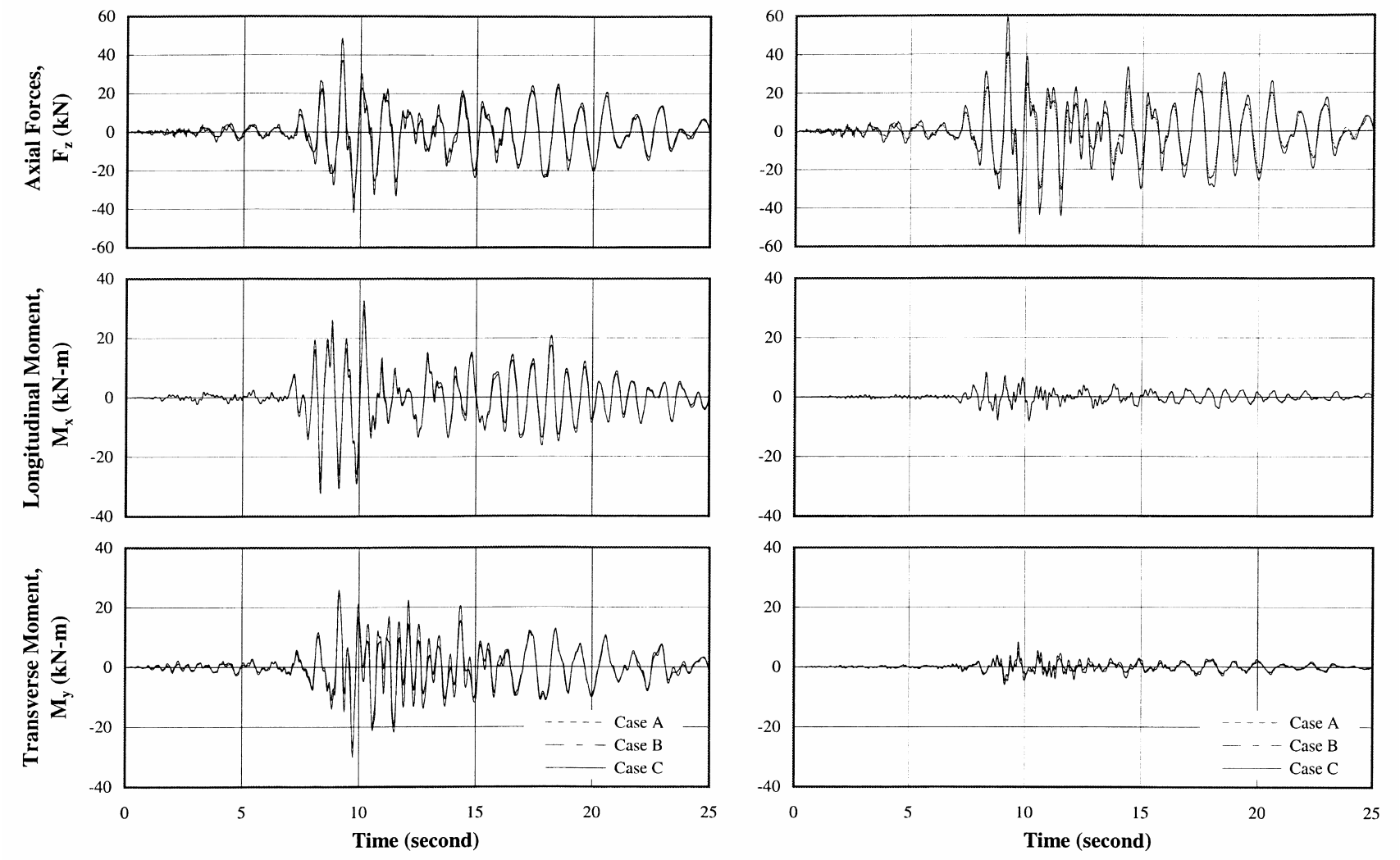

(a) At SA1 Location

(b) At SA2 Location

Figure 4.10. Computed Member Forces in the Pile at (a) SA1, and (b) SA2 Locations of Pier 6 for Different Soil Models.

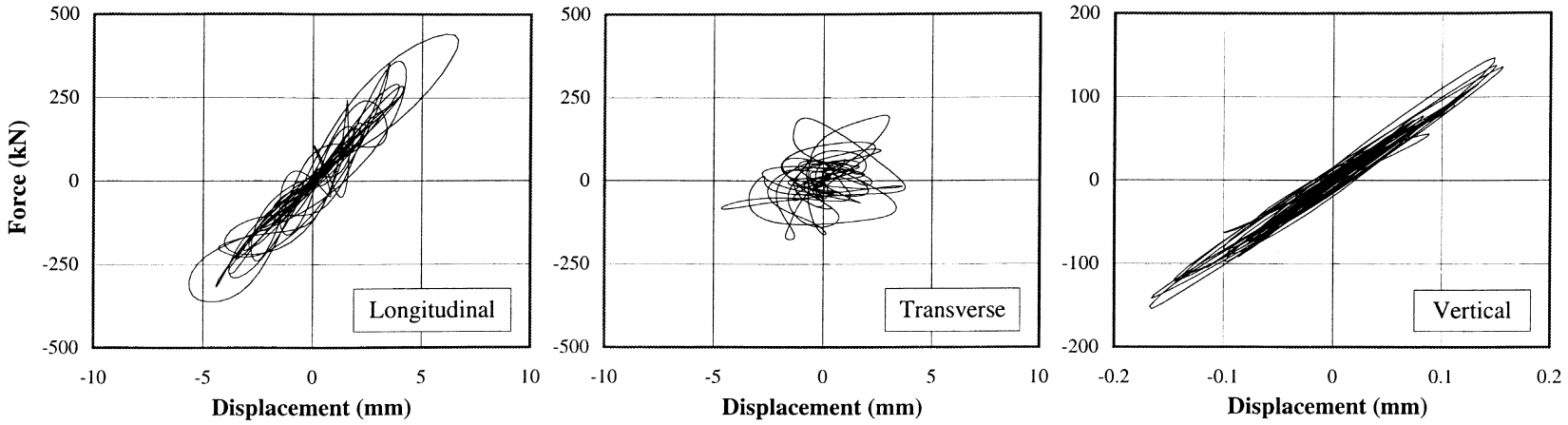

(a) Member Forces at the Base of the Pier versus Displacements at the Bent Cap of Pier 6

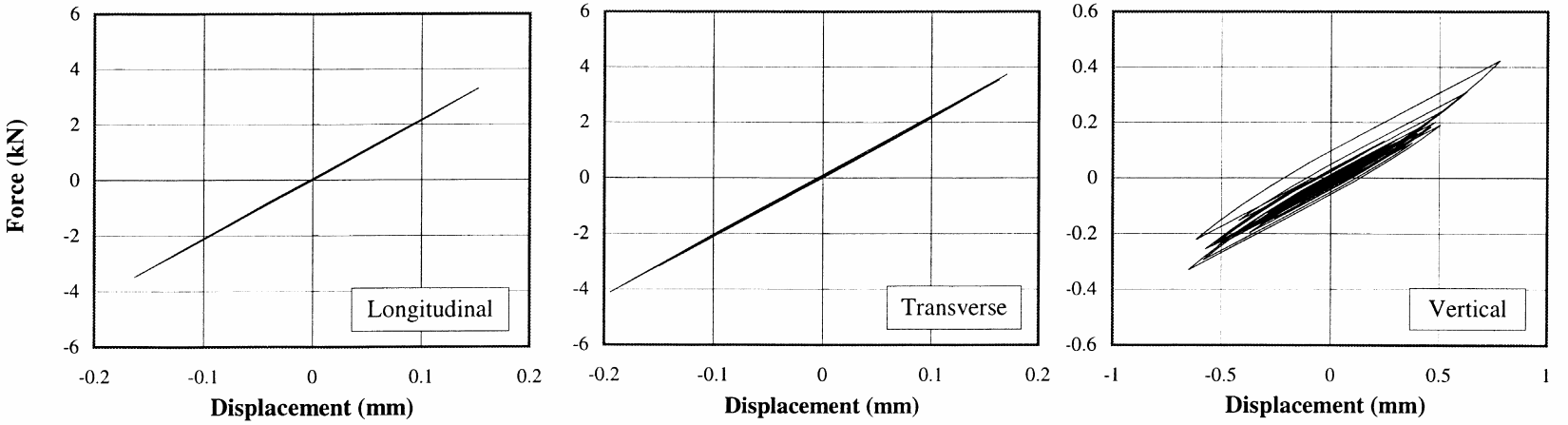

(b) Soil Reaction Histories at 1 m below Ground Surface

Figure 4.11. Force-Displacement Histories at Different Locations for Case C.

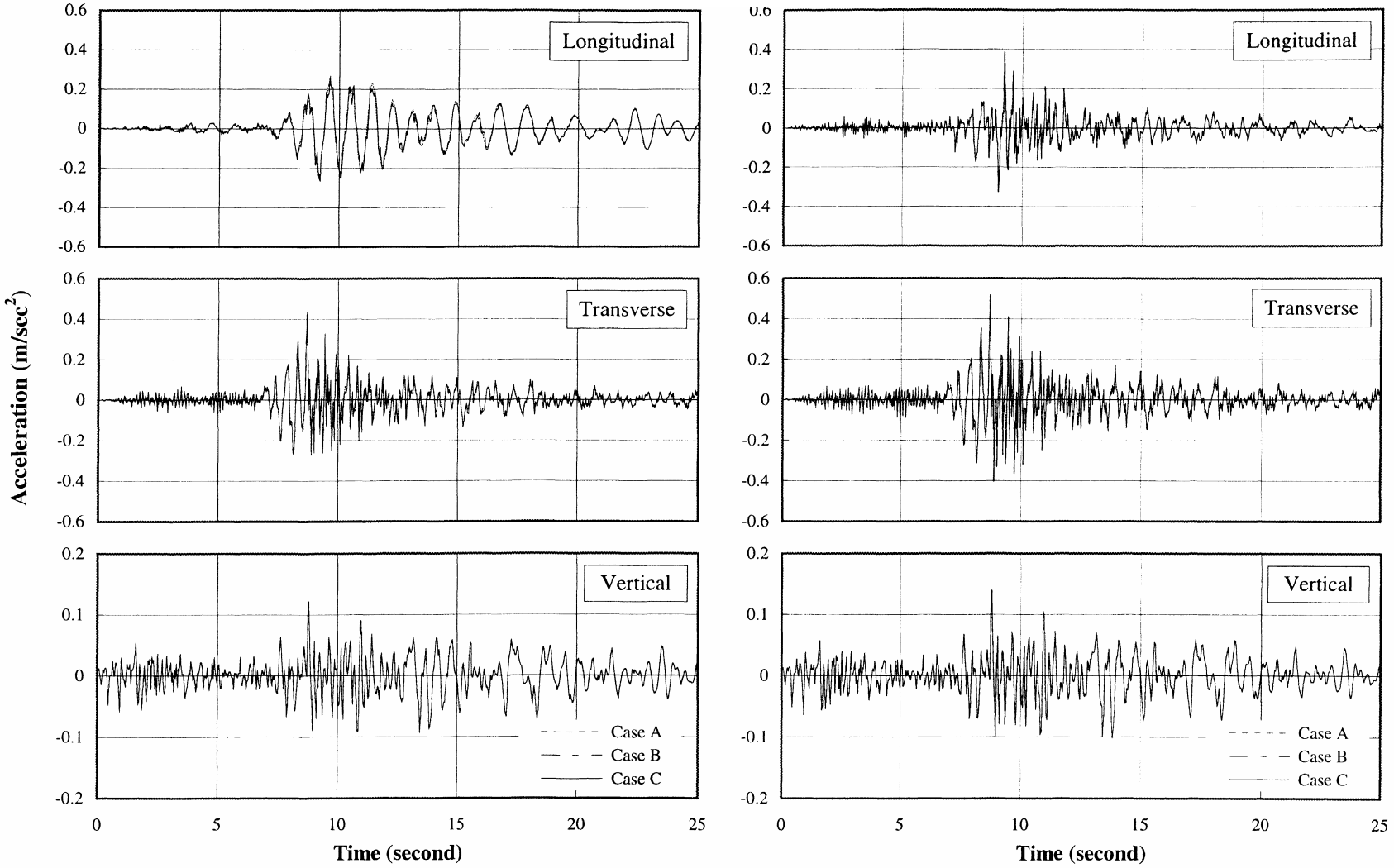

Figure 4.12. Computed Accelerations at (a) Bent Cap, and (b) Foundation of Pier 6 for Stiffer Soil Conditions.

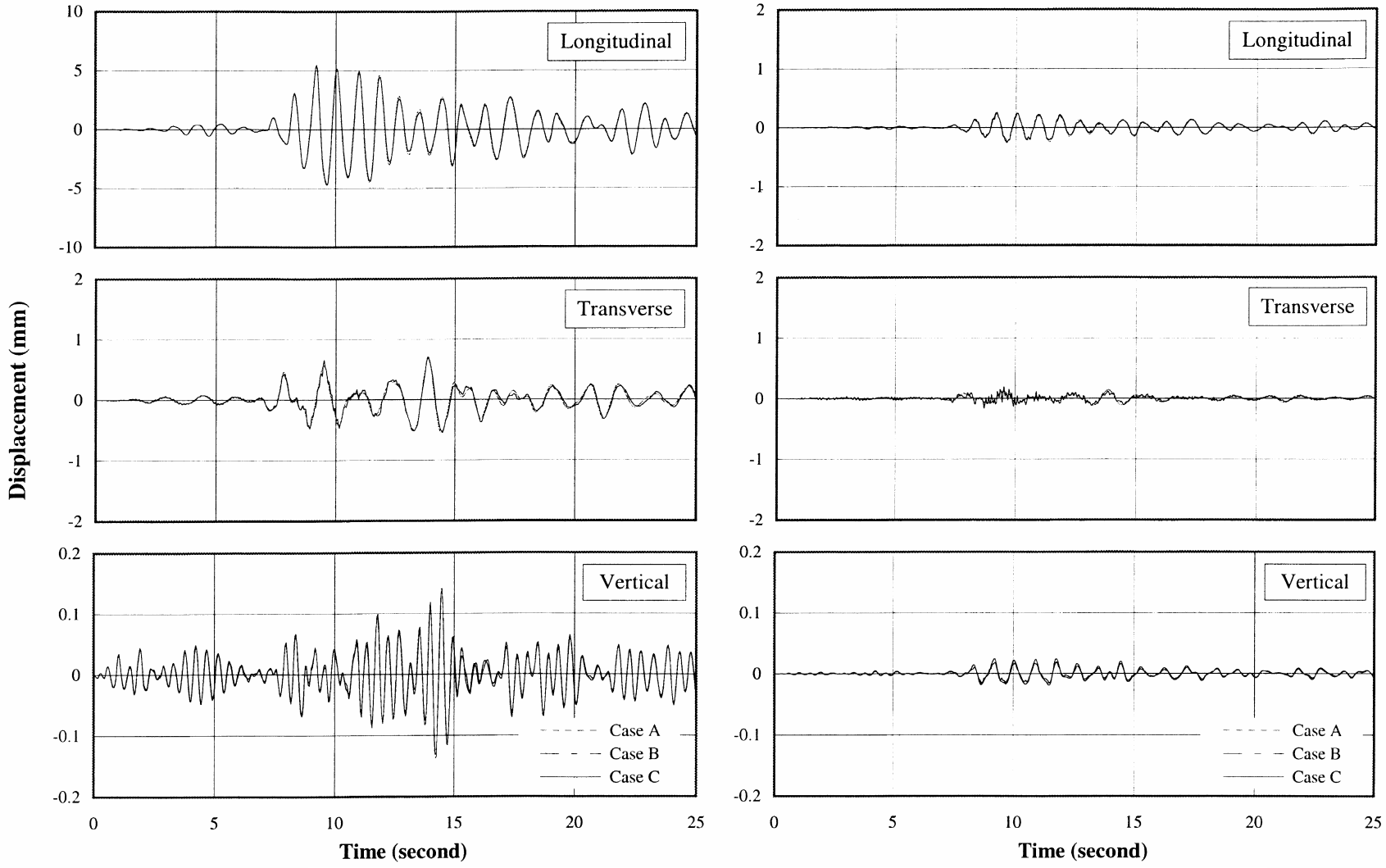

(a) Bent Cap (b) Foundation

Figure 4.13. Computed Displacement Responses at (a) Bent Cap, and (b) Foundation of Pier 6 for Stiffer Soil Conditions.

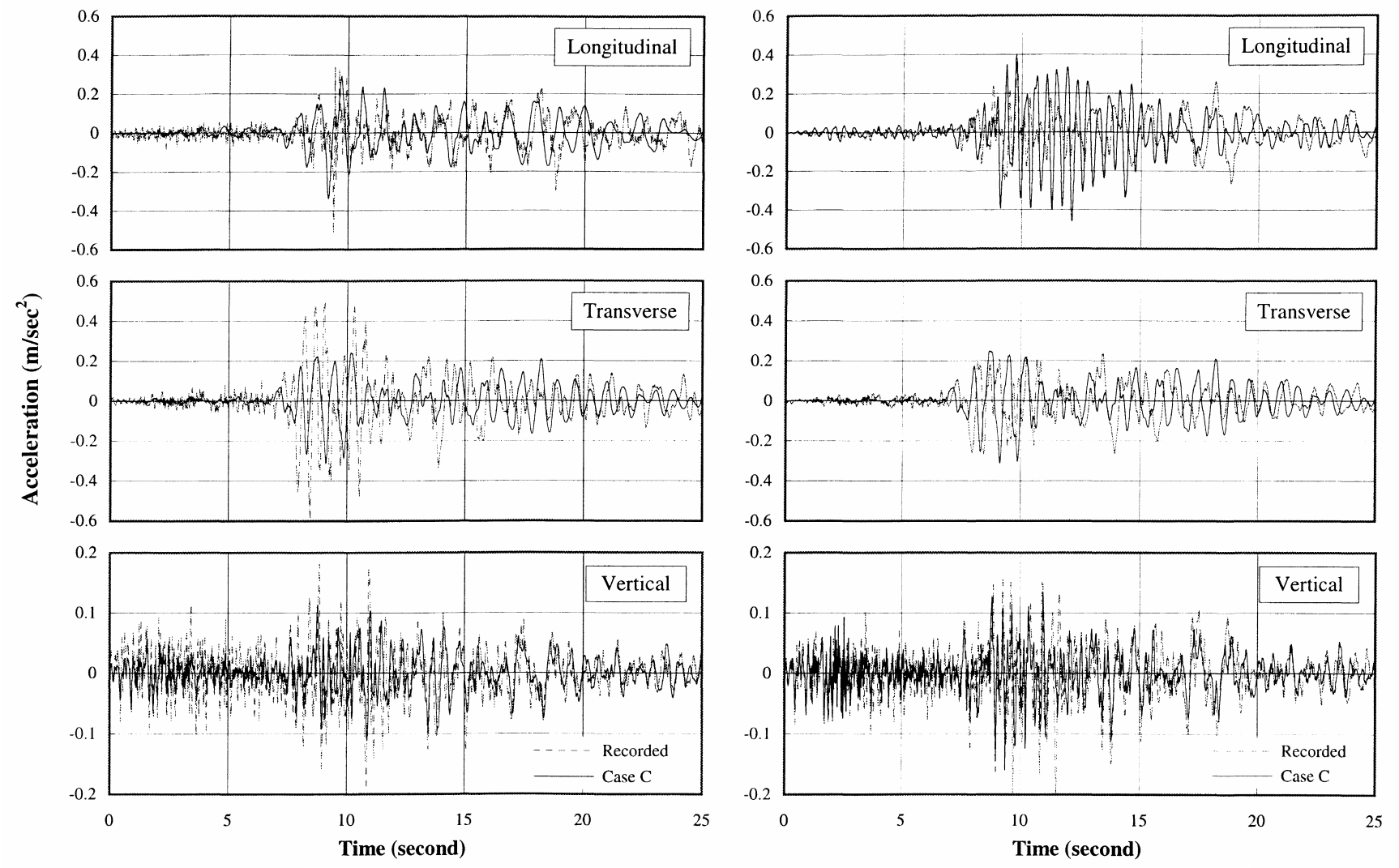

(a) Bent Cap (b) Foundation

Figure 4.14. Recorded and Computed Accelerations at (a) Bent Cap, and (b) Foundation of Pier 6.

CHAPTER 5

MODELING AND DYNAMIC ANALYSIS OF THE I-57 BRIDGE ACROSS THE MISSISSIPPI RIVER (THE CAIRO BRIDGE)

5.1 Introduction

Following the completion of Phase I of the Illinois Department of Transportation's Seismic Bridge Condition Survey in early 1991 in which bridges were ranked with respect to their potential for damage by an earthquake, six bridges with various sizes and types of construction were selected for further study in Phase II to determine preliminary seismic retrofit designs and cost estimates. Among these bridges, which were ranked within the top 20 highest risk bridges, was the bridge carrying Federal Aid Interstate Highway Route 57 over the Mississippi River at Cairo, Illinois [Anderson, Cooling and Gruendler (1994)].

Because of its long spans and highest potential for earthquake damage, the Interstate 57 Mississippi River Crossing Bridge (the Cairo Bridge) was chosen for detailed analysis and seismic performance evaluation in this study. Three-dimensional finite-element models are used for nonlinear time-history analyses of the entire bridge-foundation system. Several foundation models are used in this study including the fixed-base model, as well as the equivalent-linear and nonlinear soil spring models. In addition, the integrated soil-foundation-superstructure model of the entire bridge system is used for comparison. Since no recorded motions are available for a strong earthquake in the mid America, synthetic accelerograms are generated and site response analyses are conducted in this study to obtain the ground motions at the bridge site.

5.2 Location and Descriptions of the Bridge System

The bridge, carrying F.A.I. Route 57 over the Mississippi River at Cairo, spans across the Mississippi River, with its north abutment in Illinois and its south abutment in Missouri. Two approach structures lead into the main channel crossing. The main crossing consists of a three-continuous-span, truss-arch structure over main and auxiliary navigation channels (566 m), between Piers 9 and 12. The north approach consists of 9 spans of concrete deck supported on steel plate

girders between Piers 1 and 9 (506 m). The south approach is similar to the north approach but has only 5 spans of concrete deck supported on steel plate girders, between Piers 12 and 16 (174 m). Figure 5.1 shows an elevation view of the bridge including soil profile.

The bridge is founded on deep alluvial soil deposits with a thick layer of fine-grained soils (0-15 m thick) characterized as soft to firm low plasticity clay to clayey silt with occasional zones of fine sand. This alluvial is present beneath both bridge approaches and absent at the main river channel. Below this alluvium is a thick layer of dense to very dense clean sand and gravel (0-90 m thick). The $(N_1)_{60}$ values range from about 5 to over 40. These soil layers are underlain by a deposit of the Mississippi Embayment consisting of very dense, clayey sand, gravel and gravely clay. The Mississippi Embayment deposit is generally considered the uppermost bedrock formation in the Cairo area. The typical soil profiles under the approach (Pier 4) and main truss structures (Pier 10) are shown in Figure 5.2(a). The approximate shear wave velocity profiles from the ground surface to the bedrock are also shown in Figure 5.2(b). The preceding geotechnical information was provided by Illinois Department of Transportation (IDOT) and Illinois Geological Survey.

5.2.1 Approach Structures

The north approach consists of 9 spans (4@33.6 m, 3@47.3 m and 2@114.7 m) constructed of concrete deck acting in a composite manner with steel plate girders supported on the transverse bent cap of the piers. The south approach is of similar construction and consists of 5 spans (5@34.8 m). The typical deck system through approach spans provides for a 4-lane roadway (18.75 m wide) divided with a 1.05 m concrete median and with concrete parapets on both sides. The deck slab (21.6 cm thick) is constructed of a normal weight concrete (f'_c = 24 MPa) acting compositely with the steel girders.

The expansion joints are located at Piers 9 and 12 at the transition between the main truss and approach spans. The north approach has 2 links, one type of expansion joint, located at 1.5 m to the right of the center of Piers 4 and 7. The approach structures are supported on two types of bearings, classified as expansion and fixed bearings in Figure 5.3. The typical fixed and expansion bearings used throughout the bridge are about 0.6 m high except for Pier 8 at which the fixed bearings are 0.95 m high.

5.2.2 Main Channel Crossing

The main channel truss structure spans between Piers 9 and 12 consisting of two 158 m span and one 250 m span in the center between Piers 10 and 11. The truss members are joined together by the bolted-type connections. The typical deck system through the truss spans is constructed of reinforced concrete slab (21.6 cm thick) supported on 9 steel stringers with a spacing 1.5 m. The load from the truss is transferred to the piers by fixed bearings at Piers 10 and 11 and expansion bearings at Piers 9 and 12. The height of these bearings (Figure 5.4) is distinctive (1.17 m and 1.80 m high for expansion and fixed bearings, respectively).

5.2.3 Piers, Foundations and Abutments

The substructures of both approaches are of similar construction, consisting of reinforced concrete columns connected by spandrel beams except at Pier 8 where reinforced concrete diaphragm walls are integral with the columns throughout their length. Each pier of the approach structures is supported on a pile foundation. One of the typical piers for the approach structures (Pier 2) is shown in Figure 5.5. All pile foundations except the one supporting Pier 8 are composed of 0.3 to 0.35 m diameter cast-in-place reinforced concrete piles. The number of piles varies from 36 to 90. The foundation at Pier 8 consists of 192 steel H piles (12BP53). Some of these foundations also contain battered piles. The piles for all piers except Piers 6, 7 and 8 are completely embedded an average of 1.2 to 1.5 m in the thick layer clay. The foundations supporting Piers 6, 7 and 8 are also completely embedded about 2.5, 5.5 and 9.5 m, respectively, below ground surface. Descriptions of the foundation at each pier are given in Table 5.1.

For the main river crossing, the pier columns are connected by reinforced concrete spandrel beams and diaphragm walls from the top of the footing up to about two-thirds the height of the columns. The typical substructure for the main river crossing (Pier 10) is shown in Figure 5.6. The piers of the main channel crossing are supported on open-dredged caissons except Pier 12, which is supported on a pile group foundation. The north and south abutments are similarly constructed. They both are seat-type abutments supported on pile foundations.

Table 5.1. Descriptions of Foundations of the Cairo Bridge.

Pier	Pile Type	No. of Vertical Piles	Batter Piles		Pile Length (m)	Cap Dimensions			Depth to base* (m)
			No.	Slope (m/m)		L (m)	T (m)	H (m)	
Pier 1	CIPC	14	141 4	1:4 (+L) 1:4 (-L)	16.2	3.7	14.3	0.9	1.8
Pier 2	CIPC	36	0	-	17.7	3.2	15.9	0.8	1.2
Pier 3	CIPC	46	0	-	15.9	3.7	15.6	0.9	1.2
Pier 4	CIPC	40	0	-	12.5	3.7	15.6	0.9	1.2
Pier 5	CIPC	45	9 9	1:6 (+L) 1:6 (-L)	16.5	5.8	15.6	1.2	1.4
Pier 6	CIPC	45	9 9	1:6 (+L) 1:6 (-L)	11.9	5.8	15.6	1.2	2.4
Pier 7	CIPC	90	0	-	13.7	5.5	15.6	0.9	5.2
Pier 8	Steel 12BP53	160	16 16	1:6 (+L) 1:6 (-L)	22.2	11.5	15.0	1.8	9.5
Pier 12	CIPC	76	0	-	11.9	6.4	26.5	1.1	1.7
Pier 13	CIPC	49	0	-	11.3	4.6	15.6	0.9	1.8
Pier 14	CIPC	39	7 7	1:6 (+L) 1:6 (-L)	11.9	5.8	15.6	1.1	1.8
Pier 15	CIPC	39	7 7	1:6 (+L) 1:6 (-L)	11.6	5.8	15.6	1.1	2.3
Pier 16	CIPC	49	0	-	11.9	4.6	15.6	0.9	2.1

Notes:

1. For batter direction, +L = pile battered in longitudinal direction N or E,
   -L = pile battered in longitudinal direction S or W.
2. For pile cap dimension, L = longitudinal width, T = transverse width, and H = height.
   * denotes the depth from ground surface to base of the pile cap.
3. CIPC = cast in place concrete pile having a thin metal shell casting.
4. Piers 9, 10 and 11 are supported on open-dredged caisson.

5.3 Modeling of the Bridge Structure

An analytical model of the entire bridge was made to represent the structure as shown on as-built construction drawings provided by IDOT. To account for cracking of concrete, the flexural stiffness of pier columns and walls was determined using 50% of the gross EI, while 75% of the gross EI was used for the deck as recommended by ATC-32 (1996). The shear stiffness was based on the shape of the cross section according to established principles of mechanics of materials and was not reduced. The overall three-dimensional (3-D) model of the bridge and the global coordinate system are shown in Figure 5.7. The bridge model consists of approximately 3,410 frame elements and 38 shell elements altogether forming 9,454 degrees-of-freedom. The modeling techniques and major assumptions used in modeling of the bridge are discussed below.

5.3.1 Bridge Deck System

The bridge floor system consists of reinforced concrete deck acting compositely with 7 welded steel plate girders in the approach spans and with 9 steel plate girders in the main channel crossing. The girders are modeled using 3-D beam elements which are connected transversely by equally spaced crossing beam elements forming as a grid model. The grid model is preferable because it represents the overall characteristics of the bridge deck system with good accuracy and requires less computational time and effort than models using shell elements.

Attempts were made to simplify the modeling of the bridge deck system by using one-dimensional (1-D) longitudinal beam elements with the lumped mass at both ends of each transverse beam that is rigidly connected to the longitudinal beams (Figure 5.8). The comparison study is also conducted to investigate the effects of superstructure modeling on the overall dynamic characteristics of the bridge. It is found that the dynamic characteristics obtained from the 1-D beam model are greatly different from those obtained from the 3-D grid model, especially the torsional modes of vibration. Several unrealistic mode shapes are observed for the 1-D beam model such as the independent rotations of the transverse beam about all three principal directions, especially about the longitudinal axis (torsion). A system identification method or optimization

method may be used to obtain appropriate member properties (e.g., torsional rigidity of the longitudinal beams) to better capture the dynamic characteristics for the 1-D beam model. However, it is beyond the scope of the research study. As a result, the 3-D grid model is used to represent the bridge deck system for the following study.

5.3.2 Truss-Arch Structure

The main truss members are modeled by frame elements with the connections assumed to be rigid. Due to the stiffening effect caused by the bolted gusset plate connections and overlap of cross sections at the connection, an analysis based upon the centerline-to-centerline geometry of the members is likely to be too flexible. This stiffening effect was taken into account by using a rigid-end factor, which is defined as the length fraction of each end offset assumed to be rigid for bending and shear deformation. The value of rigid-end factor, which gives the fraction of each end offset, is specified equal to 0.85. The mass contributed by the frame element is lumped at each joint and applied to each of the three translational degrees of freedom (U_x, U_y and U_z). The total mass is apportioned to the two joints in the same way a similarly distributed transverse load would cause reactions at the ends of a simply supported beam.

5.3.3 Expansion Joint and Links

Expansion joints are located at Piers 9 and 12 at the transition between the main truss and approach spans. Calculation based on the as-built drawings with an assumption of 50°F ambient conditions indicates that the allowable expansion is +/- 0.29 m (11.5 in). In the 3-D model, the adjoining members at each side of the expansion joints were modeled as separate members connected by nonlinear gap elements. Links are located at 1.5 m to the right of the center of Piers 4 and 7. The maximum allowable rotation about horizontal y-axis is about +/- 0.147 radian and longitudinal translation is about 0.10 m (4.25 in). The gapping behavior of the joints as described above was modeled using nonlinear gap elements. An example of the idealized force-displacement relationship for the expansion joints is illustrated in Figure 5.9(a).

5.3.4 Steel Bearings

Fixed and expansion steel bearings are used throughout the bridge. The bearings were modeled in such a way that the fixed bearings could rotate and the expansion bearings could both translate and rotate within the allowable limits in the longitudinal direction. They were pinned against

transverse movements. Of particular interest are the bearings at the main truss structure (Figure 5.4). The size of these bearings is enormous, as they are required to support such a massive truss-arch structure. A careful consideration is needed to model these bearings.

From the as-built drawings furnished by IDOT, it is found that, at the main truss structure, the allowable rotation, which is defined as the rotation that can take place freely, is +/- 0.192 radian and +/- 0.250 radian for the fixed bearings and expansion (rocker) bearings, respectively. Similarly, the allowable expansion, defined as the longitudinal translation that can take place freely after which the bearings become stiff, is +/- 0.23 m (8.9 in) for the expansion bearings. These values, used in the analyses, were determined according to the as-built drawings with an assumption of 50°F ambient conditions.

The gapping and stiffening behavior of the bearings as described above is somewhat similar to that of the expansion joint except that both gap (compression only) and hook (tension only) elements are used to simulate the behavior of the bearings in the longitudinal direction. The stiffening of rotation of the fixed bearing is calculated approximately from the axial stiffness of the bearing. The stiffening of longitudinal displacement of the expansion bearing is calculated based on the stiffness of the internal (50-mm diameter) bolts. In the transverse and vertical direction, the behavior of the bearings is modeled by a beam element whose axial and flexural stiffness is computed from the stiffness of the bearings. The idealized force-displacement relationship of expansion bearings is shown in Figure 5.9(b).

5.3.5 Piers and Abutments

The piers are modeled by frame elements for the reinforced concrete columns and spandrel beams and by shell elements for the diaphragm walls. The pile cap is modeled using relatively rigid frame elements for the modeling cases in which the foundations are modeled using a set of linear or nonlinear springs attached at the centroid of the pile cap. The mass of the pile caps is also included in these cases. For a detailed foundation model, the pile cap is modeled using shell elements. Since the abutments are not integral to the bridge structure, they are not considered in modeling of the bridge, the support conditions at each end of the bridge is modeled according to the characteristics of the bearings supporting the girders.

5.4 Modeling of the Bridge Foundation

Six different foundation-modeling cases are studied. The first case is the fixed-base model. In the next 3 cases, the foundations are represented by the equivalent linear springs computed from different modeling approaches; (1) beam embedded in elastic continuum soil medium, (2) beam on inelastic foundation approach and (3) beam embedded in linear viscoelastic soil medium (dynamic impedance). The nonlinear springs determined from the proposed pile foundation model are used in modeling Case 5. In Case 6, the proposed pile foundation models are integrated with the bridge superstructure model into the complete global soil-foundation-structure model. Note that the fixed conditions are assumed for modeling of the open-dredged caissons supporting the main river crossing for all cases.

5.4.1 Case 1: The Fixed-Base Model

The first model is the bridge model in which the support conditions are assumed to be fixed for all degrees of freedom. The fixed-base model is used to evaluate effects of the foundation modeling on behavior of the bridge superstructure and also serve as a comparison case for more detailed Soil-Structure Interaction analyses.

5.4.2 Case 2: Beam Embedded in Elastic Continuum Approach

The primary assumption of this analytical approach is that the soil in which the pile is embedded is an ideal infinite elastic material as schematically illustrated in Figure 5.10. A large number of charts and closed-form expressions for estimating the displacements of the loaded piles corresponding to various distributions of soil modulus are available. The soil profile conditions are commonly represented by three soil modulus distributions as shown in Figure 5.10;

1 ***Constant soil modulus with depth*** representing the stiff, overconsolidated homogeneous clay; closed-form solutions provided by Poulos and Davis (1980) and Davies and Budhu (1986).

2 ***Parabolic variation of soil modulus with depth*** representing the cohesionless soil at small strain; closed-form solutions provided by Novak and Aboul-Ella (1978a, 1978b), Gazetas and Dobry (1984), and Gazetas and Makris (1991).

3 ***Linear variation of soil modulus with depth*** representing the soft normally consolidated clay and the cohesionless soil at moderate strain level; closed-form solutions provided by Poulos and Davis (1980), and Budhu and Davies (1987, 1988).

Since the soil condition at the Cairo site is predominantly medium to dense sand, the linear variation of soil modulus with depth is representative for this site. The linear variation of soil modulus can be reasonably used for the case in which the pile head is located at some justifiable distance (say 0-1.5 m) below ground surface. This is the case for most of the bridge foundations except for the foundation supporting Piers 6, 7 and 8 for which the embedment depth of the foundation below the ground surface is fairly large. In such case, the linear distribution of soil modulus may not be applicable for calculating the lateral stiffness of the pile since the significant lateral soil resisting zone is usually confined to a depth of 5 to 10 pile diameters form the pile head. The constant soil modulus may be best used to describe the properties of the soil in which the pile is embedded. Consequently, the embedment effect is taken into account by using the constant distribution of soil modulus whose value is equal to an average of Young's modulus of the soil over top 5 pile diameters of the pile length from the embedded pile head.

For linear variation, a coefficient of variation is obtained corresponding to the values recommended by Terzaghi (1955) and O'Neill and Murchison (1983) for sand and those recommended by Lam et al. (1991) for clay. These recommended subgrade modulus coefficients correspond to the pile head stiffness at the deflection of between 5 and 50 mm.

The stiffness of the pile foundations is computed according to a proposal by Lam and Martin (1986), included in the Seismic Design Guidelines for Highway Bridge (Federal Highway Administration, FHWA) and recommended by the American Association of State Highway and Transportation Officials (AASHTO). The equivalent-linear stiffness of each pile is calculated based on the estimated soil modulus according to an assumed level of shaking, which shall be checked against values obtained from the response-history analysis for verification. The stiffness matrices of single piles are then statically condensed to the foundation-structure-interface node to develop a 6x6-stiffness matrix for a pile group using basic matrix operations.

The pile group effects are accounted for by applying the interaction-factor method originally introduced by Poulos (1968). The static interaction factor method has been shown by a number of researchers to yield reasonable predictions of stiffness for small or typical pile group foundations (less than 50 piles in a group) during earthquake shaking. This method employs the Mindlin solution to evaluate the response of a point within the interior of a semi-infinite linearly elastic isotropic homogeneous mass (half space mass) as a result of the application of a harmonic or impulse load at another point in the half space mass. In other words, the interaction factors are to quantify the

effects of movement caused by an adjacent pile (i.e., the application of load to one pile cause the movement of the adjacent piles). The interaction factor is defined (Poulos and Davis, 1980) by:

[5.1] $$\alpha = \frac{\text{Movement caused by unit action on an adjacent pile}}{\text{Movement of the pile under unit head action}}$$

The superposition is then used to incorporate the stiffness of single piles modified by interaction factors into the pile group stiffness. As an example, the following expression is used to calculate the vertical stiffness (K_{VG}) of a pile group having n piles.

[5.2] $$K_{VG-n} = K_V \left(\sum_{i=1}^{n} \left(\frac{1}{\sum_{i=1}^{n} \alpha_{vij}} \right) \right)$$

where

K_V = vertical stiffness of an isolated pile,

α_{vij} = vertical interaction factor between pile i and pile j.

Several investigators provide a number of charts from which the interaction factors can be obtained. Alternatively, Randolph and Wroth (1979), and Randolph (1981) provided a set of simple expressions for estimating the interaction factors which is adopted in this study. A computer program was written for calculating the pile group stiffness based on the above-mentioned concepts.

The pile group stiffness matrices are then integrated with the bridge superstructure model at the base of the piers. The iteration process is performed to ensure the compatibility between the assumed and computed level of displacement. The pile group stiffness is computed corresponding to the initially estimated level of displacement and soil modulus. To verify this initially estimated soil modulus, the computed displacements at the base of the pier are compared with the assumed displacements. The determination of the pile group stiffness and the seismic analysis were repeated with the appropriately adjusted soil properties until the convergence between the assumed and computed displacements within an acceptable tolerance was reached.

5.4.3 Case 3: Beam on Inelastic Foundation Approach

The beam on inelastic foundation approach is widely used and accepted in practice to determine the pile head stiffness. One of the most well known computer programs that incorporate this approach is the COM624 program (Analysis of Stresses and Deflections for Laterally Loaded Piles, Reese and Sullivan, 1980) which is recommended by AASHTO. The concept of this approach is schematically illustrated in Figure 5.11. More details regarding the method of analysis implemented in this program can be found elsewhere and thus are not presented. In this study, the COM624 program is used to determine secant pile-head stiffness for different levels of pile-head deflections in both lateral and rotational directions. The vertical stiffness is taken similar to that obtained from the elastic continuum approach. These stiffness coefficients of each pile are then statically condensed into the 6x6 stiffness matrix of the pile group. Similar procedures to those used in Case 1 are repeated for the determination of the pile group stiffness. The embedment effect is also taken into consideration, and similar to Case 2, the static interaction factor method is used to account for the PSPI effects.

5.4.4 Case 4: Beam Embedded in Linear Viscoelastic Soil Medium Approach (Dynamic Impedance)

This analytical approach is based on a plane strain model to derive the frequency-dependent response of a pile embedded in an infinite linear viscoelastic soil medium. The fundamental concept of this approach is fairly similar to that of the beam embedded in elastic continuum approach except for the different applications of loading (static versus dynamic) and the different characterization of the soil properties. Several researchers have employed this analytical approach and come up with a number of ready-to-use, non-dimensional graphs for evaluating dynamic stiffness of the single pile. Alternatively used in this study is a set of closed-form expressions for estimating the impedance (dynamic stiffness and damping coefficients) of a single pile given by Gazetas (1991). The dynamic stiffness of a pile group is then computed using the same superposition method suggested by Lam and Martin (1986) for the static loading.

This superposition method was validated to be applicable for the dynamic loading by several investigators (Kaynia and Kausel, 1982, Sanchez-Salinero, 1983, Roesset, 1984 and Gazetas et al., 1991). However, it should be noted that this superposition method could be used with confidence for small to typical pile groups (less than 50 piles in a group). In determination of the dynamic interaction factors, expressions given by Makris and Gazetas (1992) for vertical interaction and by

Gazetas (1991) for horizontal interaction are used. More details of derivation of these expressions can be found in the above-mentioned literature and thus are not repeated. Samples of the expressions used for predicting the dynamic stiffness of the pile foundations of the Cairo Bridge are presented below.

For dynamic stiffness ($\overline{K}$) and damping coefficients (C) defining the dynamic impedance ($\overline{K} = K + i\omega C$) for flexible piles embedded in a homogeneous soil, Gazetas (1991) gives the following expressions.

For vertical impedance,

[5.3] $$K_V = 1.9 G_s D_p \left(L/D_p\right)^{2/3},$$

[5.4] $$C_V = (3/2) a_0^{-0.2} \rho_s V_s \pi L D_p \rho_d \qquad \text{for } \omega > 1.5\omega_s$$
$$= 0 \qquad \text{for } \omega \le \omega_s.$$

For lateral impedance,

[5.5] $$K_L = D_p E_s \left(E_p/E_s\right)^{0.21},$$

[5.6] $$C_L = D_p E_s \left(E_p/E_s\right)^{0.21} \left[1.6\, b/\omega + 0.35 D_p \left(E_p/E_s\right)^{0.17} V_s^{-1}\right] \qquad \text{for } \omega > \omega_s$$

[5.7] $$C_L = 1.6 (b/\omega) D_p E_s \left(E_p/E_s\right)^{0.21} \qquad \text{for } \omega \le \omega_s.$$

For vertical dynamic interaction factor, Makris and Gazetas (1992) give,

[5.8] $$a_V = \left(\frac{2s}{D_p}\right)^{-0.5} \left(e^{-b\omega s/V_s}\right)\left(e^{-i\omega s/V_s}\right).$$

For lateral and rotational interaction, Gazetas (1991) suggests the following expressions,

[5.9] $$a_L\left(90^0\right) = 3a_V/4,$$

[5.10] $$a_L\left(0^0\right) = 0.5\left(\frac{s}{D_p}\right)^{-0.5} \left(e^{-b\omega s/V_{La}}\right)\left(e^{-i\omega s/V_{Las}}\right),$$

[5.11] $$a_L(\theta) = a_L\left(0^0\right)\cos^2\theta + a_L\left(90^0\right)\sin^2\theta,$$

[5.12] $$a_{RL} \approx 0, \quad a_{RR} \approx 0.$$

where

a_0 = dimensionless frequency, $w r_0/V_s$,

D_p = diameter of the pile,

E_p = Young's modulus of the pile,

E_s = Young's modulus of the soil,

G_s = shear modulus of the soil,

L = length of the pile,

r_d = $1-e^{1.5(E_s/E_p)(L/d)^{-2}}$,

s = spacing between piles in a group,

V_{La} = average of the shear wave velocity over the depth of soil layer;

$V_{La} = 3.4V_s/\pi(1\text{-}n_s)$,

V_s = shear wave velocity of the soil,

b = damping of the soil,

n_s = Poisson's ratio of the soil,

w_s = $(\pi/2)V_s/H$: H is the soil layer thickness,

w = frequency of the input motion,

r_s = density of the soil.

The real and imaginary components of the impedances of each pile group are plotted against frequency (Hz) in Figure 5.12 for Pier 1 (14 vertical and 28 batter piles), Pier 2 (36 vertical piles), and Pier 16 (49 vertical piles). The plots show a slight variation of the stiffness (real part of the impedance) over the interested range of frequency (1-10 Hz) for vertical and lateral stiffness (K_z, K_x and K_y). It is also observed that the dynamic stiffness at low frequencies varies very little from the static stiffness. At higher frequencies, the dynamic stiffness of the pile group appears to decrease more rapidly as the number of piles in the group increases. As can be expected, the imaginary part of these impedances increases with increasing loading frequency.

In time-domain analyses, only frequency- or time-independent stiffness and damping parameters can be used. Therefore, the equivalent dynamic stiffness is chosen as the dynamic stiffness corresponding to the dominant dimensionless frequency which is computed from the characteristic frequency of the earthquake loading typically between 0.1-10 Hz (about 1 Hz and 2.4 Hz for the adopted input ground motions). Corresponding to the dominant frequency of the input acceleration

histories, the equivalent dynamic stiffness coefficients for each pile foundation can be computed for all six degrees of freedom.

5.4.5 Case 5: The Proposed Foundation Model

The proposed pile group model is used to determine the nonlinear response of the pile group foundations. Each pile in the group is modeled using 10 frame elements increasing in length with depth. The soil surrounding the pile is represented by a series of nonlinear springs in the vertical and lateral directions. The pile cap is modeled using shell elements. The pile group effects are taken into account by using *t-* and *p-*multipliers to soften the stiffness and reduce the ultimate capacity of the load transfer curves in both vertical and lateral directions. Details of modeling concepts of the single piles and pile groups were discussed in Chapters 2 and 3. A sample of the pile foundation model for Pier 7 is shown in Figure 5.13.

It is noteworthy that one advantage of using the proposed model over the traditionally used static superposition method in which the stiffness of all piles is condensed into one 6x6 stiffness at the centroid of the foundation is that the application of loads induced by the bridge superstructure to its foundation is more realistically simulated according to how the foundation is integrated with the pier columns. In addition, the soil nonlinearity can be handled directly and the mode of failure (e.g., progressive failure), which is present in most cases, can be realistically captured using the proposed model.

These nonlinear load-deformation relationships can as well be used to avoid a perplexity of selecting a representative secant stiffness which requires an iterative process so that the chosen stiffness would be compatible to the deflection level. The load-deflection and moment-rotation characteristics of selected pile foundations (Piers 1, 2 and 16) are shown in Figure 5.14. These nonlinear load-deformation relationships are used in the dynamic analysis for subsequent seismic performance evaluation of the Cairo Bridge. From these nonlinear relationships, the equivalent linear stiffness is selected at a displacement level of 15 mm and 25 mm as an upper bound for vertical and lateral stiffness, respectively. The equivalent linear rotational stiffness is specified as the secant stiffness at the rotations which induce the vertical displacement of the outermost pile of 25 mm and 12.5 mm for the rotational response about x and y axes, and the lateral displacement of 25 mm for the torsional response about z axis. For instance, the corresponding rotations for Pier 2 are equal to 0.010 radian for rotation about the x axis, 0.016 radian for rotation about the y axis, and

0.004 radian for rotation about the z axis. The equivalent linear stiffness coefficients will be used in the subsequent comparison study.

5.4.6 Case 6: The Integrated Soil-Foundation-Structure Model

The proposed pile foundation models are integrated with the bridge superstructure model into the complete global model as shown in Figure 5.15. This integrated model is used in nonlinear time-history analysis performed using the SAP2000 program. This integration allows the response of the entire bridge system including its foundation to be concurrently obtained in one analysis.

The nonlinear time-history analyses of the bridge model in which the soil surrounding the pile is modeled by nonlinear elements requires a large amount of computational time and effort and some of them may not be achievable using currently available computer analysis programs. In this study, an attempt was made to perform the nonlinear time-history analysis of the Cairo Bridge having the total of 10,266 frame elements, 751 shell elements and 5,984 nonlinear elements (44 for bearings and expansion joints and 5,940 for the soil model). The analysis could not be successfully completed using the current version of the SAP2000 Nonlinear program.

Two alternatives are considered; one is to reduce the number of the nonlinear elements for the soil model. Based on the assumption that the soil nonlinearity is expected to concentrate only at the uppermost soil layer over the depth of about 5 diameters of the pile, the number of nonlinear elements used to model the soil is reduced to 1,320 elements. The nonlinear time-history analysis of this bridge model was successfully accomplished. However, it should be noted that the larger the size of the model, the smaller the number of the modes of vibration that can be included in the analysis, and the less accurate the results. In this analysis, only 30 modes of vibration can be included. These modes include less than 70% of total mass of the bridge. The percentage of the total mass of the structure to be included in the analysis is one of several criteria that can be used to evaluate the accuracy of the results. In general, it is required that at least 90% of the total mass of the structure should be included in the analysis. More details on this subject can be found in Section 5.6; dynamic analysis of the bridge. Since the requirement of the participating mass ratio is not satisfied and only a few modes can be included in the nonlinear time-histories analysis, this model is disregarded.

The other alternative is to model the nonlinear characteristics of the soil using the equivalent linear soil springs. By eliminating a number of nonlinear elements associated with the soil modeling,

the required computational time and effort in performing the nonlinear time-history analysis is reduced substantially. The analytical results using this model are found to be satisfactory (i.e., over 98 % of the total mass of the bridge is included for all principal directions). The PSPI effects are accounted by reducing the stiffness of the soil springs by 25%. This number is partly based on the reduction of the secant stiffness of the nonlinear load-transfer curves of the soil reactions to account for the PSPI. The analytical results obtained from these detailed soil-foundation-structure models serve as a reference case in the subsequent study. Required in performing time-history analysis are the input ground motions which can be obtained through site response analysis described below.

5.5 Site Response Analysis and Input Ground Motions

Since the magnitude 8 earthquakes that had occurred in the Midwest region (1811 and 1812) predated the development of modern seismological instruments, no recorded accelerograms from such strong earthquakes are available. As a result, synthetic accelerograms (Hwang, 1998) as a function of the moment magnitude and epicentral distance are chosen to be used in the investigation. Since the bridge is located approximately 40 km. north-east from the New Madrid seismic zone, motions corresponding to a moment magnitude of 7.5 and epicentral distance of 40 km. were used as outcrop motions (Figure 5.16) in the site response analyses. The shear wave velocity of the top rock layer was assumed to be 1 km/s (3,300 ft/s).

The bridge is located over deep alluvial soil deposits with a thick layer of soft to stiff clay soils near the ground surface. For this soil profile, the bedrock motions are expected to be modified by the soft soil deposits resulting in lower frequency motions at ground surface which are believed to be critical for long period structures primarily long-span bridges. To account for such matter, site response analyses were performed for several soil profiles to determine reasonable bounds on the expected soil profile at different locations using the computer program SHAKE91 (Idriss and Sun, 1992). A schematic illustration of the site response analysis conducted in this study is shown in Figure 5.17.

Due to wave scattering or kinematic interaction effects, the support motions are generally different from the free-field motions. Nonetheless, a number of studies manifest that the foundation-input motions can be approximately considered equal to the free-field motions based upon the concept that the effects of the presence of the pile foundation on the support motions or

seismic wave scattering are expected to be insignificant if the dominant seismic wave lengths are much larger than the horizontal dimension of the foundations (Fenves et al., 1992).

At the Cairo area, the approximate shear wave velocity of the soil layer in which the pile foundations are embedded is 183 m/s (600 ft/s) and a typical length of the pile foundation is 18.3 m (60 ft) resulting in the prediction that wave scattering effects are important for periods of vibration less than 0.1 sec. Since this vibration period is small enough that wave scattering effects can be neglected for this structure, the free-field motions were used as the input motions to the bridge system. In addition, it is generally believed that the kinematic interaction is less significant than the inertial effects (i.e., the effects of dynamic response of the structural-foundation system on the movement of the supporting soil).

As a result of the site response analyses, three components of ground motions are used. Two horizontal components of the synthetic ground motions have a peak acceleration of about 0.7g. The vertical component is arbitrarily generated by scaling down the longitudinal component of the input ground motions by 30%. Therefore, the vertical component has a peak acceleration of about 0.5g. Three components of the input acceleration time histories are shown in Figure 5.18(a). The Fourier transform spectra of these histories over a frequency range of 0-15 Hz are shown in Figure 5.18(b). These Fourier spectra consist of several sharp spikes over a wide range of frequency (0.5-4.0 Hz) over which the longitudinal and transverse components of the input motions have the largest peak at the frequency of about 2.4 and 1.0 Hz or the period of about 0.4 and 1.0 second, respectively. Similar observations can be taken from the plots of the response spectra of the input motions (Figure 5.19(a)).

Also plotted in Figure 5.19(a) are the response spectra for 5% damping ratio obtained according to the NEHRP Guidelines for Seismic Rehabilitation of Buildings (FEMA-273) with the ground motions from National Seismic Hazard Mapping Project by the U.S. Geological Survey (USGS) for 50%, 10%, 5% and 2% probability of exceedance in 50 years. The response spectra of the input motions fall between those for hazards with 2% and 5% in 50 years exceedance probabilities (closer to 5% in 50 year ground motions hazards). These input motions may be considered as equivalent motions representing the 4%/50 year hazard level.

In addition to the input motions obtained from the site response analysis, three sets of input motions are generated for seismic performance evaluation of the Cairo Bridge for equivalent hazard levels of 50%, 10% and 2% probability of exceedance in 50 years or corresponding return periods

of 73, 475 and 2,475 years. These motions are obtained by scaling the original motions to match the response spectrum of the ground motions representing different hazard levels. The least sum of the square of the difference technique is used to calculate the appropriate multiplier factors to be applied to the original input motions to obtain the equivalent motions for all hazard levels over the range of the periods that is of importance for the dynamic response of the bridge (0.6 and 3.0 seconds). For the longitudinal motion, these factors are equal to 0.04, 0.29 and 2.36, and corresponding peak accelerations are about 0.03g, 0.20g and 1.65g for 50%/50, 10%/50 and 2%/50 year hazard levels, respectively. For the transverse motion, these factors are 0.04, 0.29 and 2.28, in the order previously given. The vertical motion is obtained by scaling down the longitudinal motion by a factor of 0.7. Figure 5.19(b) shows the response spectra of the modified input motions.

In conclusion, fours sets of input motions are used in the following study. The first set obtained from site response analysis (Figure 5.18) is used in comparison and parametric studies on the effects of foundation modeling on dynamic characteristics and seismic behavior of the bridge. This first set is also used for seismic performance evaluation of the bridge for the intensity of the excitation approximately corresponding to the ground motion having 4% probability of exceedance in 50 years (4%/50 year) or the return period of 1,225 years. For different excitation intensities, three additional sets of the input motions which are obtained comparable to ground motions representing the 50%/50, 10%/50 and 2%/50 year hazards are used for seismic performance evaluation of the bridge.

These motions are applied uniformly throughout the bridge during analysis. One can qualitatively argue that the uniform support motions are not appropriate for long span bridges. However, a rigorous 3-D nonlinear time-history analysis of the long-span bridge with multiple support excitations is a formidable task that goes beyond the objectives of the research projects. As a reference case, the results of the extensive nonlinear time-history analyses performed in this study can very well be used for a more rigorous analysis including the multiple support excitations in the future research. In addition, the motions from an earthquake occurring at the assumed location will be propagating mainly vertically, so there will not be a great difference in motions at each support.

5.6 Dynamic Analysis of the Bridge

There are several approaches for nonlinear time-history analysis of structures. The one implemented in the SAP2000 program used in this study is the Fast Nonlinear Analysis (FNA)

method developed by Ibrahimbegovic and Wilson (1989). This method is designed to be used for structural systems which are primarily linear elastic with a limited number of nonlinear elements. The FNA method is basically a combination of mode superposition and incremental (step-by-step integration) methods. Unlike the step-by-step integration method, the FNA uses constant stiffness iteration and load-dependent Ritz vectors to capture the behavior of the nonlinear elements. The main concept is to calculate the nonlinear modal forces using the load-dependent vectors and to treat them as the applied forces on the right-hand side of the nonlinear modal equations of motion instead of using the nonlinear stiffness matrix, which is on the left-hand side of the equation. This concept can therefore reduce the size of the modal equations to be solved at each time step. The iteration is required to obtain the solution of all modal equations at any time step. More details can be found in Wilson (1997).

The load-dependent Ritz vectors generated from the inertial loads of the structures as well as the nonlinear degrees of freedom provides not only a good representation of the response but also a realistic capture of the behavior of the nonlinear elements. This is because they directly include the modes of deformation contributing to the dynamic response of the structures. More than 300 modes of vibration are used in the nonlinear time-history analyses of the Cairo Bridge. Among these are three modes which are generated from ***static correction*** vectors for three directions (U_x, U_y and U_z). The static correction method is based upon the concept that the response in high frequency modes is essentially static and therefore the static correction vectors can be used to approximately represent high frequency modes that are not included in the analysis.

These modes include over 98% of the total mass of the structure for all principal directions. This percentage actually expresses the cumulative sums of the participating mass ratios for all modes. The participation mass ratios (r) for any mode i is corresponding to acceleration loads in the global X, Y and Z directions are given by:

[5.16] $$r_{xi} = \frac{\left(\boldsymbol{j}_i^T m_x\right)^2}{M_x},$$

[5.17] $$r_{yi} = \frac{\left(\boldsymbol{j}_i^T m_y\right)^2}{M_y},$$

[5.18] $$r_{zi} = \frac{\left(\boldsymbol{j}_i^T m_z\right)^2}{M_z},$$

where

ϕ_i^T = transpose of the mode shape i,

m_x, m_y, m_z = unit acceleration loads,

M_x, M_y, M_z = total unrestrained masses acting in X, Y and Z directions.

More details on the definition of the modal participation mass ratio can be acquired in the SAP2000 manual, Volume II. This participation mass ratio provides a simple means to determine the number of modes of vibration that is required to achieve a given level of accuracy for ground acceleration loadings. Several Building Codes require at least 90% of the participating mass to be included in the calculation of response for each principal horizontal direction. The number of modes of vibration used in this study adequately satisfies this requirement.

The load-dependent Ritz-vector analysis has several advantages over the eigenvector analysis mainly because it requires less computational time and effort and it can capture the spatial distribution of the dynamic loading as well as the static correction due to the higher mode truncation. It should be noted, however, the Ritz-vector modes do not represent the intrinsic characteristics of the structure in the way the natural modes do. The Ritz-vector modes are still considered as approximations to the eigenvector modes of the system. The approximate results are generally more accurate for the lower modes and gradually deteriorate for the higher modes.

As a result, the number of Ritz vectors included in the analysis should be sufficient to accurately capture the desired number of natural modes. In order to eliminate any uncertainty of using different numbers of modes in determining the dynamic characteristics of the bridge, the number of 300 modes is specified for all modeling cases. Note that the number of modes used in the nonlinear time-history dynamic analysis may be less than 300 depending on the size of the model. However, by applying the static correction method, the participating mass ratio is maintained over 98% for all analysis cases.

5.6.1 Specification of Damping

One of the most difficult issues in an earthquake analysis is the estimation of energy dissipation of soil-structure systems. Sources of energy dissipation may be from material damping in structures (cracking of concrete and yielding of steel), and material and radiation damping in soil deposits. The specification of damping can be divided into two categories; classical and nonclassical damping. The classical damping is appropriate for the system that is constructed of similar structural material

and structural system throughout. To construct the classical damping matrix, two procedures can be used; (1) the Rayleigh damping and Caughey damping (e.g., the mass- and stiffness-proportional damping), and (2) the superposition of the modal damping matrices. The nonclassical damping is appropriate if the system consists of two or more parts with significantly different levels of damping such as a structural-soil system. Unfortunately, the method of calculating the nonclassical damping matrix is not incorporated in most computer programs, including the one selected for this study.

The SAP2000 program provides two ways for specification of damping; the nonlinear damper element and the modal damping ratio as an overall damping of the system. In general, a bridge superstructure of truss-arch has the overall damping ratio of about 2%. However, since the Cairo Bridge consists of long approach structures and tall piers, the contribution from the concrete cracking possibly results in a higher damping ratio. In addition, higher damping ratio than 2% may be appropriate to account for the energy dissipation in the soils. As a result, a 5% damping ratio for all modes was assumed for the analyses.

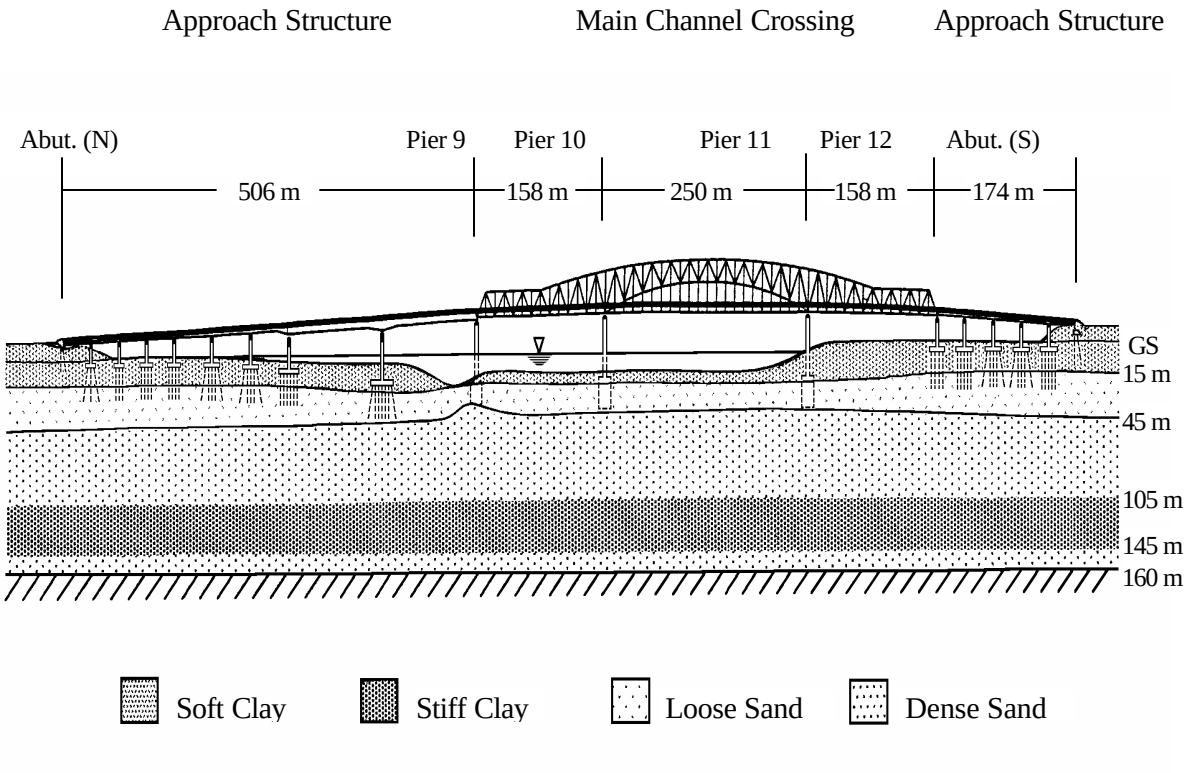

Figure 5.1. Elevation View of the Cairo Bridge.

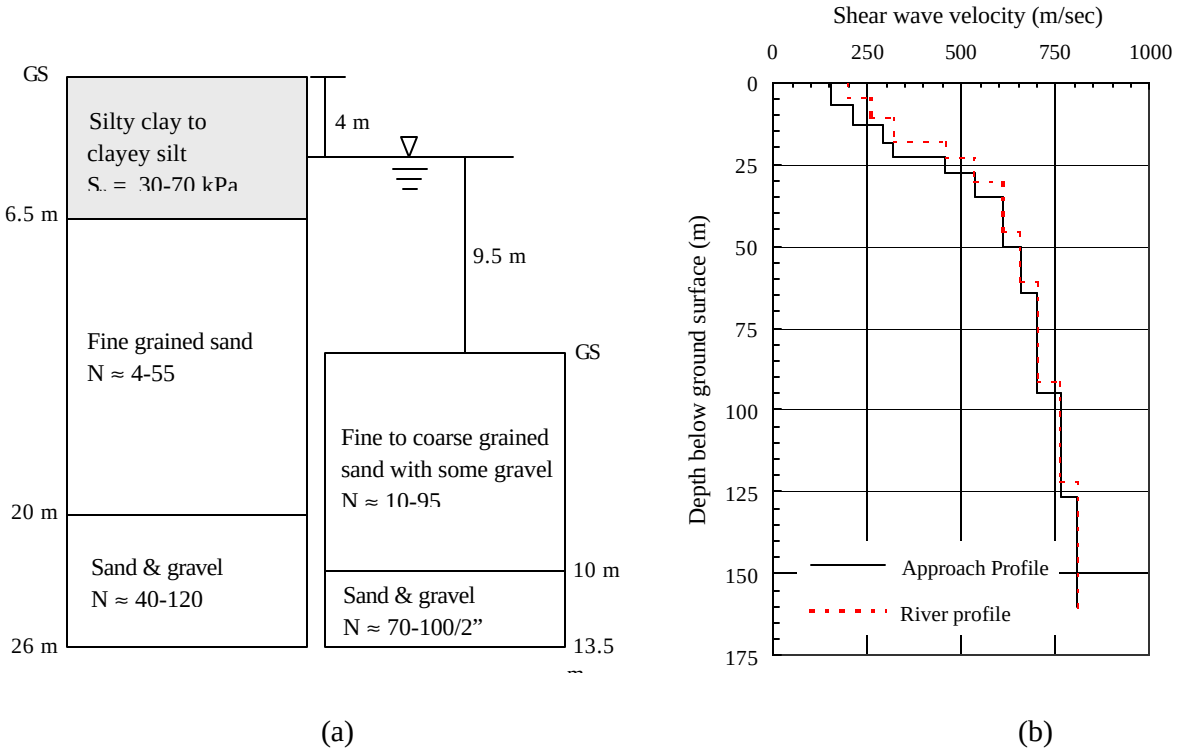

Figure 5.2. Soil Profiles (a) and Shear Wave Velocity (b) at the Bridge Site.

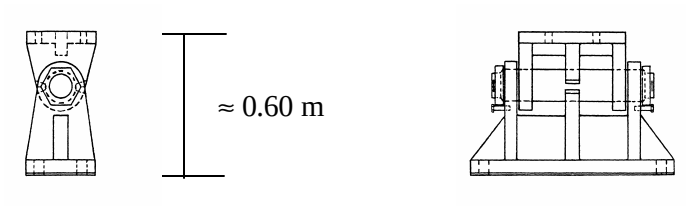

(a) Fixed Bearing

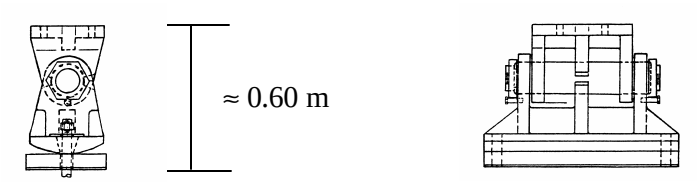

(b) Expansion Bearing

Figure 5.3. Typical bearings at the approach structures.

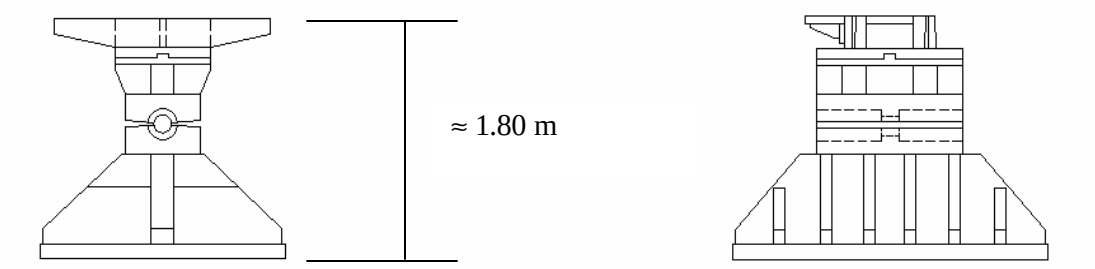

(a) Fixed Bearing

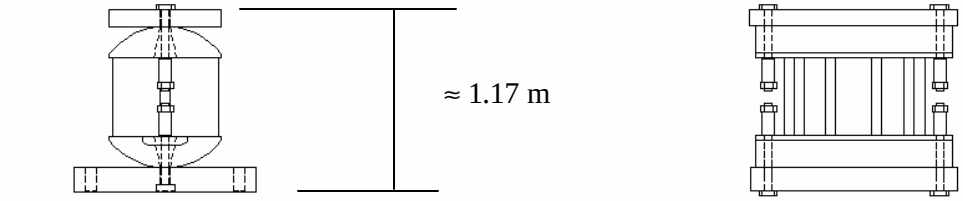

(b) Expansion Bearing

Figure 5.4. Bearings at the Main Truss Structure.

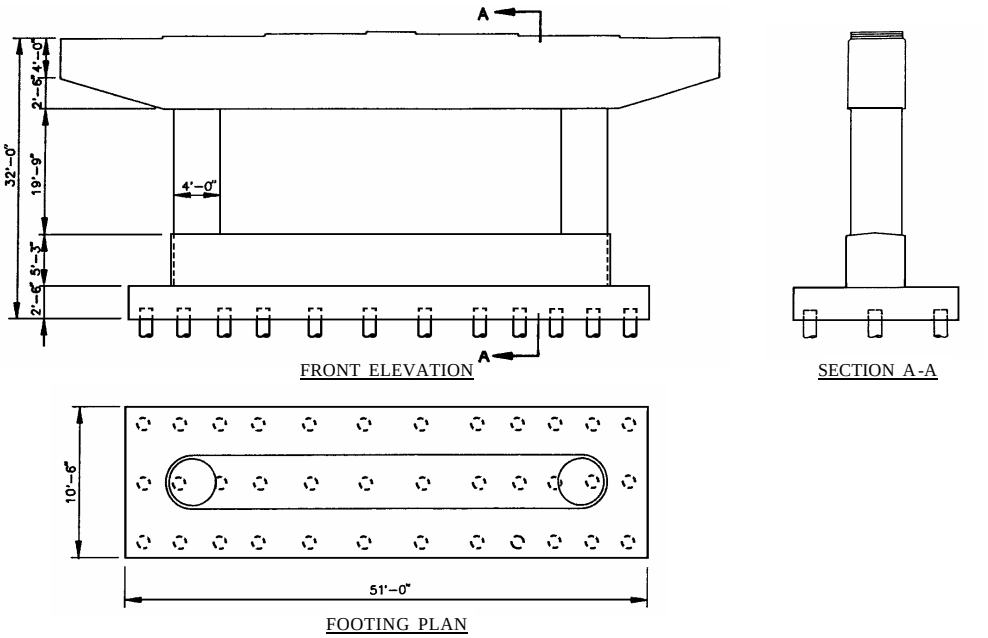

Figure 5.5. Typical Piers for the Approach Structure (Pier 2).

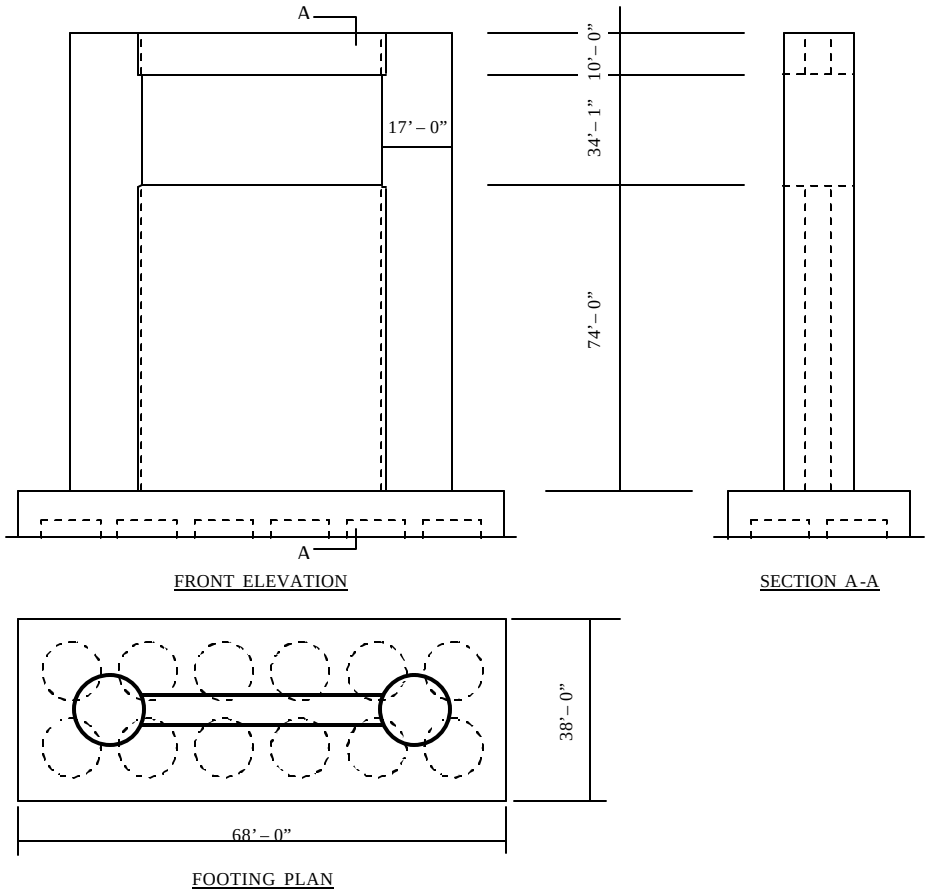

Figure 5.6. Typical Piers for the Main River Crossing (Pier 10).

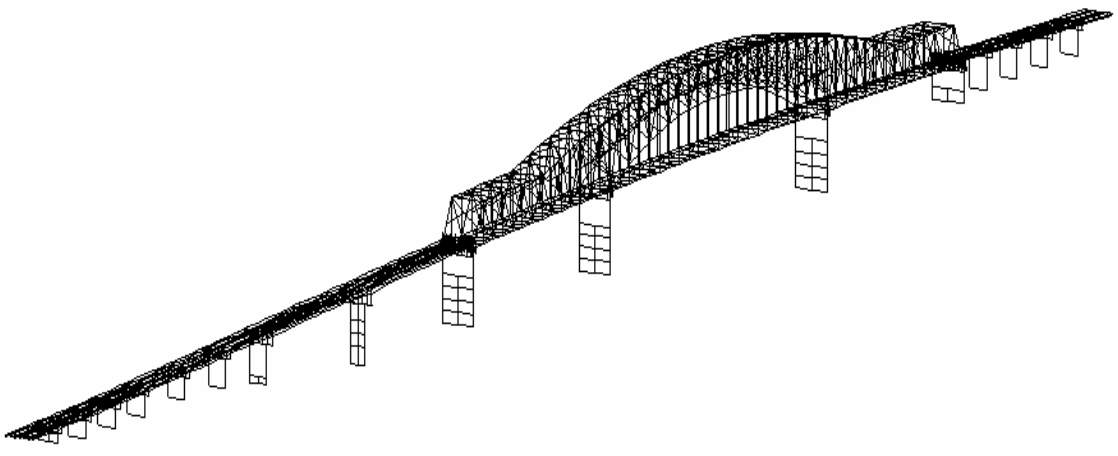

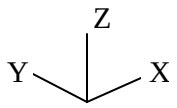

Figure 5.7. Structural Model of the Cairo Bridge.

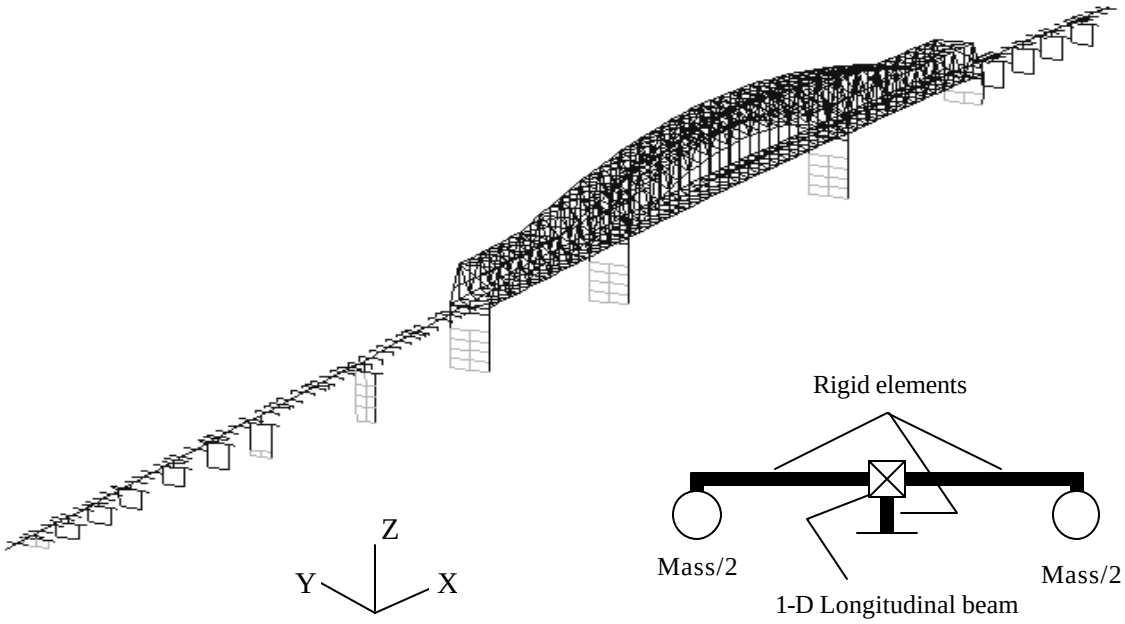

Figure 5.8. Schematic 1-D Beam Model for the Bridge Deck System.

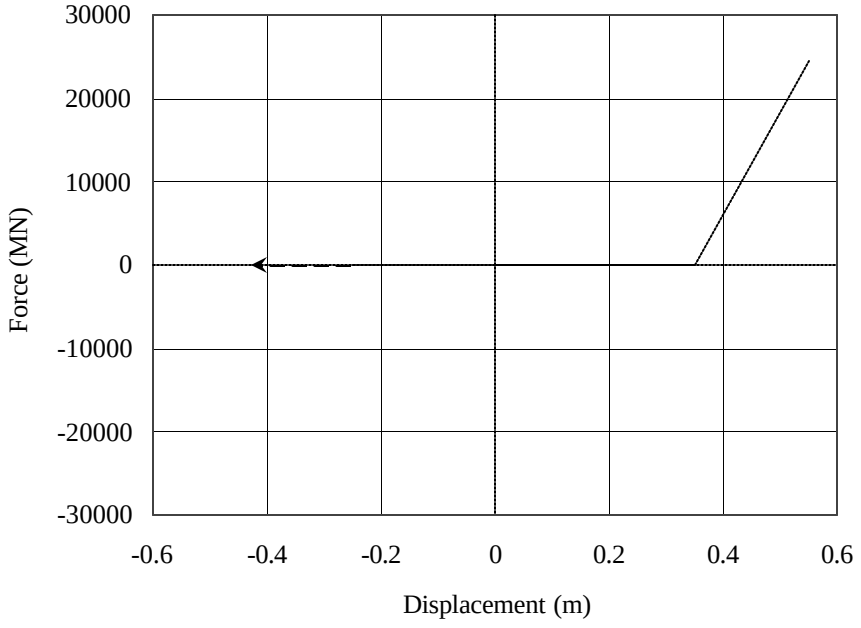

(a)

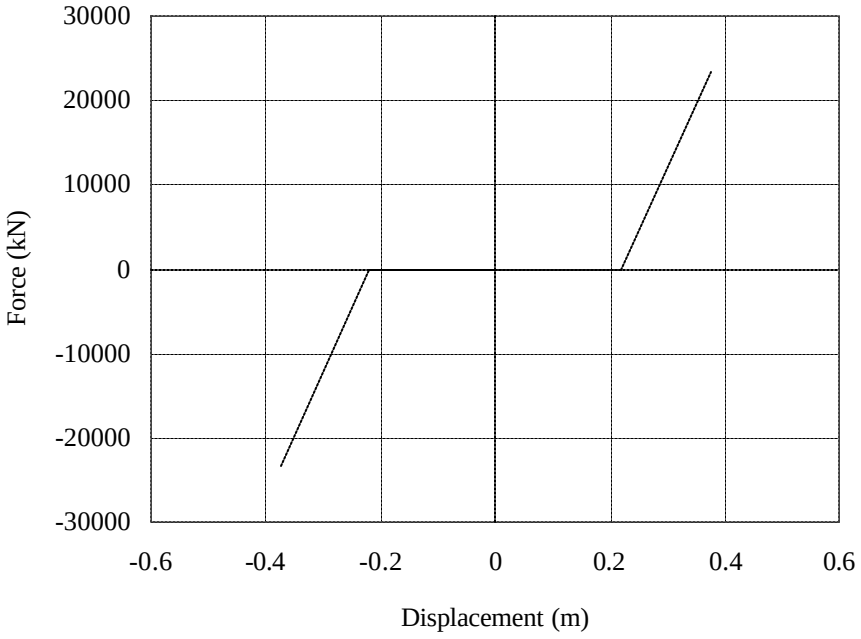

(b)

Figure 5.9. Idealized Force-Displacement Relationships for (a) Expansion Joints, and (b) Expansion Bearings at the Main Truss Structure.

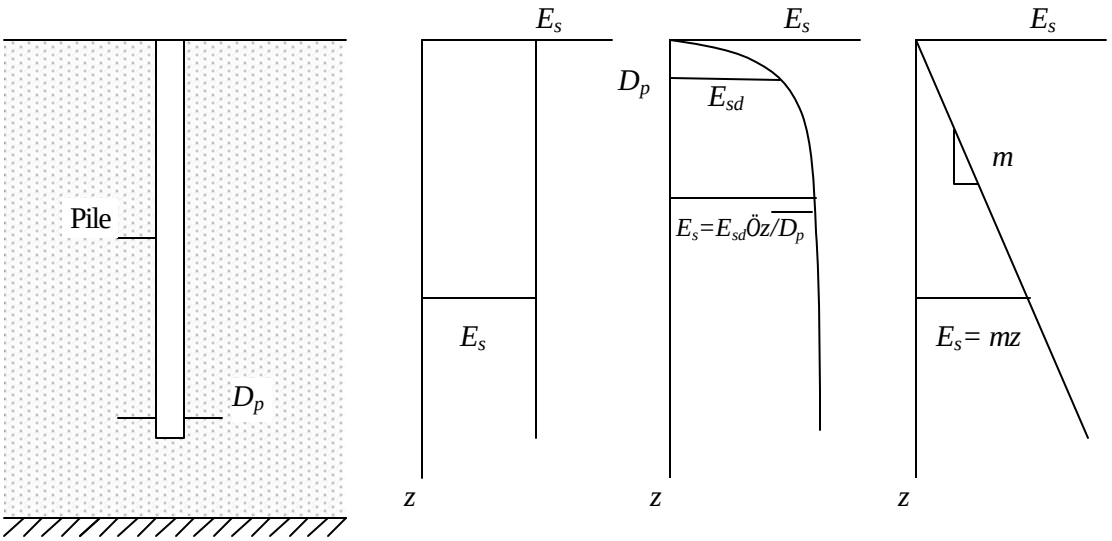

Figure 5.10. Schematic Illustration of the Beam Embedded in Elastic Continuum Approach.

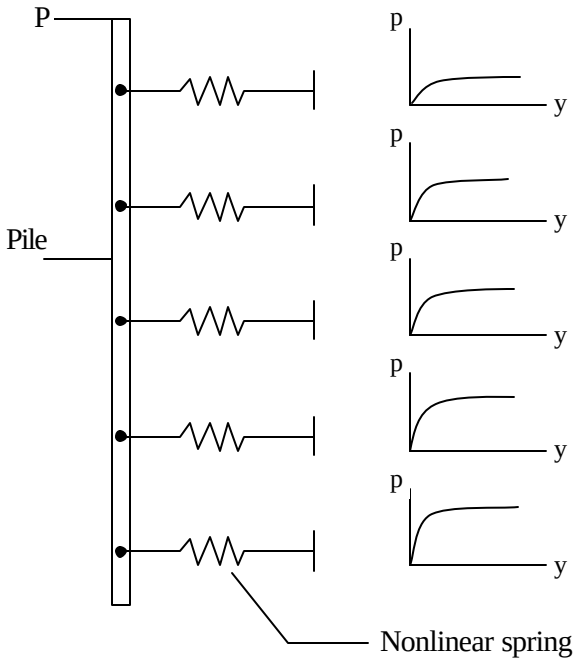

Figure 5.11. Schematic Illustration of the Beam on Inelastic Foundation Approach.

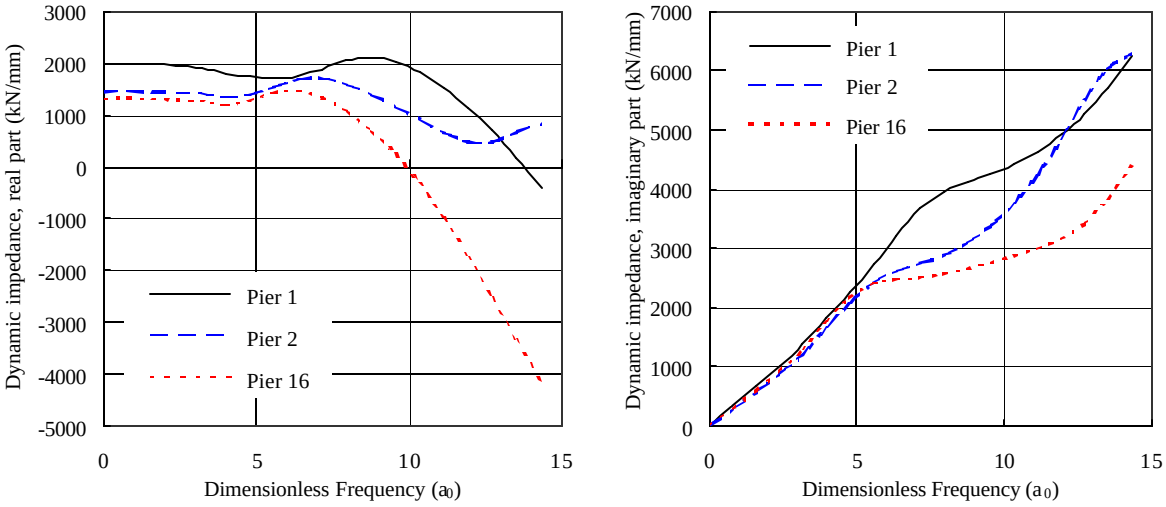

(a) Vertical Direction (z-axis)

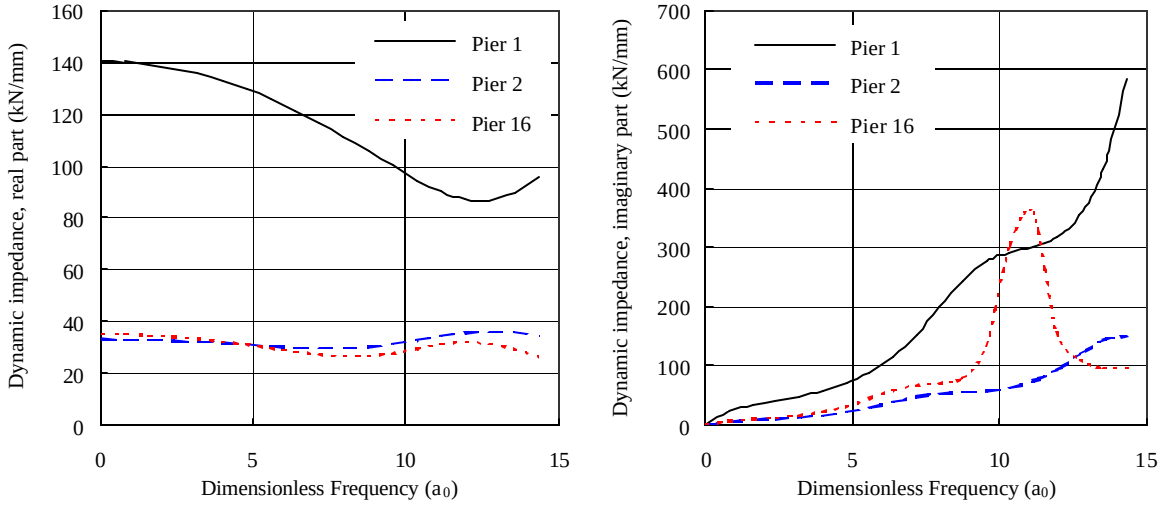

(b) Longitudinal Direction (x-axis)

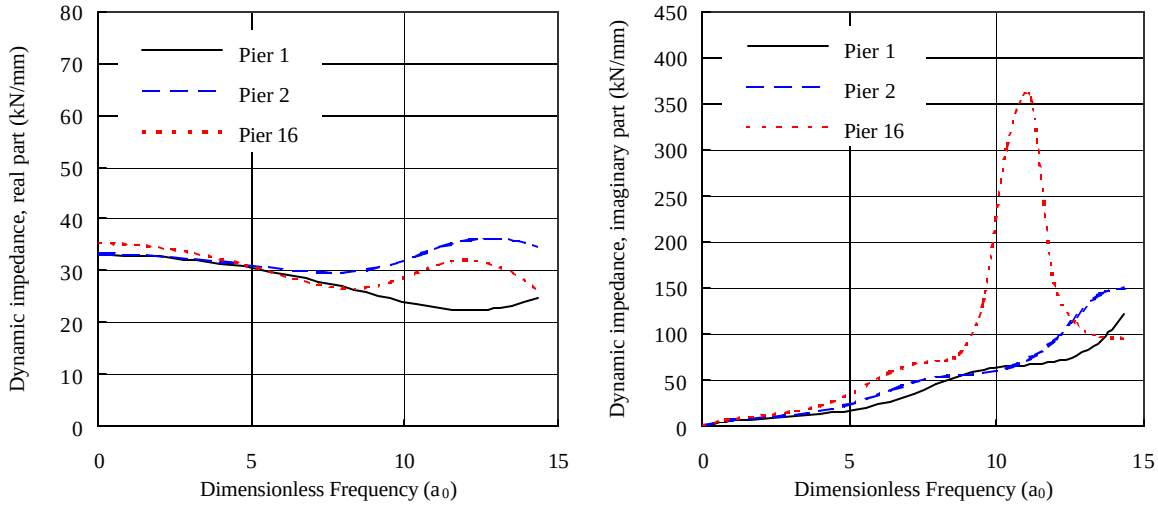

(c) Transverse Direction (y-axis)

Figure 5.12. Vertical and Horizontal Dynamic Impedance of Foundations for Piers 1, 2 and 16.

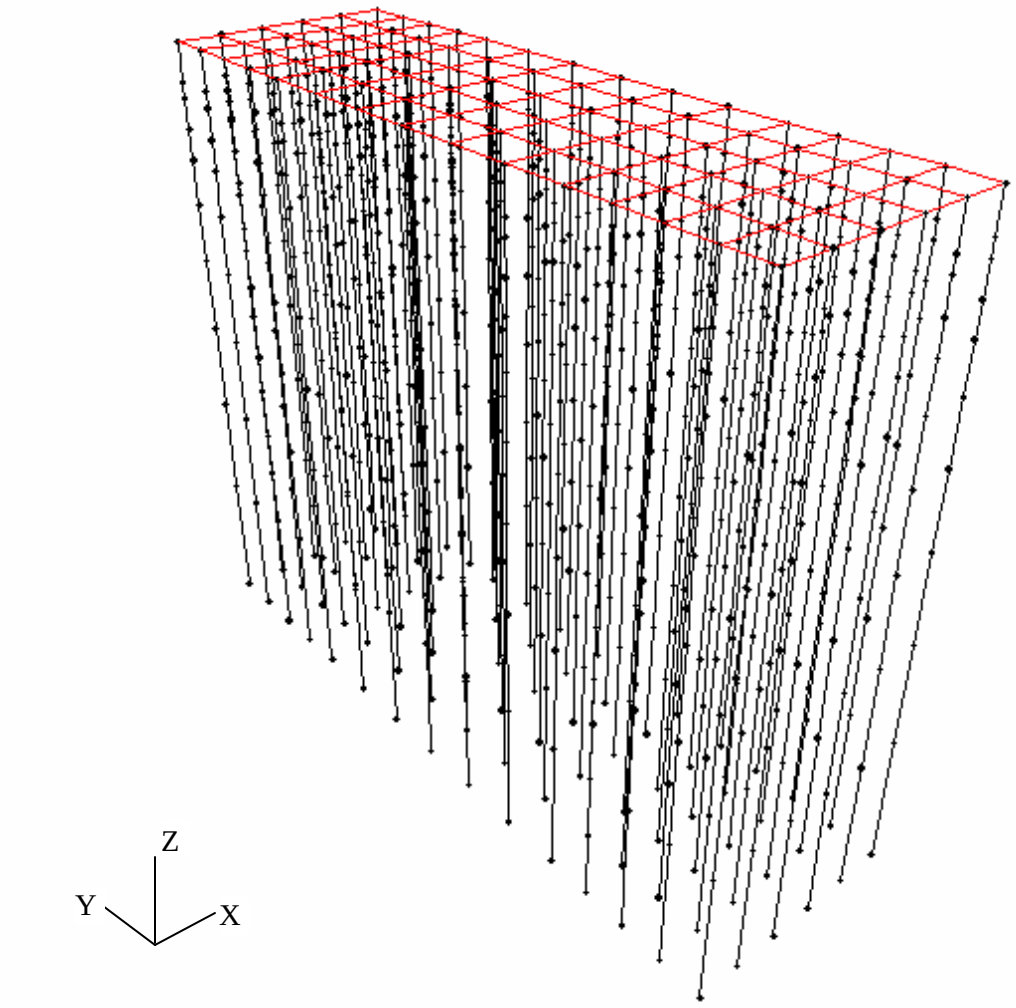

Figure 5.13. The Proposed Pile Foundation Model for Pier 7.

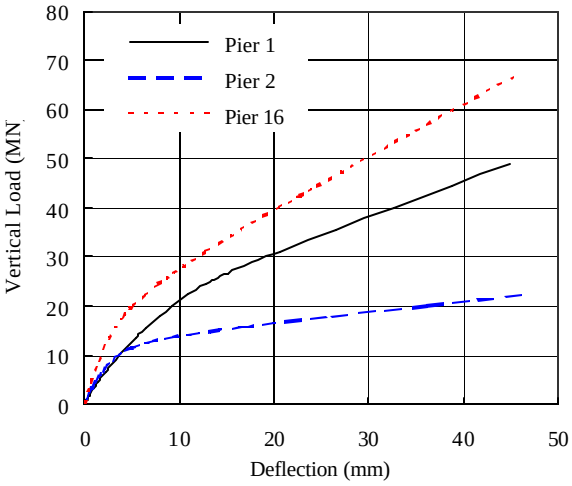

(a) Vertical Direction (z-axis)

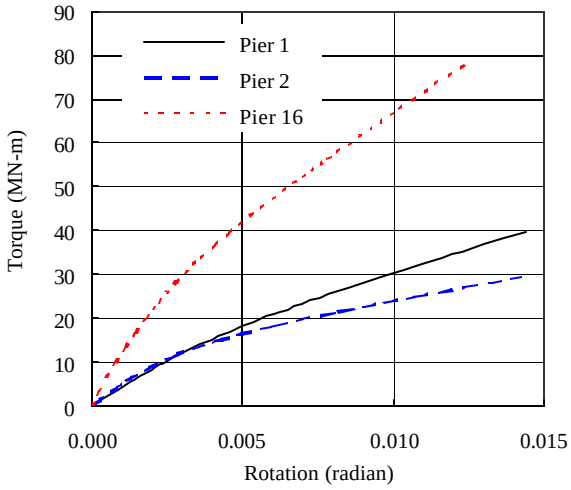

(b) Rotation about z axis

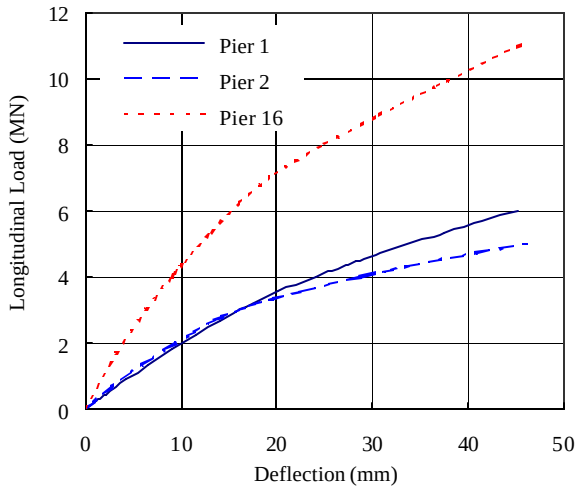

(c) Longitudinal Direction (x-axis)

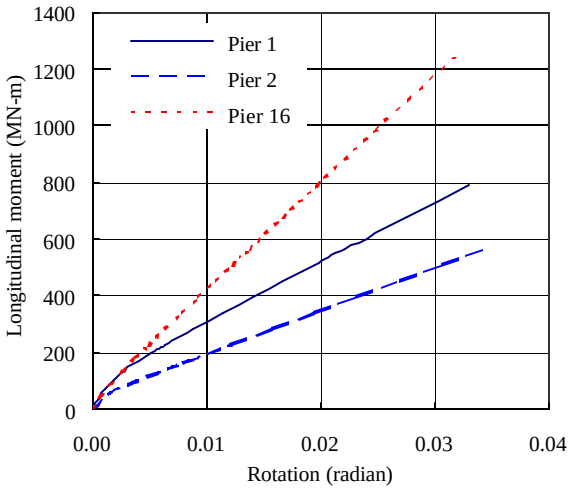

(d) Rotaion about x-axis

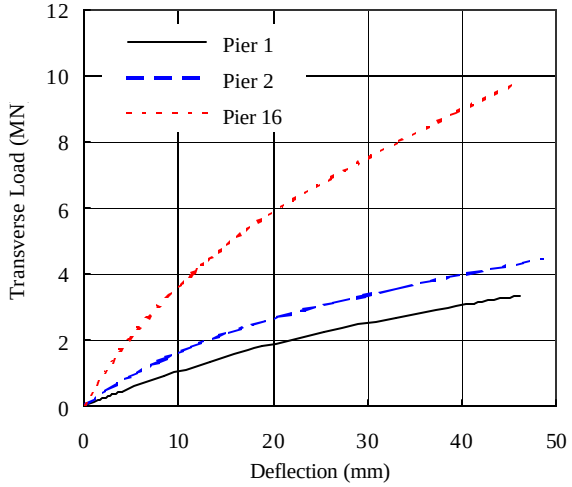

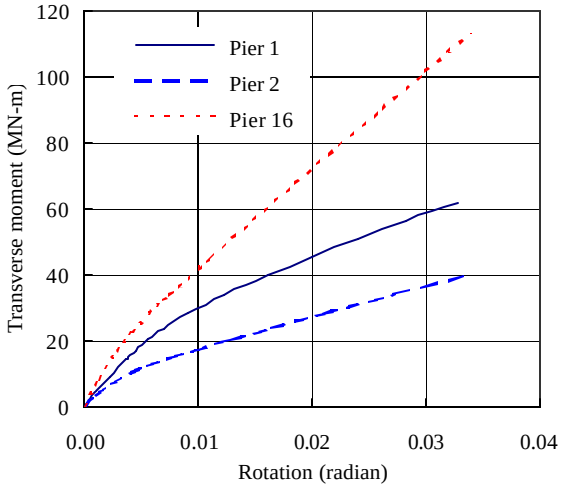

(e) Transverse Direction (y-axis)

(f) Rotaion about y-axis

Figure 5.14. Load-Deflection and Moment-Rotation Characteristics of Foundations at Piers 1, 2 and 16 using the Proposed Pile Foundation Model.

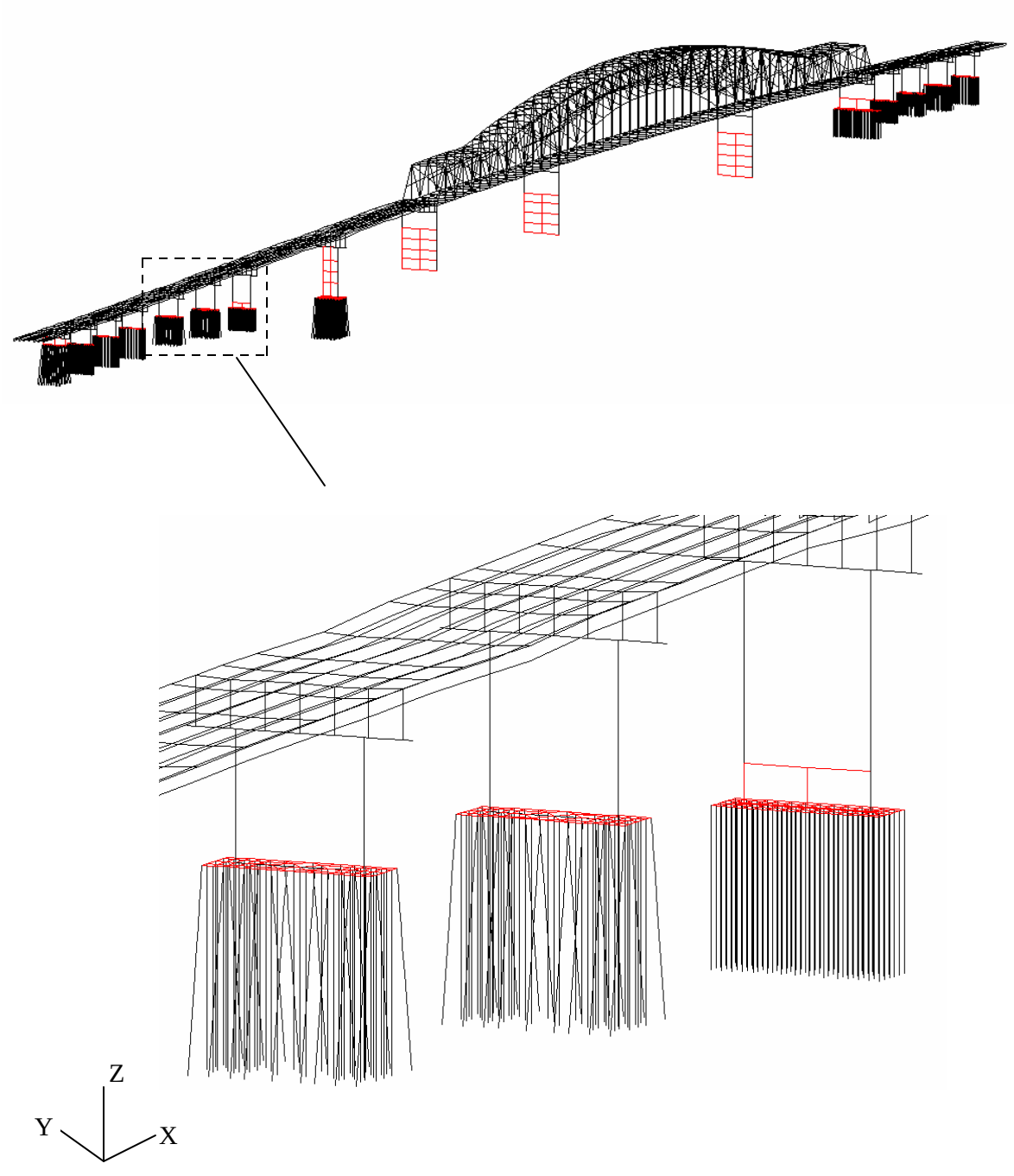

Figure 5.15. The Complete Integrated Soil-Foundation-Structure Model (Case 6).

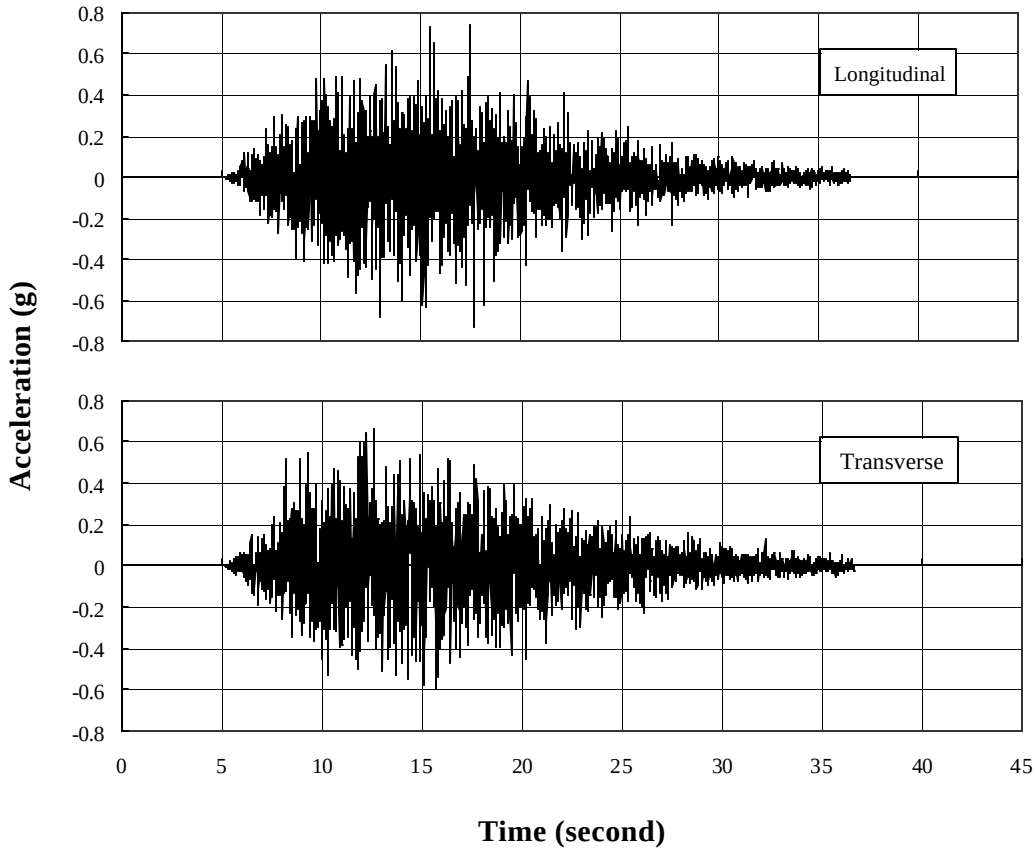

Figure 5.16. Outcrop Acceleration Histories Used in Site Response Analysis.

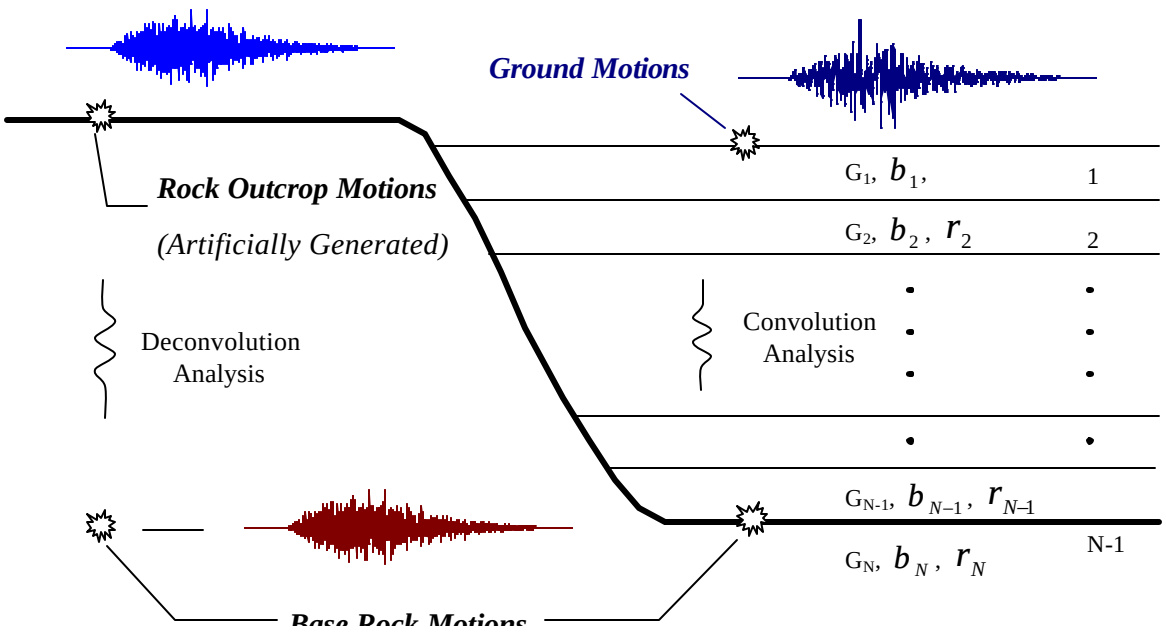

Figure 5.17. Schematic Illustration of Site Response Analysis Conducted in this Study.

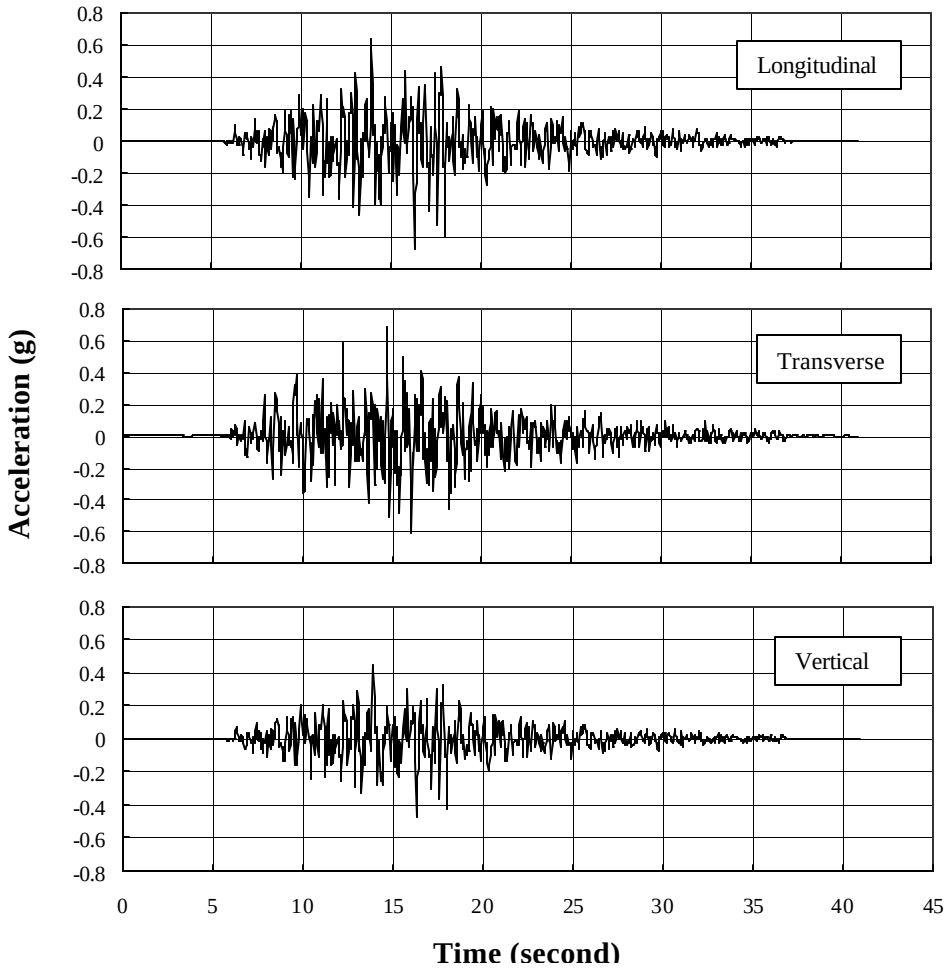

(a)

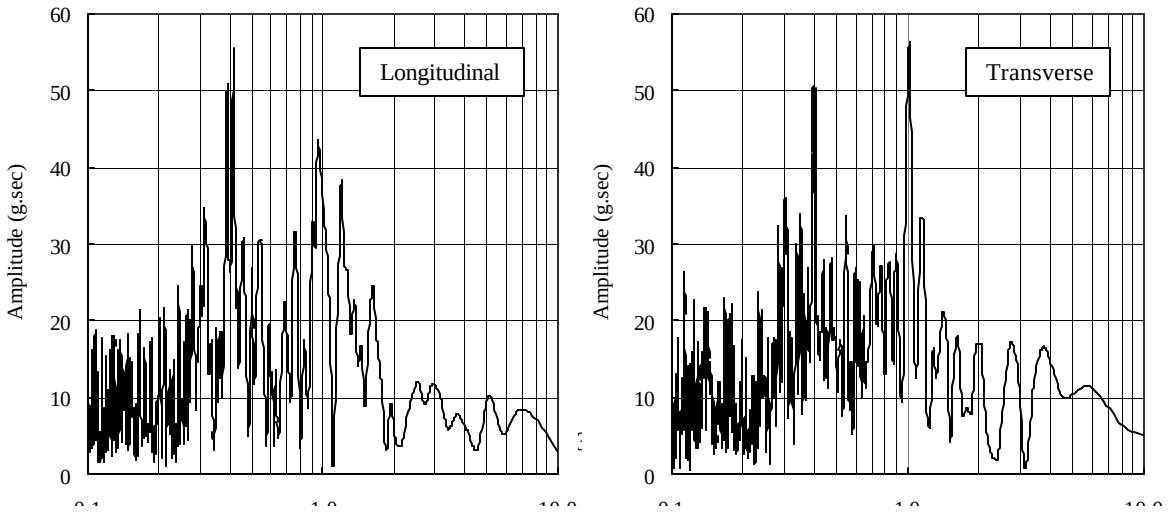

(b)

Figure 5.18. Input Ground Motions and Corresponding Fourier Response Spectra.

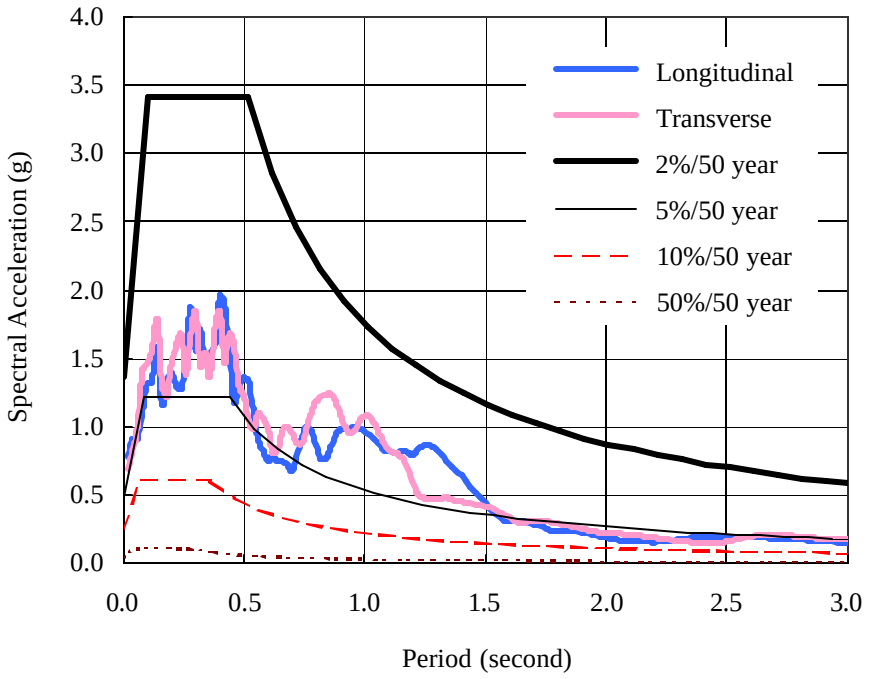

(a)

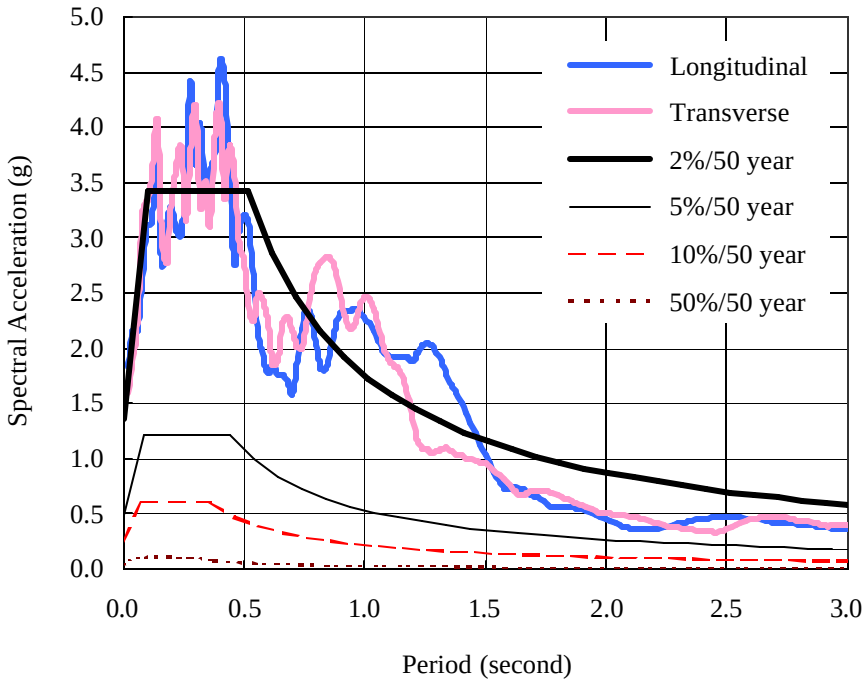

(b)

Figure 5.19. Response Spectra of (a) Original, and (b) Modified Input Ground Motions.

CHAPTER 6

SEISMIC PERFORMANCE EVALUATION OF THE CAIRO BRIDGE

6.1 Introduction

For the seismic response analyses conducted in this study, several bridge models, each of which has a different foundation model described in Chapter 5, are used. The foundation models obtained from various modeling approaches are employed for evaluating the effects of foundation modeling on dynamic characteristics and seismic behavior of the bridge. This evaluation is done through extensive comparison and parametric studies, which are divided into three parts.

First, the equivalent linear stiffness coefficients of foundations calculated from different foundation models are compared. Since the bridge response directly depends on the dynamic characteristics (modal periods and shapes) of the entire structural system, which in turn depends on the foundation flexibility, the modal periods from different bridge models are then compared. Also being compared are seismic responses of the bridge such as the response of piers (e.g., displacements, rotations, forces and moments) as well as the reactions at critical locations such as the expansion joints and bearings under the main truss structure. A comparison of the response of selected piles from different pile foundations is also presented. These responses are obtained from nonlinear time history analyses of the bridge model with different foundation models and with different intensity levels of the input motions presented in Chapter 5.

6.2 Summary of Bridge Modeling Cases

Several foundation modes are used in the dynamic analysis of the Cairo (Illinois) Bridge. Each bridge modeling case represents the bridge model in which the properties of the foundations are determined from one of the six modeling approaches discussed in the preceding chapter. Summarized in Table 6.1 are the descriptions of the six modeling cases of the Cairo Bridge.

In all cases except Case 1, the foundation models are further divided into two models according to how the PSPI effect is taken into account. The letters A and B are used to describe these different models. For instance, Case 2A refers to the model for which the foundation

characteristics are determined based on the beam on elastic continuum approach without considering the PSPI effect. Case 2B refers to the model in which the PSPI effect is considered using a conventional static IF method.

Table 6.1. Cases Considered in Seismic Analysis of the Cairo Bridge.

Case	Descriptions of foundation models
1	Fixed-base model
2	Equivalent linear 6x6 stiffness matrix: beam on elastic continuum
3	Equivalent linear 6x6 stiffness matrix: beam on inelastic foundation
4	Equivalent dynamic springs: beam in linear viscoelastic medium
5	Nonlinear springs: pile foundation model
6	The proposed integrated soil-foundation-structure model

6.3 Comparison of Foundation Stiffness

Tables 6.2 to 6.7 summarize the equivalent linear foundation stiffness coefficients computed from various cases. The values given in parenthesis represent the ratio of the stiffness computed from the model in which the PSPI is accounted for in a conventional manner (i.e., the PSPI effect is assumed present among all piles in a group) to that without the PSPI.

6.3.1 Vertical Stiffness

It is observed from Table 6.2 that the vertical stiffness coefficients obtained from all foundation modeling cases except Case 4 (Dynamic impedance) are somewhat comparable. It should be noted that the stiffness values listed in Case 4 are computed using the soil properties at small strains (level of soil-strain in the range of 10^{-4}%) whereas the soil properties at large strains are used in other cases. For small-strain behavior, the stiffness is much greater than that for larger strains. The small-strain soil modulus can be as high as five to ten times greater than the large strain soil modulus. Accordingly, the stiffness coefficients computed from Case 4 should be reduced corresponding to the level of soil strains.

Table 6.2. Comparison of Vertical Stiffness Coefficients (K_z) from Different Cases.

Bent	Vertical Stiffness Coefficients, K_z (kN/mm)			
	Case 2	Case 3	Case 4	Case 5
Pier 1	2,411.0 (0.11)	2,407.5 (0.11)	17,940.7 (0.11)	1,962.2 (0.93)
Pier 2	2,727.8 (0.16)	2,727.9 (0.16)	11,073.2 (0.13)	1,157.5 (0.94)
Pier 3	3,485.6 (0.13)	3,485.6 (0.13)	14,149.1 (0.10)	1,635.3 (0.98)
Pier 4	3,031.0 (0.15)	3,031.0 (0.15)	12,303.6 (0.12)	1,995.4 (0.99)
Pier 5	5,212.7 (0.11)	5,212.3 (0.11)	16,624.5 (0.08)	4,207.5 (0.97)
Pier 6	5,227.4 (0.07)	5,217.3 (0.07)	16,624.5 (0.08)	3,729.9 (0.99)
Pier 7	9,377.1 (0.06)	9,377.1 (0.06)	17,008.8 (0.05)	3,936.3 (1.00)
Pier 8	27,083.4 (0.02)	27,074.3 (0.02)	80,508.9 (0.03)	19,008.6 (1.00)
Pier 12	8,633.2 (0.10)	8,633.2 (0.10)	21,948.7 (0.08)	5,265.0 (0.97)
Pier 13	5,105.3 (0.14)	5,105.3 (0.14)	9,260.4 (0.10)	2,060.9 (0.95)
Pier 14	5,484.3 (0.14)	5,484.3 (0.14)	9,946.2 (0.09)	2,770.8 (0.98)
Pier 15	4,875.2 (0.14)	4,875.4 (0.14)	11,911.5 (0.09)	4,119.5 (0.99)
Pier 16	4,084.2 (0.13)	4,084.2 (0.13)	13,029.6 (0.10)	3,456.1 (0.95)

Table 6.3. Comparison of Longitudinal Stiffness Coefficients (K_x) from Different Cases.

Bent	Longitudinal Stiffness Coefficients, K_x (kN/mm)			
	Case 2	Case 3	Case 4	Case 5
Pier 1	295.7 (0.21)	209.2 (0.21)	943.0 (0.15)	181.4 (0.92)
Pier 2	176.7 (0.24)	127.9 (0.24)	191.7 (0.17)	177.0 (0.84)
Pier 3	225.8 (0.20)	163.4 (0.20)	244.9 (0.14)	255.8 (0.83)
Pier 4	196.4 (0.22)	184.1 (0.22)	213.0 (0.16)	203.0 (0.83)
Pier 5	347.7 (0.18)	303.4 (0.18)	463.2 (0.11)	423.0 (0.84)
Pier 6	1,285.9 (0.24)	937.9 (0.18)	1,351.4 (0.10)	1,061.8 (0.88)
Pier 7	3,100.5 (0.18)	1,748.3 (0.12)	3,825.6 (0.07)	2,215.4 (0.87)
Pier 8	13,839.7 (0.12)	11,829.8 (0.07)	14,054.6 (0.04)	17,248.8 (0.86)
Pier 12	676.0 (0.17)	598.5 (0.17)	665.0 (0.10)	637.9 (0.83)
Pier 13	258.1 (0.20)	254.7 (0.20)	260.9 (0.13)	287.0 (0.88)
Pier 14	316.9 (0.21)	313.2 (0.21)	352.2 (0.12)	350.4 (0.85)

Pier 15	312.5 (0.21)	344.7 (0.21)	366.5 (0.12)	518.3 (0.88)
Pier 16	258.1 (0.20)	252.1 (0.20)	260.9 (0.13)	380.2 (0.84)

Table 6.4. Comparison of Transverse Stiffness Coefficients (K_y) from Different Cases.

Bent	Transverse Stiffness Coefficients, K_y (kN/mm)			
	Case 2	Case 3	Case 4	Case 5
Pier 1	206.2 (0.21)	116.1 (0.21)	223.6 (0.15)	99.1 (0.88)
Pier 2	176.7 (0.24)	127.9 (0.24)	191.7 (0.17)	148.3 (0.79)
Pier 3	225.8 (0.20)	163.4 (0.20)	244.9 (0.14)	186.7 (0.82)
Pier 4	196.4 (0.22)	184.1 (0.22)	213.0 (0.16)	184.2 (0.76)
Pier 5	309.3 (0.17)	264.6 (0.18)	335.4 (0.11)	348.8 (0.81)
Pier 6	1,254.8 (0.24)	904.1 (0.18)	1,267.9 (0.11)	952.7 (0.89)
Pier 7	3,100.5 (0.18)	1,748.3 (0.12)	3,825.1 (0.08)	2,327.2 (0.86)
Pier 8	13,779.0 (0.12)	18,681.6 (0.07)	13,779.0 (0.04)	13,193.6 (0.84)
Pier 12	676.0 (0.17)	598.5 (0.17)	665.0 (0.10)	553.5 (0.81)
Pier 13	258.1 (0.20)	254.7 (0.20)	260.9 (0.13)	239.6 (0.81)
Pier 14	279.2 (0.21)	275.5 (0.21)	282.2 (0.13)	255.9 (0.82)
Pier 15	279.2 (0.21)	311.6 (0.21)	282.2 (0.13)	417.9 (0.82)
Pier 16	258.1 (0.20)	252.1 (0.20)	260.9 (0.13)	380.2 (0.84)

Table 6.5. Comparison of Torsional Stiffness Coefficients (K_{rz}) from Different Cases.

Bent	Torsional Stiffness Coefficients, K_{rz} (kN-m) x 10^6			
	Case 2	Case 3	Case 4	Case 5
Pier 1	5.828 (0.34)	4.074 (0.33)	17.973	4.020 (0.93)
Pier 2	4.327 (0.41)	3.141 (0.41)	4.690	4.078 (0.83)
Pier 3	6.429 (0.30)	4.664 (0.30)	6.927	5.829 (0.85)
Pier 4	5.766 (0.33)	5.409 (0.33)	6.249	5.676 (0.83)
Pier 5	9.988 (0.27)	8.691 (0.27)	12.769	13.452 (0.85)
Pier 6	37.469 (0.34)	27.275 (0.26)	39.060	32.655 (0.90)
Pier 7	76.490 (0.28)	43.180 (0.20)	94.338	56.177 (0.90)
Pier 8	416.190 (0.17)	434.022 (0.11)	420.224	469.269 (0.88)
Pier 12	53.518 (0.26)	47.390 (0.26)	52.658	48.269 (0.85)
Pier 13	7.368 (0.31)	7.270 (0.31)	7.447	7.874 (0.83)

Pier 14	8.861 (0.31)	8.755 (0.31)	9.718	9.935 (0.85)
Pier 15	8.748 (0.31)	9.659 (0.31)	10.046	14.865 (0.86)
Pier 16	7.355 (0.31)	7.184 (0.31)	7.435	10.331 (0.84)

Table 6.6. Comparison of Rotational Stiffness Coefficients (K_{rx}) from Different Cases.

Bent	Rotational Stiffness Coefficients: Longitudinal, K_{rx} (kN-m) x 10^6			
	Case 2	Case 3	Case 4	Case 5
Pier 1	45.446 (0.25)	45.218 (0.25)	336.226 (0.29)	47.478 (0.89)
Pier 2	64.157 (0.25)	64.039 (0.25)	258.900 (0.30)	37.049 (0.95)
Pier 3	94.940 (0.18)	94.791 (0.18)	384.200 (0.19)	44.568 (0.93)
Pier 4	85.385 (0.20)	85.286 (0.20)	345.780 (0.22)	37.379 (0.98)
Pier 5	135.558 (0.15)	135.368 (0.15)	431.050 (0.16)	78.317 (0.99)
Pier 6	136.176 (0.17)	135.571 (0.15)	431.050 (0.16)	77.634 (~1.0)
Pier 7	209.118 (0.12)	208.586 (0.15)	377.420 (0.11)	107.037 (~1.0)
Pier 8	516.421 (0.13)	510.090 (0.09)	1,515.080 (0.10)	240.426 (~1.0)
Pier 12	648.010 (0.97)	647.367 (0.97)	1,649.800 (0.11)	342.424 (~1.0)
Pier 13	135.758 (0.22)	135.567 (0.22)	246.340 (0.18)	43.836 (~1.0)
Pier 14	137.137 (0.24)	137.036 (0.24)	246.860 (0.19)	62.604 (~1.0)
Pier 15	121.950 (0.20)	121.828 (0.20)	297.190 (0.20)	72.809 (~1.0)
Pier 16	108.679 (0.18)	108.552 (0.18)	345.780 (0.19)	45.935 (~1.0)

Table 6.7. Comparison of Rotational Stiffness Coefficients (K_{ry}) from Different Cases.

Bent	Rotational Stiffness Coefficients: Transverse, K_{ry} (kN-m) x 10^6			
	Case 2	Case 3	Case 4	Case 5
Pier 1	3.360 (0.32)	3.153 (0.29)	22.320 (0.33)	3.786 (0.93)
Pier 2	2.637 (0.40)	2.520 (0.37)	9.830 (0.42)	1.546 (0.83)
Pier 3	4.294 (0.55)	4.144 (0.54)	16.317 (0.90)	2.245 (0.85)
Pier 4	3.617 (0.51)	3.517 (0.50)	13.711 (0.74)	1.839 (0.83)
Pier 5	17.838 (0.27)	17.633 (0.27)	55.562 (0.31)	9.373 (0.85)
Pier 6	18.312 (0.26)	17.817 (0.27)	55.562 (0.31)	9.391 (0.90)
Pier 7	23.913 (0.47)	23.378 (0.40)	41.959 (0.49)	16.377 (0.90)
Pier 8	315.688 (0.18)	316.911 (0.14)	909.763 (0.13)	186.142 (0.88)
Pier 12	37.718 (0.54)	37.076 (0.53)	92.879 (0.77)	29.587 (0.85)

Pier 13	9.429 (0.37)	9.335 (0.36)	16.690 (0.42)	3.822 (0.83)
Pier 14	18.705 (0.32)	18.597 (0.32)	33.400 (0.38)	8.228 (0.85)
Pier 15	16.677 (0.32)	16.555 (0.31)	39.941 (0.38)	9.308 (0.86)
Pier 16	7.615 (0.36)	7.489 (0.35)	23.384 (0.42)	4.706 (0.84)

It is found that the difference of vertical stiffness values from between Cases 2 and 3 is very small. It is because the vertical stiffness coefficients of each pile in a group are calculated from the same expression. Consequently, the vertical stiffness of the pile groups consisting of only vertical piles from these two cases is similar. Even for the pile groups having battered piles, the difference of stiffness coefficients between these two cases is still rather small. The vertical stiffness coefficients obtained from Cases 2 and 3 appear to be slightly stiffer than those from the proposed foundation model.

The stiffness coefficients calculated from Cases 2, 3 and 4 with and without inclusion of the PSPI are of notable difference. The vertical stiffness is reduced to about 7-21% of the one without the PSPI effects for most foundations (36-50 piles in a group) and to as low as 2% for the foundation supporting Pier 8 consisting of 192 piles. In fact, the comparison results show that by accounting for the PSPI using the interaction factor (IF) method, the stiffness of 192-pile foundation is less than that of the 90-or-less pile foundations. Such a huge reduction in stiffness may result from the contribution of the interaction factors between the considered pile and the piles farther away, which are supposedly small. However, these small interaction factors are added up and become important for a relatively large pile group. Unfortunately, there is little data on the behavior of large pile groups; therefore, more specific explanations for this distinctive reduction are difficult to establish. Nonetheless, it is strongly believed that the interaction factor method greatly overpredicts the PSPI effects, and it is not applicable for large pile groups.

It is also observed that the percentage of stiffness reduction due to the PSPI effect is fairly similar for the static IF method (Cases 2 and 3) and dynamic IF method (Case 4). This is not surprising because both methods are based on the same assumption of using the superposition technique and because the dominant frequency of the input motions is somewhat low (about 1 to 2.4 Hz); thus, the dynamic PSPI for this loading case may not be as significant as for a high-frequency loading case. Note that the PSPI effect is not as significant for the proposed model case. This is owing to the fact that the t-multiplier is applied only to the clay, which is a top layer soil, to account

for the PSPI. However most of the axial pile resistance at the Cairo site is derived from the deeper soil layer which is mostly medium to dense sand to which no t-multiplier is applied.

6.3.2 Lateral Stiffness

The lateral stiffness coefficients obtained from all cases are comparable for all foundations except for the longitudinal stiffness of the foundation supporting Pier 1 (Case 4, Table 6.3). A plausible cause of this distinctively high longitudinal stiffness is the effect of batter piles. Twenty-eight out of forty-two piles in the foundation at Pier 1 are battered in the longitudinal direction. The vertical stiffness of these battered piles plays an important role in deriving the longitudinal stiffness coefficient. Since the vertical stiffness computed from Case 4 is much higher than that from other cases, the longitudinal stiffness computed from Case 4 is expected to be higher than that from other cases, accordingly. In addition to a small variation of the lateral stiffness computed among all cases, it is found that the variation of lateral stiffness is smaller than that of the vertical stiffness.

It is also observed that for lateral stiffness, the reduction of stiffness due to the PSPI using the IF method is not as much as that for vertical stiffness. It varies between 10-30% for most foundations and highest of 4% for the foundation at Pier 8. However, for the proposed pile foundation model, the PSPI effect is more pronounced for lateral response than for vertical response of the pile group. This is because a significant lateral resisting zone, which is usually confined to a depth of the lower 5 to 10 pile diameters from the ground surface, is predominantly clay to which the p-multiplier is applied to account for the PSPI.

6.3.3 Rotational Stiffness

The variation of the computed torsional stiffness (K_{rz}) for all cases is less than that of the other two rotational stiffnesses (K_{rx} and K_{ry}). This is due to the fact that most of the torsional stiffness is derived from the lateral stiffness which has less deviation than the vertical stiffness from which most of the rotational stiffness is derived.

For the proposed pile group model, it is observed from the analytical results that the peripheral piles reach their capacity at a small rotation. As the applied load level increases, the adjacent piles closer to the center of loading continuously reach their capacity resulting in the so-called progressive failure which cannot be simulated by using the traditional static condensation method. Since the foundation responds nonlinearly to a relatively small applied torsion or moment, the rotational

stiffness coefficients of the foundations predicted by the proposed model are smaller than those predicted by any other method in which the soil-pile nonlinearity is not directly accounted for. For all foundation modeling cases, the reduction of the rotational stiffness coefficients due to the PSPI is not as much as that of the vertical and lateral stiffness. It is evidently shown in Tables 6.2 to 6.7 that the rotational interaction between piles is less than that for vertical and horizontal interaction.

6.4 Comparison of Dynamic Characteristics of the Bridge

Unlike static response, the dynamic response of the structure depends primarily on the overall dynamic characteristics of the structure and in turn depends on the modeling of the foundations. The modal periods of the structure are required for performing dynamic analysis using the response spectrum method. Therefore, the effects of foundation modeling on the dynamic characteristic of the bridge are investigated. Dynamic characteristics computed from different foundation models are listed in Tables 6.8 to 6.9. The values in parenthesis represent the ratio of the presented modal period to that computed from the fixed-base model. The modal periods of the bridge for different cases are also summarized in graphical form in Figure 6.1 in order to illustrate the effects of foundation modeling as compared to the fixed-based model. The first 8 modes of vibration for all cases are shown in Figures 6.2 to 6.7.

6.4.1 Effects of Foundation Modeling on Modal Periods

When the deformations of the foundation and soil are included in the model, the natural periods of vibration increase. The modal periods of the bridge are elongated more than 100% when the foundation flexibility is considered. The periods of the structure are elongated by about 1-40% for the modeling cases in which the PSPI effects are not considered and about 3-160% for the case in which the PSPI effects are included. It is observed that the first three modal periods increase quite significantly as the foundation flexibility is considered, while an increase of the periods of the higher modes is relatively small (Figure 6.1). Although the overall foundation stiffness coefficients are reduced by a factor of about 5 to 10 for the cases in which the PSPI is taken into account, the modal periods of the bridge are not affected as much.

The modal periods for Cases 2A, 3A, 4A, 5A and 5B are not much different. For Cases 2B and 3B, most of the modal periods are also comparable except for the first mode of each case which involves the longitudinal vibration of the north approach structure. The periods computed for Case 4B fall between the no-PSPI modeling cases and the PSPI modeling cases. The modal

periods and shapes obtained form Cases 5A and 5B are very similar and so are those from Cases 6A and 6B. The difference of the periods for these modes is indeed less than 0.5%. This small difference is due to the fact that the vibration modes of the structure are initially computed based upon the elastic or initial stiffness of the nonlinear elements. Consequently, in addition to a similarity of the results for Cases 5A and 5B and those for Cases 6A and 6B, the periods of the bridge computed for these cases are smaller than those computed for other modeling cases.

Table 6.8. Modal Periods for Cases 1, 2A, 3A, 4A, 5A and 6A (No-PSPI Cases).

Mode	Modal Period (second)					
	Case 1	Case 2A	Case 3A	Case 4A	Case 5A	Case 6A
1	2.285	2.832 (1.24)	2.831 (1.24)	2.734 (1.20)	2.821 (1.23)	2.781 (1.22)
2	2.172	2.594 (1.19)	2.773 (1.28)	2.285 (1.05)	2.419 (1.11)	2.299 (1.06)
3	1.649	2.285 (1.39)	2.285 (1.39)	2.077 (1.26)	2.285 (1.39)	2.285 (1.39)
4	1.529	1.536 (~1.0)	1.536 (~1.0)	1.534 (~1.0)	1.535 (~1.0)	1.563 (1.02)
5	1.505	1.507 (~1.0)	1.507 (~1.0)	1.507 (~1.0)	1.509 (~1.0)	1.533 (1.02)
6	1.281	1.468 (1.15)	1.469 (1.15)	1.444 (1.13)	1.507 (1.18)	1.508 (1.18)
7	1.272	1.286 (1.01)	1.286 (1.01)	1.285 (1.01)	1.289 (1.01)	1.300 (1.02)
8	1.233	1.233 (1.00)	1.233 (1.00)	1.233 (1.00)	1.233 (1.00)	1.286 (1.04)
9	1.198	1.198 (1.00)	1.198 (1.00)	1.198 (1.00)	1.199 (1.00)	1.233 (1.03)
10	1.026	1.154 (1.12)	1.156 (1.13)	1.118 (1.09)	1.198 (1.17)	1.188 (1.17)
11	1.025	1.084 (1.06)	1.088 (1.06)	1.037 (1.01)	1.181 (1.15)	1.141 (1.11)
12	1.007	1.045 (1.04)	1.047 (1.04)	1.027 (1.02)	1.031 (1.02)	1.105 (1.10)
13	0.999	1.027 (1.03)	1.027 (1.03)	1.026 (1.03)	1.027 (1.03)	1.029 (1.03)
14	0.876	1.026 (1.17)	1.026 (1.17)	1.005 (1.15)	1.026 (1.17)	1.026 (1.17)
15	0.864	0.876 (1.01)	0.877 (1.02)	0.876 (1.01)	0.907 (1.05)	0.939 (1.09)

Table 6.9. Modal Periods for Cases 1, 2B, 3B, 4B, 5B and 6B (PSPI Cases).

Mode	Modal Period (second)					
	Case 1	Case 2B	Case 3B	Case 4B	Case 5B	Case 6B
1	2.285	3.196 (1.40)	3.640 (1.60)	3.070 (1.34)	2.821 (1.23)	2.781 (1.22)
2	2.172	3.180 (1.46)	3.186 (1.47)	2.498 (1.15)	2.419 (1.11)	2.299 (1.06)
3	1.649	2.285 (1.39)	2.285 (1.39)	2.285 (1.39)	2.285 (1.39)	2.285 (1.39)
4	1.529	1.623 (1.06)	1.726 (1.13)	1.574 (1.03)	1.535 (~1.0)	1.563 (1.02)
5	1.505	1.588 (1.06)	1.595 (1.06)	1.551 (1.03)	1.509 (~1.0)	1.533 (1.02)
6	1.281	1.542 (1.20)	1.540 (1.20)	1.539 (1.20)	1.507 (1.18)	1.508 (1.18)
7	1.272	1.518 (1.19)	1.521 (1.19)	1.413 (1.11)	1.289 (1.01)	1.300 (1.02)

8	1.233	1.283 (1.04)	1.285 (1.04)	1.339 (1.09)	1.233 (1.00)	1.286 (1.04)
9	1.198	1.249 (1.04)	1.282 (1.07)	1.277 (1.07)	1.199 (1.00)	1.233 (1.03)
10	1.026	1.234 (1.20)	1.234 (1.20)	1.234 (1.20)	1.198 (1.17)	1.188 (1.17)
11	1.025	1.198 (1.17)	1.198 (1.17)	1.198 (1.17)	1.181 (1.15)	1.141 (1.11)
12	1.007	1.169 (1.16)	1.177 (1.17)	1.193 (1.18)	1.031 (1.02)	1.105 (1.10)
13	0.999	1.130 (1.13)	1.173 (1.17)	1.142 (1.14)	1.027 (1.03)	1.029 (1.03)
14	0.876	1.125 (1.28)	1.164 (1.34)	1.133 (1.29)	1.026 (1.17)	1.026 (1.17)
15	0.864	1.030 (1.19)	1.030 (1.19)	1.132 (1.31)	0.907 (1.05)	0.939 (1.09)

6.4.2 Effects of Foundation Modeling on Mode Shapes

The fundamental vibration mode of the fixed-base bridge model (Figure 6.2) involves longitudinal vibration of the main truss structure primarily because the taller piers and longer spans of the main truss result in more flexible structure than the approach structure. The second mode involves longitudinal vibration of the south approach structure which consists of much fewer spans than the north approach does. The longitudinal vibration of the north approach is activated by the third mode. The forth model involves the vertical vibration of the two distinctively long spans (span 8 and 9) of the north approach. After the first mode, the main truss structure is excited again by the fifth mode involving the transverse vibration of the main truss structure.

The vibration modes are essentially the same for modeling Cases 2A, 3A and 4A (Figure 6.3). The vibration modes computed from the modeling Cases 2B and 3B are also similar (Figure 6.4). This phenomenon can be anticipated from the fact that the differences of the stiffness coefficients computed for these cases (e.g. Cases 2A versus 3A and Cases 2B versus 3B) are relatively small. It is also observed that the vibration modes computed from Case 4B (Figure 6.5) are basically a combination of the previously mentioned modes. This is because the dynamic stiffness values computed for Case 4B including the PSPI effect are smaller than those without the PSPI effect (Case 4A) but larger that the static stiffness values with the PSPI effect (Cases 2A and 3A). Therefore, the corresponding vibration modes for Case 4B appear to contain modes similar to those from other cases. The vibration modes for Cases 5A and 5B (Figure 6.6) are similar. For the integrated model (Cases 6A and 6B), the vibration modes are also alike. Figure 6.7 shows that the mode shapes of the integrated soil-foundation-structure models are fairly similar to those of other models.

It is clear (Figures 6.2 to 6.7) that the vibration modes of the bridge model in which the foundations are modeled by a set of either linear or nonlinear springs or by a detailed soil-pile model are essentially similar, especially for the first three modes. The general difference is the ordering of the modes (different mode ordering for different foundation models). It is noteworthy that vibration modes of the main truss and its approach structures are uncoupled. These uncoupled motions are indeed anticipated because the truss is isolated from its approaches by the expansion joints at Piers 8 and 12, and because the main truss bearings at these piers are of expansion-bearing type, which allows the truss to longitudinally move and rotate independently of the piers and vice versa. These independent movements of the main truss and its approaches may lead to beating or pounding of the two structures at the expansion joints (Piers 9 and 12), which may possibly lead to structural failures. Further investigation of the response at these vulnerable locations is carried out in the subsequent study.

6.5 Response of the Cairo Bridge to Seismic Loading

The seismic induced force and displacement demand is dependent not only on the modeling of the structure but also the modeling of the foundation. How the foundations are modeled directly affects the seismic response of the bridge structure. The following comparison study is devoted to an investigation of the effects of different foundation modeling on the bridge response. First, the comparison of the displacement and rotation response of the bridge at the base of the piers as well as at the bent cap is conducted. The response of the bridge at such vulnerable locations as the expansion joints and truss bearings is then examined. The member forces and moments in the pier columns are also investigated. In addition, the member forces and moments in the piles from selected pile foundations computed from different modeling cases are compared.

Furthermore, the seismic performance evaluation of the bridge is conducted. Four sets of input motions are used. The first set, which is used in all of the above-mentioned comparison study, is obtained from the site response analysis discussed in Chapter 5. These input motions may be considered as an equivalent of 4% probability of exceedance in 50 years (4%/50 year hazard level), which represents a return period of 1,225 years. These motions have a peak acceleration of about 0.7g and represent the motions from an earthquake having moment magnitude of 7.5 and an epicenter at the New Madrid seismic zone, which is 40 km from the Cairo Bridge. Three other sets are used for seismic performance evaluation of the bridge only. These three sets are equivalent ground motions representing 50%/50, 10%/50 and 2%/50 hazard levels corresponding to a return

period of 73, 475 and 2,475 years, and a peak acceleration of 0.03g, 0.20g and 1.65g, respectively. The seismic performance evaluation for different excitation intensities is performed using the modeling Case 5A in which the foundation characteristics are represented by the nonlinear load-deflection and moment-rotation relationships obtained from the pile foundation model.

6.5.1 Response at Base of the Piers

The maximum earthquake-induced displacements and rotations computed at the base of the piers (center of the pile cap) for all cases are presented in graphical form in Figures 6.8 to 6.13. The positive and negative values indicate the maximum magnitude of the displacements and rotations in the positive and negative direction, respectively. The maximum response at the base of each pier computed from all cases is compared for each degree of freedom. The displacement responses at the base of Piers 1 and 12 computed for Cases 2A, 2B and 6A are also shown in Figures 6.14 to 6.15. To develop an insight on the level of excitation and nonlinearity, the load-displacement histories of the nonlinear foundation springs obtained for Case 5A at the base of Piers 1 and 12 are shown in Figures 6.16 to 6.19 for the hazard level of 50%, 10%, 4% and 2% probabilities of exceedance in 50 years, respectively.

It is shown from Figures 6.8 to 6.13 that the variation of the computed maximum response among all cases is somewhat scattered. This scatter is indeed expected because the distribution of the foundation stiffness is different among all cases. In addition, since the entire bridge model is used in these analyses, the change in the foundation characteristics affects the distribution of the response of the structure both locally and globally. However, by plotting the response of all cases together, several interesting results are observed.

The computed maximum longitudinal and transverse responses compare reasonably well for Cases 2A and 3A and for Cases 2B and 3B although the responses for Case 3 are slightly larger than those from Case 2. It is also observed that, among the no-PSPI cases (Cases 2A, 3A, 4A, 5A and 6A), the maximum and minimum lateral and vertical displacements are comparable. This implies that the calculated shear forces at the top of the pile caps are roughly the same for each case. For Cases 2, 3 and 4, the vertical displacement response appears to be most influenced by the PSPI effect. This is due to the fact that the vertical stiffness of the foundations computed using the interaction factor method to account for the PSPI is reduced to the range of 2-15% of the stiffness without the PSPI. In contrast, the difference between Cases 5A and 5B is quite small, and

so is the difference between Cases 6A and 6B. For Case 5B, although the lateral stiffness of the foundations is reduced by about 10-25% due to the PSPI, an increase in maximum response is less than 15%. Similarly for Case 6B, the effect of reducing the stiffness of the lateral soil springs by 25% on the maximum response at the base of the piers is not consequential at all.

For the longitudinal rotation response, the comparison (Figure 6.12) shows a similar trend of increasing maximum response for the piers of the north approach, as they are closer to the main channel. The maximum longitudinal rotation experienced at Pier 8 for Case 6A (0.0043 radian) corresponds to the vertical displacement at the outermost pile of 18.8 mm, which is about 9.5 times larger than the vertical displacement shown in Figure 6.10.

For the transverse rotation response which is about 5 to 10 times as large in magnitude as the other two rotations, the largest maximum rotation occurs at Pier 1 and the maximum responses experienced by the piers closer to the main channel are decreasing. The maximum transverse rotation experienced at Pier 1 for Case 6A (0.018 radian) corresponds to the vertical displacement of the outermost pile of 12.7 mm, which is 6.4 times larger than the vertical displacement shown in Figure 6.10.

The torsional response at the base of the piers of the north and south approaches appears to be similar to a beat pattern with its highest amplitudes at Piers 1, 5 and 12. The maximum torsion experienced at Pier 1 for Case 6A (0.0009 radian) corresponds to the lateral displacement of the outermost pile of 5.1 mm, which is small compared to the longitudinal and transverse displacements shown in Figures 6.8 and 6.9.

These results indicate that the largest vertical displacements and, therefore, vertical pile forces occur due to rocking of the piers. The largest transverse and longitudinal displacements result from translations of the piers. In addition, it is well to note that the difference of the maximum rotations experienced at the base of the piers computed from the no-PSPI cases is significant for Cases 2, 3 and 4 where the interaction factor method was used to account for the PSPI. This means that the maximum vertical pile forces will be underestimated for modeling Cases 1, 2A, 3A and 4A. The transverse rotation and torsional responses appear to be less influenced by the PSPI than is the longitudinal rotation response.

The displacement histories at the base of the selected piers for Cases 2A, 2B and 6A are compared in Figures 6.14 and 6.15. The computed responses for Case 2B contain higher amplitude

and longer period motions than those for Case 2A. The responses for Case 2B are also smoother. These characteristics are indeed anticipated from the much more flexible structure as the PSPI effects are accounted for using the static IF method. Note that the motion histories of other piers, although not shown here, also suggest a similar trend.

It is observed from Figures 6.16 and 6.19 (Case 5A) that higher intensity levels of input motions lead to a much higher degree of nonlinearity experienced at the foundations. The intensity level of the motions representing the 50%/50 year hazard is so small that the foundations behave in an elastic range. For the 10%/50 year hazard level, the results show minor excursions into nonlinear behavior of the foundations. Much higher degrees of nonlinearity are observed at the foundation responses for the 40%/50 and 2%/50 year hazard levels. The maximum longitudinal and transverse displacements experienced at the foundations computed for the 2%/50 year hazard level are as much as 4 times larger that those computed from the 4%/50 year hazard level (the original input motions) although the motions representing the 2%/50 year hazard are obtained by multiplying the original motions by a factor of 2.36 for the longitudinal motion and 2.28 for the transverse motion.

Despite such highly nonlinear response observed for both longitudinal and transverse direction for the 2%/50 year hazard, the foundation response in the vertical direction does not go as much into nonlinear region as that for other directions. Although the performance of these existing foundations to resist earthquake-induced vertical loads is somewhat satisfactory, they are found to be highly vulnerable for seismic loading in the horizontal directions. The maximum longitudinal and transverse displacements experienced at Pier 1 and the transverse displacement at Pier 12 are so large that they are expected to be damaging to both the foundations and the overall bridge structural and nonstructural system. In fact, it is strongly believed that bridge would be severely damaged, or might even collapse if subjected to this equivalent 2%/50 year hazard level.

6.5.2 Response of the Bridge Superstructure

The maximum displacements at the bent cap of the piers for the 4%/50 year hazard level computed from all modeling cases are compared in Figures 6.20 to 6.22. The computed absolute displacement histories of Piers 1, 9 and 16 for Cases 2A, 2B and 6A are shown for comparison in Figures 6.23 to 6.25. By comparing the maximum response obtained from the foundation-modeling cases with the fixed-base model case, it is evident that the maximum displacements are sensitive to the foundation modeling. It is observed that the bent caps of most piers at the approach structures

undergo higher displacement as the flexibility of the foundation is considered. However, there are some piers where the displacements computed from the fixed-base model are actually higher than those from other modeling cases (e.g., the longitudinal displacement at Piers 11 and 15).

The general statement that by including the flexibility of the foundation, the maximum horizontal displacements of the superstructure increase does not necessarily apply for such a long span bridge as the Cairo Bridge. In addition, it has been demonstrated that the effect of reducing the foundation stiffness due to the PSPI does not always increase the maximum lateral displacement experienced at the superstructure as generally expected. A decrease in the maximum lateral displacements at the bent cap at several piers is observed for the PSPI cases. The fluctuation of the maximum seismic response is hard to predict for this case study since the Cairo Bridge not only consists of several spans, but it also consists of different structural systems (truss structure for the main channel and steel plate girders for the approach structures).

The vertical response of the bridge seems to be sensitive to the foundation flexibility, especially for the PSPI cases. However, it should be noted that most of the absolute maximum vertical displacement experienced at the bent cap is attributed to the motions of the vertical displacement of the foundation. The relative displacement between the foundation and the bent cap is in fact very small. For the longitudinal and transverse directions, the PSPI effects on the response of the structure appear to be less significant than those on the response of the foundations. A rational explanation is that for the PSPI cases (more flexible foundations), the input energy is absorbed through the strain energy of the foundations rather that other parts of the structure. For the stiffer foundations, less energy is absorbed through the foundations and more through other parts of the structure. In other words, the more flexible the foundation characteristics, the higher the displacement experienced at the foundations but the lower the relative displacement between the foundation and the superstructure. This compensation of the displacement at the foundation and the relative displacement experienced by the superstructure explains why the PSPI effects on the superstructure response are less significant than those on the foundation response.

The results show that the maximum displacements at the bent caps computed for Case 6 is slightly greater than those computed for Case 5, although both of them show a similar trend of the displacement distribution along the bridge. The flexibility of the foundations for Case 5 and Case 6 is undoubtedly similar. However, by integrating the soil and pile foundations to the bridge structure,

the mass, the stiffness and the distribution of the stiffness (and thus distribution of the force) of the structure change.

Shown in Figures 6.23 to 6.25 are the motions at the bent cap of selected piers (Pier 1 from the north approach, Pier 9 from the main channel and Pier 16 from the south approach). The computed displacement motions at most piers from Case 2B not only contain higher amplitude but also longer periods than those computed from Cases 2A and 6A as can be expected from more flexible structure. The computed motions from these two cases appear to be more in agreement at the main channel and south approach structure. The variation of the response of the main channel structure among all cases is small. Such a small difference between the computed motions for Cases 2A and 6A and for Cases 2A and 2B is not surprising because these piers are supported on caissons which are assumed to be fixed for all degrees of freedom.

6.5.3 Response of the Main Truss Structure

The stress check of the truss members is performed using the SAP2000 program. The program allows users to examine the stress ratios for steel design computed in accordance with the user-specified design code. The stress ratios refer to the ratio of the design load combination for selected design code experienced at the member to the strength of that member. In this study, the AISC-LRFD93 specification for steel is used along with three load combinations of 1.4(Dead load), 1.2(Dead load)+1.0(Earthquake load), and 0.9(Dead load)+ 1.0(Earthquake load). The results presented herein are obtained from the largest among these three load combinations. Figure 6.26 shows the stress ratios computed by the program for the north half of the main truss for different modeling cases for the motions representing the 4%/50 year hazard. The stress ratios computed for different excitation intensities are also shown in Figure 6.27. These results are from modeling Case 5A.

For the 4%/50 year hazard level, the results show that a number of truss members, especially at the supports, are overstressed. The stress ratios or demand/capacity ratios are found to be greater than 1 for several members. The D/C ratios computed for Case 1 are found to be smaller than those computed from other foundation modeling cases. For instance, by considering the same truss member (the first horizontal member from the left) the D/C ratio computed from Case 1 is equal to 2.65 whereas the D/C ratio computed from Cases 5A and 6A is about 3.31 and 4.00, respectively.

Although these D/C ratios are so large that the truss members would behave nonlinearly, the D/C ratio computed from Case 1 is less than that from Case 6A or other cases by a factor of about 1.5, implying that the fixed-base model may be unconservative in predicting the forces in the truss members for the Cairo Bridge.

It is shown from Figure 6.27 that, at higher intensity level of the input motions, larger numbers of the truss members are overstressed and the degree of overstressing or the D/C ratio of these members are also higher. The D/C ratio of the same first horizontal truss member is equal to 0.68, 1.38, 3.31 and 10.73 for the motions representing the 50%/50, 10%/50, 4%/50 and 2%/50 hazard levels, respectively. For the 50%/50 and 10%/50 year hazard levels, a few truss members are slightly overstressed. The truss members for these excitation levels are not expected to suffer any significant damage. For the 4%/50 year hazard level, the D/C ratios of the members at the end support are about twice as much as those for the 10%/50 year hazard level. Some damage is probable for this level of excitation. For the 2%/50 year hazard level, it is found that almost all of the primary load-carrying truss members are greatly overstressed. Severe damage of the truss structure particularly at the support locations can be expected. It is likely that the bridge would collapse into the river.

It is of interest to note that several truss members undergo a significant minor-axis bending moment. For instance, the D/C ratio of the horizontal member to the left of the middle support for the 2%/50 year hazard (Figure 6.27(d)) is 1.85, 37% of which results from the minor-axis bending moment. This high moment in the truss member is induced by the assumed partially-fixed connection between the floor beam system and the truss structure in the analytical model. This connection is usually modeled as a pinned connection in typical design and analysis of truss structures. However, in reality, the connection between the floor beam and the truss is not a pinned but rather a partially-fixed connection, which is assumed in modeling of the main truss structure. As a result, the bending moments in the truss members are expected from the analytical model as they would be expected in reality.

A note should be made regarding a limitation of using a linear elastic modeling and analysis for the truss. Under the 2%/50 year hazard level, several members undergo a relatively high bending moment. Plastic hinges are likely to develop at both ends of the truss members, which cannot be captured using the linear elastic analysis. The formation of plastic hinges reduces the moments experienced by the members. Consequently, the truss members whose axial compression or tension

capacity is not exceeded may be able to sustain the applied load without any significant damage or collapse.

However, for the truss members where the Euler buckling strength is exceeded (the first diagonal members at the end support (Figure 6.27(d) for the 2%/50 year hazard level), failures associated with local buckling can be anticipated. In addition, by considering the same members for the 4%/50 year hazard level, it is observed a fairly high D/C ratio attributed to the axial compression forces (1.52 out of 2.79). Although the formation of plastic hinges helps reduce the moments applied to the members, the compression force is so much larger than the strength of the member that a local failure is very likely to occur.

6.5.4 Response of Expansion Joints and Truss bearings

The computed relative longitudinal displacements across the expansion joint at Pier 12 for no-PSPI cases are presented in Figure 6.28. In these plots, a dash line represents the maximum allowable displacements after which the expansion joints are closed. It is shown that there is no impact during the analysis at the expansion joints for Case 1. For other cases, the nonlinear time-history analyses indicate that the pounding of the steel girders occurs at the expansion joint at pier 14 and only for Cases 2B and 3B where the pounding occurs at both locations of the expansion joints (Piers 9 and 12). The maximum compression forces experienced by the member upon impact for the 4%/50 year hazard level are summarized in Table 6.10.

Table 6.10. Number of Impacts and Maximum Forces Experienced at Expansion Joints.

Case	Pier 9		Pier 12	
	No. of impact	Maximum force (kN)	No. of impact	Maximum force (kN)
1	-	-	-	-
2A	-	-	3	43,300 @ 16.77 sec
2B	1	3,131 @ 15.75 sec	1	31,810 @ 16.90 sec
3A	-	-	2	11,520 @ 16.78 sec
3B	3	12,135 @ 15.52 sec	1	15,370 @ 17.03 sec
4A	-	-	2	45,800 @ 19.15 sec
4B	-	-	2	51,730 @ 16.86 sec
5A	-	-	2	60,800 @ 19.18 sec
5B	-	-	2	50,840 @ 19.20 sec

6A	-	-	3	64,000 @ 19.28 sec
6B	-	-	3	87,340 @ 19.24 sec

The analytical results of all modeling cases indicate that the impact occurs at all locations of the expansion bearings at the main truss (Piers 9 and 12). Figure 6.29 shows the relative longitudinal displacement response experienced at the expansion bearing at Pier 12 for no-PSPI cases. The dash lines in these figures represent the allowable maximum bound of the longitudinal displacements that can take place freely after which the bearings become stiff. For every modeling case, the results indicate that the allowable longitudinal displacement is exceeded several times during the analysis. In addition, since the longitudinal stiffness of the bearings is very small, the bearings undergo larger displacement than the allowable value after the impact. The maximum forces experienced by the expansion bearings upon the impact are listed in Table 6.11. No impact or pounding is observed at any of the fixed bearings at the main truss or other bearings throughout the approach structures.

Had the nonlinear elements not been used to model the expansion joints and truss bearings, the nonlinear (opening and closing characteristics at these joints) would not have been properly represented and the impact forces would not have been obtained. To investigate the response at such vulnerable locations which are prone to pounding or impact as the expansion joints and bearings, the nonlinear model is therefore required to appropriately represent the nonlinear behavior of these articulations. The modeling of the foundation is also important. The overestimation of the foundation stiffness may lead to unconservative results. As the study shows no impact at any of the expansion joints when the fixed-base model is used, whereas pounding does occur for other foundation modeling cases.

Table 6.11. Number of Impacts and Maximum Forces Experienced at Expansion Bearings.

Case	Pier 9		Pier 12	
	No. of impact	Maximum force (kN)	No. of impact	Maximum force (kN)
1	18	6,343 @ 16.58 sec	2	2,080 @ 13.28 sec
2A	13	5,489 @ 17.11 sec	5	3,044 @ 15.75 sec
2B	7	3,777 @ 16.59 sec	8	4,060 @ 14.84 sec

3A	13	5,597 @ 17.12 sec	6	3,226 @ 14.76 sec
3B	11	4,800 @ 16.56 sec	8	3,818 @ 14.88 sec
4A	18	5,959 @ 17.09 sec	5	2,163 @ 16.42 sec
4B	10	4,615 @ 16.60 sec	7	2,725 @ 16.58 sec
5A	11	4,408 @ 17.12 sec	6	4,221 @ 14.80 sec
5B	10	4,510 @ 17.12 sec	6	3,991 @ 14.81 sec
6A	12	3,684 @ 17.08 sec	4	2,766 @ 14.84 sec
6B	9	3,809 @ 16.59 sec	5	2,597 @ 14.86 sec

6.5.4.1 Forces in the Truss Bearings

Some of the maximum forces induced by the impacts at the expansion bearings (Table 6.11) are higher than the ultimate shear strength of the bearing, which is governed by the ultimate shear strength (5,366 kN) of two 51-mm (2-in) diameter high strength bolts (tensile strength ˜ 828 MPa (120 ksi) and four 51-mm (2-in) pintles. This value is calculated in accordance with the AISC-LRFD93 specification for strength of connections for both welds and bolts. The transverse shear experienced at the expansion bearings is also checked against the ultimate shear strength and presented in the form of the demand/capacity ratios, which are listed in Table 6.12 for Cases 1, 5A and 6A. The shear forces are calculated from the higher force in one direction plus 30% of the lower shear force in the other direction. It is evident from the large D/C ratios that the expansion bearings are vulnerable for transverse shears. This vulnerability in resisting the transverse shear is indeed anticipated from the rocker-type bearings (Figures 5.3(b) and 5.4(b)).

The performance evaluation of the fixed bearings is also conducted for both shears and tensions. The calculation of the shear strength and tension strength of the fixed bearing is also based on the AISC-LRFD93 specification, and similar to the expansion bearing, the shear strength and the tension strength of the fixed bearing are governed by the bolts. The shear strength is computed to be approximately equal to 48,293 kN for sixteen 76-mm (3-in) diameter high strength bolts. The D/C ratio of the fixed bearings is evaluated for both shears and tensions and presented in Table 6.12. The performance of the fixed bearings appears to be satisfactory for the 4%/50 year hazard level (i.e., the D/C ratio is less than 1 for all comparisons). Note that the difference of the D/C ratios of the truss bearings obtained from different foundation modeling cases is small.

Table 6.12. Demand/Capacity Ratios for the Truss Bearings.

Case	Expansion Bearing				Fixed Bearing			
	Pier 9		Pier 12		Pier 10		Pier 11	
	F_v	F_t	F_v	F_t	F_v	F_t	F_v	F_t
For 50%/50 year								
Case 5A	0.13	*	0.08	*	0.02	*	0.02	*
For 10%/50 year								
Case 5A	1.00	-	0.59	*	0.10	*	0.12	*
For 4%/50 year								
Case 1	3.14	-	1.87	-	0.44	*	0.44	*
Case 5A	3.21	-	1.88	-	0.42	*	0.39	*
Case 6A	2.94	-	2.21	-	0.42	*	0.42	*
For 2%/50 year								
Case 5A	4.23	-	2.69	-	0.83	-	0.62	-

Notes:

1. * denotes no tension forces experienced in the bearings.
2. – denotes no tension capacity left in the bearings.

The seismic performance evaluation of the expansion and fixed bearings is also conducted for different hazard levels. The D/C ratios are presented in Table 6.12. The truss bearings are not expected to experience any damage for the 50%/50 and 10%/50 year hazard levels. The fixed bearings are found to be satisfactory for all hazard levels. Deficiencies of the expansion bearings associated with excessive transverse shears are revealed for the excitation level of the 4%/50 year hazard and higher. The shear and/or tension failure of the bolts of the expansion bearings can be expected.

6.5.5 Member Forces and Moments in the Pier Columns

The reactions (forces and moments) in the west and east columns of all piers for Cases 1, 2A, 2B and 6A are presented in Figures 6.30 to 6.35. These reactions include the static forces and moments under dead load as well as the maximum and minimum seismic-induced forces and moments. The magnitude and distribution of the reactions experienced at the pier columns for

Cases 1 and 6A are compared to examine the effects of soil-foundation-structure interaction. The computed forces and moments for Cases 2A and 2B are also compared to evaluate the pile-soil-pile interaction effects. Note that there are no member forces presented for Pier 1 where reinforced concrete diaphragm is used instead of reinforced concrete columns.

6.5.5.1 Axial Forces

The east and west columns (Figure 6.30) undergo both compression and tensile forces. These forces are especially high at the piers supporting the main river crossing. The largest axial force occurs at Pier 8 ranging from a compression of about 94,072 kN to a tensile force of 60,201 kN in the east column for Case 1. The range of axial force is even higher (a compression force of 126,052 kN and a tensile force of 93,425 kN) for Case 6A. These forces are smaller than the axial load capacity of Pier 8 (circular reinforced concrete column having 3.66-m diameter and 0.02% reinforcement ratio). The axial load capacity is about 346,319 kN for compression and 140,029 kN for tension. The demand/capacity ratios of the axial forces for Case 6A are equal to 0.36 for compression, and 0.67 for tension. The forces at other pier columns are also smaller than the axial load capacity of the columns. The comparison of the axial forces for Case 2A and 2B show a quite similar magnitude and variation of the axial forces in the columns of most piers except Pier 8. A note is made that in spite of a significant difference in the vertical displacement computed from these two models, the discrepancy of variation and magnitude of axial forces in the columns is rather small.

6.5.5.2 Shear Forces and Moments

The comparison of shear forces in the pier columns is shown in Figure 6.31 for the longitudinal direction and Figure 6.32 for the transverse direction. These values are obtained for the motions representing the 4%/50 year hazard. Unlike the longitudinal shear, the transverse shear is less in magnitude and its distribution is more uniform. The distribution of the transverse shear fluctuates in such a way that the shear force experienced at the pier columns is larger for the pier closer to the main channel with the largest magnitude at Piers 7 and 15 and then decreases. The shear force starts increasing again at Piers 10 and 13, and the largest transverse shear force occurs at Piers 11 and 12. This up and down variation of the transverse shear is associated with the longitudinal overturning moment. It is shown from Figures 6.32 and 6.34 that the distributions of the longitudinal moments and transverse shears are somewhat similar as can be expected. It is also observed that

the distribution patterns of the longitudinal shears and the transverse moments as well as the torsional moments (Figures 6.31, 6.33 and 6.35) are quite similar.

One common observation is made from Figures 6.30 to 6.35 is that the foundation flexibility evidently has an influence on the member forces and moments in the pier columns (i.e., it can either increase or decrease the maximum member forces experienced at the pier columns as compared to the fixed base model). For instance, the results show that the maximum transverse shear force at Pier 8 computed from Case 6A (4,396 kN) is greater than that computed from Case 1 (2,919 kN), but the longitudinal shear force for Case 6A which is about 3,874 kN is less than that for Case 1 (5,047 kN). The general belief that the incorporation of the foundation flexibility into the structural model decreases the member forces is not necessarily applicable for such a long span bridge as the Cairo Bridge. In addition, it is clear that the member forces and moments at the pier columns are less sensitive to the PSPI effects than are the displacement and rotational responses.

The shear forces and moments are compared with the ultimate strength of the reinforced concrete members computed according to American Concrete Institute (ACI 318-95), and presented in form of demand/capacity ratios (D/C ratios) in Table 6.13 for Cases 1, 5A and 6A. The values listed in this table correspond to the motions representing the 4%/50 year hazard. The shear and moment demands are approximately computed from the higher force and moment in one direction plus 30% of the lower force and moment in the other direction. It is evident that although the forces and moments experienced at the pier columns at the main channel are much higher than those at the approach piers, the D/C ratio is less for the pier columns at the main channel. This is because the pier columns at the approach structure are relatively small (about 1.5-to-2.0-m diameter) as compared to the large pier columns at the main channel (5.2-m diameter for Piers 10 and 11) as they are required to resist enormous loads from the main truss. Note that the D/C ratios for different modeling cases are somewhat similar, indicating that the member forces and moments in the pier columns are not sensitive to different foundation modeling.

Table 6.13. Demand/Capacity Ratios for Shears and Moments in Pier Columns for Different Cases.

Pier	Shear			Moment		
	Case 1	Case 5A	Case 6A	Case 1	Case 5A	Case 6A
Pier 2	**1.12**	**1.51**	**1.38**	**3.15**	**4.16**	**3.79**

Pier 3	**2.00**	**2.05**	**1.58**	**4.78**	**4.94**	**3.71**
Pier 4	**1.82**	**1.84**	**1.40**	**4.67**	**4.47**	**3.57**
Pier 5	**2.34**	**1.54**	**1.46**	**1.97**	**1.31**	**1.37**
Pier 6	**1.82**	**1.37**	**1.36**	**1.88**	**1.42**	**1.37**
Pier 7	**2.28**	**1.57**	**1.85**	0.57	**1.54**	0.47
Pier 8	0.50	0.33	0.47	0.63	0.31	0.49
Pier 9	0.52	0.56	0.61	**1.12**	**1.24**	**1.27**
Pier 10	0.58	0.58	0.64	0.57	0.49	0.63
Pier 11	0.62	0.58	0.57	0.63	0.55	0.57
Pier 12	0.48	0.59	0.43	**1.19**	0.99	0.53
Pier 13	0.73	0.81	0.86	**2.56**	**2.13**	**2.51**
Pier 14	**1.43**	**1.12**	**1.26**	**2.04**	**1.79**	**1.78**
Pier 15	**1.47**	**1.28**	**1.43**	**1.99**	**1.80**	**1.96**
Pier 16	0.82	0.72	0.85	**2.00**	**1.84**	**1.79**

The D/C ratios of the pier columns for various excitation intensities are listed in Table 6.14. These values are obtained from modeling Case 5A. No deficiency of the pier columns is observed for the 50%/50 year hazard level. The shear capacity of the pier columns is also found to be adequate for the 10%/50 year hazard level; however, the moment capacity of the columns at Piers 2, 3 and 4 is exceeded by a factor of 1.26, 1.54 and 1.57, respectively. For higher excitation level (the 4%/50 year hazard level), more column vulnerabilities are observed. The primary deficiencies are either insufficient column shear capacity (most of the north and south approach piers) or inadequate flexural ductility (all piers except Piers 7, 8, 10 and 11). The D/C ratios significantly increase for the 2%/50 year hazard level. At Pier 7, the D/C ratio for moment increases about 5 times as much as that for 4%/50 year motions. The D/C ratios are found to exceed one for all piers except Pier 8. It can also be observed that the D/C ratios are much higher for both the approach structures than for the main channel. The approach structures are expected to be badly damaged by the 2%/50 year ground motion hazards.

Table 6.14. Demand/Capacity Ratios for Shears and Moments in Pier Columns for Different Excitation Intensities.

Pier	Shear	Moment

	50%/50	10%/50	4%/50	2%/50	50%/50	10%/50	4%/50	2%/50
Pier 2	0.06	0.45	**1.51**	**2.73**	0.18	**1.26**	**4.16**	**7.65**
Pier 3	0.09	0.65	**2.05**	**3.34**	0.22	**1.54**	**4.94**	**8.10**
Pier 4	0.08	0.58	**1.84**	**2.90**	0.21	**1.51**	**4.47**	**7.67**
Pier 5	0.07	0.50	**1.54**	**2.52**	0.06	0.40	**1.31**	**3.01**
Pier 6	0.06	0.44	**1.37**	**2.84**	0.06	0.45	**1.42**	**3.01**
Pier 7	0.08	0.58	**1.57**	**3.05**	0.08	0.57	**1.54**	**7.89**
Pier 8	0.01	0.10	0.33	0.96	0.01	0.10	0.31	0.80
Pier 9	0.02	0.16	0.56	**1.10**	0.05	0.32	**1.24**	**1.83**
Pier 10	0.02	0.18	0.58	**1.33**	0.02	0.18	0.49	**1.26**
Pier 11	0.03	0.20	0.58	**1.47**	0.03	0.20	0.55	**1.44**
Pier 12	0.03	0.20	0.59	**1.21**	0.05	0.35	0.99	**1.63**
Pier 13	0.04	0.26	0.81	**1.27**	0.10	0.68	**2.13**	**3.81**
Pier 14	0.06	0.41	**1.12**	**1.96**	0.08	0.59	**1.79**	**3.79**
Pier 15	0.06	0.41	**1.28**	**2.36**	0.08	0.56	**1.80**	**4.06**
Pier 16	0.04	0.24	0.72	**1.46**	0.09	0.63	**1.84**	**3.91**

6.5.6 Member Forces and Moments in the Piles

The member forces and moments in three piles in the selected pile foundations (Piers 2 and 16) are compared in Tables 6.15 and 6.16. The typical location of the selected piles in the group is shown in Figure 6.36.

For Cases 1, 2A and 2B, the member forces and moments of the piles are computed using basic matrix operations; multiply the stiffness matrix of the single pile by the pile-head deformation vector which is computed from the displacements and rotations of the foundation springs obtained from the analysis. For Case 1 (the fixed-base model), the displacements and rotations of the pile group are computed from a product of the vector of maximum forces and moments experienced at the base piers and the flexibility matrix from the foundation modeling Case 2A. The stiffness matrix of single piles obtained from Case 2A is also used to calculate the pile-head displacements for Case 1. The pile-head displacements for Cases 1, 2A and 2B are evaluated using a pile-group-to-pile coordinate transformation matrix. A computer program is written to incorporate all these steps and perform the calculation of the pile-head response.

Note that a set of the pile group displacements and rotations, which are used in calculation of the pile head forces and moments, is a combination of the maximum computed responses of the foundation springs in positive and negative directions. The directions of maximum displacements and rotations are selected in such a way that the pile on one side of the foundation (Pile 3) experiences the largest forces and moments (e.g., the largest compression force (-) for the vertical degree of freedom). For all other degrees of freedom, the directions of the maximum pile group displacements and rotations are chosen to produce the largest positive forces and moments (positive direction) at Pile 3.

Table 6.15. Member Forces and Moments of Selected Piles in the Foundation at Pier 2 (36 Piles).

Pile/Case	Force (kN)			Moment (kN-m)		
	Axial	Long. Shear	Trans. Shear	Torsion	Long. Moment	Trans. Moment
Pile 1						
Case 1	+258.7	18.9	81.3	0.24	78.10	26.50
Case 2A	+459.4	21.3	111.3	0.34	107.40	29.30
Case 2B	+119.4	61.2	109.7	0.73	278.16	129.03
Case 6A	985.3	75.7	135.3	0.12	145.63	61.99
Case 6B	994.6	71.5	145.6	0.12	153.40	61.95
Pile 2						
Case 1	-147.1	29.1	81.3	0.24	78.10	36.19
Case 2A	-116.4	33.1	113.4	0.34	107.40	40.54
Case 2B	-167.5	56.7	83.4	0.71	243.30	137.75
Case 6A	17.2	75.7	150.9	0.17	150.96	68.35
Case 6B	19.9	72.0	149.9	0.18	159.51	69.22
Pile 3						
Case 1	-583.8	37.4	81.3	0.24	78.11	44.08
Case 2A	-758.1	47.6	113.7	0.34	107.41	54.35
Case 2B	-646.2	78.2	109.8	0.73	278.18	173.19
Case 6A	1,047.6	71.7	147.2	0.16	146.37	58.94
Case 6B	1,001.0	68.3	146.2	0.17	154.53	59.53

Table 6.16. Member Forces and Moments of Selected Piles in the Foundation at Pier16 (49 Piles).

Pile/Case	Force (kN)			Moment (kN-m)		
	Axial	Long. Shear	Trans. Shear	Torsion	Long. Moment	Trans. Moment
Pile 1						
Case 1	+389.5	26.5	61.7	0.26	57.92	31.83
Case 2A	+512.7	36.5	67.0	0.30	63.25	41.49
Case 2B	+116.5	63.9	44.3	0.70	123.37	159.60

Case 6A	762.4	76.2	128.2	0.08	108.54	58.93
Case 6B	771.7	72.7	128.1	0.08	114.95	58.99
Pile 2						
Case 1	-125.0	36.9	61.7	0.26	57.92	38.64
Case 2A	-112.7	47.7	67.0	0.30	63.25	51.88
Case 2B	-128.9	63.8	38.5	0.72	122.59	178.48
Case 6A	66.3	83.8	134.9	0.08	118.01	68.54
Case 6B	72.1	80.2	134.8	0.10	125.15	69.20
Pile 3						
Case 1	-639.5	46.1	61.7	0.26	57.92	49.88
Case 2A	-738.1	58.9	67.0	0.30	63.25	62.27
Case 2B	-445.5	77.1	44.3	0.70	123.39	197.47
Case 6A	985.4	84.2	125.8	0.15	107.72	66.97
Case 6B	957.5	80.2	125.7	0.16	114.21	67.11

It is noteworthy that the maximum or minimum displacements and rotations of the foundation springs may not occur at the same time (i.e., at any time step of the analysis, the responses of the foundation springs may consist of the largest movement in one degree of freedom but may or may not consist of the largest movement in all other degrees of freedom). The more representative calculation of the pile head forces than the above-mentioned procedure is to compute the displacements and rotations of the pile foundations in all six degrees of freedom at each time step and then calculate the corresponding forces and moments of the piles. Comparison of these forces and moments computed for all time steps is required to obtain the maximum values, which again may or may not occur at the same time step. The time-history analyses conducted in this study contain a total of 4,095 time steps during which the maximum responses are expected to be within the 1,000th and 3,000th time step. That means the calculation of pile group response and pile-head response at each time step for a total of 2,000 time steps is needed. A computer program may be written to perform this calculation. However, the adopted procedure discussed in the previous paragraph may very well be used to calculate the upper-bound values of the reactions experienced by each pile, which is of main interest in this study.

For Cases 6A and 6B, the maximum and minimum member forces and moments in the piles as well as their distribution along the pile length can be directly obtained from the analytical models. The distribution of the pile response along its length may be essential especially when the piles are embedded in a layered soil system having a significant variation of soil properties for each layer. The response of the pile at the discontinuity location between layers may be of main concern for

seismic performance evaluation of the bridge. These issues can be readily taken care of using the integrated soil-foundation-structure model. It is well to note that these forces and moments are the maximum values experienced by the piles during the entire time-history analysis. Therefore, the forces and moments listed for Cases 6A and 6B in Tables 6.14 to 6.15 are the maximum absolute values. That means the presented values are the larger between the maximum (+) and minimum (-) forces and moments experienced by the piles. However, an observation is made that the magnitude of the maximum and minimum responses is fairly similar.

It is first observed from these tables that most of the forces and moments computed from Case 1 are less than those computed from other cases. The fixed-base model clearly underpredicts the displacements and rotations at the foundations as well as the maximum forces and moments experienced in the piles at Piers 2 and 16. The comparison between Cases 2A and 2B indicates a notable difference in both forces and moments in the piles. It is observed that for the central pile (Pile 2) all forces and moments except the transverse shear increase for Case 2B. For the corner piles (Piles 1 and 3), the longitudinal shear force and moments for all components (torsion, and other two moments) increase, whereas the axial force decreases quite significantly especially for the tensile force at Pile 1. Although the seismic-induced vertical displacement computed for Case 2B are much greater than that for Case 2A, the maximum axial compression force is less for Case 2B. This is because of a significant reduction of vertical stiffness of single piles due to the PSPI effects taken into account using the interaction factor method.

On the contrary, by comparing the computed pile responses from Cases 6A and 6B, it is observed that the difference between the forces and moments is relatively small. The difference is indeed less than 10% for most components. Due to a fluctuation of these pile responses both in the same foundation and among different foundations, it is difficult to establish a clear trend. Nonetheless, one evident conclusion is that the effect of softening the soil reactions is insignificant not only for the overall dynamic characteristics and response of the bridge as previously discussed, but for the response of the piles as well.

The comparison also shows that a majority of forces and moments in the piles computed from Cases 1 and 2A are smaller than those computed from Case 6A. It is worth repeating once again that the forces and moments computed for Cases 1 and 2 are the maximum possible or the upper-bound values. These upper-bound values appear to be less than those computed for Case 6, which may possibly raise a question concerning conservatism of applying the fixed-based model or the

equivalent linear or nonlinear foundation springs in seismic performance evaluation of the bridge foundation system.

In addition, it should be noted that the axial capacity of the pile is about 430 kN for compression and 415 kN for tension considering the ultimate shear and end-bearing resistance of the soils. The axial capacity of a 0.3-m diameter cast in place concrete pile with a minimum reinforcing steel is about 2,020 kN for compression and 590 kN for tension. The shear and moment capacities of the pile are 20 kN and 70 kN-m, respectively. Most of the forces and moments in the piles exceed the ultimate capacity. For instance, at Pier 2, the D/C ratio for moment of Pile 3 (the higher moment in one direction plus 30% of the lower moment in the other direction) computed from Case 6A is 2.5.

6.6 Recommended Retrofit Strategy for the Cairo Bridge

The Cairo Bridge was ranked within the 20 highest risk bridges with respect to their potential damage during earthquake; therefore, it was selected for preliminary seismic analysis and retrofit design by IDOT. Geotechnical and structural evaluations were performed in accordance with current FHWA Seismic Retrofit Guidelines [ATC (1983)]. The geotechnical and structural retrofits recommended by IDOT [Anderson et al. (1994)] are first reviewed. Following that are discussions on plausible additional retrofits of superstructure and substructure based upon the detailed seismic performance evaluation of the bridge conducted in this study for an equivalent of 4% probability of exceedance in 50 years (corresponding return period of 1,225 years or a peak acceleration of 0.7g).

6.6.1 Geotechnical Retrofits

The geotechnical retrofits are not of main concern in this research study; therefore, only a brief review of the geotechnical analysis and retrofit recommendation made by IDOT is presented here. The geotechnical analysis indicated a potential of widespread liquefaction at both the north and south approaches, with minimal liquefaction in the river channel. Consequences of liquefaction include bearing capacity failure of foundations, slope failure of abutment fills, and lateral spreading of the ground surface. The caisson foundations supporting the main river crossing are not expected to be significantly affected by liquefaction, and thus no geotechnical retrofit is required.

Three options of liquefaction mitigation are considered. The first option is to prevent liquefaction from developing or to improve soil strength by densification (vibro-compaction, compaction grouting) or by adding cohesion (permanent grouting). The second option is to underpin

the bridge piers by installing new piles around the perimeter of the existing pile cap. The new piles are to be driven below the liquefaction zone. This option is somewhat similar to foundation retrofits which will be discussed subsequently. The third option is a combination of the first and second options. Both soil improvement and underpinning (the third option) are recommended to alleviate the liquefaction problems at the approach piers of the Cairo Bridge.

6.6.2 Structural Retrofits

The structural retrofits may be divided into two categories, (1) superstructure retrofit which involves the expansion joints and bearings, and (2) substructure retrofit which includes structural retrofitting of columns, piers and foundations.

6.6.2.1 Superstructure Retrofits

Installation of restraining devices such as cable restrainers and structural steel restrainers (restraining beam) at the expansion joints and links is recommended to control movement of the superstructure at expansion joints and to prevent expansion bearings from toppling as a result of excessive longitudinal displacements. To accommodate large longitudinal displacements, extension of seat length is also suggested. The support length may be increased by adding corbels or brackets or installing seat extension devices developed by Caltrans (1993). Upgrading transverse restraint system is also recommended to maintain stability of the superstructure in the transverse direction.

This above-mentioned retrofit scheme is unlikely to be adequate for the expansion bearings at the main truss. The analytical results indicate excessive forces as well as displacements at the expansion bearings. The forces in the truss members especially at the supports are also found to be particularly high. Replacing all existing truss bearings with seismic isolation bearings is strongly recommended not only to accommodate the excessive displacements but also to reduce the seismic forces to be transmitted to the superstructure or the truss members.

6.6.2.2 Substructure Retrofits

Retrofit strategies as recommended by IDOT for reinforced concrete pier columns focused on improving column ductility rather than increasing column strength. The ductility of the columns can be greatly improved through increased confinement and enhanced ductility. The steel column jackets are recommended to increase the flexural ductility and shear strength of the columns at selected piers. The installation of a partial height steel jacket is required to increase the column

flexural ductility at the top and bottom of Piers 2, 3 and 4. The installation of a full height of steel jacket is required at Piers 5, 6, 7, 9, 10, 11, 12, 13, 14 and 15 to increase the shear capacity. Reconstruction of existing joints between column and foundation and between column and bent cap is also necessary to enhance the shear strength at Piers 12, 13, 14 and 15. Column retrofit is not required at Piers 8 and 16.

The seismic performance of the pier columns of the Cairo Bridge is investigated in this study. It is shown that seismic deficiencies in the columns are found in all the piers at both the north and south approaches. The pier columns are found to be deficient in both flexural ductility and shear capacity at all piers except Pier 8 at the north approach; Piers 9 and 10 at the main river channel; Pier 7 where only inadequate shear capacity is found; and Piers 12, 13 and 16 where only inadequate flexural ductility is found (Table 6.13). Consequently, it is recommended that in addition to column joint reconstruction, column retrofits for both flexural ductility and shear capacity be applied to all piers except Piers 8, 10, 11, 12, 13 and 16. Piers 8, 10 and 11 do not require column retrofitting. Piers 12, 13 and 16 require column retrofitting for flexural ductility only. Contrary to IDOT's recommendation, column retrofits are needed for Piers 16 and are not needed for Piers 10 and 11.

As previously discussed, underpinning of the foundations with new piles is recommended for failure associated with liquefaction at the approach structures. In combination with this retrofit, the flexural and shear capacity of the pile cap is increased by adding reinforcement and concrete section, and by post-tensioning the pile cap. For the Cairo Bridge, increasing the pile cap thickness for shear is recommended only at Piers 5, 6 and 7, and post-tensioning the pile cap is recommended only at Pier 1. Although no quantitative evaluation of the pile caps is performed, it is strongly believed that foundation retrofit by increasing the pile cap thickness should be recommended for several more piers than three piers (Piers 5, 6 and 7). This is because the axial forces in the piles are observed to be relatively high at the foundations supporting Piers 2 and 16 (Tables 6.14 and 6.15). Similar observation is also made at other piers.

6.7 Summary and Conclusions

The comparison studies conducted in this research have provided valuable lessons for investigating the sensitivity of the seismic response and dynamic characteristics of a long span bridge to uncertainties in defining system parameters such as structural, soil, and foundation

properties. In modeling of the Cairo Bridge, the structural properties are carefully and elaborately modeled based on justifiable modeling techniques and concepts. The soil properties are properly characterized according to the geotechnical information furnished by both IDOT and Illinois Geological Survey. The foundation properties are modeled using several approaches, some of which are recommended by several code specifications and adopted in practice, some are widely accepted among researchers, and some are proposed in this study.

One of the primary objectives of this research study is to apply the currently available modeling techniques to account for the soil-structure interaction for bridges and then compare the results obtained from these models with those obtained from the soil-foundation-structure model proposed in this study. The comparison and parametric study was conducted to examine the effects of different modeling techniques on the dynamic characteristics and seismic response of the Cairo Bridge. The study was divided into four parts; (1) comparison of the foundation stiffness, (2) comparison of the dynamic characteristics, (3) comparison of the seismic response of the bridge, and (4) seismic performance of the bridge for different excitation intensities. The concluding remarks obtained from each part are summarized below.

Comparison of foundation stiffness

The stiffness coefficients obtained from the elastic continuum and the beam on inelastic foundation approaches are comparable. In addition, the variation of the dynamic stiffness with respect to loading frequencies is somewhat uniform for the frequency range of interest for earthquake loading; therefore, at low frequency loading, the static stiffness may be properly used. It is well to note that the conventional static and dynamic interaction factor method for taking into account the PSPI effects significantly reduces the stiffness of the pile group foundation especially for large pile groups (i.e., the vertical stiffness is reduced to as low as 2% of the original foundation stiffness without the group effect). In contrast, for the proposed foundation model case, the lateral and torsional stiffness of the foundations reduce by about 10-30% due to the PSPI. The vertical and rotational stiffness is not much influenced by the PSPI mainly because the soil conditions from which most of the vertical stiffness is derived are predominantly sands for which the PSPI is not expected to be strongly pronounced. Using the multiplier method for modeling the PSPI can take into account the layering nature of the soil profile as well as the soil conditions more realistically than the static interaction factor method.

Comparison of dynamic characteristics of the bridge

Modeling of the foundations causes the period of the structure to increase. The modal periods of the bridge are elongated by 5-160% when the foundation flexibility is considered. The modal periods of the structure reduce quite significantly for the cases in which the IF method is applied to account for the PSPI effects as compared to those from other cases. The PSPI effects on the modal periods of the bridge are not of great consequence for the modeling cases in which the foundation characteristics are represented by nonlinear springs obtained from the proposed foundation model. For the integrated soil-foundation-structure modeling case, the effects of softening the stiffness of soil springs by 25% are insignificant (i.e., the difference of the periods from the models with and without considering the PSPI is less than 2%). An observation is made that the mode shapes of the bridge from all modeling cases are similar. In addition, it is noteworthy that the vibration of the main truss and its approach structures are uncoupled for all three principal directions, which may result in independent movements and thus lead to beating or pounding of the bridge superstructures.

Comparison of seismic response of the bridge

The flexibility of the foundations and the PSPI effects may either increase or decrease the design values (base shear and overturning moment) and the response (horizontal displacements and rotations) of such a long span bridge as the Cairo Bridge. The effects of reducing the foundation stiffness do not always increase the maximum displacements experienced at the superstructure, or decrease the member forces and moments in the pier columns as generally believed. The responses of the long span bridge depend not only on the foundation stiffness of an individual pier but also on the distribution of the foundation stiffness among all piers. For instance, an increase of the member forces and moments in the pier columns is mainly caused by the stiffer foundation of the considered pier relative to that of other piers.

It is also found that the displacement and rotational responses of the bridge superstructure are less sensitive to the PSPI effects than those of the responses of the foundations are. The comparison study also shows that the member forces and moments at the pier columns are least sensitive to the PSPI effects (less than the displacement and rotation responses of the superstructure and the foundations). The effects of softening the soil stiffness by 25% for the

integrated soil-foundation-structure model on the response of both bridge superstructure and its pile foundations are found to be insignificant.

An overestimation of the foundation stiffness may lead to unconservative results. The study shows no impact at any of the expansion joints when the fixed-base model is used, whereas pounding does occur for other foundation modeling cases. In addition, a majority of forces and moments experienced in the piles computed from the fixed-base model are to be less than those computed from other modeling cases. It is important to emphasize once again that the fixed-base model underpredicts the bridge responses in several aspects such as displacements and rotations at both the superstructure and foundations, potential pounding of the bridge superstructures at expansion joints, and forces in truss members. Furthermore, the study indicates that using equivalent linear springs to model the foundation characteristics may lead to unconservative prediction of the pile responses. The forces and moments in the piles are underestimated by a factor of 2 using the spring-base model as compared to those predicted by the integrated soil-foundation-structure model.

Seismic performance of the bridge for different excitation intensities

The nonlinear time-history analyses are performed using different excitation intensities of the input motions. The results show no major deficiency of the overall bridge responses except for a few truss members that are slightly overstressed for the 50%/50 year hazard level (a return period of 73 years or a peak acceleration of 0.03g). Deficiencies associated with excessive shear forces at the expansion bearings of the main truss and the piles, and excessive moments in the columns of the north approach piers (Piers 2, 3 and 4) are discovered for the 10%/50 year hazard level (a return period of 475 years or a peak acceleration of 0.2g).

For the 4%/50 year hazard level (a return period of 1,225 years or a peak acceleration of 0.7g), the results indicate excessive seismic-induced longitudinal displacements at the expansion joints, which may lead to a loss of support for the superstructure and possibly structural damage of the bridge. The analytical results of all modeling cases reveal several occurrences of impact at the expansion bearings supporting the main truss, which are not present at lower excitation levels. The maximum longitudinal force induced by the impacts as well as the transverse shears substantially exceeds the bearing capacity, indicating a high potential for toppling that may lead to a major structural damage of the main truss structure. Shear forces and moments at the pier columns

especially at both the north and south approaches are much greater than the ultimate capacity, and thus failures of the pier columns are very likely. Foundation failures at the approach piers are also probable as a consequence of inadequate flexural and shear strength of the piles and excessive displacements and rotations of the foundations. For the excitation level of the 2%/50 year hazard (a return period of 2,475 years or a peak acceleration of 1.65g), the analytical results show that almost all structural members are most likely to be heavily damaged. A significant destruction of the bridge is plausible for the 2%/50 year hazard level.

All these concluding remarks are obtained corresponding to the results of the nonlinear time-history analyses of the Cairo Bridge with a selected set of input ground motions. Careful consideration should be given to the extent of interpreting and applying these findings to other long span bridges since they are based exclusively upon the seismic response of the Cairo Bridge. However, it is not the response of the bridge that is important but the technique of modeling and analyzing the bridge that is most important. The modeling technique is one thing that can be applied for all pile-supported bridges regardless of the length, configuration or types of construction. Presented in this study is the technique of modeling the bridge by integrating the soil and foundation model into the bridge structure model.

This integrating technique may be considered to be an initiation of incorporation of both the geotechnical and structural points of view in seismic analysis of the bridge. The presented integrating technique may also be used to simulate several aspects that could not be realistically captured using the foundation spring model. These several aspects include modeling of multi-layer soil system, modeling of nonlinear behavior and hysteresis damping property of the soil, and simulating the soil-foundation-structure interaction effects for both the inertial interaction (the effects of the response of superstructure on the foundation and its surrounding soil) and the kinematic interaction (the effects of differences between the motions of the foundation and the far-field motions). In addition, the proposed soil-pile-foundation model can be applied to performance evaluation of the foundation retrofits. Application of the proposed model is further discussed in the following chapter.

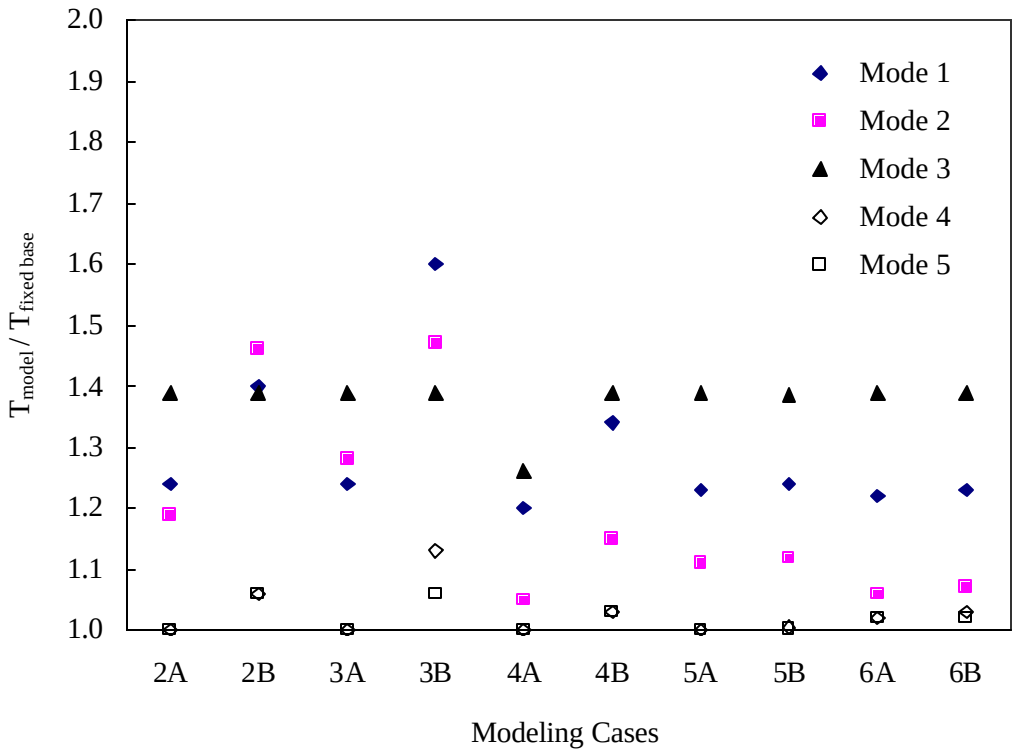

Figure 6.1. Comparison of Periods (T) Computed from Different Foundation Modeling Cases.

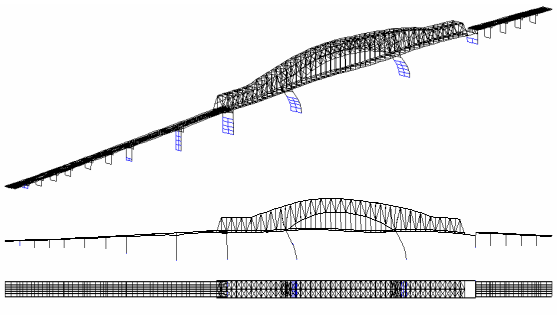

Mode 1 : Period = 2.285

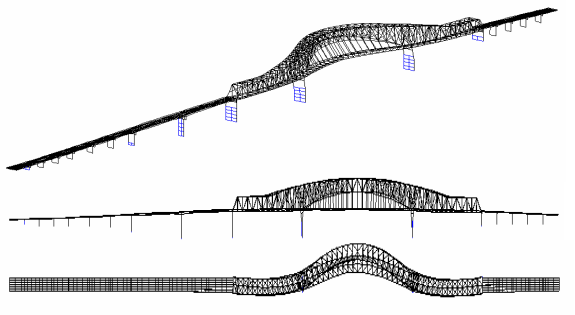

Mode 5 : Period = 1.505

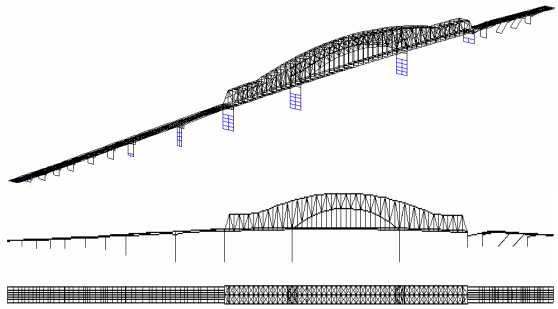

Mode 2 : Period = 2.175

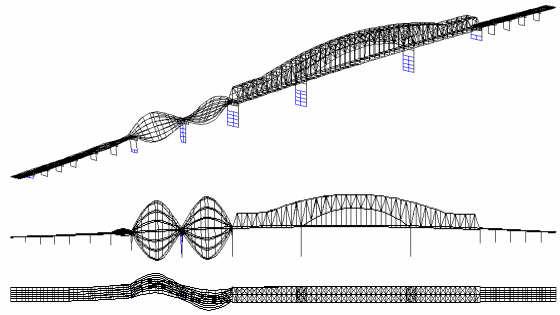

Mode 6 : Period = 1.281

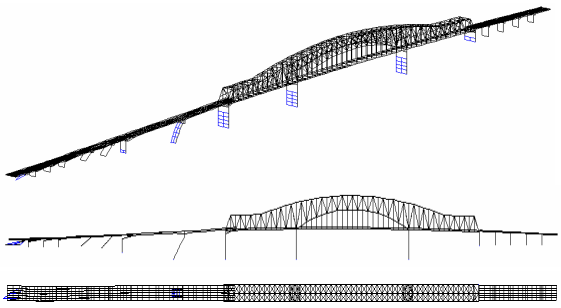

Mode 3 : Period = 1.649

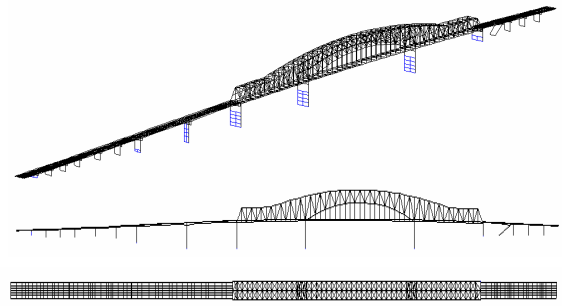

Mode 7 : Period = 1.272

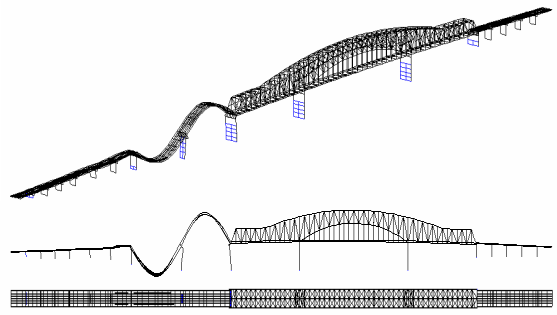

Mode 4 : Period = 1.529

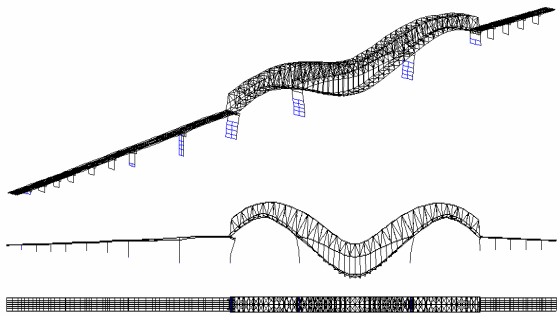

Mode 8 : Period = 1.233

Figure 6.2. Lower Eight Vibration Modes for Case 1.

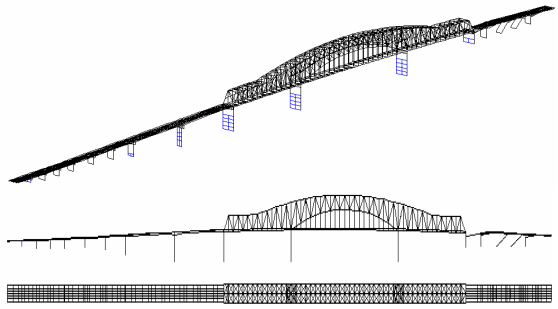

Mode 1

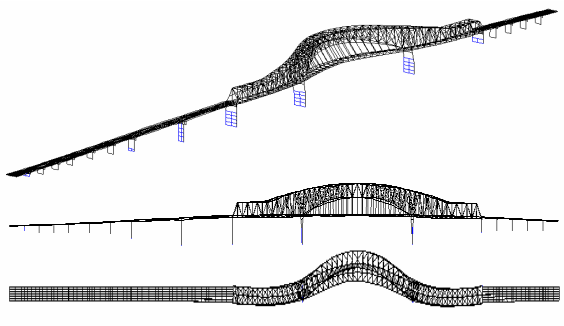

Mode 5

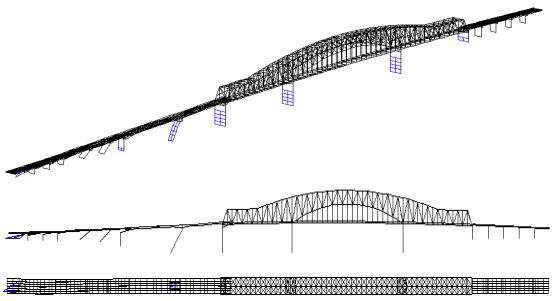

Mode 2

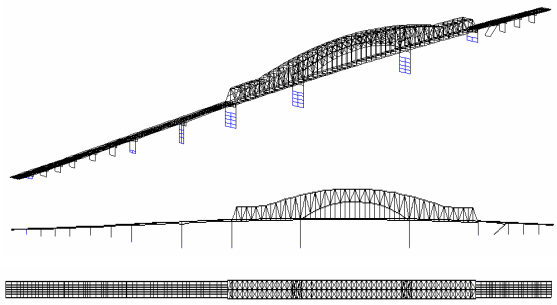

Mode 6

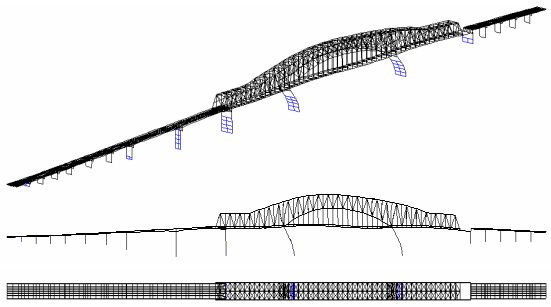

Mode 3

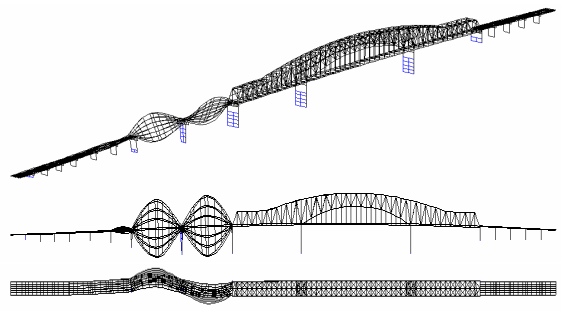

Mode 7

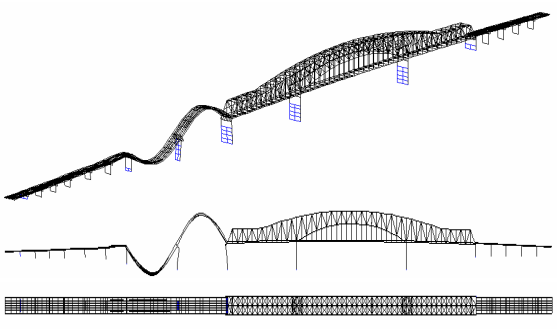

Mode 4

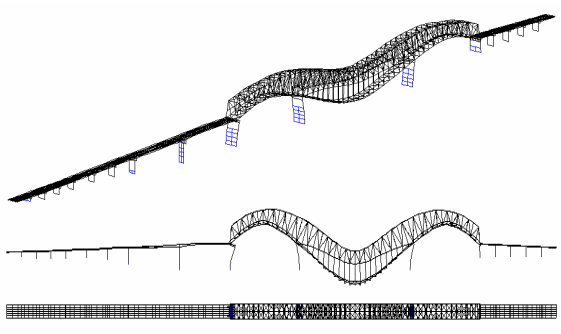

Mode 8

Figure 6.3. Lower Eight Vibration Modes for Cases 2A, 3A and 4A.

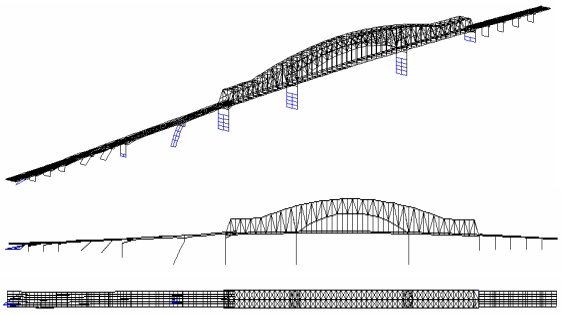

Mode 1

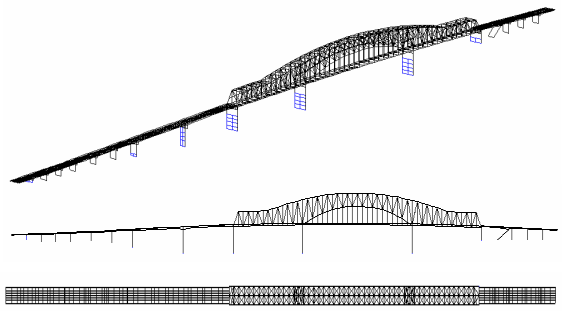

Mode 5

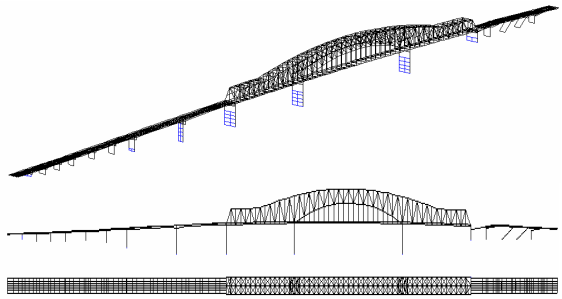

Mode 2

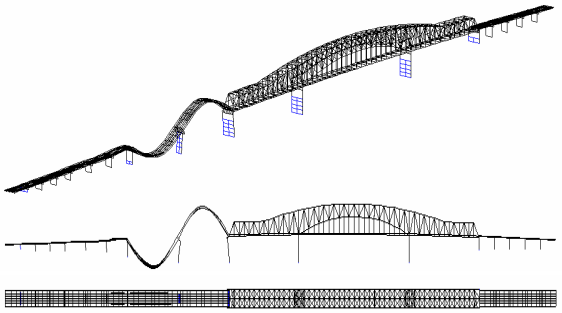

Mode 6

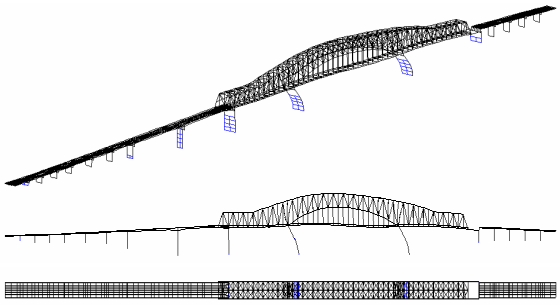

Mode 3

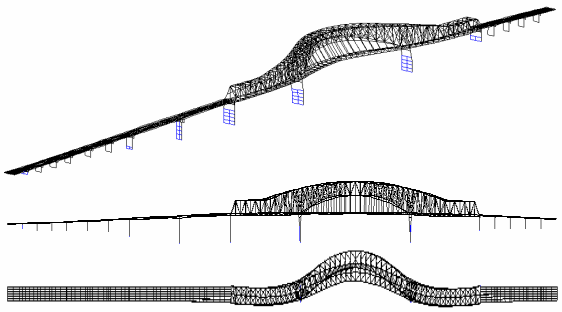

Mode 7

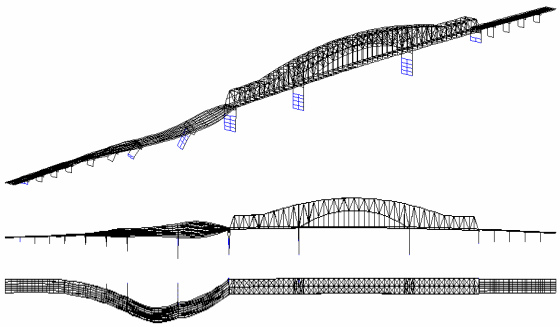

Mode 4

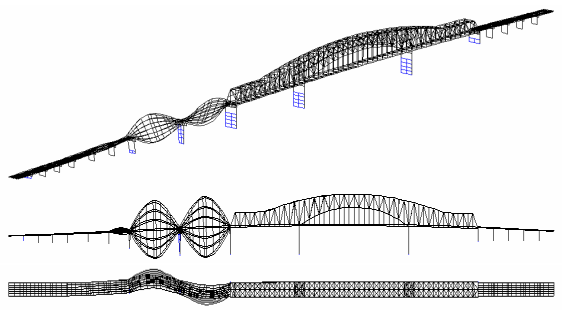

Mode 8

Figure 6.4. Lower Eight Vibration Modes for Cases 2B and 3B.

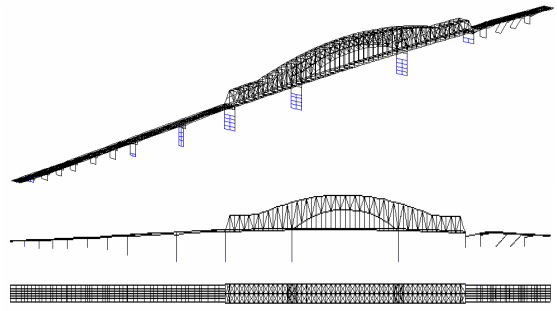

Mode 1

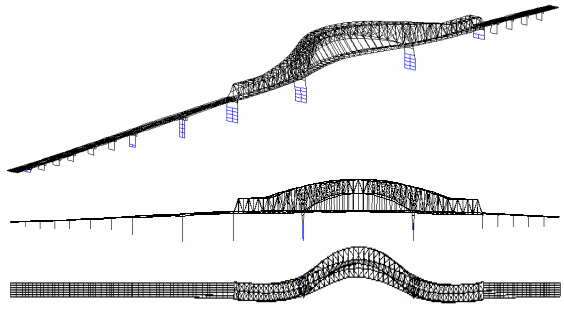

Mode 5

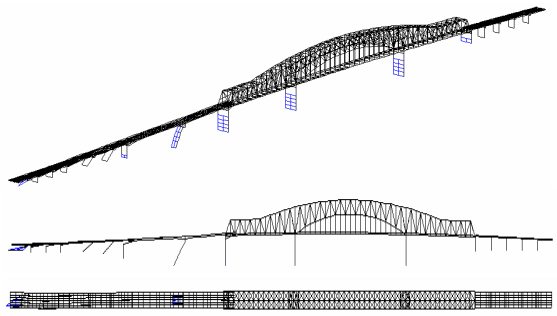

Mode 2

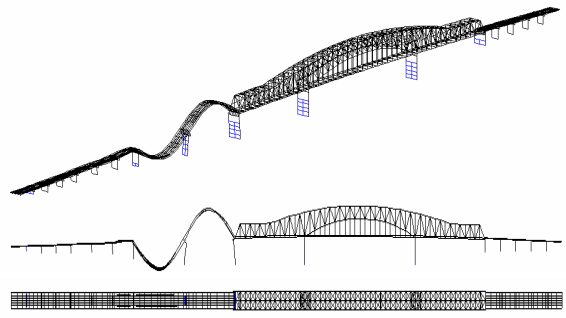

Mode 6

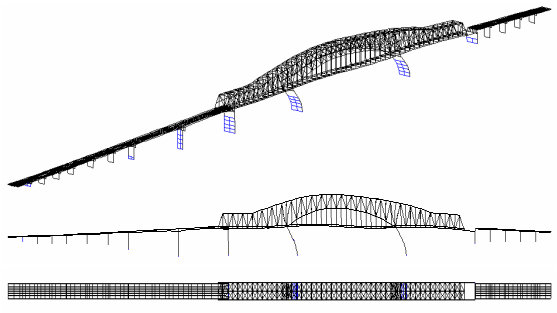

Mode 3

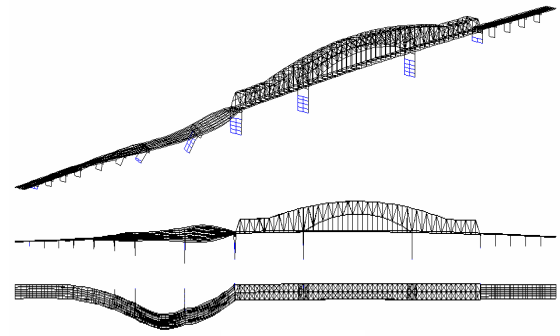

Mode 7

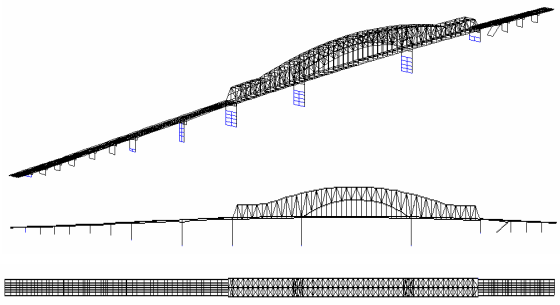

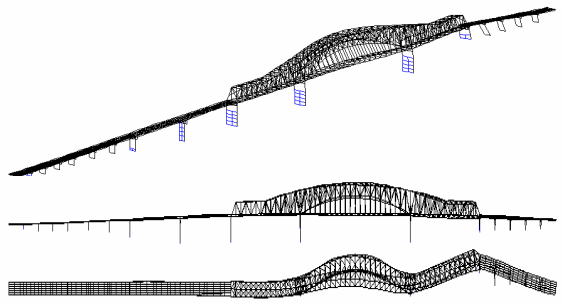

Figure 6.5. Lower Eight Vibration Modes for Case 4B.

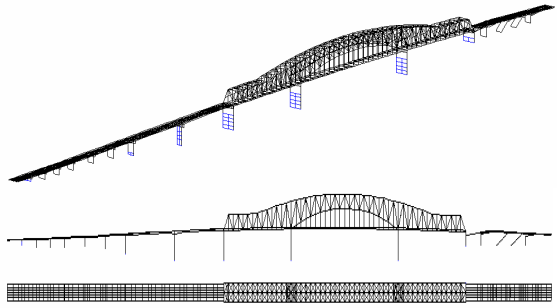

Mode 1

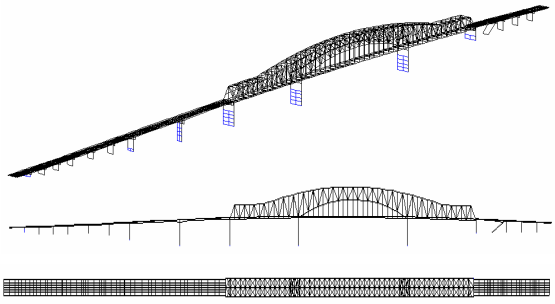

Mode 5

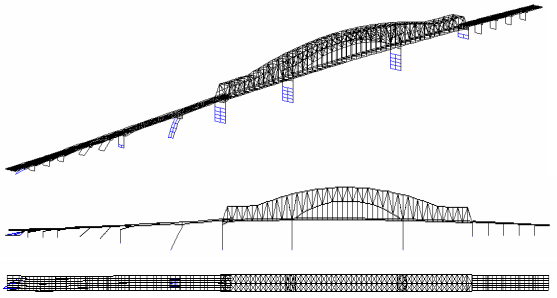

Mode 2

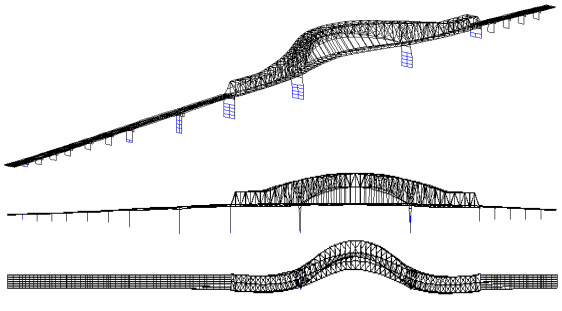

Mode 6

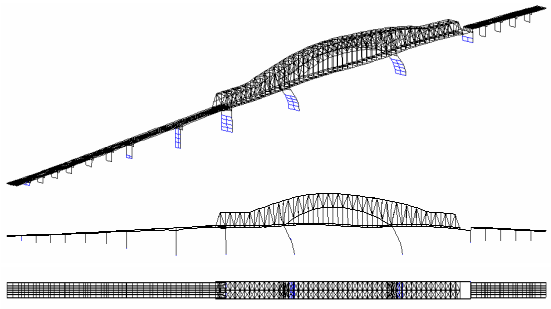

Mode 3

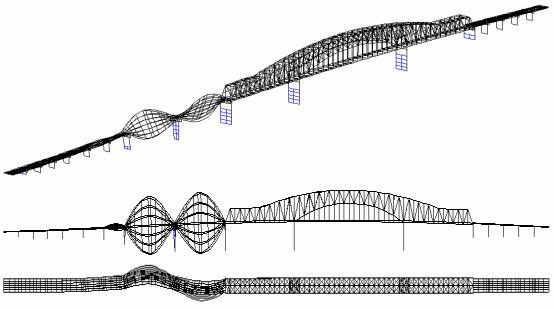

Mode 7

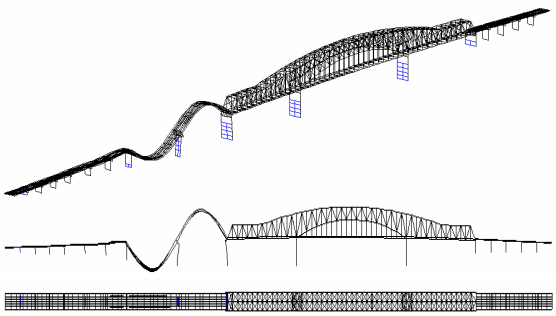

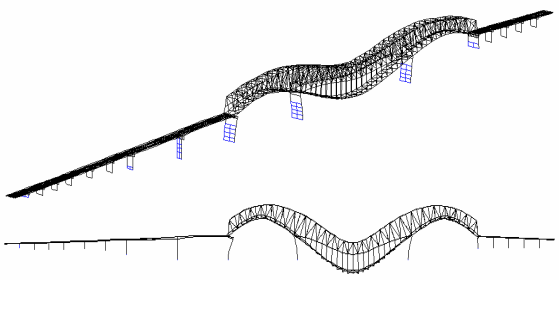

Figure 6.6. Lower Eight Vibration Modes for Cases 5A and 5B.

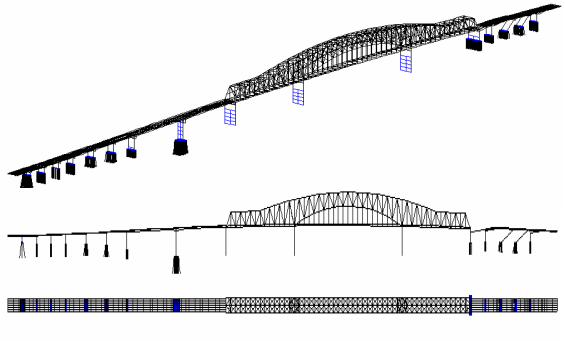

Mode 1

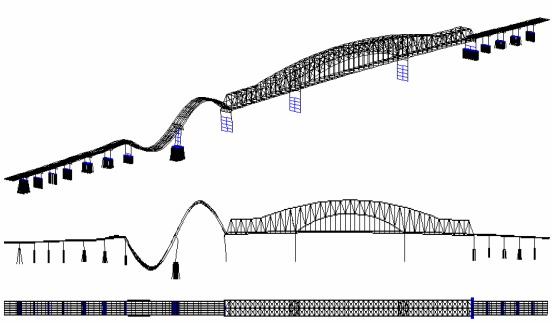

Mode 5

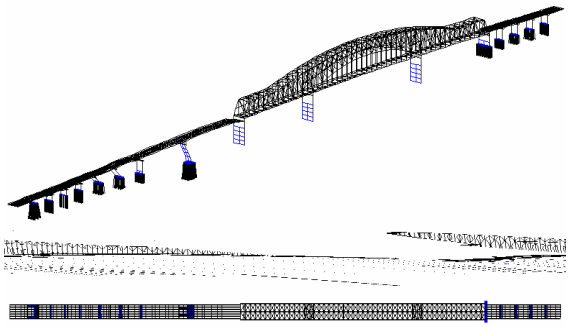

Mode 2

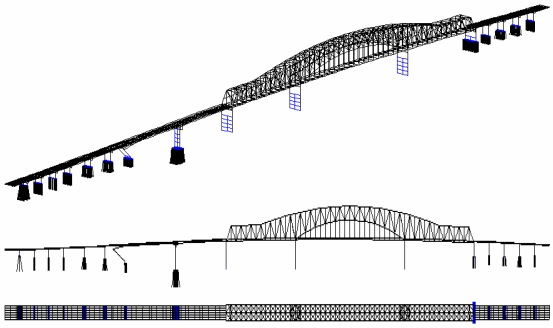

Mode 6

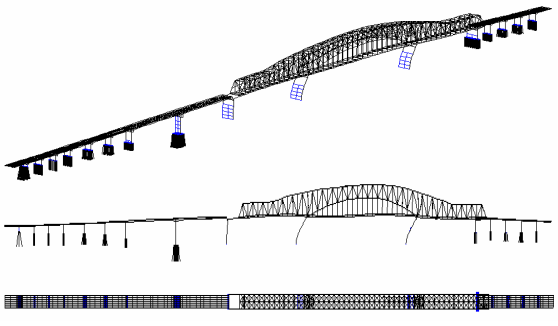

Mode 3

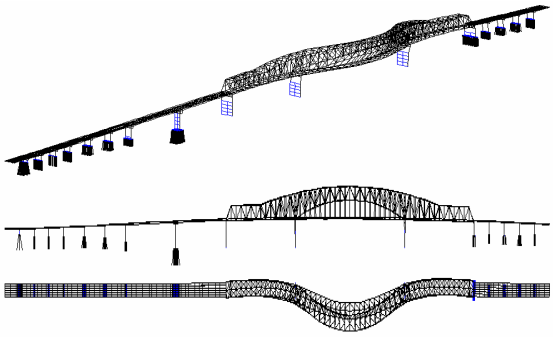

Mode 7

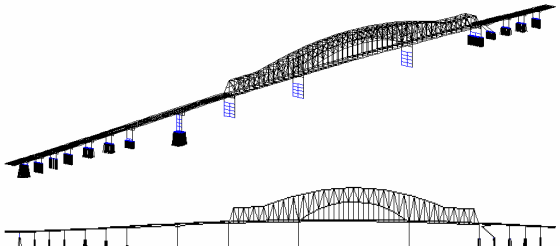

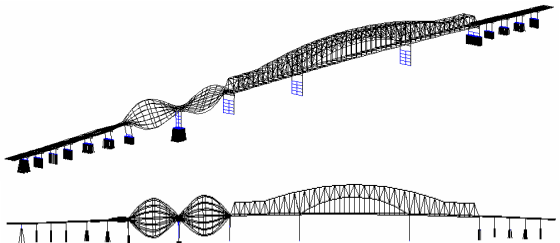

Figure 6.7. Lower Eight Vibration Modes for Cases 6A and 6B.

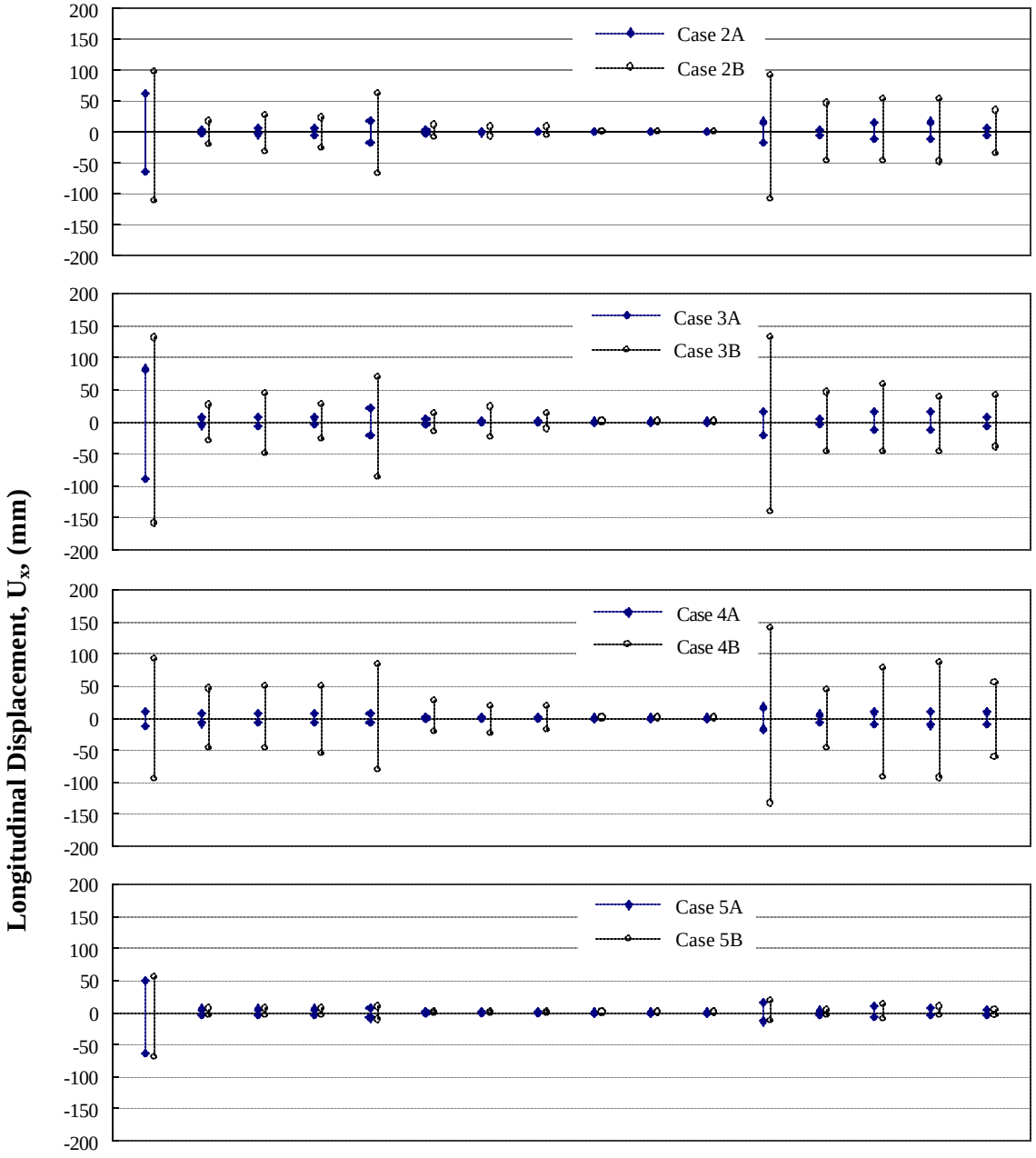

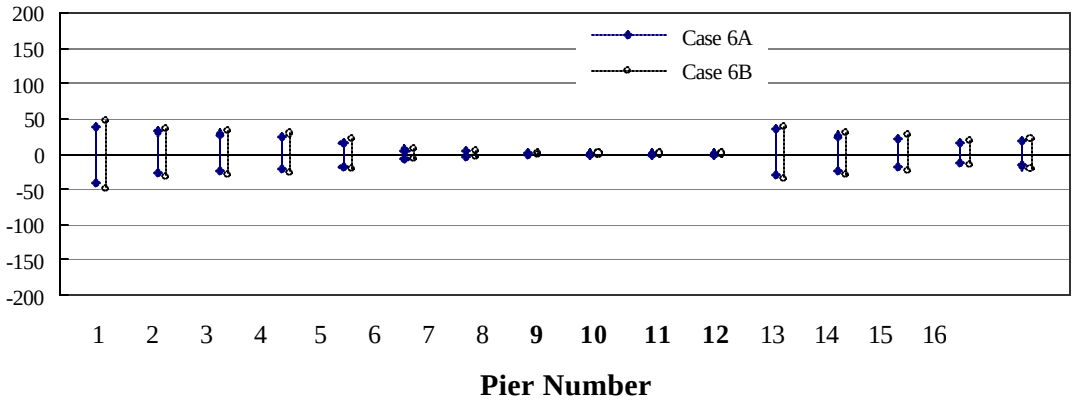

Figure 6.8. Computed Maximum Seismic-Induced Longitudinal Displacements at Foundations.

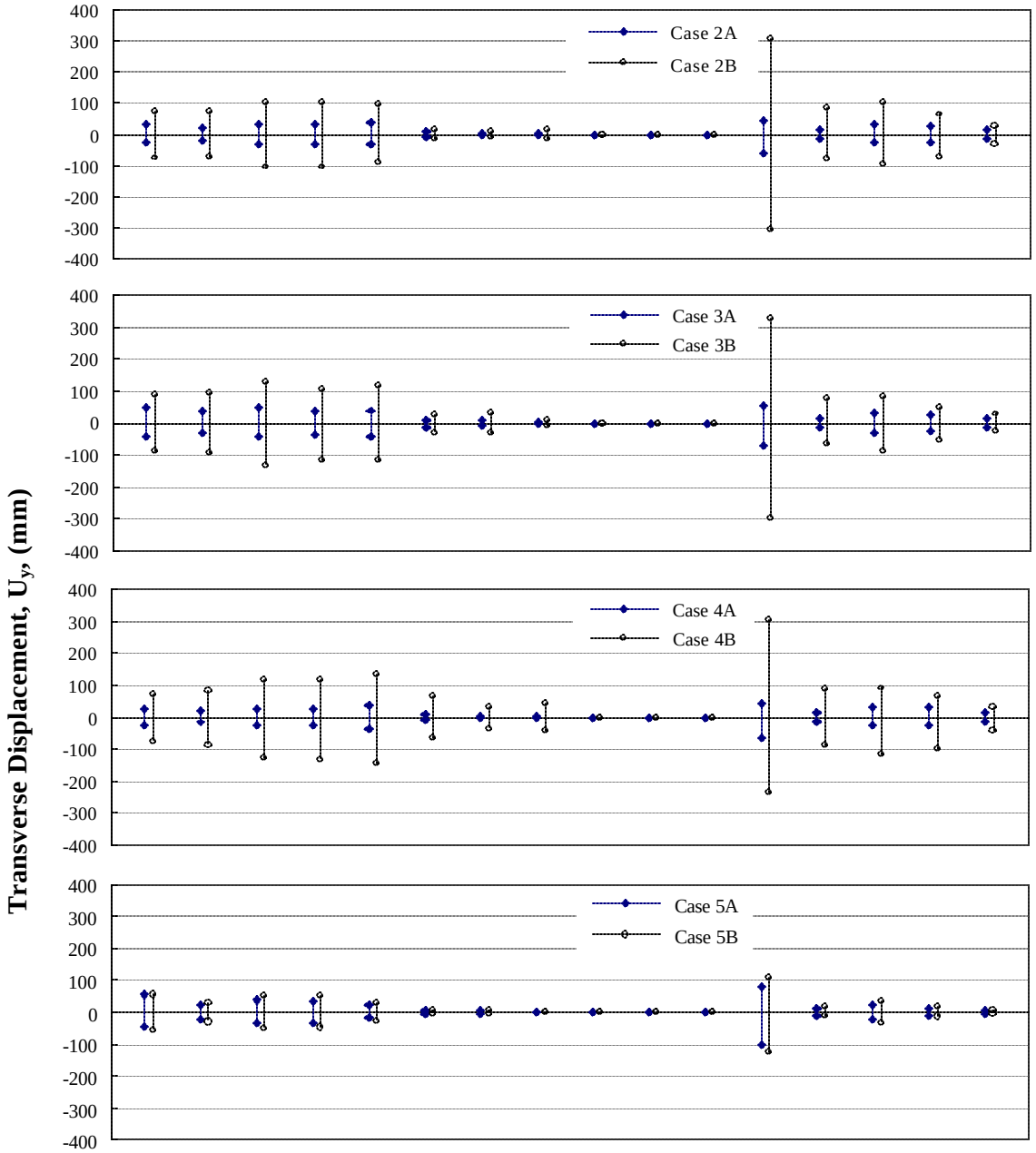

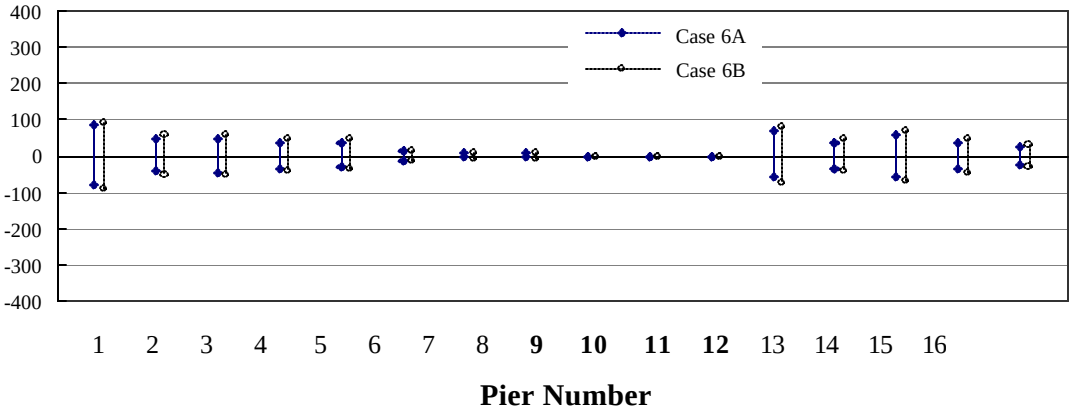

Figure 6.9. Computed Maximum Seismic-Induced Transverse Displacements at Foundations.

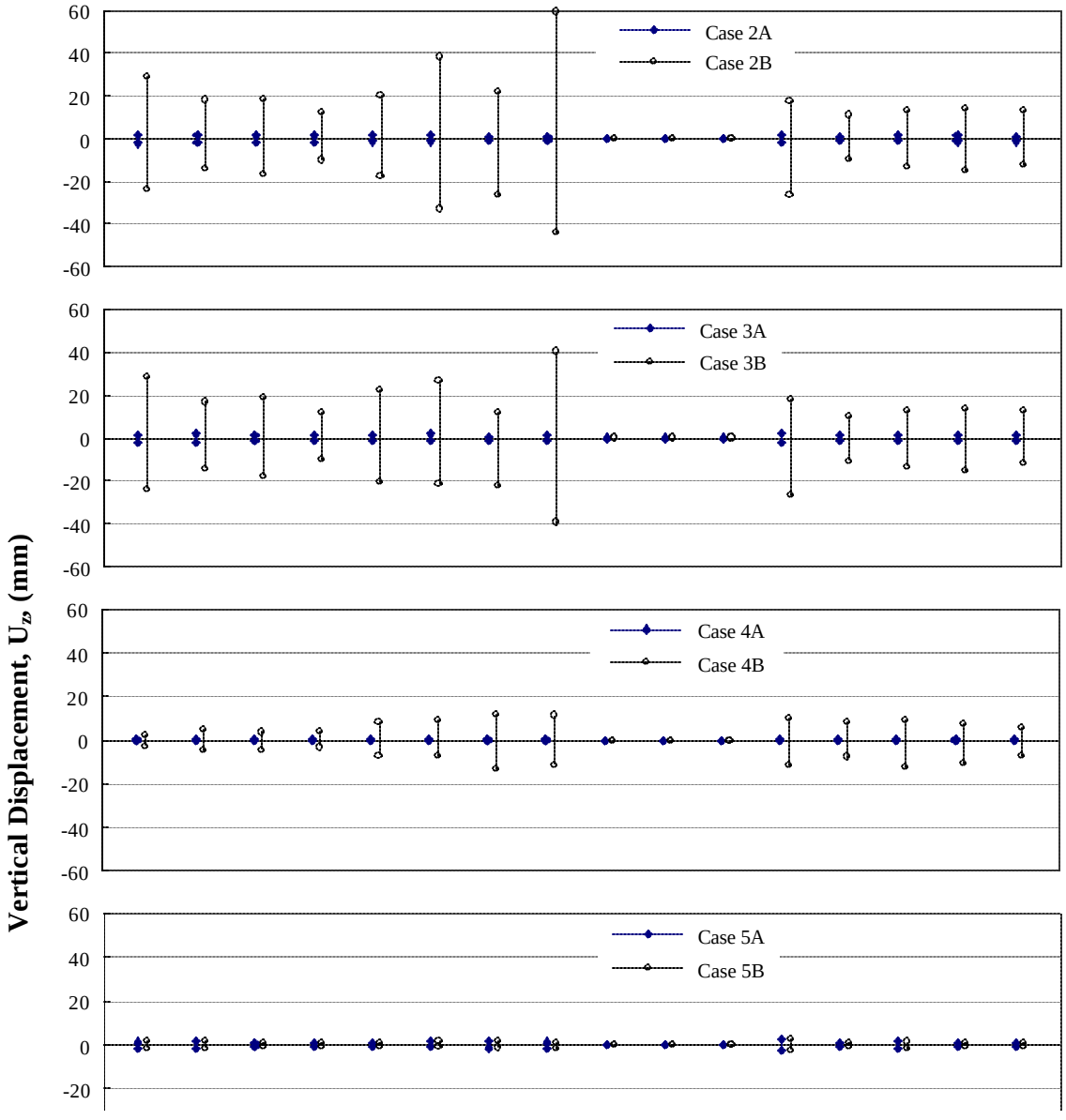

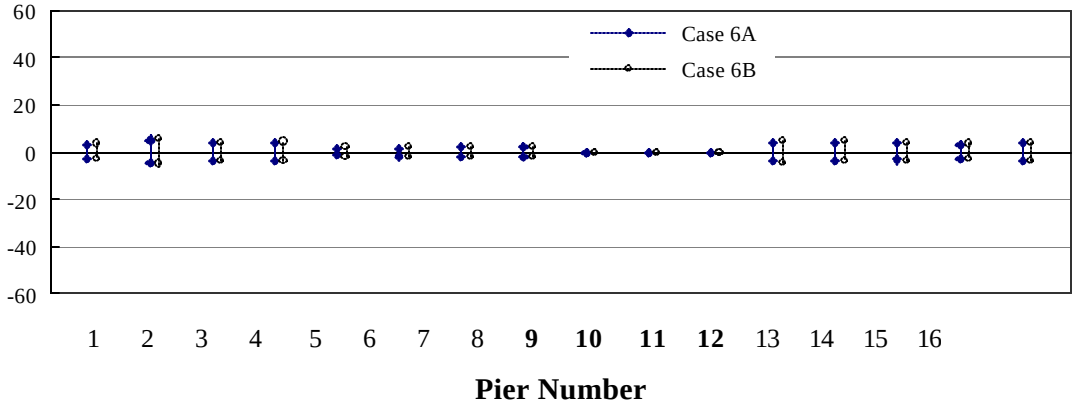

Figure 6.10. Computed Maximum Seismic-Induced Vertical Displacements at Foundations.

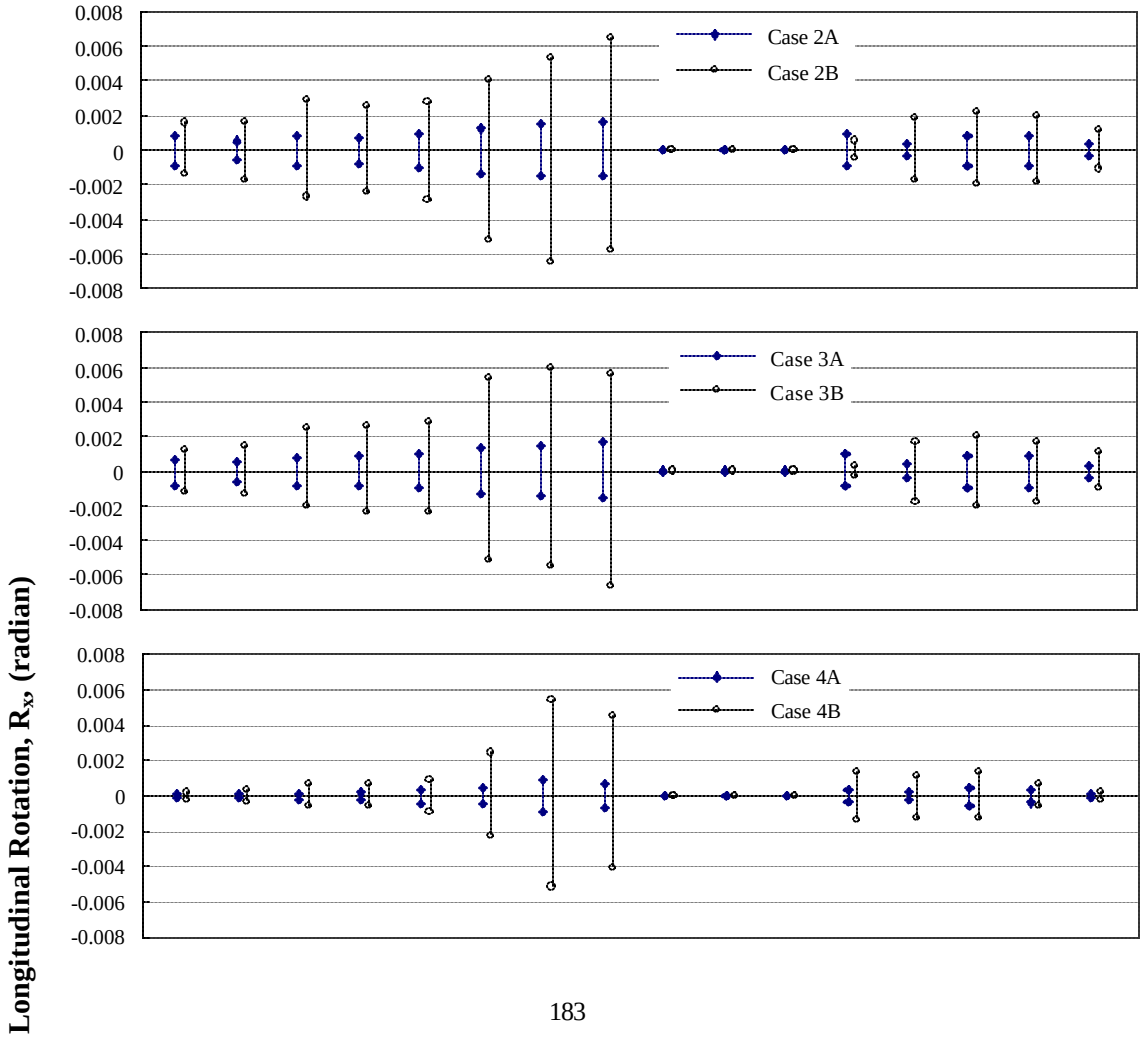

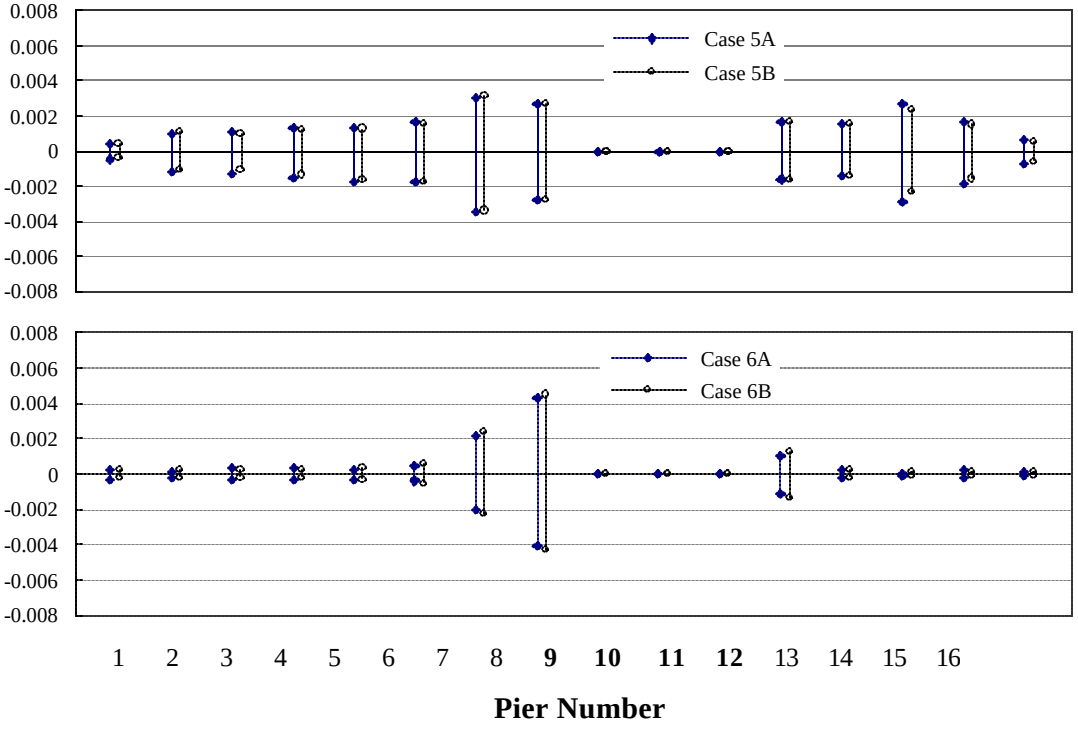

Figure 6.11. Computed Maximum Seismic-Induced Longitudinal Rotations at Foundations.

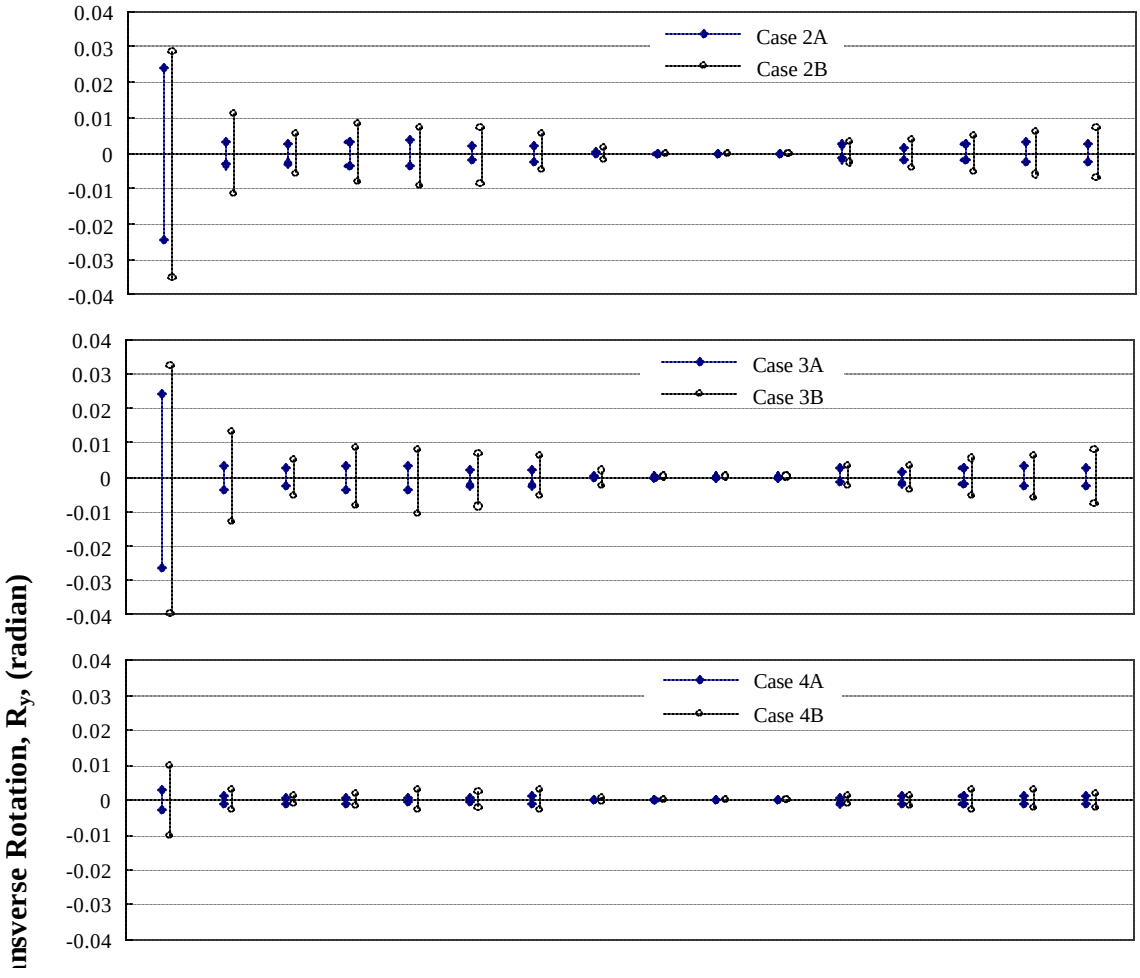

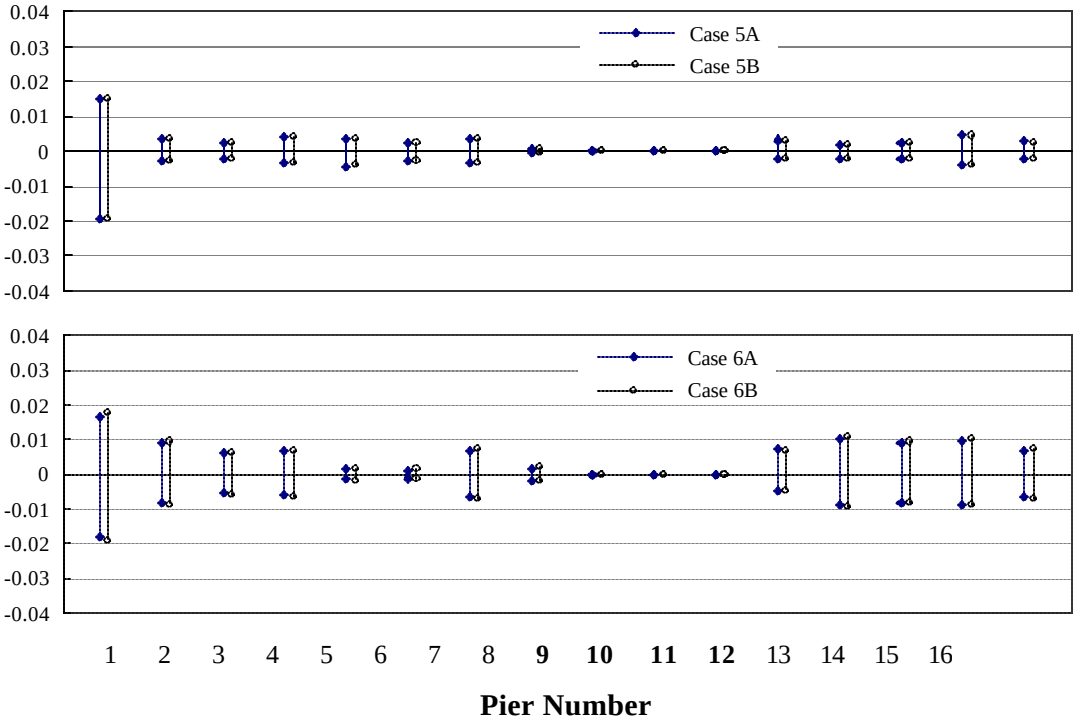

Figure 6.12. Computed Maximum Seismic-Induced Transverse Rotations at Foundations.

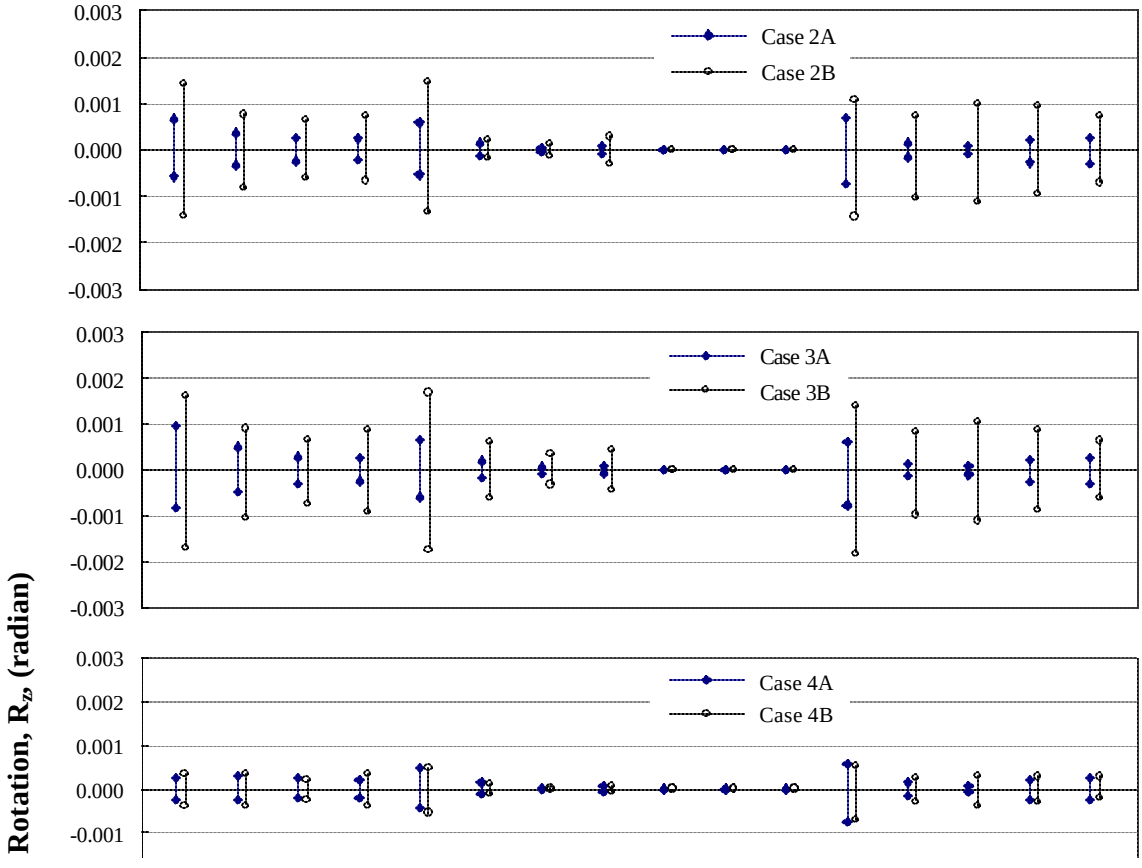

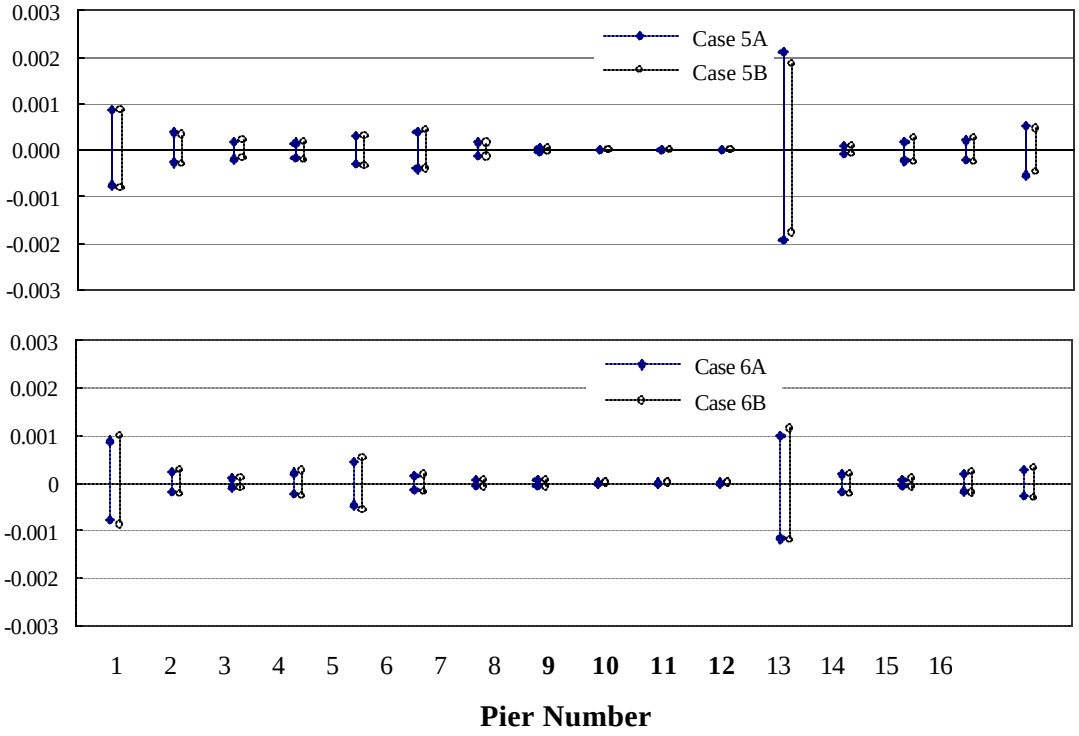

Figure 6.13. Computed Maximum Seismic-Induced Torsional Rotations at Foundations.

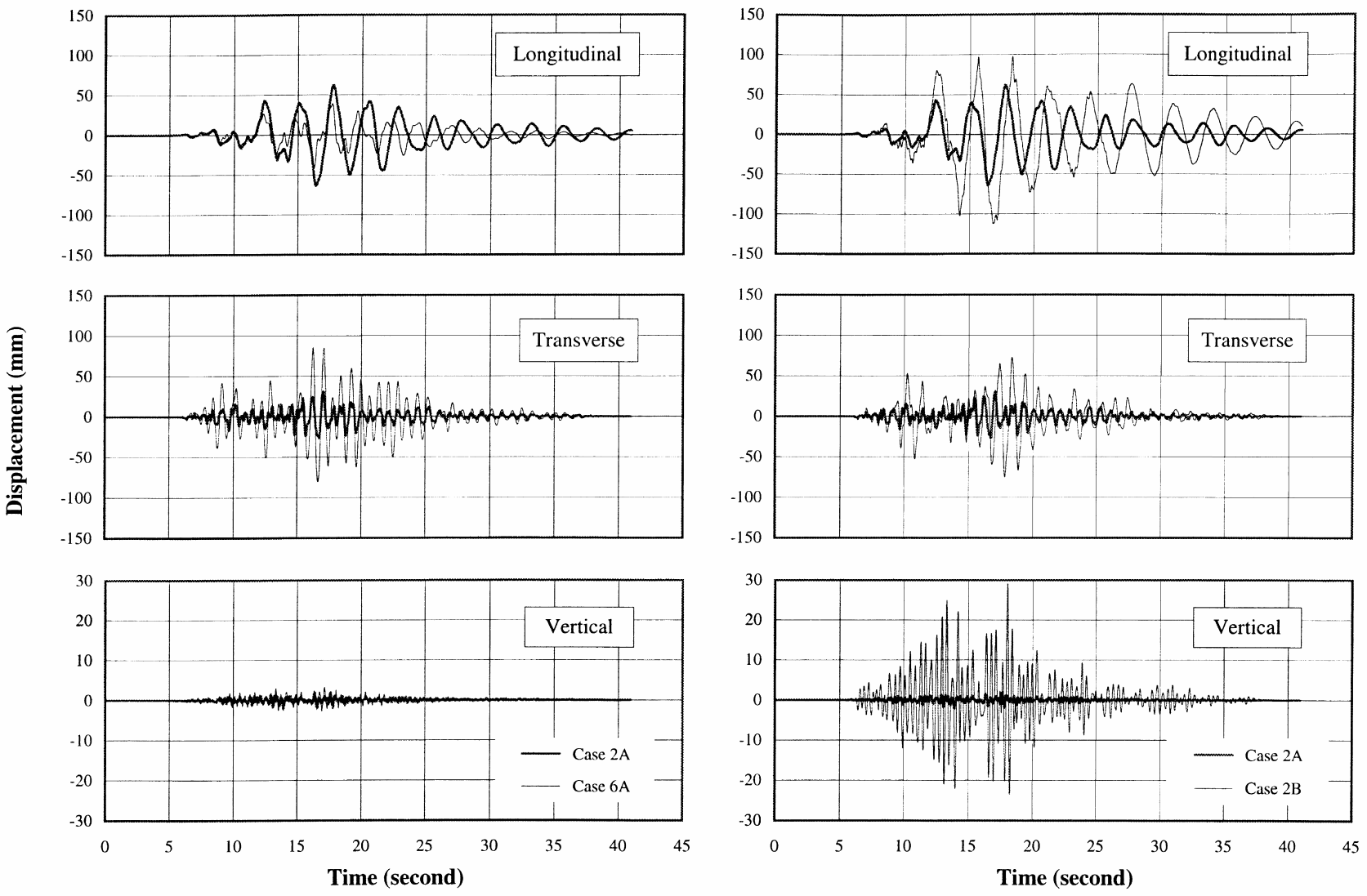
Longitudinal
Transverse
Vertical
Displacement (mm)
Time (second)
Case 2A
Case 6A
Case 2B

Figure 6.14. Computed Displacements at the Foundation of Pier 1.

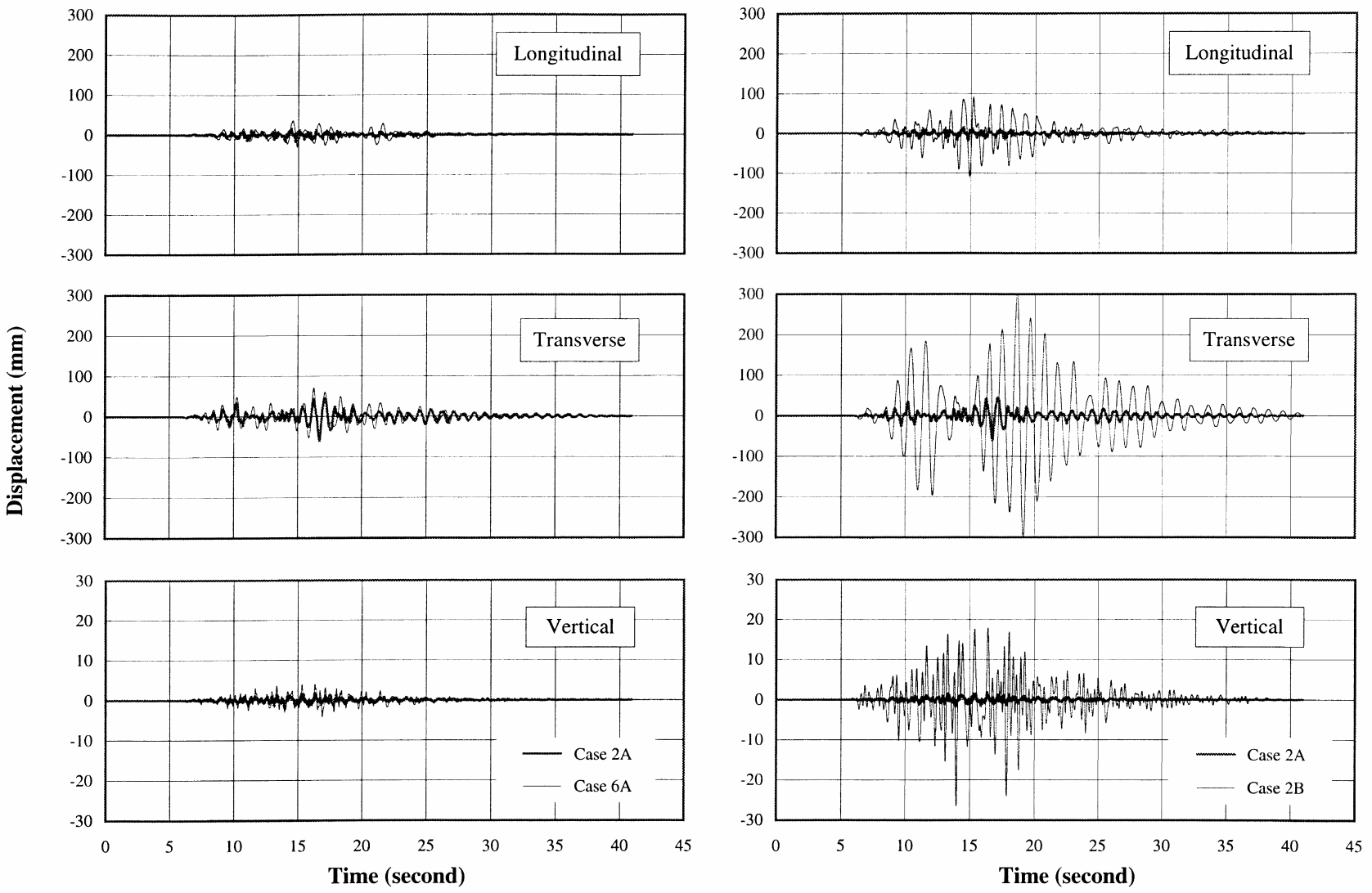

Figure 6.15. Computed Displacements at the Foundation of Pier 12.

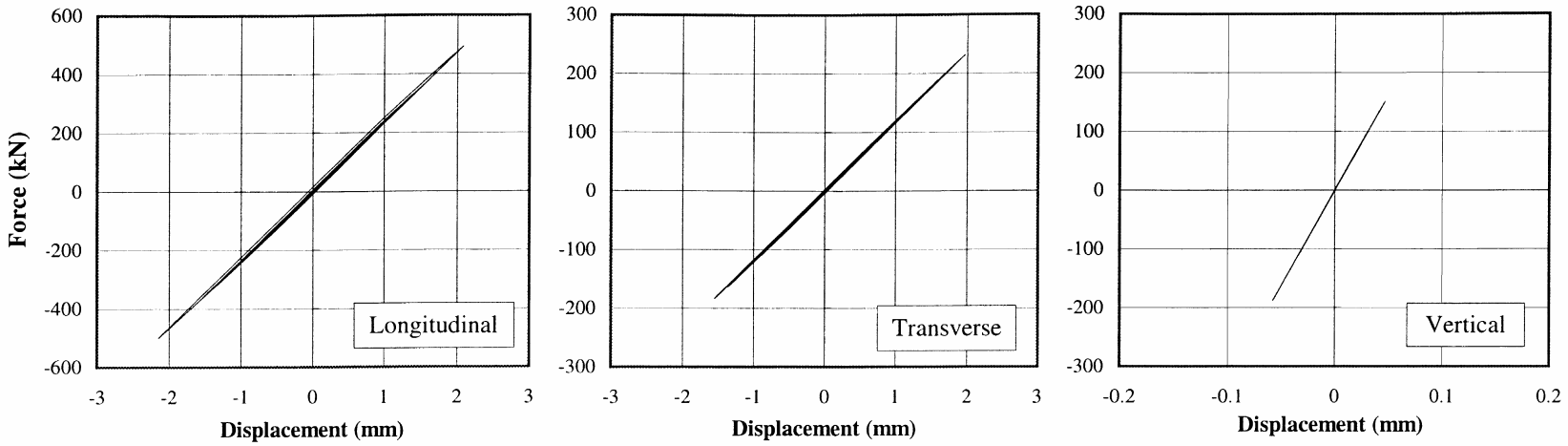

(a) Nonlinear Responses at the Foundation of Pier 1

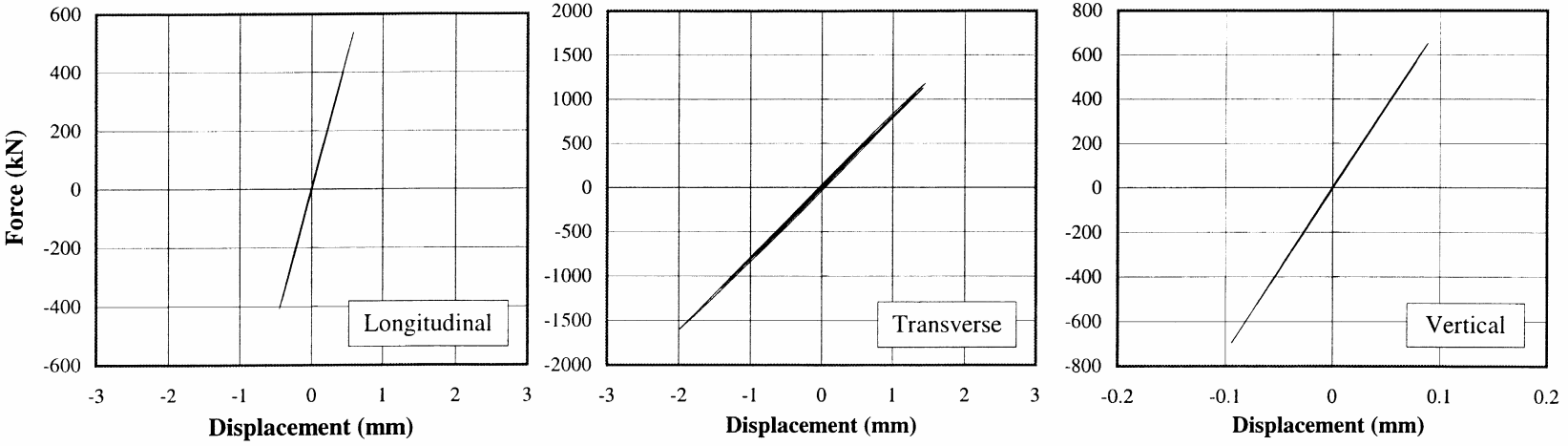

(b) Nonlinear Responses at the Foundation of Pier 12

Figure 6.16. Force-Displacement Histories at the Foundation of Piers 1 and 12 for the 50%/50 Year Hazard Level.

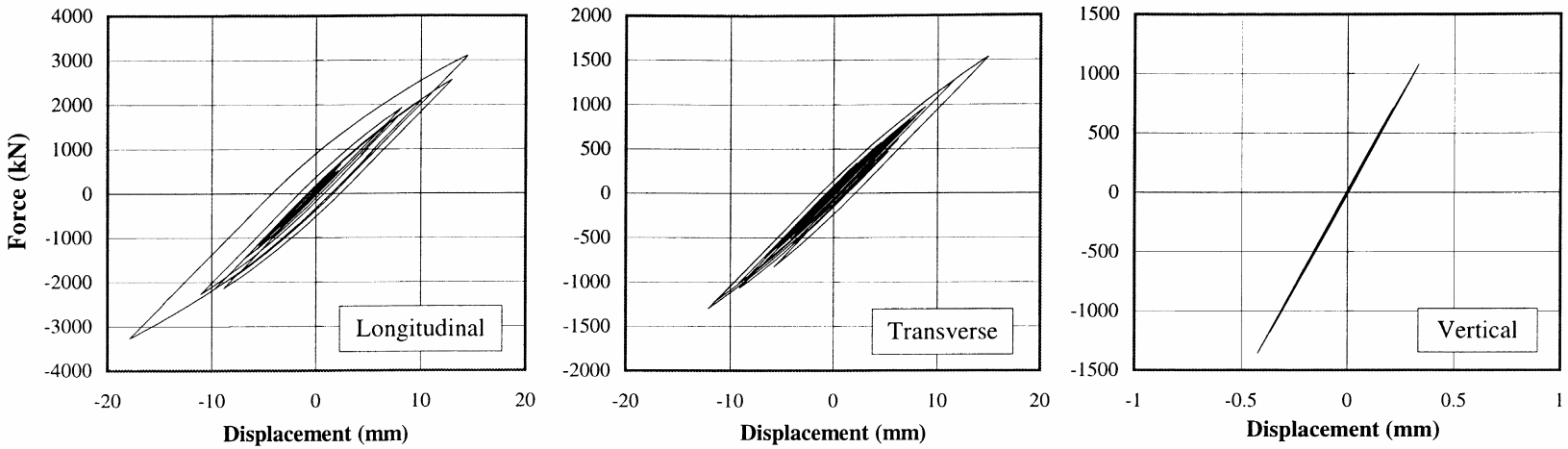

(a) Nonlinear Responses at the Foundation of Pier 1

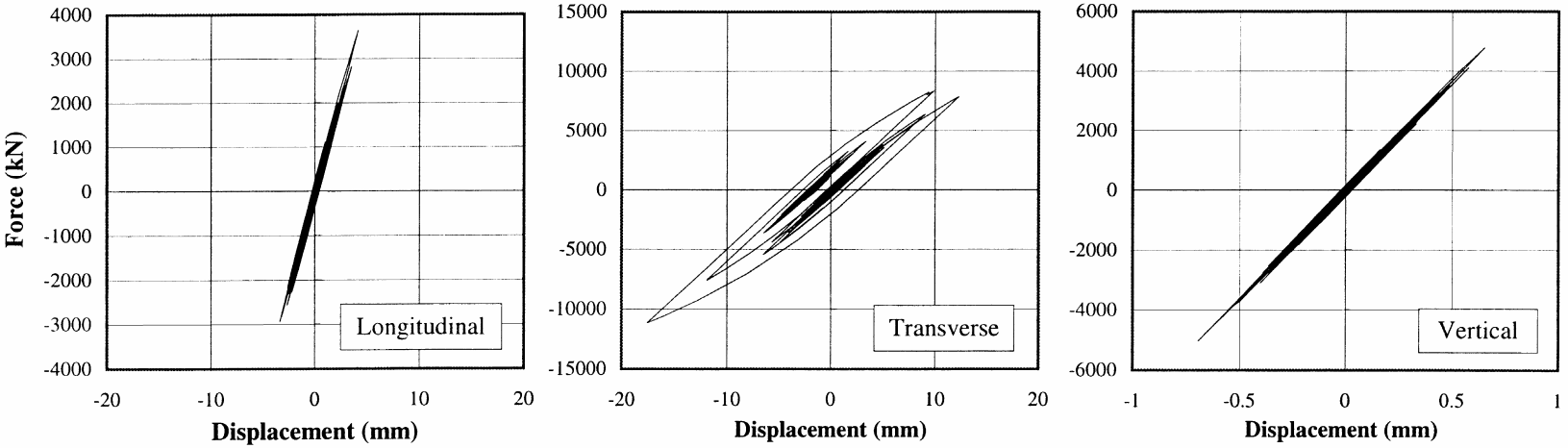

(b) Nonlinear Responses at the Foundation of Pier 12

Figure 6.17. Force-Displacement Histories at the Foundation of Piers 1 and 12 for the 10%/50 Year Hazard Level.

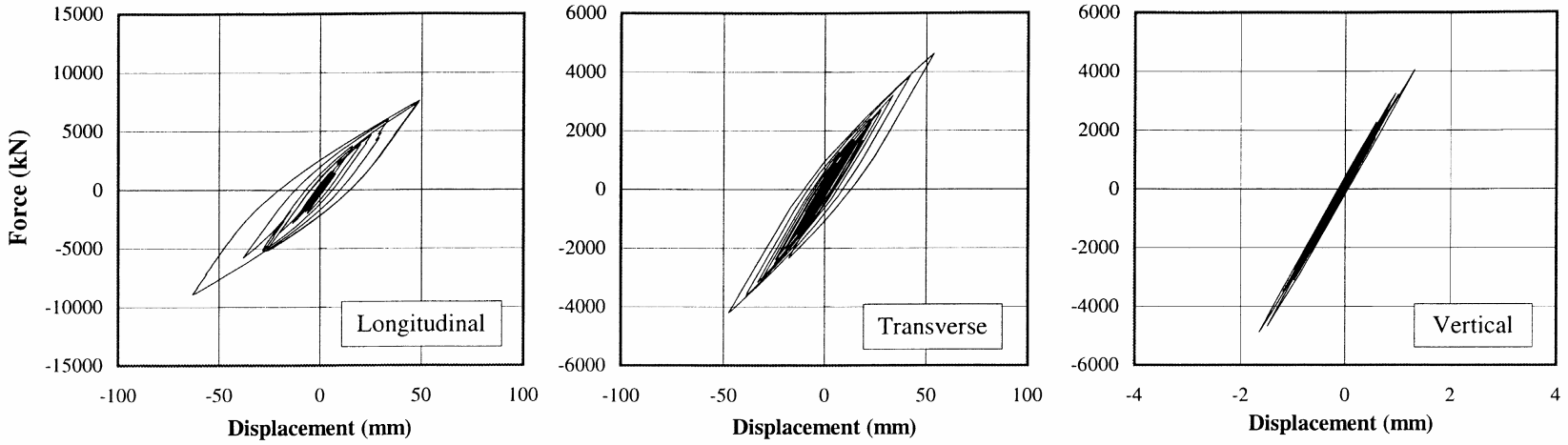

(a) Nonlinear Responses at the Foundation of Pier 1

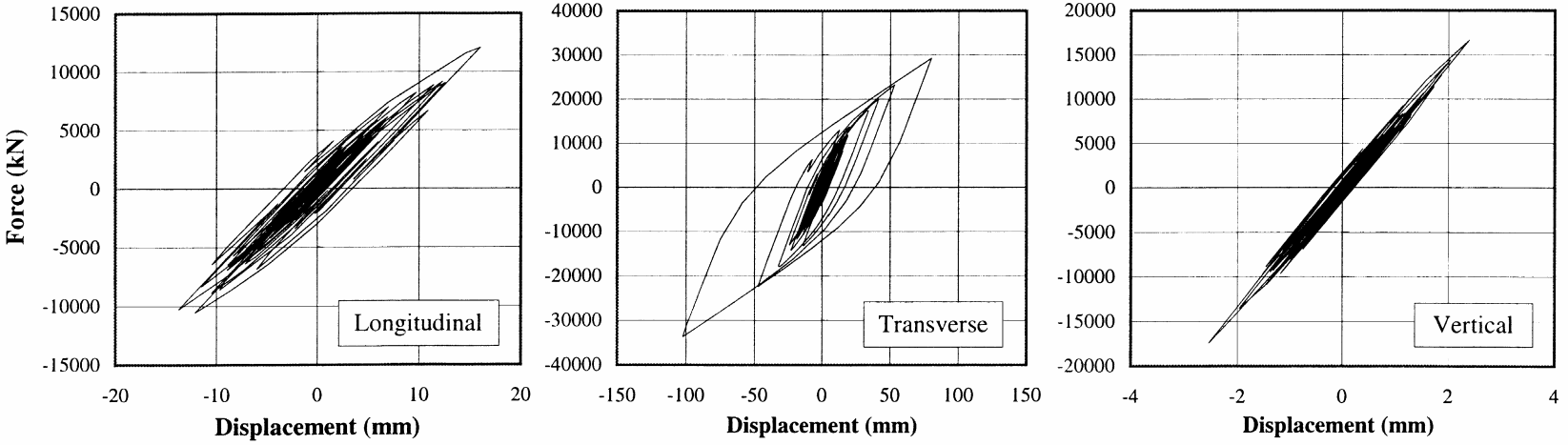

(b) Nonlinear Responses at the Foundation of Pier 12

Figure 6.18. Force-Displacement Histories at the Foundation of Piers 1 and 12 for the 4%/50 Year Hazard Level.

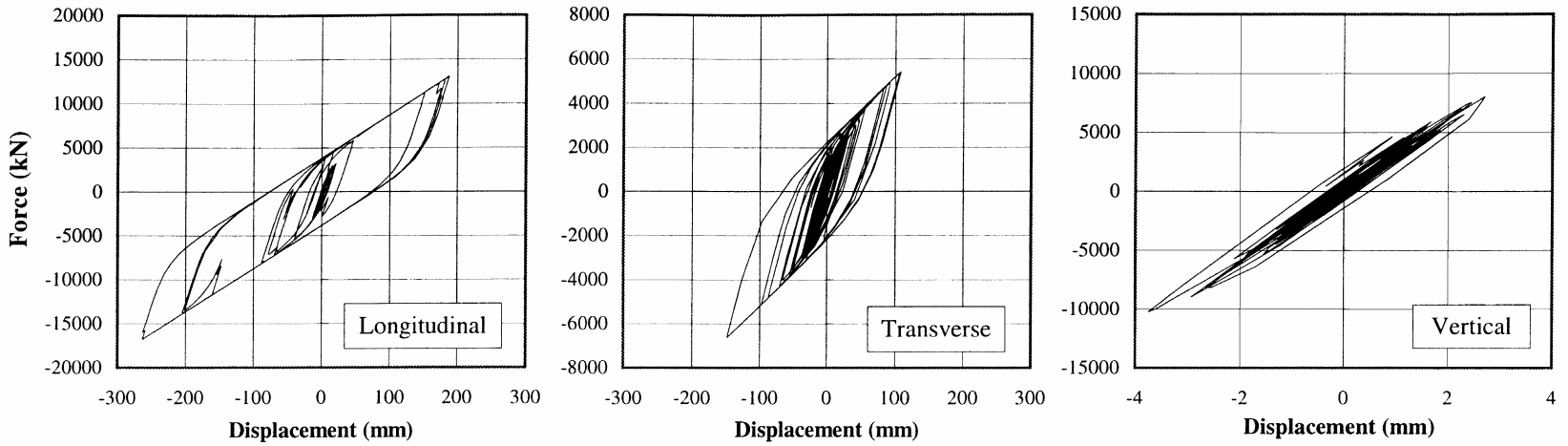

(a) Nonlinear Responses at the Foundation of Pier 1

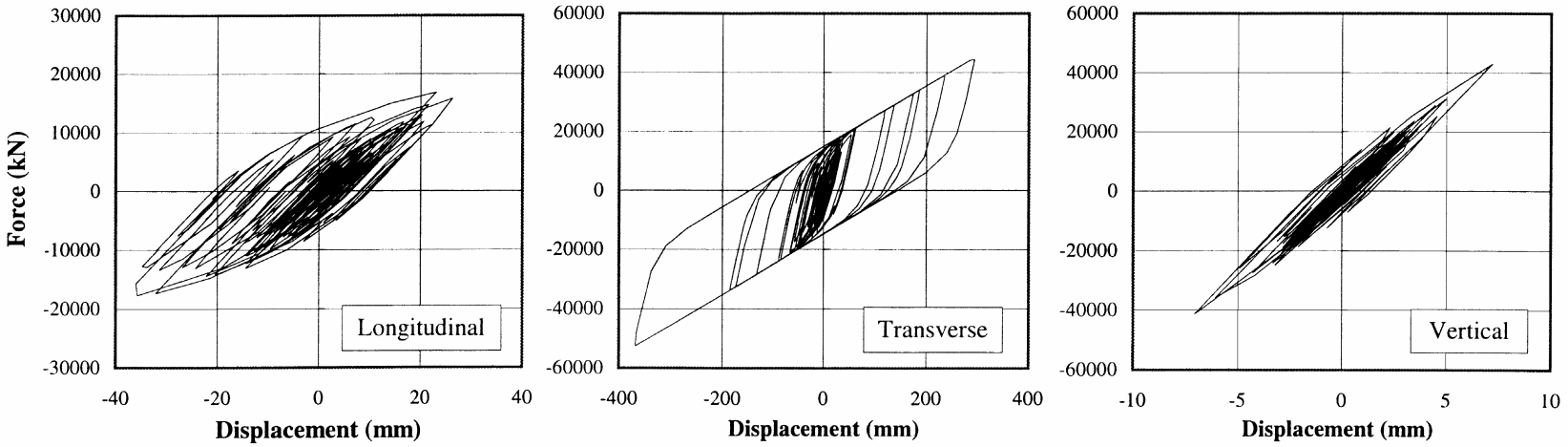

(b) Nonlinear Responses at the Foundation of Pier 12

Figure 6.19. Force-Displacement Histories at the Foundation of Piers 1 and 12 for the 2%/50 Year Hazard Level.

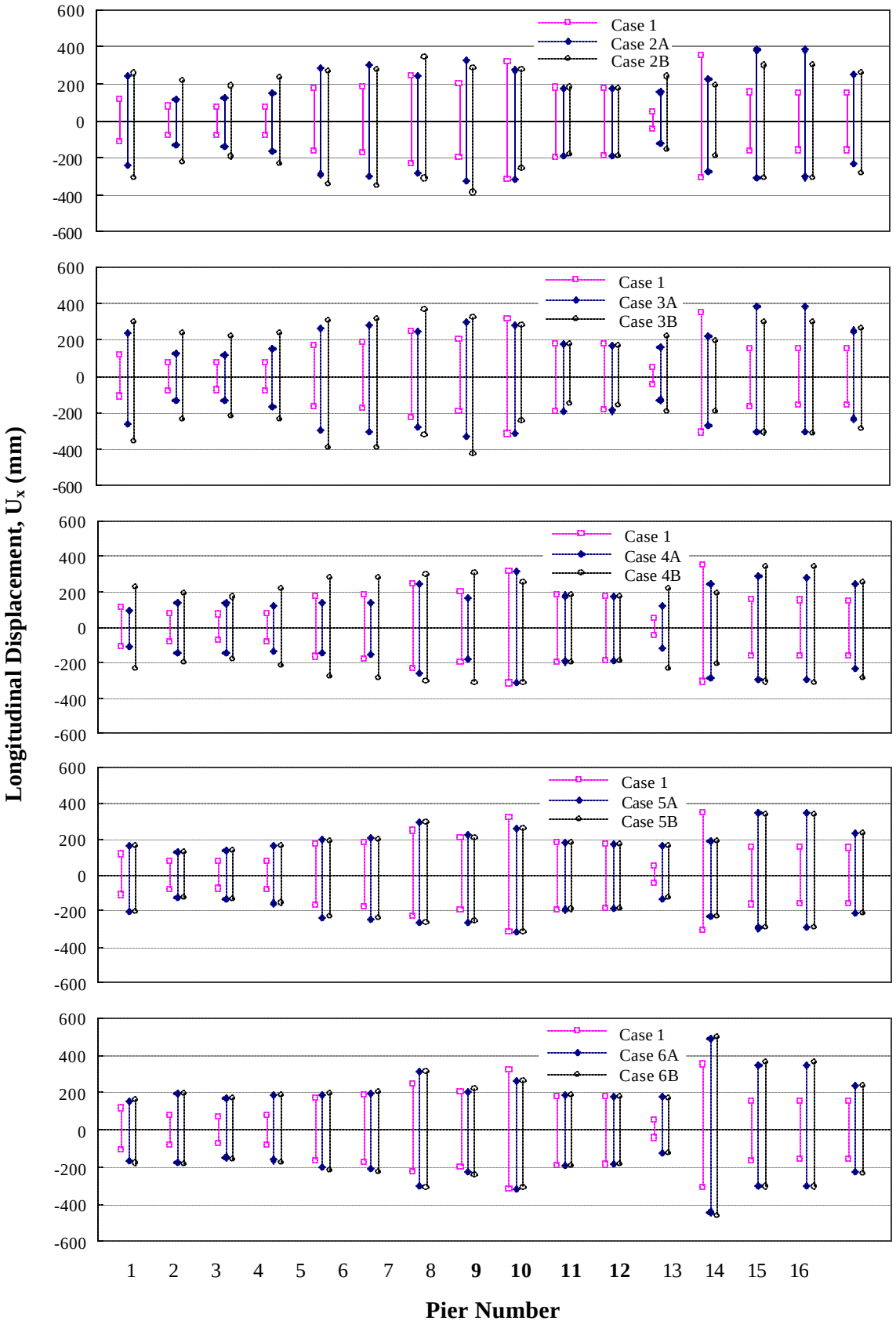
Case 1
Case 2A
Case 2B
Case 1
Case 3A
Case 3B
Case 1
Case 4A
Case 4B
Case 1
Case 5A
Case 5B
Case 1
Case 6A
Case 6B
600
400
200
0
-200
-400
-600
1 2 3 4 5 6 7 8 9 10 11 12 13 14 15 16
Pier Number
Longitudinal Displacement, U_x (mm)

Figure 6.20. Computed Maximum Seismic-Induced Longitudinal Displacements at Bent Caps.

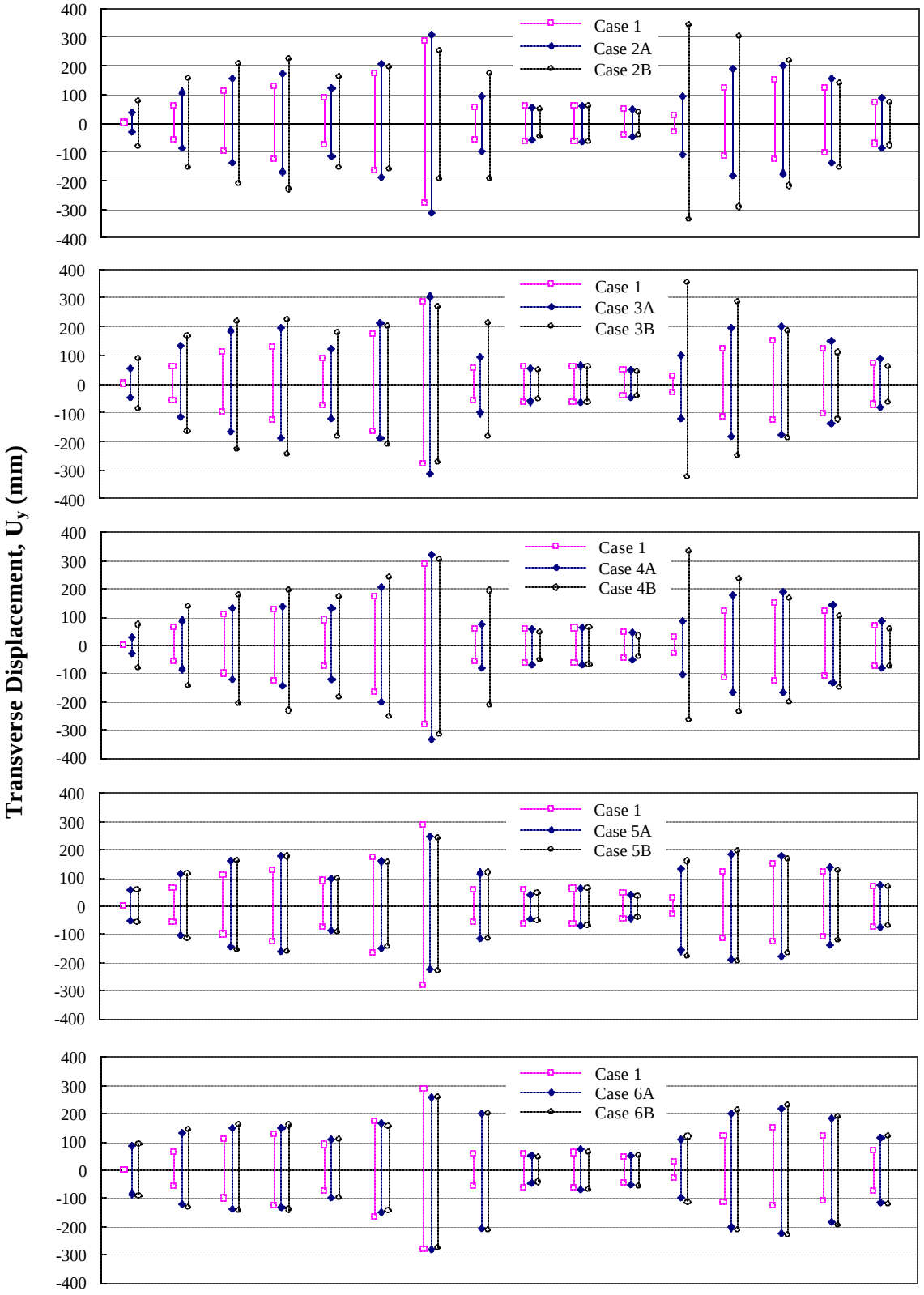

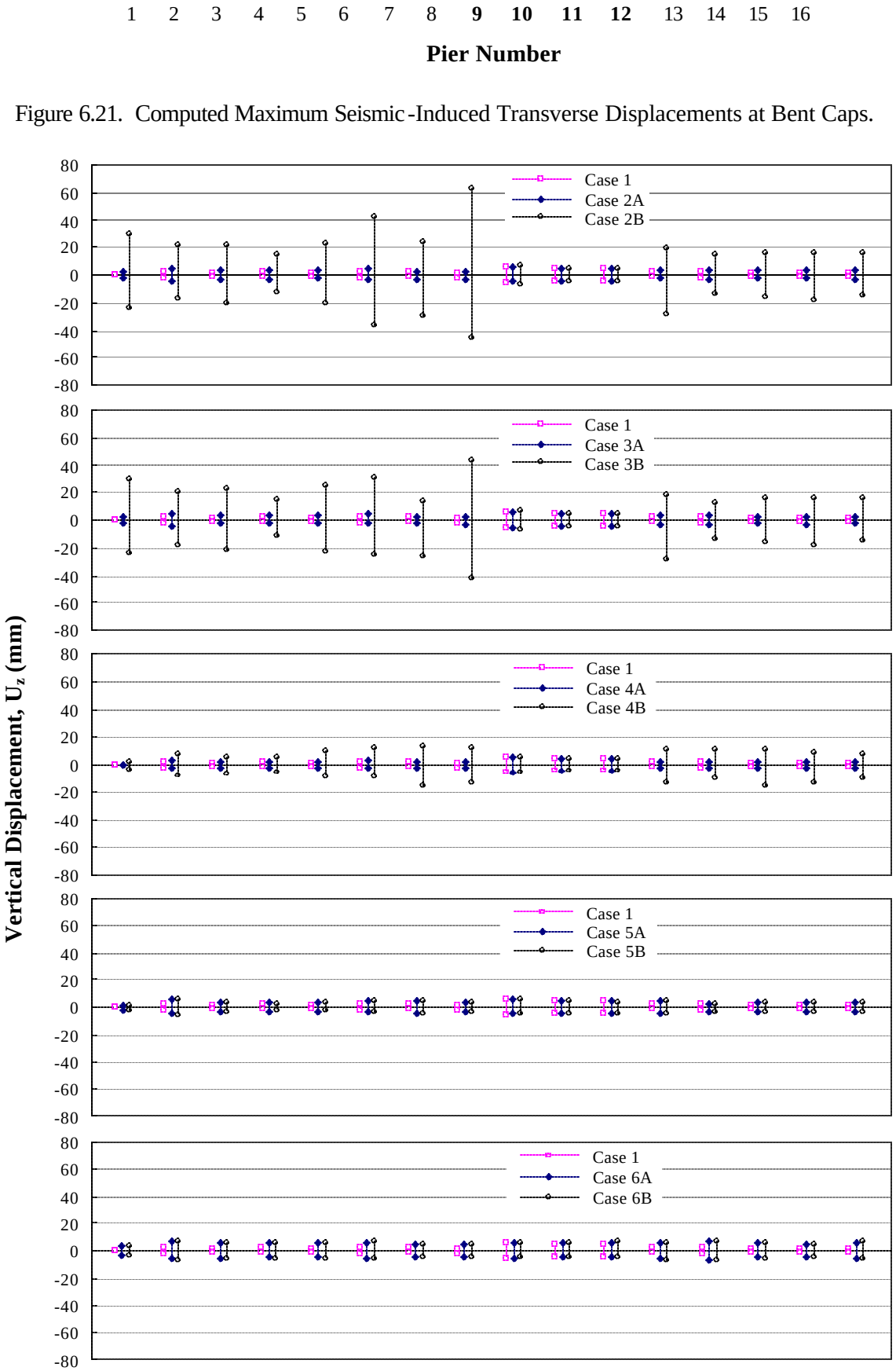

Figure 6.21. Computed Maximum Seismic-Induced Transverse Displacements at Bent Caps.

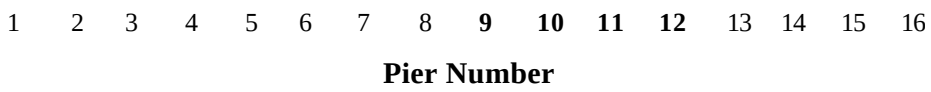

Figure 6.22. Computed Maximum Seismic-Induced Vertical Displacements at Bent Caps.

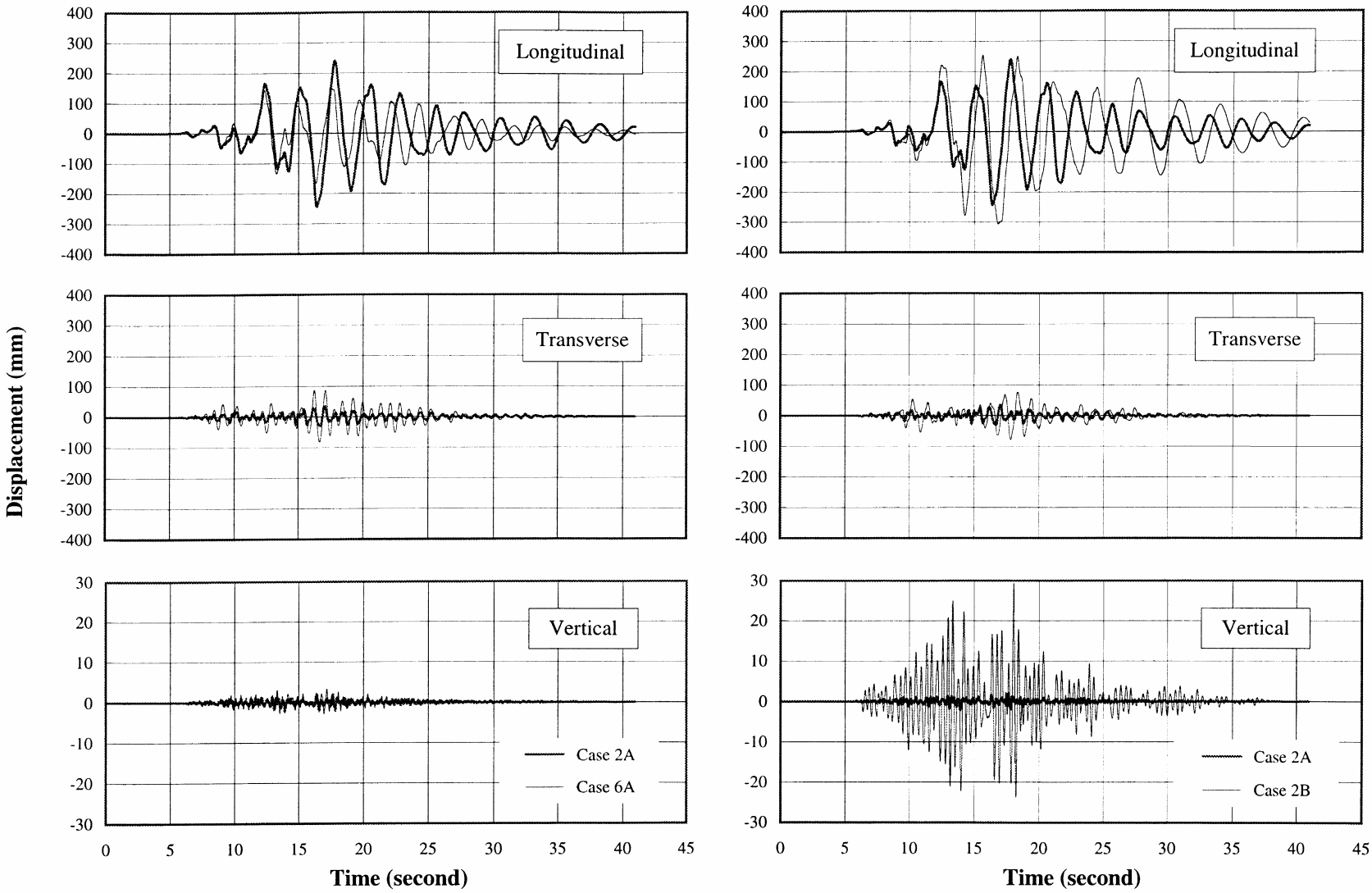
Longitudinal
Transverse
Vertical
Case 2A
Case 6A
Case 2B
Displacement (mm)
Time (second)
400
300
200
100
0
-100
-200
-300
-400
30
20
10
0
-10
-20
-30
0
5
10
15
20
25
30
35
40
45

Figure 6.23. Computed Displacements at the Bent Cap of Pier 1.

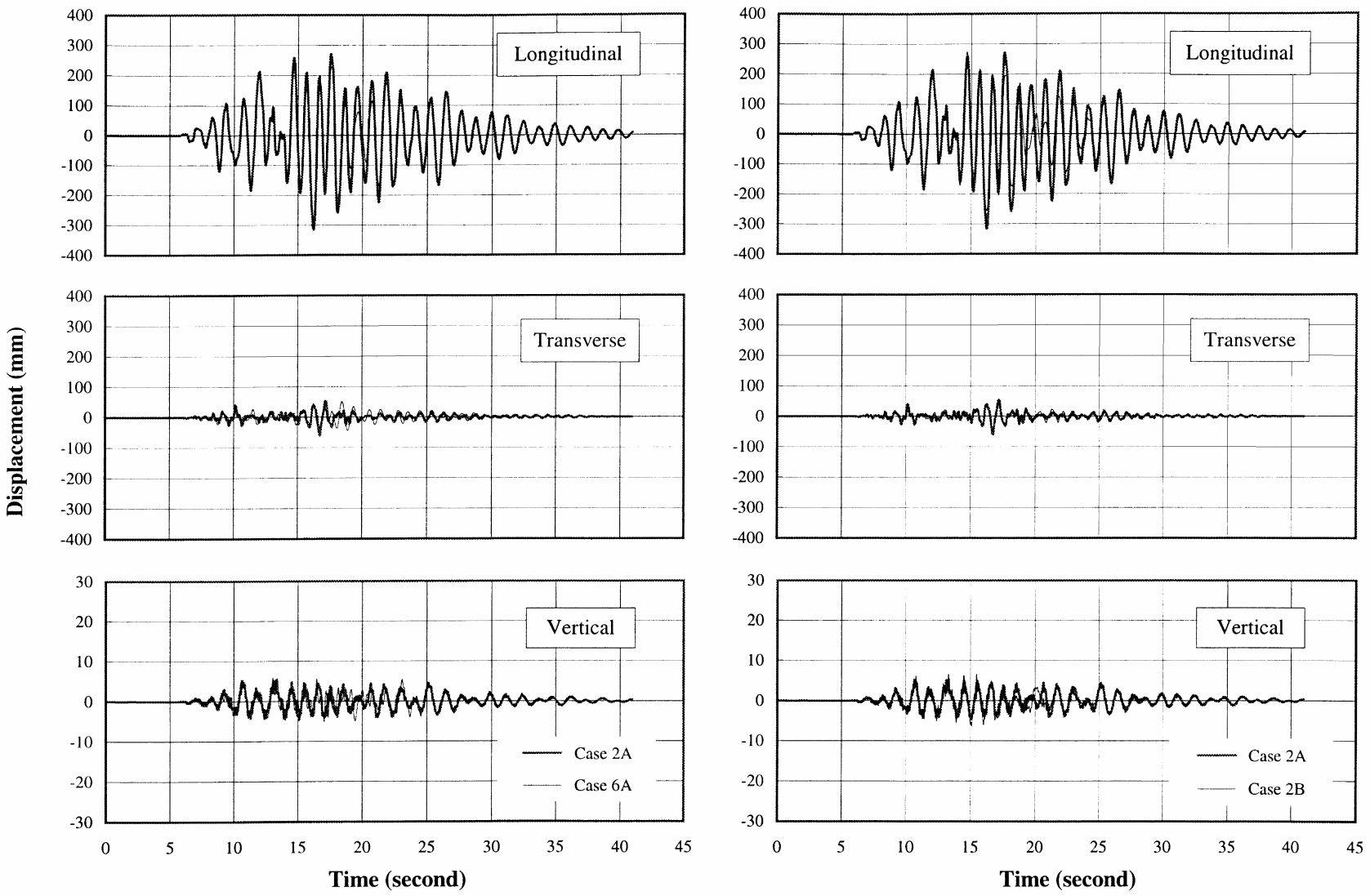

Figure 6.24. Computed Displacements at the Bent Cap of Pier 9.

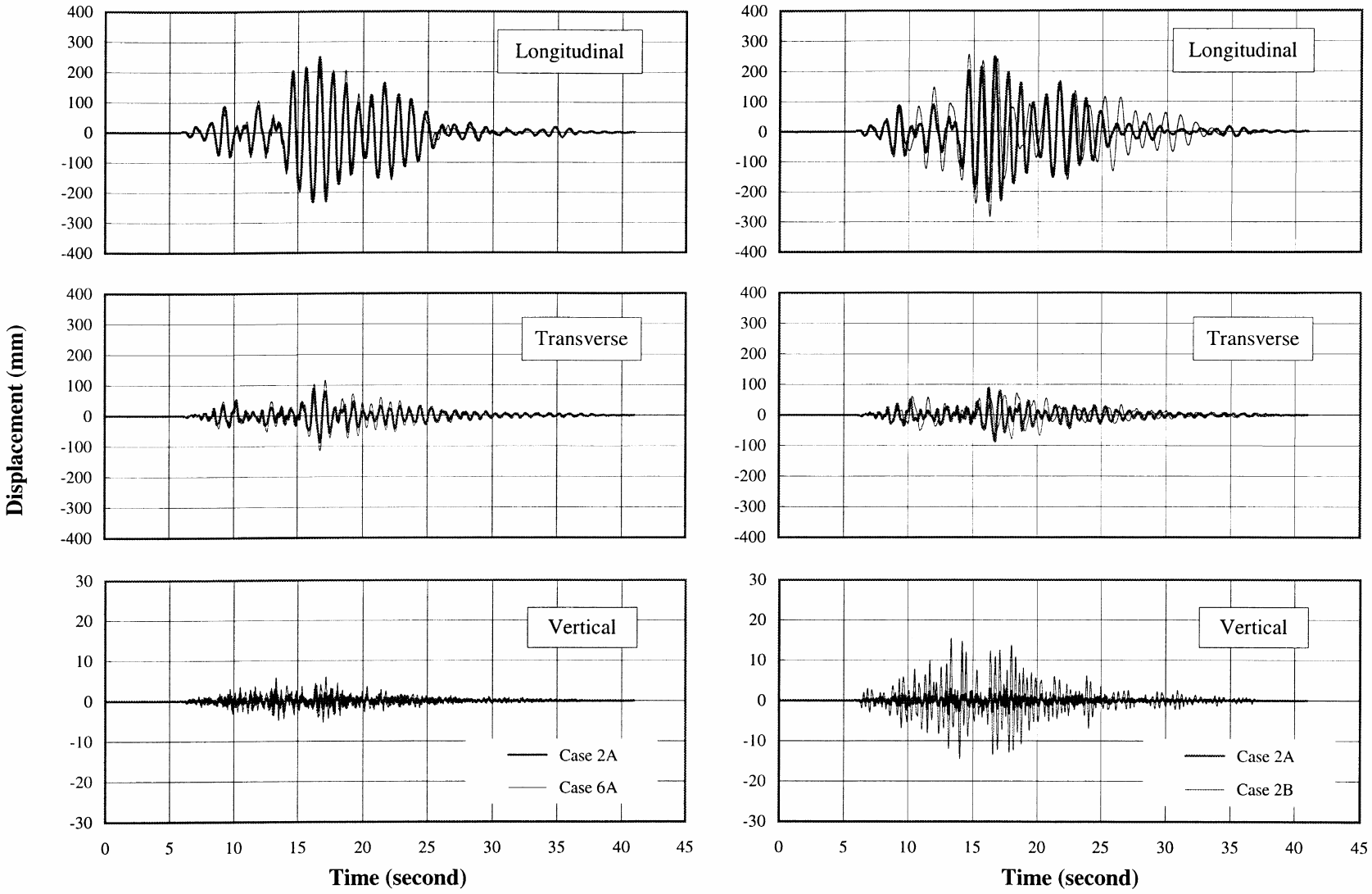

Figure 6.25. Computed Displacements at the Bent Cap of Pier 16.

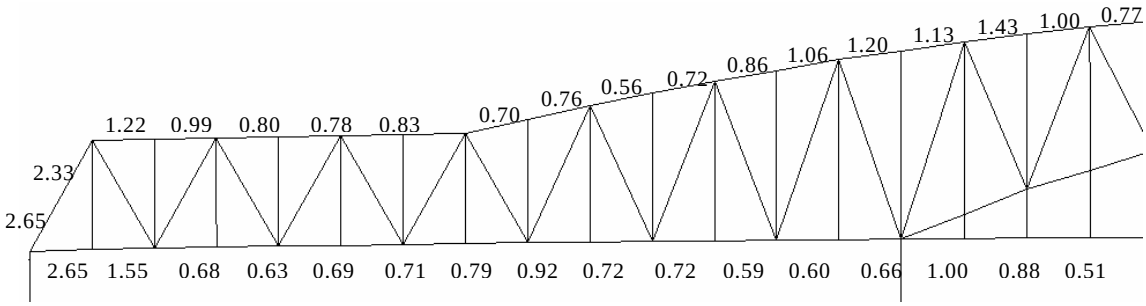

(a) Case 1

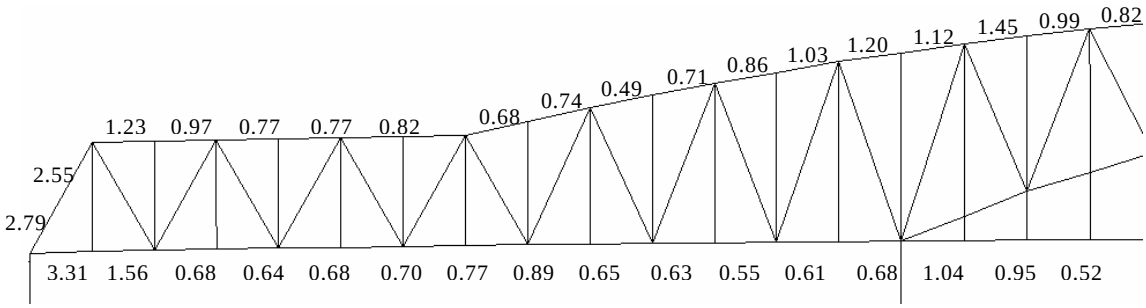

(b) Case 5A

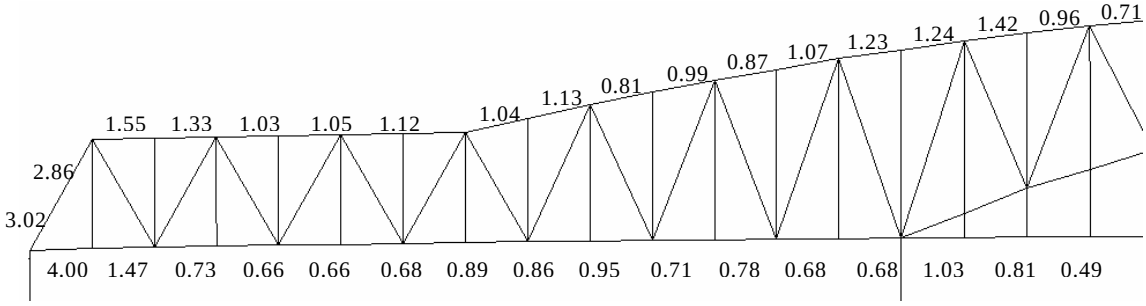

(c) Case 6A

Figure 6.26. Stress Ratios of Truss Members for Different Modeling Cases.

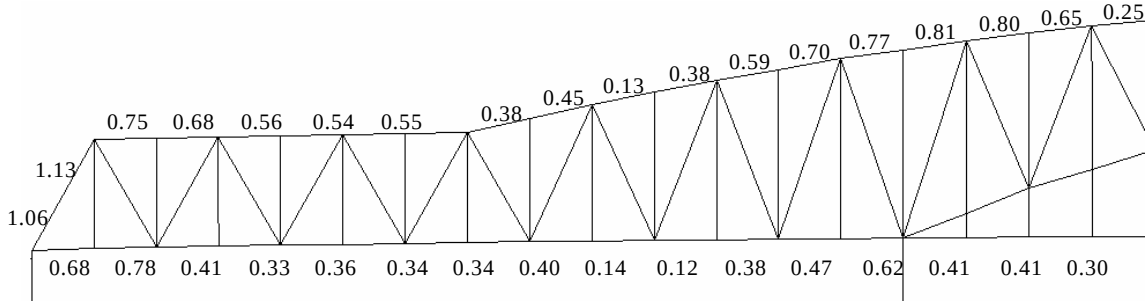

(a) For the 50%/50 Year Hazard Level

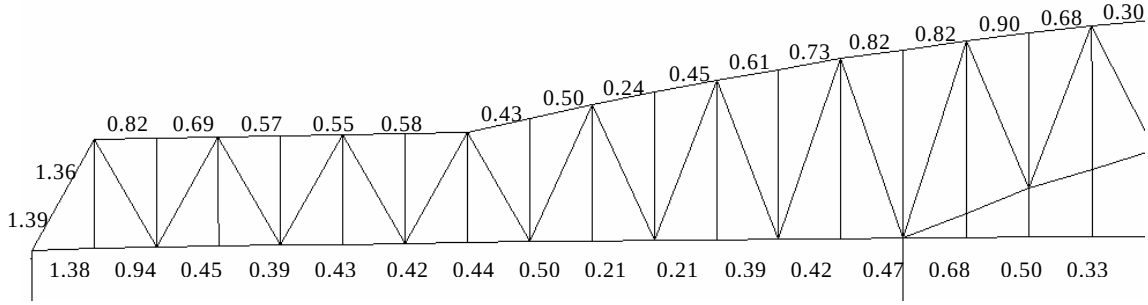

(b) For the 10%/50 Year Hazard Level

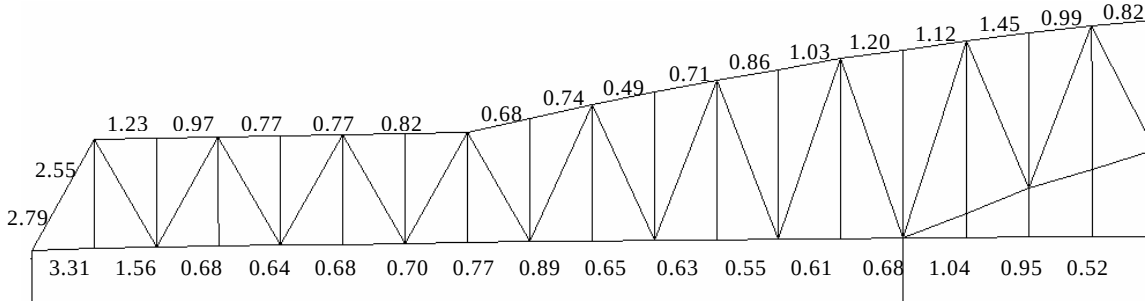

(c) For the 4%/50 Year Hazard Level

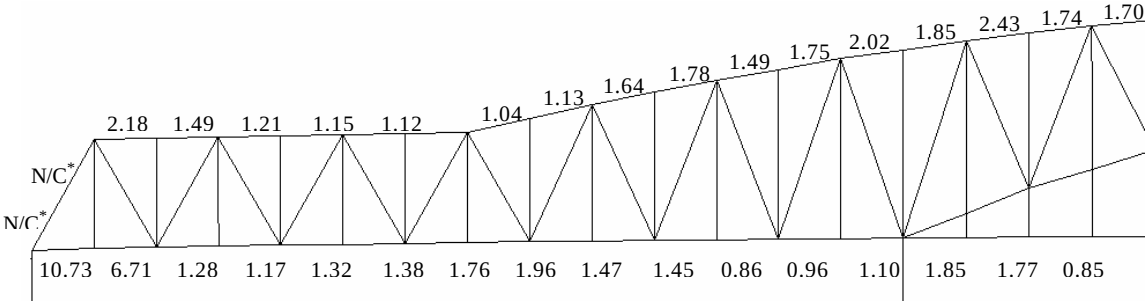

Note: N/C^* denotes Euler buckling strength of the element is exceeded.

(d) For the 2%/50 Year Hazard Level

Figure 6.27. Stress Ratios of Truss Members (Case 5A) for Different Excitation Intensities.

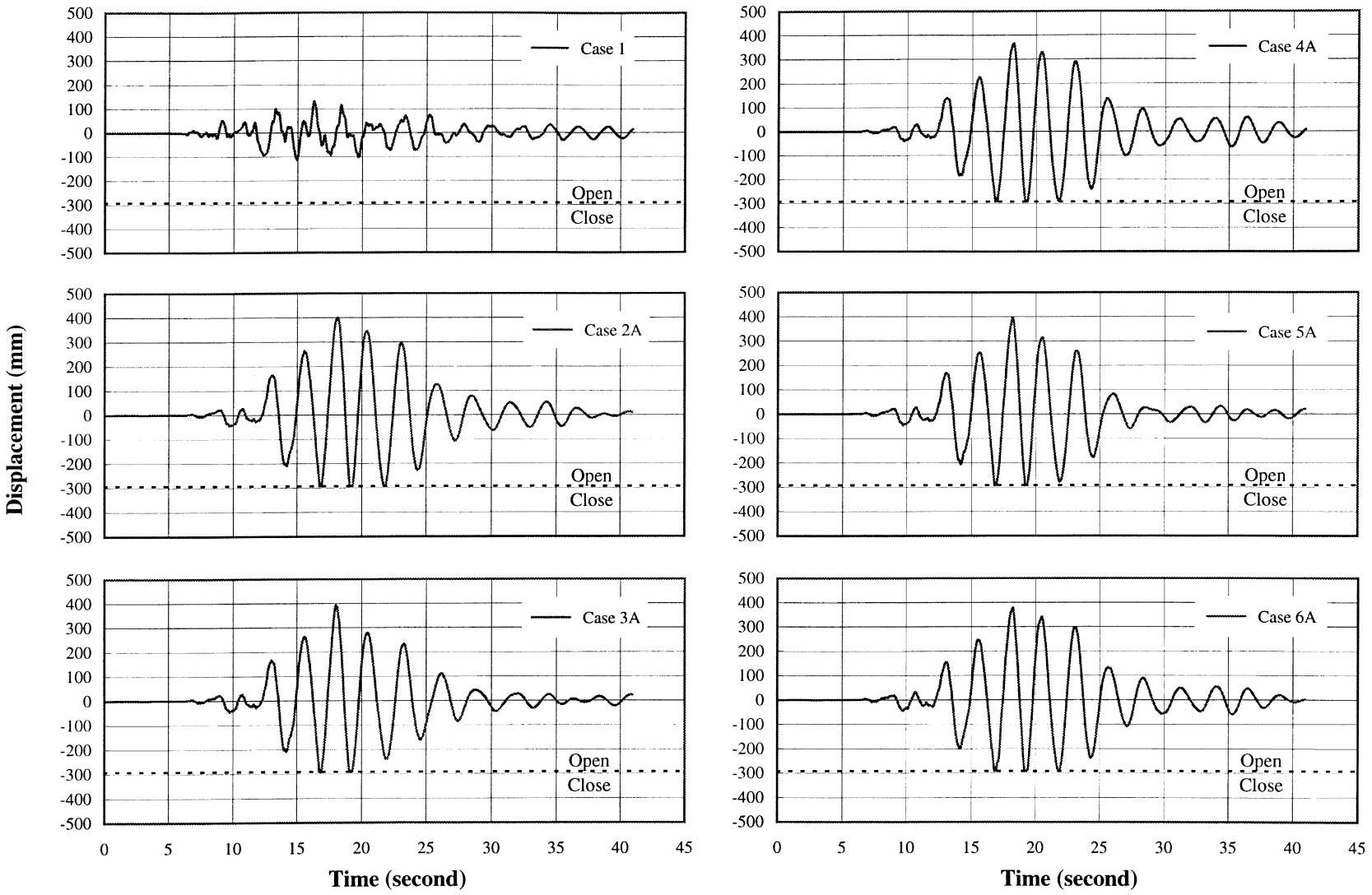
Displacement (mm)
Case 1
Case 2A
Case 3A
Case 4A
Case 5A
Case 6A
Open
Close
500
400
300
200
100
0
-100
-200
-300
-400
-500
0
5
10
15
20
25
30
35
40
45
Time (second)

Figure 6.28. Computed Relative Displacements of the Expansion Joint at Pier 12 for No-PSPI Cases.

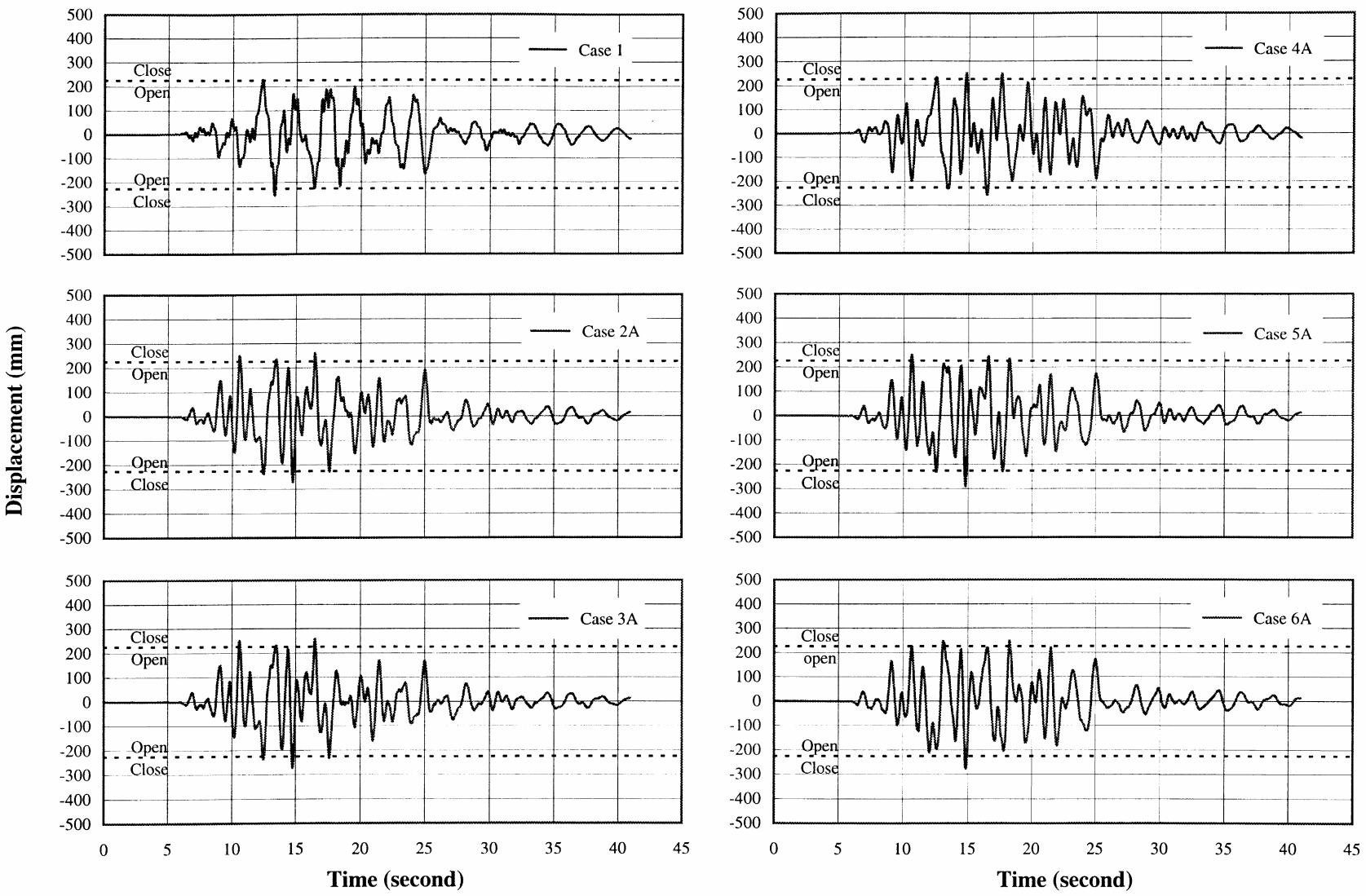

Figure 6.29. Computed Relative Displacements of the Expansion Bearing at Pier 12 for No-PSPI Cases.

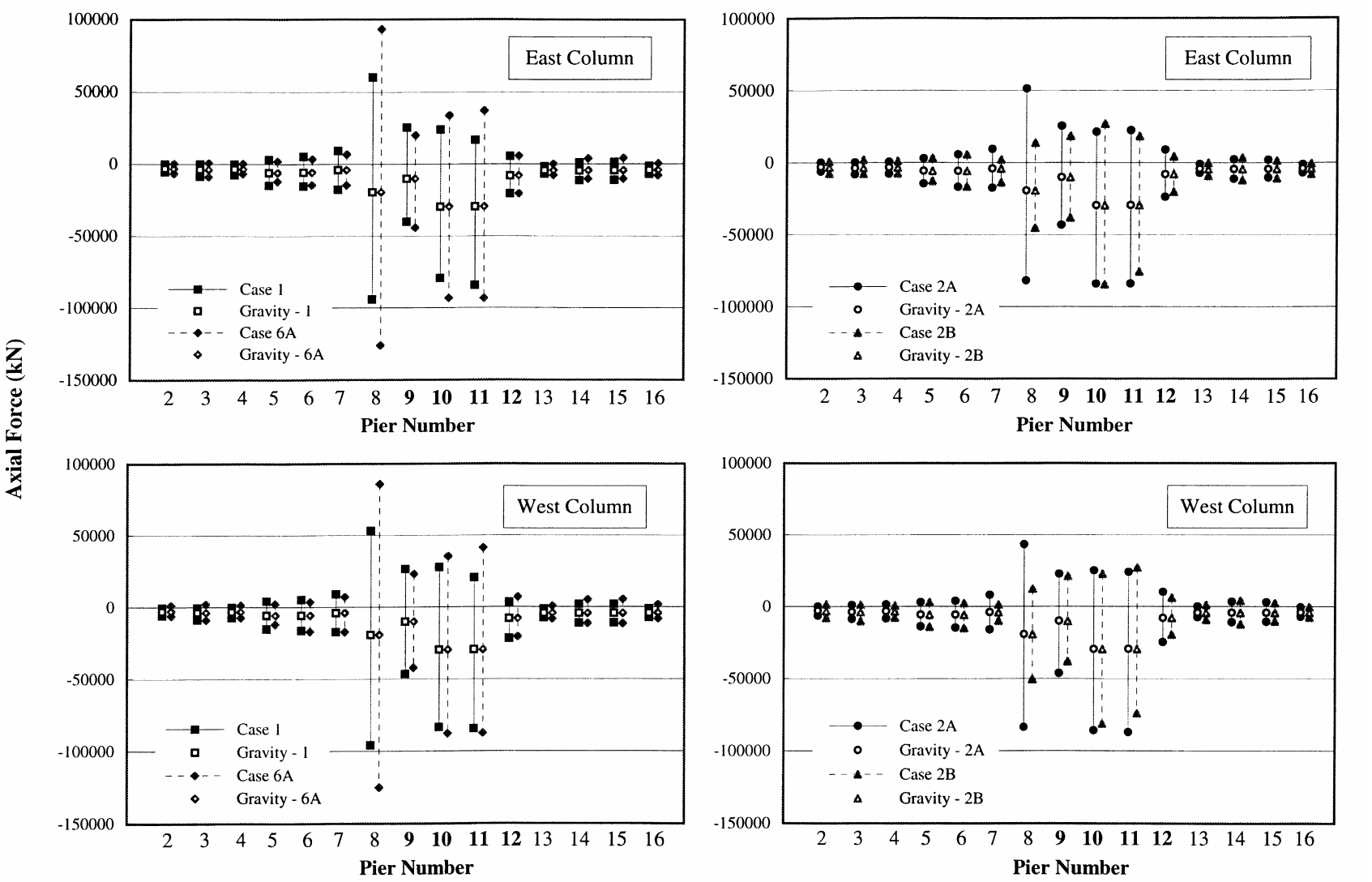
East Column
Case 1
Gravity - 1
Case 6A
Gravity - 6A
Case 2A
Gravity - 2A
Case 2B
Gravity - 2B
West Column
Axial Force (kN)
Pier Number
100000
50000
0
-50000
-100000
-150000
2 3 4 5 6 7 8 9 10 11 12 13 14 15 16

Figure 6.30. Computed Axial Forces in Pier Columns for Cases 1, 6A, 2A and 2B.

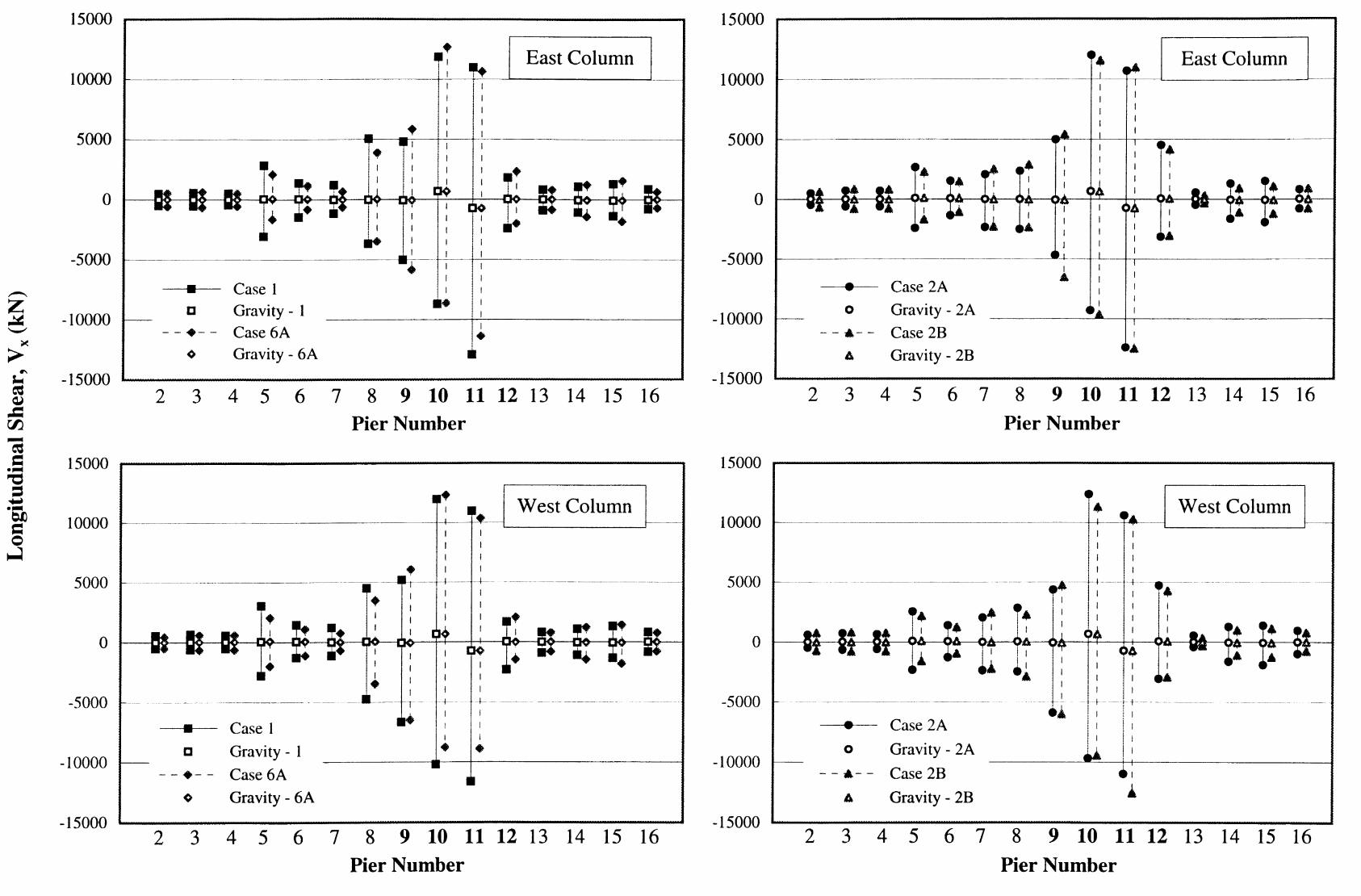

Figure 6.31. Computed Longitudinal Shears in Pier Columns for Cases 1, 6A, 2A and 2B.

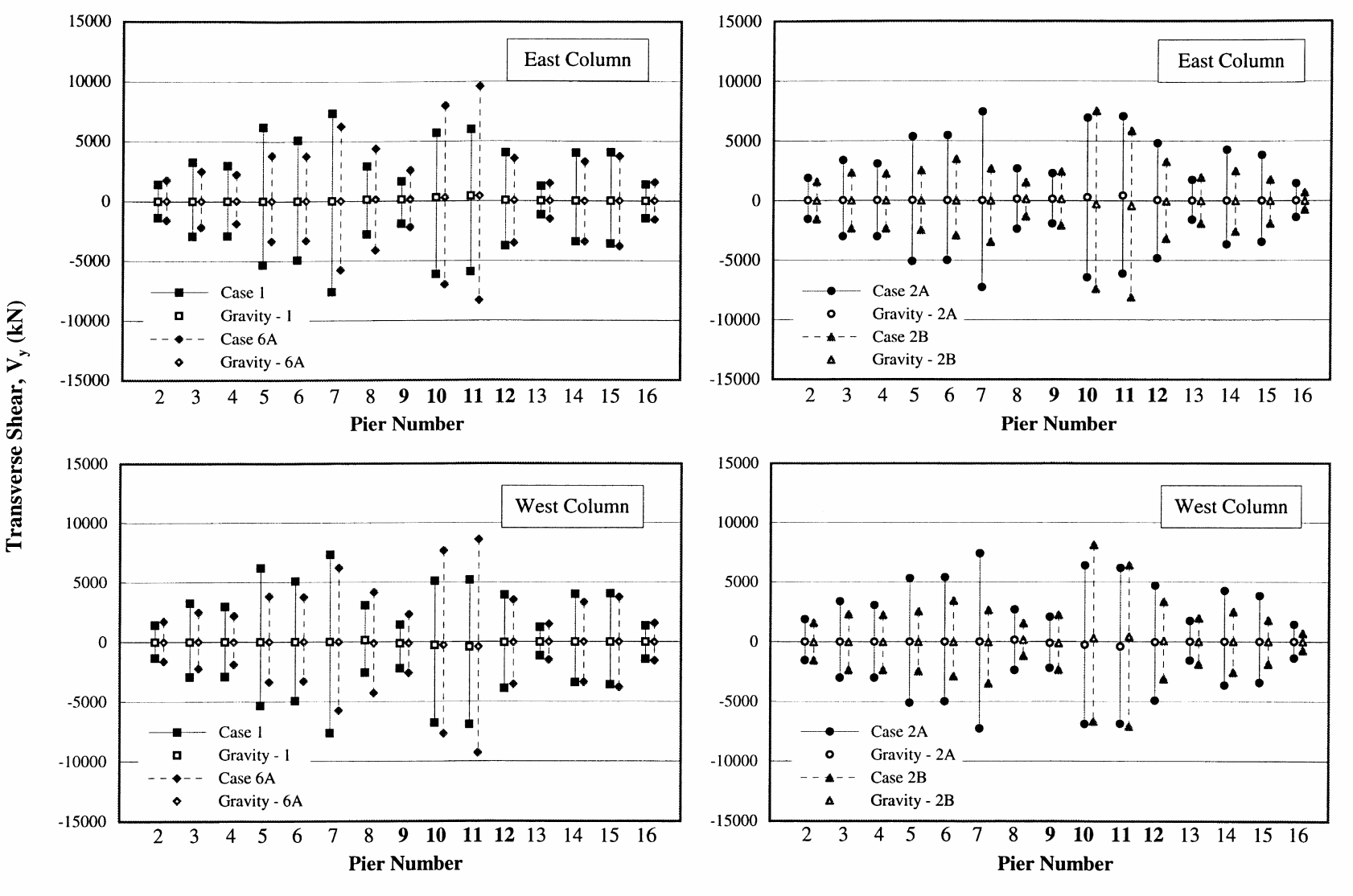

Figure 6.32. Computed Transverse Shears in Pier Columns for Cases 1, 6A, 2A and 2B.

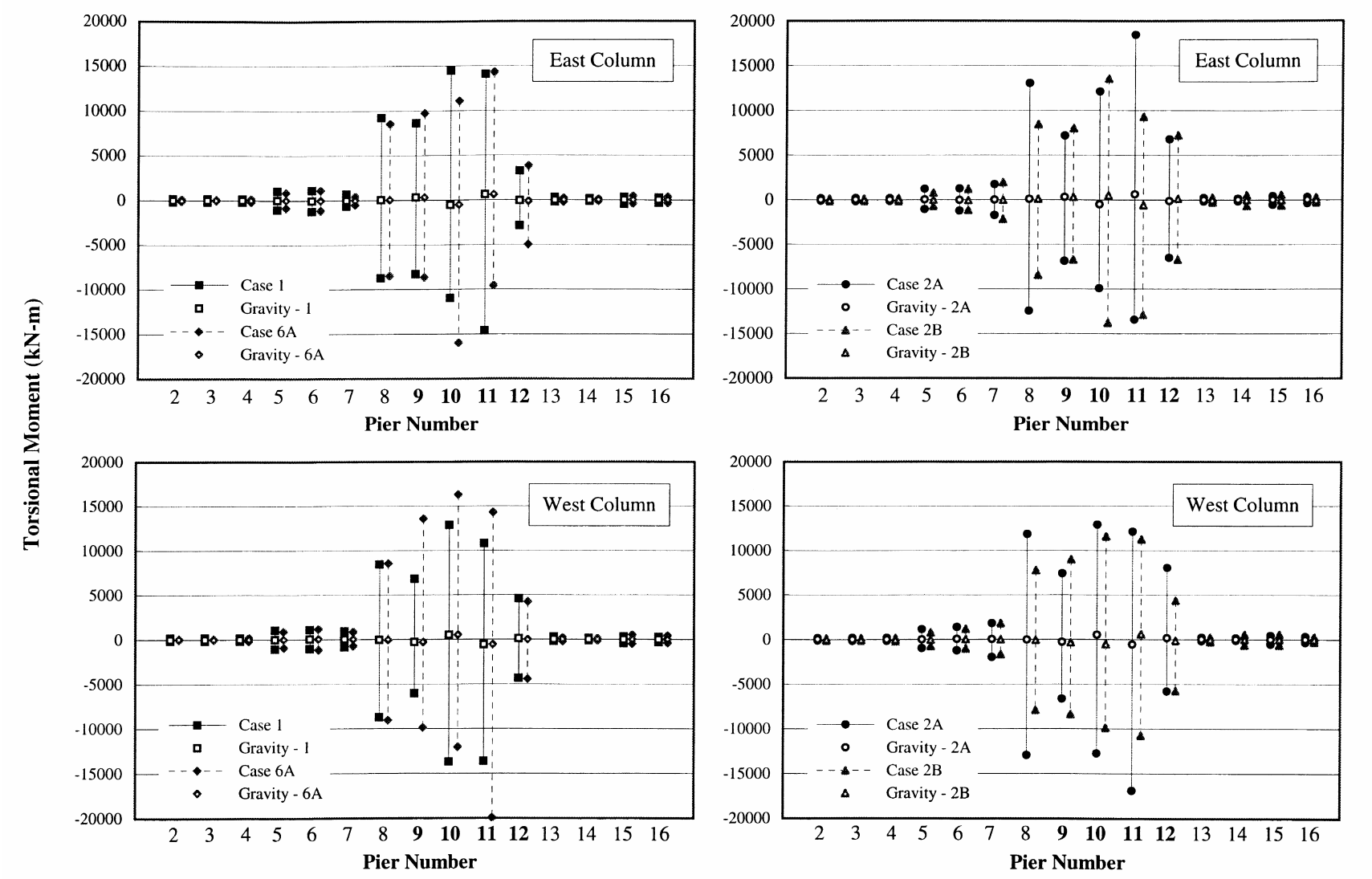

Figure 6.33. Computed Torsional Moments in Pier Columns for Cases 1, 6A, 2A and 2B.

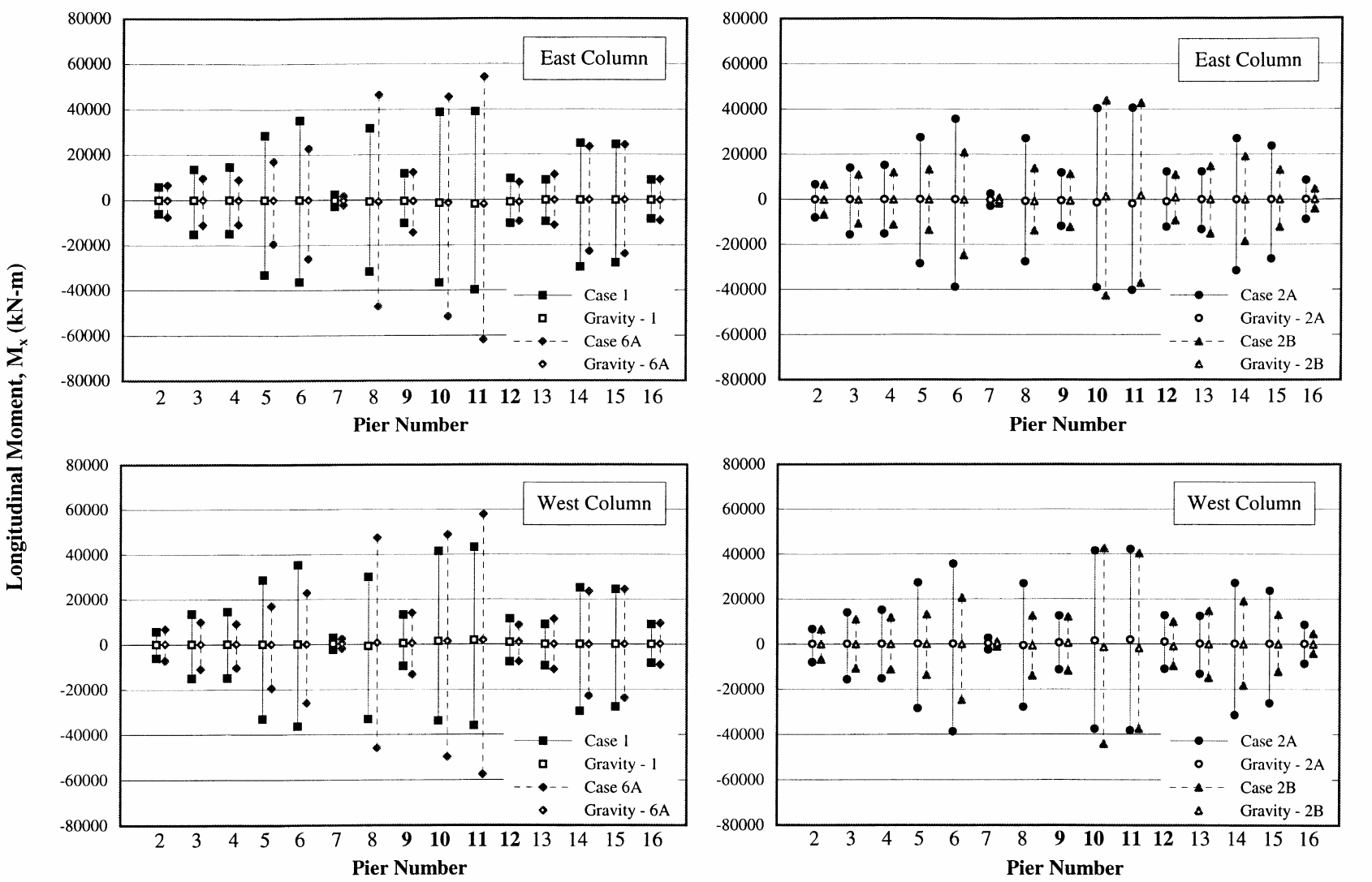

Figure 6.34. Computed Longitudinal Moments in Pier Columns for Cases 1, 6A, 2A and 2B.

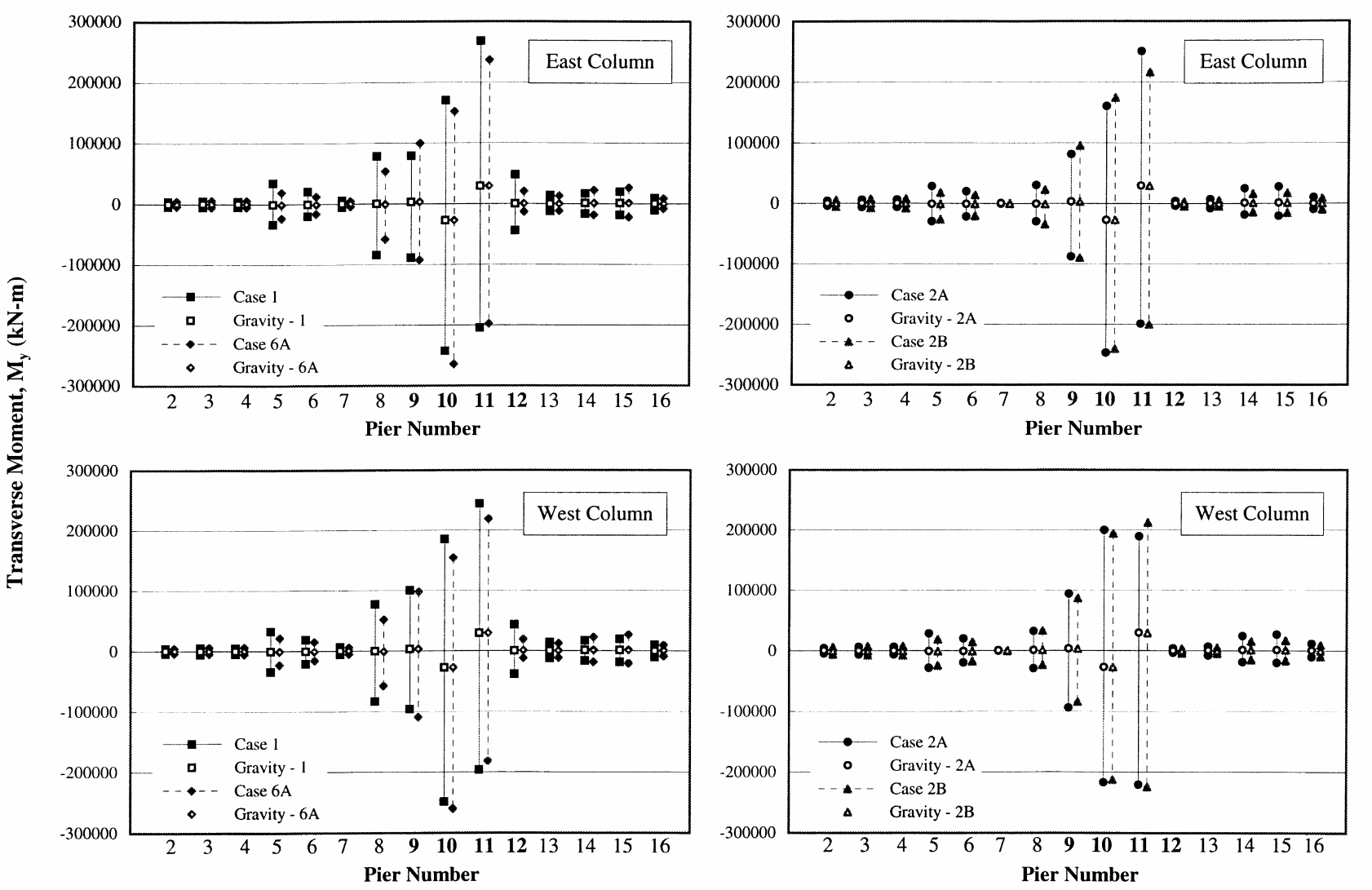
Transverse Moment, M_y (kN-m)
300000
200000
100000
0
-100000
-200000
-300000
East Column
Case 1
Gravity - 1
Case 6A
Gravity - 6A
Case 2A
Gravity - 2A
Case 2B
Gravity - 2B
West Column
2 3 4 5 6 7 8 9 10 11 12 13 14 15 16
Pier Number

Figure 6.35. Computed Transverse Moments in Pier Columns for Cases 1, 6A, 2A and 2B.

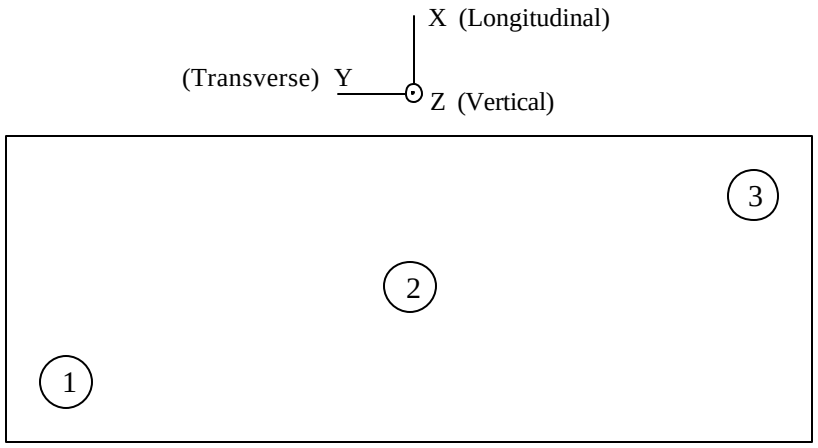

Figure 6.36. Typical Location of the Piles Selected for Comparison Studies.

CHAPTER 7

APPLICATION OF THE PROPOSED PILE-FOUNDATION MODEL

7.1 Introduction

The pile-foundation model was used to investigate the behavior of retrofitted foundations for the Cairo Bridge. In the previous study on the Cairo Bridge foundation (Chapter 6), the analytical results indicated inadequate flexural and shear strength of the piles in the foundations. This finding agrees with the results obtained from the seismic condition survey and performance analysis of the Cairo Bridge conducted by Illinois Department of Transportation (IDOT). Of interest in this study is the behavior of the retrofitted foundations (as suggested by IDOT) and predicted using the proposed pile-foundation models.

In addition, an attempt is made to apply the proposed foundation model to develop a simple alternative for characterizing the pile foundations in the form of a set of equivalent linear springs. To be of great benefit to practitioners, the simplified method developed in this study is interpreted in form of ready-to-use charts from which the pile group stiffness can be obtained as a function of foundation configurations as well as soil and pile properties.

7.2 Application of the Proposed Model to Response Analysis of Retrofitted Foundations

The foundation retrofits recommended for the Cairo Bridge involve increasing the pile cap thickness and adding more piles. This retrofit scheme is recommended for foundations supporting all piers except Piers 9, 10 and 11 which are supported on open-dredge caissons. In this study, the retrofitted foundation for Pier 2 is selected for static response evaluation. Also investigated herein is the effect of loading history (i.e., the different state of stress at service load experienced by the existing and retrofitted members) on the foundation response. Details of modeling the retrofitted foundation of Pier 2 are given as follows.

7.2.1 Modeling of the Retrofitted Foundation

The existing foundation consists of 36 vertical, 0.31-m-diameter reinforced concrete piles. The piles are approximately 17.70 m long and embedded about 0.31 m into the pile cap. The pile cap has a dimension of 3.20 m for longitudinal width, 15.86 m for transverse width and 0.76 m for vertical depth. The pile cap is enlarged to a 6.96 m wide, 17.70 m long and 2.14 m thick. A steel pipe pile having an outside diameter of 0.32 m has been selected as a typical retrofit pile. The drilled-in piling type is recommended to minimize the possible detrimental effects from installation of the retrofit piles on the existing bridge. The length of the piles may vary to ensure the penetration depth into a stratum of very dense sand, which is about 18 to 25 m below the ground surface. A schematic of the retrofitted foundation is shown in Figure 7.1.

The piles are modeled using frame elements and the pile cap is modeled using shell elements. Figure 7.2 shows the analytical model of the retrofitted foundation. The soil is modeled using nonlinear elements. To account for the PSPI effects, the t- and p-multipliers are used to soften the stiffness and reduce the ultimate capacity of the soil reactions in both vertical and lateral directions. The gap elements are used at the pile tip to deactivate the end-bearing soil reactions when the piles are subjected to tension load. These modeling concepts are applied to both new and existing foundations.

The difference between the retrofit and existing structure is the state of stress at service condition experienced by the structure. The existing structure has already carried a majority part of the service load (dead load) whereas the retrofit structure is put in only to resist the additional loads (live load and loads for which it is designed). In other words, the dead load is carried solely by the existing structure and any additional load is carried by both the existing and retrofit structure acting in a composite manner. This loading sequence can be simulated using the proposed mechanism as shown in Figure 7.2. The gap element is used to replicate the application of dead load to the existing piles. The open width of the gap elements is specified as the settlement of the existing foundation due to dead load only. That is the retrofit pile will resist only the additional applied load which is transmitted through the gap elements for compression and the hook elements for tension.

7.2.2 Static Behavior of the Retrofitted Foundation

The proposed pile foundation model is used in nonlinear response analyses of the retrofitted foundation. The nonlinear load-deformation relationships obtained from these analyses are compared with those previously obtained for the existing foundation. The comparison is done for

the foundation response for all degrees of freedom. In addition, the load-deflection responses of the retrofit and existing pile to vertical and lateral loading are shown for comparisons.

Vertical response

The load-settlement relationships for single retrofit and existing piles are shown in Figure 7.3(a) and those for retrofitted and existing foundations are compared in Figure 7.3 (b). In Figure 7.3(b), the solid line represents the load-settlement curve of the existing foundation. The dash line is obtained from the model in which the loading history is neglected. The lighter solid line with open circle represents the load-settlement curve obtained from the modeling case in which the loading sequence is modeled. The secant stiffness specified at 5-mm settlement increases about 54% and the ultimate compression load capacity specified at 25-mm settlement increases about 29% after applying the foundation retrofits.

Figure 7.3(b) is enlarged for the region (0-5 mm) at which the deviation among load-settlement curves is found most distinguishable (Figure 7.4). It is observed from Figure 7.4 that the curve for the retrofitted foundation considering the loading sequence (the lighter solid line with open circle) follows the curve for the existing foundation (the solid line) initially and starts deviating at about 1 mm and merges close to the curve for retrofitted foundation without the loading sequence (the dash line with closed circle) at about 2 mm. The abrupt change of the curve occurs when the gap elements are closed or when the retrofitted and existing foundation starts acting as a whole, and thus resulting in a stiffer structural system. This abrupt change in stiffness occurs only at the initial part of the curve (0-2 mm) and it is hardly noticeable in Figure 7.3(b) implying that the effects of loading sequence in this case on the load-settlement relationship of the retrofitted foundation are insignificant and may be neglected.

Lateral response

The load-deflection responses of the retrofit and existing pile to lateral loads are shown in Figure 7.5. The load-displacement relationships of the retrofitted and existing foundation to longitudinal and transverse loads are shown in Figure 7.6. Since the lateral force experienced at the foundation under service load is relatively small, and the load-displacement curves for lateral loading are uncoupled with that for vertical loading, the effects of loading sequence are anticipated to be insignificant and therefore neglected.

The analytical results show that by increasing the size of the pile cap and adding more piles, the secant stiffness and ultimate load capacity increase by 32% and 35% for the longitudinal direction and 40% and 43% for the transverse direction, respectively. The secant stiffness is computed at the lateral displacement of 25 mm and the ultimate load capacity is computed at the load at the lateral displacement of 50 mm. These increases are somewhat significant considering that only 8 more piles are added. However, the new piles are of steel pipe pile type whose flexural stiffness (EI = 30,606 kN.m^2) is about 6 times larger than the flexural stiffness of the existing reinforced concrete piles (EI = 4,843 kN.m^2). Furthermore, the increased depth of the pile cap results in a more even distribution of the applied load to all the piles in the group and thus leading to greater stiffness as well as greater ultimate load capacity for the retrofitted foundations.

Rotational response

The rotational response of the retrofitted foundation is quite different from the lateral response. The rotation response is strongly dependent on the vertical response which is dependent on the loading history. If the foundation is loaded vertically up to the service load before applying the moment at the center of the pile cap, the rotational response of the foundation will be different from that obtained from the foundation to which no vertical load is applied. The difference between the rotational responses obtained from the model with and without considering the load sequence is investigated.

The moment-rotation curves about x and y axes for the existing and retrofitted foundations are shown in Figure 7.7. It is first observed from these figures that the difference of the moment-rotation curves for retrofitted and existing foundation is fairly significant. The secant stiffness increases about two times for rotational response about the x axis and as much as four times for rotational response about the y axis for the retrofitted foundation. The ultimate moment capacity of the retrofitted foundation also increases significantly for both directions (three times and seven times as much as that of the existing foundation for rotational response about x and y axes, respectively). Note that the secant rotational stiffness and ultimate moment capacity are specified at the rotations which induce the vertical displacement of the outermost existing pile (Pile A) for rotational response about the x axis of 25 mm and 50 mm and the vertical displacement of the outermost existing pile (Pile B) for rotational response about the y axis of 12.5 mm and 25 mm, respectively. Figure 7.7(d) shows the location of indicative piles (Piles A and B). For rotational response about the x axis for both retrofitted and existing foundation, these rotations are approximately equal to 0.004 and 0.010

radian. For rotational response about the y axis, these rotations are about 0.009 and 0.020 radian. The rotational response of the foundation is found to be more sensitive to the retrofit measures than the response in other degrees of freedom.

In Figure 7-7, the moment-rotation curves obtained from the model with and without considering the loading sequence are also shown for comparison. Note that the gap and hook elements are not yet implemented in the analytical models. The effects of loading sequence on the rotational response of the existing foundation appear to be more significant than those on the rotational response of the retrofitted foundation. This is probably because of the fact that the foundation retrofits not only strengthen the structural system but also stiffen the pile cap and thus resulting in a more even distribution of the applied load. In other words, the stiffer pile cap lessens occurrences of local failure of individual piles and thus leading to a stiffer structural system.

A possible explanation for a close agreement between the moment-rotation curves computed with and without considering the loading sequence for the retrofitted structure is that the studied pile foundation is of friction-pile type for which the compression and tension capacity of the pile are somewhat similar. For end-bearing-type foundation, the tension capacity is much less than the compression capacity of the pile. Therefore, the downward force due to applied dead load plays an important role in counterbalancing the applied moment-induced tensile force, thus resulting in larger discrepancies between the moment-rotation curves computed from the models with and without considering the loading-sequence effects.

It should be noted that an attempt has been made to incorporate the proposed mechanism to capture the rotation-induced tensile and compressive force on the retrofit piles. Unfortunately, the nonlinear analyses could not be successfully completed. There experienced both computational and technical problems with the computer. Hopefully, with a rapid growth in development of computer programming technology, more advanced computer systems and also more improved computer programs may soon become available and the incorporation of the proposed mechanism may become achievable as well. Nonetheless, it is believed that had the analysis been completed, the computed moment-rotation curve of the retrofitted foundation would have been very similar to the computed curves with and without the loading sequence shown in Figure 7.7.

The difference between the torsional response of the retrofitted and existing foundation (Figure 7.7(c)) is less than that of the other two rotational responses. The secant torsional stiffness increases about 65% and the ultimate capacity increases about 80%. The torsion-induced lateral

displacements at the outermost existing pile (pile A in Figure 7.7(d)) of 25 mm (q_z = 0.003 radian) and 50 mm (q_z = 0.007 radian) are used to compute the torsional stiffness and ultimate capacity. The torsional response of the retrofitted foundation has similar characteristics to the lateral response which is not dependent on the loading sequence but mostly on the flexural stiffness of the retrofit piles and the increased depth of the pile cap.

The increases in the secant stiffness and ultimate capacity of the foundation certainly affect the response of the bridge. In general, it is believed that the stiffer foundation system results in smaller displacements and rotations but larger forces and moments experienced at the foundation. The statement is applicable for such simple structures as one- or two-span bridges. However, for long span bridges, the previous study on the Cairo Bridge indicated that the overall bridge response was dependent not only on one individual element but also on all elements of the structural systems. The change in properties of one element affects the response of all other elements and by changing the stiffness of one foundation, the displacements or forces experienced at that foundation could either increase or decrease depending on the stiffness of other foundations or other elements in the structural system. Consequently, to properly investigate the efficiency of the retrofit measures on the bridge response, the global model of the bridge including its foundation system is recommended.

7.3 Application of the Proposed Model to Development of a Simplified Foundation Model

In view of practicality, a simplified foundation model such as a linear or nonlinear spring model has found considerable appeal for preliminary seismic performance evaluation of pile-supported bridges. Several approaches have been proposed to evaluate appropriate coefficients for representing the foundation springs. However, a majority of these approaches are not applicable for large pile groups for which the pile-soil-pile interaction is of great consequence. An attempt has been made in this research study to provide a simple alternative to account for the PSPI effects for large pile groups and in order to be of practical use for practitioners in both geotechnical and structural engineering fields, the proposed foundation model has been applied to establish ready-to-use charts from which the pile group stiffness can be evaluated as a function of number of piles in a group, pile properties and soil properties. The assumptions and steps taken to develop this chart are discussed below.

7.3.1 Development of Charts for Stiffness Coefficient Evaluation

As a demonstration case, similar properties of the piles used for the Cairo Bridge are adopted. The piles are cast-in-place, reinforced concrete, circular piles having a diameter of 0.3 m. The pile length is sufficient to be considered as a long pile for which the mode of failure is governed by the pile flexibility rather than the rigid body movement. The adopted criteria for long piles are presented in Chapter 3 (Equation 3.1).

A homogenous soil stratum of various soil types (loose, medium-dense, and dense sand) is chosen and the linear distribution of the modulus of subgrade reaction is assumed for all soil types. As for typical properties of loose sand, the angle of internal friction of 30° is used and the corresponding coefficient of subgrade reaction (the rate of increase in initial modulus of subgrade reaction with increasing depth, k_s) obtained according to API's recommendation (Figure 7.8) is set equal to 12 MN/m^3. For medium dense and dense sand, the angles of internal friction of 35° and 40° are specified and the corresponding coefficients of subgrade modulus are 36 and 75 MN/m^3, respectively. The pile-flexibility factor (PF) is introduced to evaluate the relative stiffness of the pile and its surrounding soil. The PF factor is defined as the ratio of flexural stiffness of the pile to coefficient of subgrade soil reactions (k_s) given as,

[7.1] $$PF = \frac{E_p I_p}{k_s},$$

The pile-flexibility factor for each soil type is listed in Table 7.1.

Table 7.1. Pile-Soil Stiffness, and Corresponding Pile-Flexibility Factor for Each Soil Type.

Soil type	Flexibility of pile section, E_pI_p (kN.m^2)	Coefficient of subgrade modulus, k_s (kN/m^3)	Pile-flexibility Factor (m)
Loose sand	4,847	12,000	0.404
Medium-dense sand	4,847	36,000	0.135
Dense sand	4,847	75,000	0.065

The soil reactions on pile foundations may be divided into two components; soil reactions on the pile and the pile cap. The soil reactions at the piles are characterized using the *p-y* criteria proposed

by O'Neill and Murchinson (1983) and also recommended by the API (1991). The soil reactions at the pile cap are not considered and the pile cap is assumed to be rigid. As an illustration case, two conditions of the pile-to-pile-cap connections (fixed-head and free-head conditions) are used in constructing the stiffness curves. For the fixed-head pile condition, the piles are assumed to be rigidly capped into the pile cap and for the free-head condition, the piles are free to rotate independently of the pile cap.

Theoretically, the number of piles in the group should not have any effect on the pile group response to lateral loads computed by the proposed pile group model in which each pile is modeled independently if the loading and pile configuration are symmetrical and the pile cap is rigid. Therefore, to be computationally efficient, the 2x2 pile group is used to construct the stiffness curves for lateral loading as a function of pile spacing to diameter ratio (s/d). Various s/d ratios are used to investigate the effects of the PSPI on the lateral stiffness of pile group foundations. For each s/d ratio, the p-multiplier is assigned corresponding to a relationship given in Figure 7.9. For s/d ratio equal to 3, the p-multiplier is equal to 0.5 and for s/d ratio greater than 10, the p-multiplier is equal to 1.0. For s/d ratios between 3 and 10 and less than 3, the p-multiplier varies linearly.

A number of nonlinear analyses are performed to establish the stiffness curve for different s/d ratios and pile-flexibility factors. The pile group stiffness coefficients obtained from these analyses are normalized as a ratio of the pile group stiffness to the product of the single pile stiffness and the number of piles in the group. The stiffness for both single pile and grouped piles is defined as the secant stiffness at the lateral displacement of 25 mm.

For the fixed-head condition, the load-displacement relationships of the single pile for different pile-flexibility factors are shown in Figure 7.10(a). The secant stiffness corresponding to the lateral displacement of 25 mm is about 9.5, 16.3 and 22.4 kN/mm for loose, medium-dense and dense sand respectively. These values conform well to those computed using the elastic continuum method, which is equal to 8.5, 15.6 and 22.3 kN/mm in the order previously given. These values correspond to the coefficients of secant subgrade modulus set equal to 10 MN/m^3 for loose sand, 30 MN/m^3 for medium-dense sand, and 55 MN/m^3 for dense sand above water table. For free-head condition, the load-displacement curves of the single pile are also shown in Figure 7.10(b) and the secant stiffness is approximately 3.6, 7.1 and 9.7 kN/mm for loose, medium-dense sand and dense sand, respectively. These values also conform well to those computed using the elastic continuum

methods which are about 3.3, 6.0 and 8.5 kN/mm corresponding to the previously specified coefficients of secant subgrade modulus in the order given.

The stiffness curves relating the normalized pile-group-to-single-pile stiffness factor and the s/d ratios for different pile-flexibility factors and pile-to-pile-cap conditions are shown in Figure 7.11 and the calculated values are also listed in Table 7.2. As can be expected, the stiffness curves approach 1.0 as the s/d ratio increases and reach 1.0 at the s/d ratio equal to 10. Although the p-multiplier varies linearly with the s/d ratio, the pile-group stiffness appears to vary nonlinearly and the degree of nonlinearity increases as the pile-flexibility factor increases. For the fixed-head condition, the pile-flexibility factor decreases 3 times as much from loose sand to medium-dense sand while the pile-group-to-single-pile stiffness factor decreases only 13% maximum at the s/d ratio equal to 2. Similar observation can also be made for the free-head condition. As the pile-flexibility factor decreases 6 times from loose sand to dense sand, the stiffness factor decreases by only 16% at the s/d ratio equal to 2. Although the PSPI effect is more strongly pronounced for stiffer soil (i.e., the pile-group-to-single-pile stiffness factor decreases), it is observed that the reduction rate of the pile group stiffness decreases as the soil stiffness increases.

Table 7.2. Pile-Group-to-Single-Pile Stiffness Factors for Different s/d Ratios and PF Factors.

Pile-flexibility factor/ Soil type	Pile-group-to-single-pile-stiffness factor for different s/d ratios								
	2	3	4	5	6	7	8	9	10
PF = 0.404 m (Loose sand)									
(a) Fixed-head	0.77	0.82	0.86	0.89	0.92	0.94	0.97	0.98	1.00
(b) Free-head	0.85	0.89	0.92	0.94	0.96	0.97	0.98	0.99	1.00
PF = 0.135 m (Medium sand)									
(a) Fixed-head	0.67	0.72	0.76	0.81	0.85	0.89	0.93	0.96	1.00
(b) Free-head	0.66	0.72	0.77	0.81	0.86	0.90	0.93	0.96	1.00
PF = 0.065 m (Dense sand)									
(a) Fixed-head	0.65	0.70	0.75	0.79	0.84	0.88	0.92	0.96	1.00
(b) Free-head	0.66	0.71	0.76	0.81	0.85	0.89	0.93	0.96	1.00

It is of interest to note that the stiffness curves for fixed-head and free-head conditions are comparable for medium-dense and dense sands. For loose sand (the largest PF factor), the stiffness curve deviates from others. A rational explanation is that as the pile-flexibility factor increases (piles in soft soils), the flexural stiffness of the piles becomes more dominant in the lateral stiffness of the pile foundations. In other words, the effects of pile-soil-pile interaction are less influential with increasing pile-flexibility factor. In case the piles are embedded in very soft soils, the pile-group-to-single-pile stiffness factor will be less sensitive to the PSPI or s/d ratios. In case the piles are embedded in stiffer soils, the soil stiffness or the PSPI effects become more pronounced, and the variation of pile-group-to-single-pile stiffness factor will be similar to the assumed linear variation of the p-multipliers with s/d ratios.

It appears that the free-head pile foundation in loose sand has the highest group efficiency or pile-group-to-single-pile stiffness factors. It should be pointed out however that the single pile or pile group stiffness for free-head condition is less than those for fixed-head condition. In addition, it is observed from the analytical results that at the specified displacement for computed the secant stiffness, the moments experienced in the piles are relatively low and the moments are distributed over a greater portion of the pile length for the free-head condition.

This distribution of moments at greater depth below ground surface for the free-head condition indicates that the soil resistance at greater depth is derived more efficiently and thus resulting in higher group efficiency or larger pile-group-to-single-pile stiffness factors than that for the fixed-head condition. As the soil stiffness increases from medium-dense to dense sand, the contribution of the soil resistance at greater depth becomes less significant. That is the displacement of the soil at greater depth is relatively small and therefore a close agreement between the stiffness curves obtained for medium-dense and dense sand and also those for fixed-head and free-head conditions can be anticipated.

These stiffness charts can be readily used to determine the pile group stiffness for a variety of soil and pile properties. The first step is to compute the single pile stiffness either from the proposed single pile model or from other analytical models. The lateral stiffness of the pile group foundation can then be computed as the product of the sum of the single pile stiffness for all piles in the group and the pile-group-to-single-pile stiffness factor which can be obtained from the presented charts as a function of s/d ratio and pile-flexibility factor. These steps can be repeated for different configurations and material properties of the pile and its surrounding soils. A similar concept of

constructing the stiffness chart for lateral response can also be applied for constructing the stiffness chart for vertical response and rotational response, for various types of soils and for different pile-head fixity conditions as well.

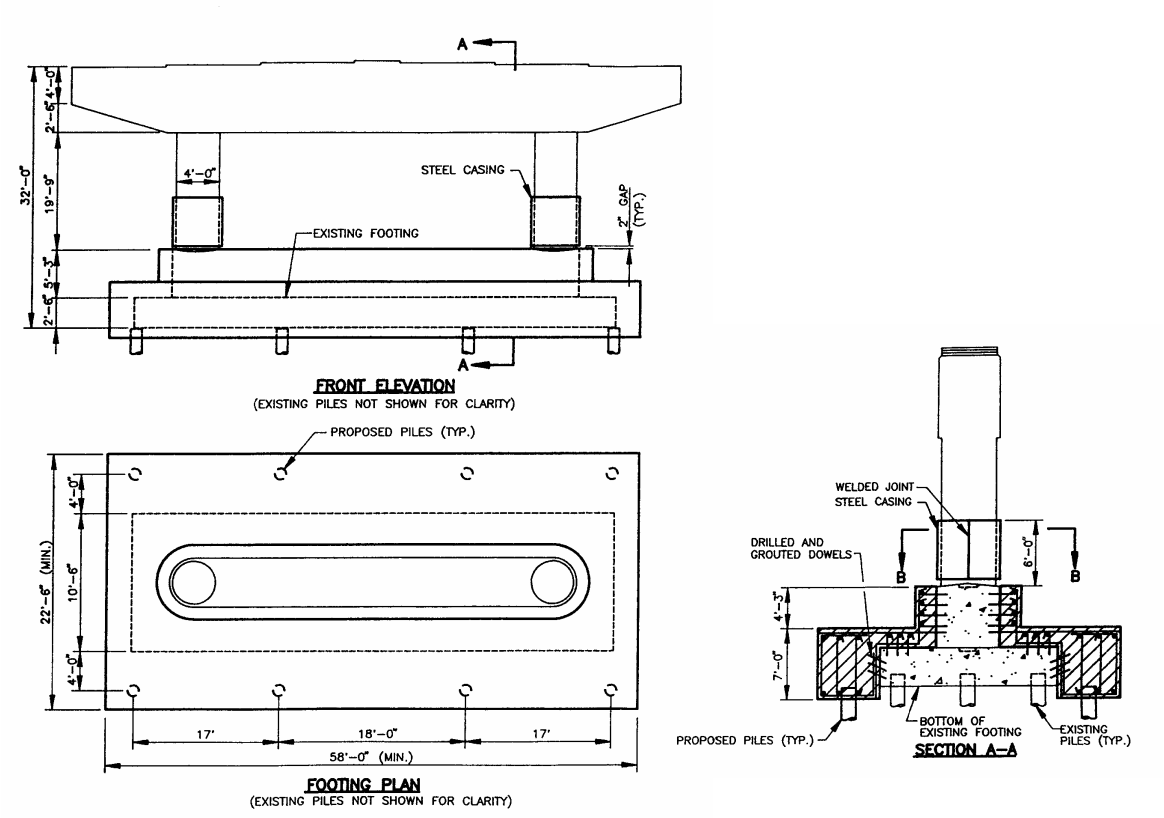

Figure 7.1. Details of Foundation Retrofits for Pier 2 of the Cairo Bridge.

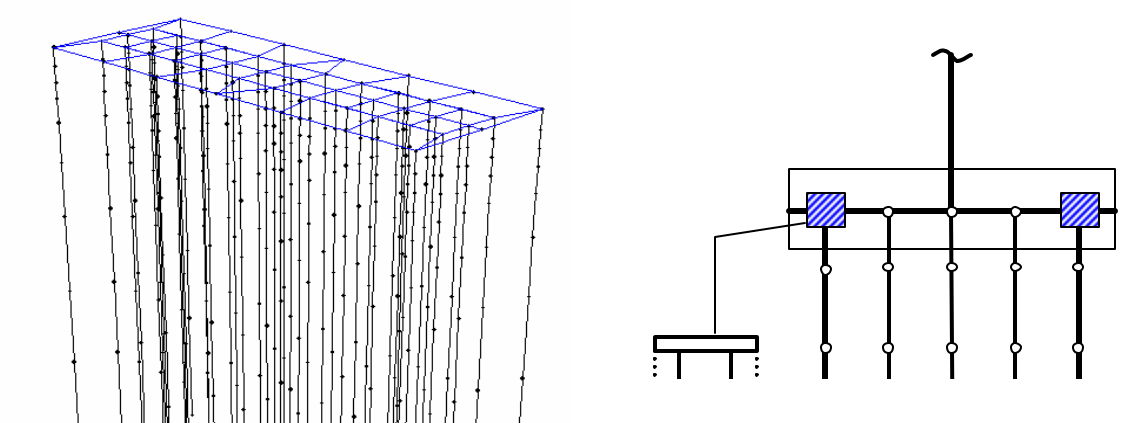

Figure 7.2. Foundation Model and Proposed Mechanism for Simulating Loading Sequences.

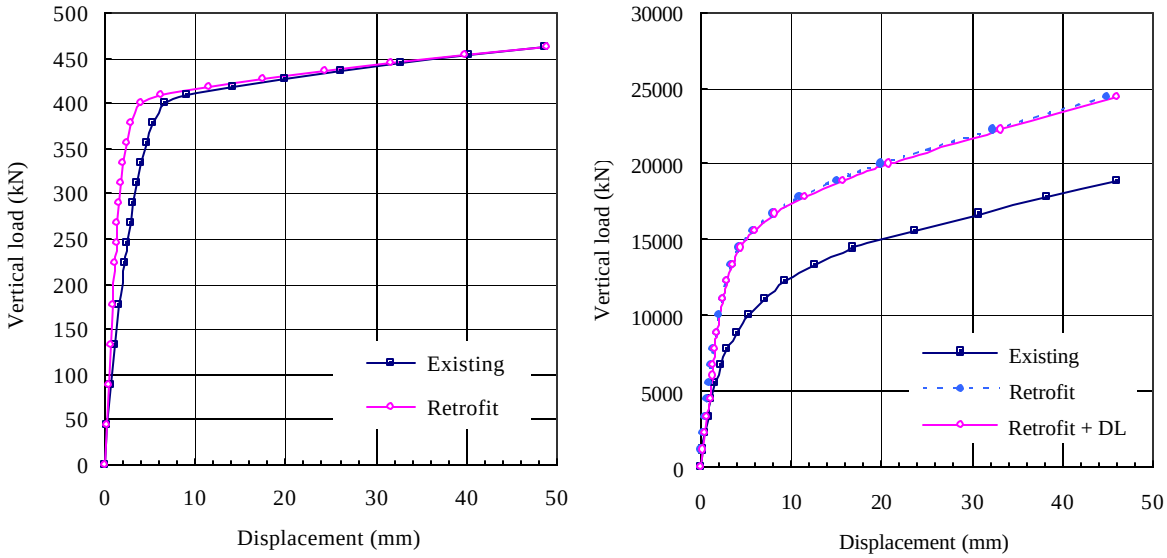

(a) Single Pile Response (b) Pile Foundation Response

Figure 7.3. Vertical Load-Displacement Responses: (a) Single Retrofit and Existing Pile, and (b) Retrofitted and Existing Foundation.

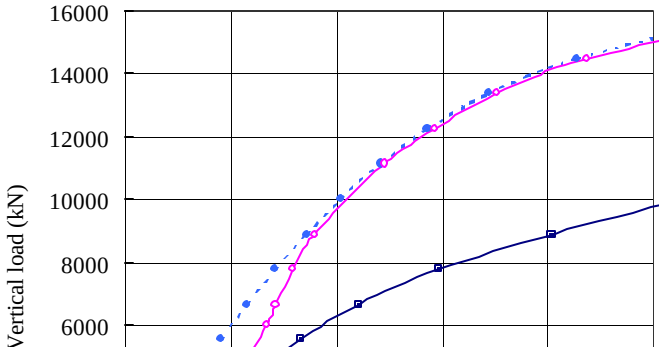

Figure 7.4. Enlarged Vertical Load-Displacement Response of Retrofitted and Existing Foundation.

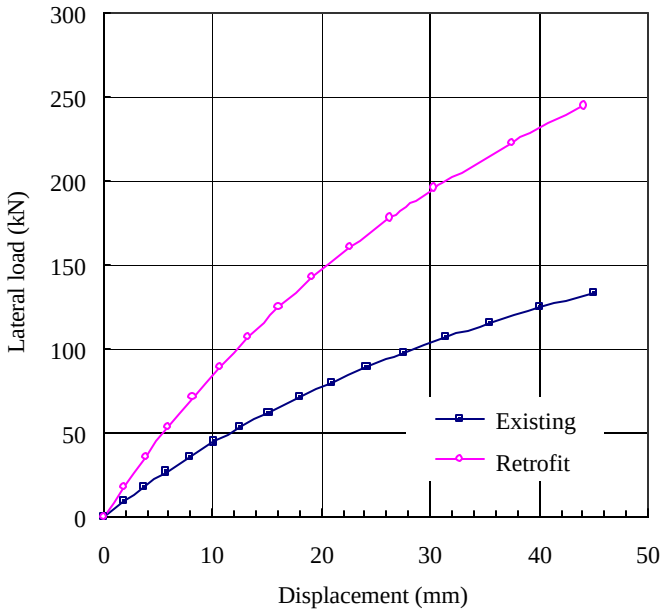

Figure 7.5. Lateral Load-Displacement Responses of Single Retrofit and Existing Pile.

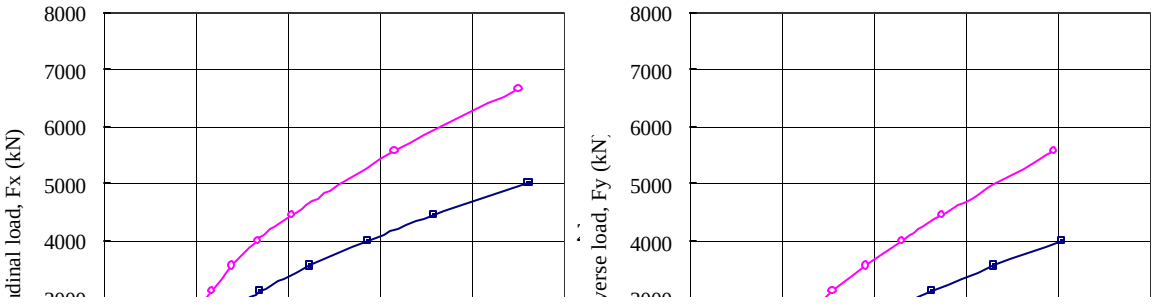

(a) Longitudinal response (b) Transverse response

Figure 7.6. Lateral Load-Displacement Responses of Retrofitted and Existing Foundation.

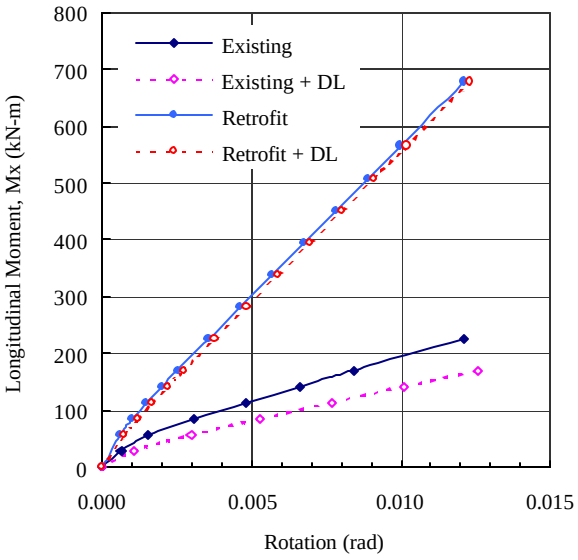

(a) Rotational Response about x-axis

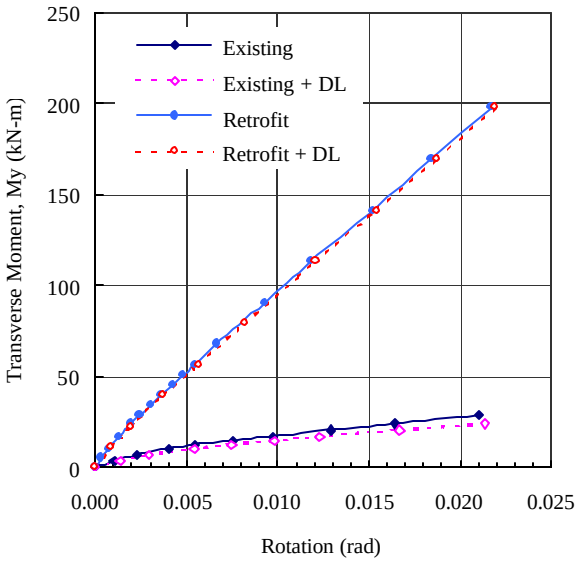

(b) Rotational Response about y-axis

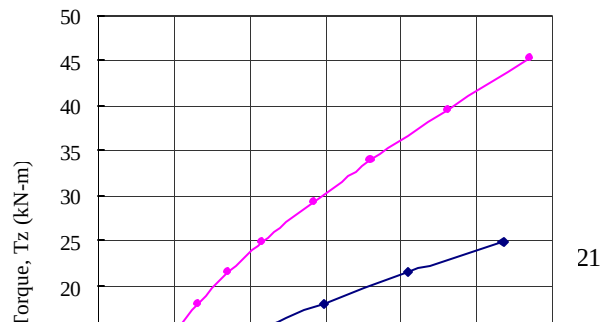

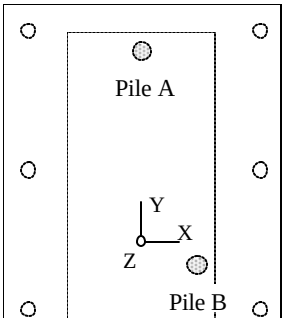

(c) Rotational Response about z-axis (d) Location of Indicative Piles

Figure 7.7. Moment-Rotation Responses about x, y and z axes, and Location of Indicative Piles for Specifying the Stiffness and Ultimate Capacity of the Foundation.

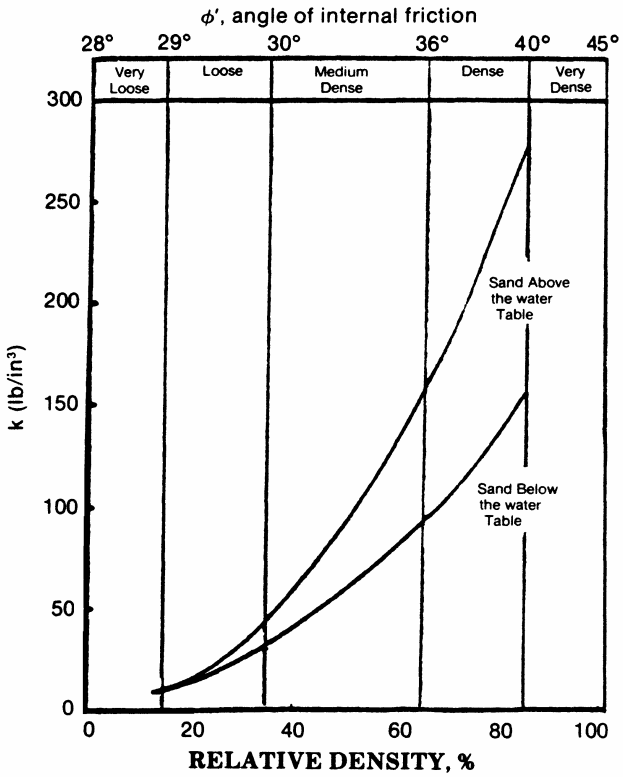

Figure 7.8. Coefficient of Initial Modulus of Subgrade Reaction [API (1991)].

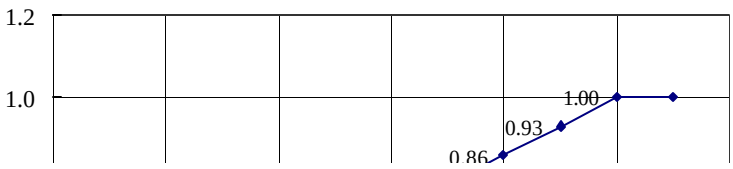

Figure 7.9. Relationship between p-Multiplier and S/D ratios.

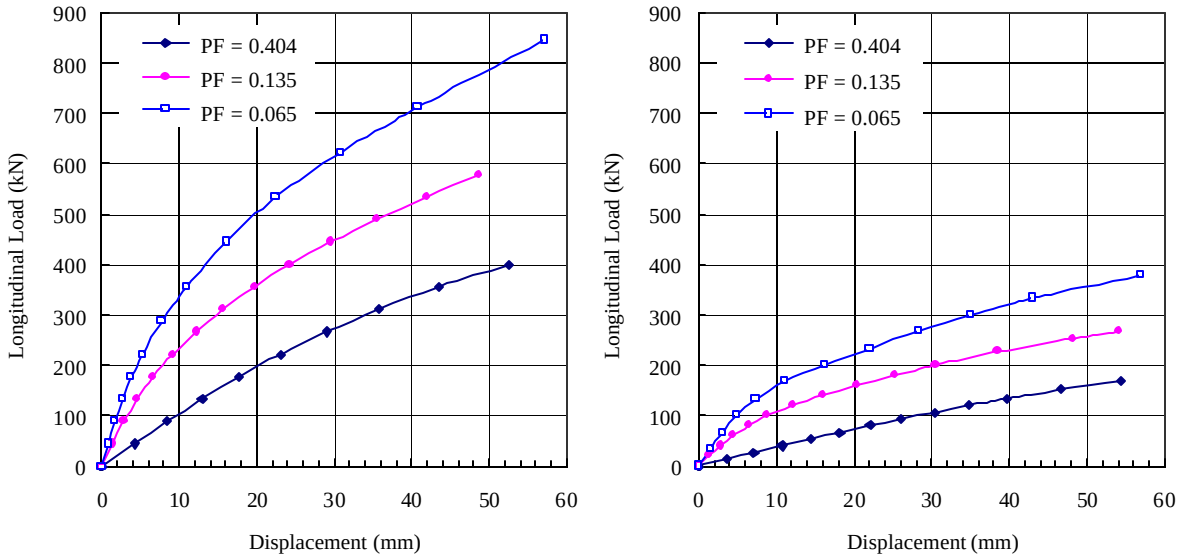

(a) Fixed-Head Condition (b) Free-Head Condition

Figure 7.10. Load-Displacement Relationships of Single Piles Computed from Different Pile-Flexibility Factors for (a) Fixed-Head, and (b) Free-Head Conditions.

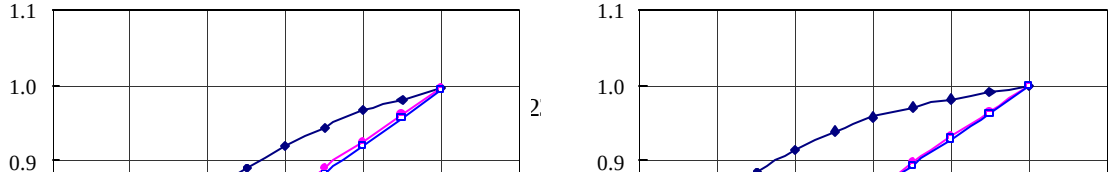

(a) Fixed-Head Condition (b) Free-Head Condition

Figure 7.11. Stiffness Curves for Computing Pile-Group Stiffness from Different Pile-Flexibility Factors for (a) Fixed-Head, and (b) Free-Head conditions.

CHAPTER 8

SUMMARY AND CONCLUSIONS

8.1 Summary

An analytical technique of integrating a bridge structure and its soil-foundation system into the complete global model is proposed for seismic soil-foundation-structure interaction analysis of pile-supported bridges. In a process of implementing the integrating concept, a simple yet realistic pile-soil model is required in modeling of pile group foundations. Existing methods of modeling soil characteristics are reviewed. Among these methods, the dynamic p-y soil modeling method based on Winkler's hypothesis is adopted. This modeling method is chosen in consideration of its performance in accurately representing nonlinear behavior and radiation damping properties of the soils, and its application to seismic analysis of bridges with justified amount of computational time and effort.

Several methods have been proposed to characterize nonlinear load deflection relationships for near-field soil reactions, and to derive stiffness and radiation damping coefficients for far-field soil reactions. Adopted in this study are the criteria for constructing the load deflection curves recommended by AASHTO, FHWA and API. The expressions derived from a plane-strain model are employed in calculation of stiffness and damping coefficients for the far-field soil model. An adjustment is needed in implementing these adopted criteria to comply with the available nonlinear and damping models provided in the selected computer program (SAP2000) to perform nonlinear time-history analyses in this study. The performance of the adjusted pile-soil model in predicting static and dynamic responses of single piles to vertical and lateral loads is validated through comparison studies with experimental results from field tests. Parametric studies are also conducted to evaluate the sensitivity of the results to uncertainties in determining model parameters.

Once a satisfactory pile-soil model for single piles is found, it is integrated into a pile group foundation model. Similar to the single pile model, the performance of the pile group model is investigated though comparison studies with experimental data. Parametric studies are also conducted to investigate the sensitivity of the results to model parameters such as the number of pile elements, the size of soil mass to be included, the far-field soil model, and the pile-soil-pile

interaction. Through these studies, the capability of the proposed pile group model in capturing the behavior of pile foundations subjected to both vertical and lateral loading is justified.

The pile foundation model is verified for its ability to predict the static and dynamic responses of the pile group to vertical and lateral loads applied at the pile cap; in other words, its ability to capture the inertial interaction effects of the superstructure on the foundation response. However, the pile cap loading condition is certainly different from the seismic loading condition. For complete confidence of applying the foundation model for seismic analysis of pile-supported bridges, a comparison study with recorded responses of a road bridge in Japan (the Ohba-Ohashi Bridge) during earthquakes is conducted. The performance of the integrated soil-pile-foundation-structure model for the Ohba-Ohashi Bridge in predicting the bridge responses is found to be satisfactory. A sensitivity study is also conducted to examine the effects of far-field soil model (radiation damping) on the overall bridge response.

The integrated soil-foundation-structure modeling technique can be applied for seismic soil-structure interaction analysis of different bridge types such as truss, plate-girder, tied-arch and cable-stayed bridges. Chosen for a case study in this research project is an existing truss-arch bridge spanning across the Mississippi River with its north abutment in Illinois and its south abutment in Missouri (the Cairo Bridge). The nonlinear time-history analysis of the Cairo Bridge is performed using input motions obtained from ground response analysis of bedrock motions artificially generated for the Cairo area. Comparison studies of the seismic response and dynamic characteristics of the bridge obtained from the integrated model with those obtained from other models (the fixed-base model, and the equivalent linear and nonlinear foundation spring models) are conducted. The results promote the use of the integrated model and emphasize the importance of the soil-structure interaction in seismic analysis of pile-supported bridges. In addition, the proposed model is applied to perform seismic performance evaluation of the Cairo Bridge for different intensity levels of input motions.

An attempt is made to apply the pile foundation model to investigate the behavior of retrofitted foundations and to develop a simple alternative to account for the group effects in evaluation of the foundation characteristics in the form of equivalent linear or nonlinear load deflection relationships. For preliminary analysis and design, the equivalent linear spring model is often used in practice. Therefore, to be of great benefit to practitioners, the proposed pile foundation model is applied to

develop ready-to-use stiffness charts from which the pile group stiffness can be evaluated as a function of the number of piles in a group, pile properties and soil properties.

8.2 Conclusions

Based on the comparison and parametric studies previously summarized as well as the seismic performance evaluation of the Cairo Bridge, the following conclusions, which are divided into four categories according to how they are derived, can be drawn.

Comparison and parametric studies for single pile and pile group foundation models

1. For a relatively homogeneous soil deposit, the number of pile elements of greater than 10 elements increasing in length with depth can be efficiently and accurately used in modeling of the pile for static and dynamic response analysis of single piles and grouped piles to vertical loading. For lateral loading, it is recommended that at least 5 elements be used to model the top 10 pile diameters of the pile length.
2. The pile cap can be adequately modeled using 4-node shell elements with each node representing one individual pile in a group.
3. The effects based on the size of cylindrical soil mass to be included in the model on the dynamic response of single piles and grouped piles are negligible.
4. The effects of far-field soil models on static and dynamic response of pile group foundations are found to be inconsequential for a frequency range typical for earthquake loading (0.1-10 Hz).
5. For the high-frequency and low-amplitude loading, the far-filed soil model (radiation damping) plays an important role in predicting the pile group response.
6. The uniform p-multiplier can be properly used to account for group effects in modeling of the pile group foundation.
7. The effects of loading sequence (e.g., different state of stress experienced by the retrofit and existing structures at service conditions) on the behavior of the retrofitted foundations, which are of friction-pile type, are insignificant.

Comparison studies on effects of foundation modeling on seismic responses of the Ohba-Ohashi Bridge

1. The capability of the integrated soil-foundation-structure model in predicting the overall bridge response is found satisfactory.
2. The effects of the far-field soil model on seismic response of the bridge are insignificant for either soft or stiff soil conditions. The far-field soil models can be disregarded in modeling of the soils in the pile foundation model.
3. The near-field soil model alone can be accurately used in modeling the soil components of the integrated soil-foundation-structure model.

Sensitivity studies on effects of foundation modeling on seismic responses of the Cairo Bridge

1. The conventional static and dynamic interaction factor method for taking into account the PSPI effects significantly reduces the foundation stiffness for large pile groups. This method significantly overestimates the PSPI effects.
2. The variation of the dynamic stiffness with loading frequencies is fairly uniform for the frequency range of interest for earthquake loading; therefore, for low frequency loading, the static stiffness may be properly used.
3. The modal periods of the bridge are elongated by 5 to 160% when the foundation flexibility is considered. For higher modes, an increase of the periods is relatively smaller than for lower modes. The mode shapes of the bridge from different foundation modeling cases are essentially similar.
4. At lower modes, the vibration mode of the main truss and its approach structures are uncoupled for all three principal directions.
5. For the integrated soil-foundation-structure model, the effects of softening the soil reactions by 25% are insignificant on the dynamic characteristics and seismic response of the bridge.
6. The general belief that by including the flexibility of the foundations, the maximum horizontal displacements of the superstructure increase and the maximum forces at the base piers decrease does not necessarily apply for such a long span bridge as the Cairo

Bridge. The study shows that an increase or decrease of the maximum displacements or forces for a long span bridge depends not only on the foundation stiffness of an individual pier but also on the distribution of the foundation stiffness among all piers.

7. Overestimation of the foundation stiffness may lead to unconservative results. The fixed-base model underpredicts the bridge response in several aspects such as the displacement and rotation response of the superstructure and foundations, potential pounding of the bridge superstructures at expansion joints, and forces experienced in the truss members and in the piles.

8. The equivalent linear foundation spring models underestimate the shear forces and moments in the piles by a factor of 2 as compared to those obtained from the integrated model.

Seismic performance evaluation of the Cairo Bridge for different excitation intensities

1. No major deficiencies of the overall bridge responses except for a few truss members that are slightly overstressed are observed for the 50%/50 year hazard level.

2. Deficiencies associated with excessive shear forces in the piles (D/C ratio ˜ 2), and excessive moments in the columns (D/C ratio ˜ 1.3 to 1.5) of the north approach piers (Piers 2, 3 and 4) are discovered for the 10%/50 year hazard level.

3. For an equivalent of the 4%/50 year hazard level, the results indicate excessive longitudinal displacements at the expansion joints and several occurrences of pounding and impact at the expansion joints and bearings at the main truss structure. The forces induced by the impacts as well as the transverse forces experienced at the expansion bearings substantially exceed its capacity (D/C ratio ˜ 2 to 3), indicating a high potential for toppling which could possibly lead to a major structural damage of the main truss structure unless retrofits are implemented.

4. Flexural and shear failures at the approach piers are probable for the 4%/50 year hazard level. Column retrofits are required to enhance flexural ductility and shear capacity for almost all piers at the approach structures. Foundation retrofits are also recommended to mitigate a consequence of inadequate flexural and shear strength of the piles and excessive displacements and rotations of the foundation.

5. Seismic performance evaluation of the Cairo Bridge for an equivalent of 2%/50 year hazard level indicates a high possibility of a significant destruction of the bridge. Almost all truss members are overstressed especially at the supports. The forces experienced at the expansion bearings of the main truss structure greatly exceed its ultimate shear and tension strength. It is likely that the main truss would collapse into the river. Severe damage to pier columns and pile foundations is expected for this level of excitation intensity.

REFERENCES

AASHTO (1996). *Standard Design Specifications for Highway Bridges*, American Association of State Highway And Transportation Officials, Washington, D.C.

ACI (1995). *Building Code Requirements for Reinforced Concrete* (ACI 318-95) and *Commentary* (ACI 318R-95), American Concrete Institute, Detroit, MI.

AISC (1993). *Manual of Steel Construction: Load & Resistance Factor Design*, Vol. 1 and 2, AISC-LRFD93, American Institute of Steel Construction, Chicago, IL.

API (1991). *Recommended Practice for Planning, Designing, and Constructing Fixed Offshore Platforms*, American Petroleum Institute, Washington D.C.

ATC (1996). *Improved Seismic Design Criteria for California Bridges: Provisional Recommendations*, ATC-32, Applied Technology Council, California.

ATC (1983). *Seismic Retrofitting Guidelines for Highway Bridges*, ATC-6-2, Applied Technology Council, California.

Anderson, R. E., Cooling, T. L. and Gruendler, J. J. (1994). "Illinois Department of Transportation Seismic Bridge Condition Survey, Phase II," *Proceedings of 5th U.S. National Conference on Earthquake Engineering*, Chicago, Illinois

Aschenbrener, T. B. and Olson, R. E. (1984). "Prediction of Settlement of Single Piles in Clay," *Proceedings of Symposium on Analysis and Design of Pile Foundation*, ASCE, San Francisco, pp. 41-58.

Badoni, D. and Makris, N. (1997) "Analysis of the Nonlinear Response of Structures Supported on Pile Foundations," Earthquake Engineering Research Center, Report No. UCB/EERC-97/07.

Badoni, D. and Makris, N. (1996). "Nonlinear Response of Single Piles under Lateral Inertial and Seismic Loads," *Soil Dynamics and Earthquake Engineering*, Vol. 15, pp. 29-43.

Barden, L. and Monckton, M. F. (1970). *Tests on Model Pile Groups in Soft and Stiff Clay*, Geotechnique, Vol. 20, No. 1, pp. 94-96.

Berger, E., Mahin, S. A., and Pyke, R. (1977). "Simplified Method for Evaluating Soil-Pile Structure Interaction Effects, *Proceedings of 9th Offshore Technology Conference*, Houston, Texas, pp. 589-598.

Blaney, G. W. and O'Neill, M. W. (1989). "Dynamic Lateral Response of a Pile Group in Clay," *Geotechnical Testing Journal*, ASTM, Vol. 12, No. 1, pp. 22-29.

Blaney, G. W., Mahar, L. J., and O'Neill, M. W. (1987). "Vertical Vibration Test of a Full-Scale Pile Group," *Dynamic Response of Pile Foundations*, Geotechnical Special Publication No. 11, ASCE, pp. 149-165.

Blaney, G. W. and O'Neill, M. W. (1986). "Measured Lateral Response of Mass on Single Pile in Clay," *Journal of Geotechnical Engineering*, ASCE, Vol. 112, No. 4, pp. 443-457.

Brand, E. W., Muktabhant, C., and Taechathummarak, A. (1972). "Load Tests on Small Foundation in Soft Clay," *Proceedings of the Special Conference on Performance of Earth and Earth-Supported Structure*, ASCE, Purdue University, Vol. 1, No. 2, pp. 903-928.

Broms, B. B. (1981). *Precast Piling Practice*, Thomas Telford Ltd., London, England.

Broms, B. B. (1964a). "The Lateral Resistance of Piles in Cohesive Soils," *Journal of Soil Mechanics and Foundations Division*, ASCE, Vol. 90, No. SM2, pp. 27-63.

Broms, B. B. (1964b). "The Lateral Resistance of Piles in Cohesionless Soils," *Journal of Soil Mechanics and Foundations Division*, ASCE, Vol. 90, No. SM3, pp. 123-156.

Brown, D. A. (1985). "Behavior of a Large Scale Pile Group Subjected to Cyclic Lateral Loading," Ph.D. Dissertation, University of Texas at Austin.

Brown, D. A., Morrison, C., and Reese, L. C. (1988). "Lateral Load Behavior of a Pile Group in Sand," *Journal of Geotechnical Engineering*, ASCE, Vol. 114, No. 11, pp. 104-121.

Brown, D. A., Reese, L. C., and O'Neill, M. W. (1987). "Cyclic Lateral Loading of a Large-Scale Pile Group," *Journal of Geotechnical Engineering*, Vol. 113, No. 11, pp. 1326-1343.

Budhu, M. and Davies, T. G. (1988). "Analysis of Laterally Loaded Piles in Soft Clays," *Journal of Geotechnical Engineering*, Vol. 114, No. 1, pp. 21-39.

Budhu, M. and Davies, T. G. (1987). "Nonlinear Analysis of Laterally Loaded Piles in Cohesionless Soils," *Canadian Geotechnical Journal*, Vol. 24, No. 2, pp. 289-296.

Caltrans. (1993). *Bridge Design Specification*, California Department of Transportation, Sacramento, CA.

Castilla, F., Martin, P. and Link, J, (1984). "Fixity of Members Embedded in Concrete," Technical Report CERL M-339, US Army Corps of Engineers, Champaign, IL.

Chaemmangkang, P. (2001). "Behavior of Batter Piles in Sand," A thesis Submitted for the Degree of Doctor of Philosophy in Civil Engineering, University of Illinois at Urbana-Champaign, Urbana, Illinois.

Coduto, D. (2001), *Foundation Design*, Prentice Hall

Cox, W. R., Reese, L. C., and Grubbs, B. R. (1974). "Field Testing of Laterally Loaded Piles in Sand," *Proceedings of 6th Annual Offshore Technology Conference*, Vol. 2, Houston, Texas.

Coyle, H. M. and Reese, L. C. (1966). "Load Transfer for Axially Loaded Piles in Clay," *Journal of the Soil Mechanics and Foundations Division*, ASCE, Vol. 92, No. SM2, pp. 1-26.

Crouse, C. B. (1992). "Estimation of Foundation Stiffness of Meloland Road Overcrossing Bridge from Forced Vibration Test Data," Report to California Department of Transportation, CA.

Crouse, C. B., Hushmand, B. and Martin, G. R. (1987). "Dynamic Soil-Structure Interaction of a Single-span bridge," *Earthquake Engineering and Structural Dynamics*, Vol. 15, pp. 711-729.

Crouse, C. B., Kramer, L., Mitchell, R., and Hushmand, B. (1993). "Dynamic Tests of Pipe Pile in Saturated Peat," *Journal of Geotechnical Engineering*, Vol. 119, No. 10.

Davies, T. G. and Budhu, M. (1986). "Nonlinear Analysis of Laterally Loaded Piles in Heavily Overconsolidated Clays," *Geotechnique*, Vol. 36, No. 4, pp. 527-538.

Douglas, B. M., Maragakis, E. A. and Vrontinos, S. (1991). "Parameter Indentification Studies of the Meloland Overcrossing," *Proceedings of the Pacific Conference of Earthquake Engineering*, Auckland, New Zealand.

Douglas, B. M., Maragakis, E. A., Vrontinos, S. and Douglas, B. J. (1990). "Analytical Studies of the Satic and Dynamic Response of the Meloland Road Overcrossing," *Proceedings of the 4th U.S. National Conference on Earthquake Engineering*, pp. 987-992.

El-Marsafawi, H., Han, Y. C., and Novak, M. (1992). "Dynamic Experiments on Two Pile Groups," *Journal of Geotechnical Engineering*, ASCE, Vol. 118, No. 6, pp. 839-855.

El-Naggar, M. H. and Novak, M. (1996). "Nonlinear Analysis for Dynamic Lateral Pile Response," *Journal of Soil Dynamics and Earthquake Engineering*, Vol. 15, pp. 223-244.

El Sharnouby, B. and Novak, M. (1985). "Static and Low Frequency Response of Pile Groups," *Canadian Geotechnical Journal*, Vol. 22, No. 1, pp. 79-94.

Fan, K. (1992). "Seismic Response of Pile Foundations Evaluated Through Case Histories," A thesis Submitted for the Degree of Doctor of Philosophy in Civil Engineering, State University of New York at Buffalo, New York.

FEMA (1997). *NEHRP Guidelines for Seismic Rehabilitation of Buildings*, Report No. FEMA-273, Federal Emergency Management Agency, Washington, D.C.

Fenves, G. L. Filippou, F. C., and Sze, D. T. (1991). "Evaluation of the Dumbarton Bridge in the Loma Prieta Earthquake," Report No. UCB/EERC-92/02, Earthquake Engineering Research Center, University of California at Berkeley, California.

Gadre, A. (1997). "Lateral Response of Pile-Cap Foundation Systems and Seat-Type Bridge Abutments in Dry Sand," A thesis Submitted for the Degree of Doctor of Philosophy in Civil Engineering, Rensselaer Polytechnic Institute.

Gazetas, G. (1991). "Foundation Vibrations," in *Foundation Engineering Handbook*, 2nd Edition, Edited by H-Y Fang, Van Nostrand Reinhold, pp. 553-593.

Gazetas, G. and Dobry, R. (1984). "Horizontal Response of Piles in Layered Soils," *Journal of Geotechnical Engineering*, Vol. 110, No. 1, pp. 20-40.

Gazetas, G., Fan, K., Kaynia, A., and Kausel, E. (1991). "Dynamic Interaction Factors for Floating Pile Groups," *Journal of Geotechnical Engineering Division*, ASCE, Vol. 117, No. 10, pp. 1531-1548.

Gazetas, G. and Makris, N. (1991). "Dynamic Pile-Soil-Pile interaction, Part I: Analysis of Axial Vibration." *Earthquake Engineering and Structural Dynamics*, Vol. 20, pp. 115-132.

Heydinger, A. G. (1989). "Prediction of Driven Pile Behavior Using Load Transfer Functions." *Predicted and Observed Axial Behavior of Piles*, Geotechnical Special Publication No. 23, ASCE, pp. 117-128.

Hwang, H. M. (1998). Personal Communication, Center for Earthquake Research and Information, University of Memphis.

Ibrahimbegovic, A.and Wilson, E. L. (1989). "Simple Numerical Algorithms for the Mode Superposition Analysis of Linear Structural Systems with Nonproportional Damping," *Computers and Structures*, Vol. 33, No. 2, pp. 523-531.

Idriss, I. M. and Sun, J. I. (1992). *User's Manual for Shake91*, Department of Civil Environmental Engineering, University of California, Davis, California.

Kagawa, T. and Kraft, L. M., Jr. (1980a). "Seismic p-y Response of Flexible Piles," *Journal of the Geotechnical Engineering Division*, ASCE, Vol. 106, No. GT8, pp. 899-918.

Kagawa, T. and Kraft, L. M., Jr. (1980b). "Lateral Load-Deflection Relationship of Piles Subjected to Dynamic Loadings," *Soils and Foundations*, Vol. 20, No. 4, pp. 19-36.

Kaynia, A. M. and Kausel, E. (1982). "Dynamic Stiffness and Seismic Response of Pile Groups," Research Report R82-03, Massachusetts Institute of Technology, Massachusetts.

Khan, M. N. (1993). "Idealization of Pile to Pile-Cap Connection with Respect to Lateral Loads," A thesis Submitted for the Degree of Doctor of Philosophy in Civil Engineering, University of Illinois at Urbana-Champaign, Urbana, Illinois.

Kraft, L. M., Ray, R. P., and Kagawa, T. (1981). "Theoretical *t-z* Curves," *Journal of the Geotechnical Engineering Division*, ASCE, Vol. 107, No. GT11, pp. 1543-1561.

Laier, J. E. (1989). "Predicting the Ultimate Compressive Capacity of a Long 12-H-74 Steel Pile," *Proceedings of the International Conference on Design and Construction of Deep Foundations*, Orlando, FL, Vol. III, pp. 1804-1818.

Lam, P. and Kapuskar, M. (1998). "Modeling of Pile Footings for Seismic Design," Technical Report, National Center for Earthquake Engineering Research (NCEER), pp. 110-136.

Lam, I. P. and Cheang, L. C. (1995). "Dynamic Soil-Pile Interaction Behavior in Submerged Sands," in *Earthquake-Induced Movements and Seismic Remediation of Existing Foundations and Abutments*, ASCE Geotechnical Special Publication No. 55, pp. 110-136.

Lam, I. P. and Law, H. (1994). "Soil-Foundation-Structure Interaction – Analysis Considerations by Empirical p-y Methods," *Proceedings of 4th Caltrans Seismic Research Workshop*, California Department of Transportation, Sacramento.

Lam, I. P., Martin, G. R., and Imbsen, R. (1991). "Modeling Bridge Foundations for Seismic Design and Retrofitting," Transportation Research Record 1290.

Lam, I. P. and Martin, G. R. (1986). "Seismic Design of Highway Bridge Foundations, Vol. II: Design Procedures and Guidelines," Final Report to the Office of Engineering and Highway Operations, Federal Highway Administration.

Long, J. H. (1996). "Input Guide to Axpill Pile Response due to Axial Loading," Class Material of CEE485, University of Illinois at Urbana-Champaign, Urbana, Illinois.

Makris, N. and Gazetas, G. (1992). "Dynamic Pile-Soil-Pile Interaction, Part II: Lateral and Seismic Response," *Earthquake Engineering and Structural Dynamics*, Vol. 21, pp. 145-162.

Maragakis, E. A., Douglas, B. M. and Abdel-Ghaffar, S. M. (1994). "An Equivalent Linear Finite Element Approach for the Estimation of Pile Foundation Stiffnesses," *Earthquake Engineering and Structural Dynamics*, Vol. 23, pp. 1115-1124.

Matlock, H. (1970). "Correlations for Design of Laterally Loaded Piles in Soft Clay," *Proceedings of 2nd Annual Offshore Technology Conference*, Houston, Texas, pp. 577-594.

Matlock, H., Foo, H. C., and Bryant, L. M. (1978). "Simulation of Lateral Pile Behaviour under Earthquake Motion," *Proceedings of Specialy Conference on Earthquake Engineering and Soil Dynamics*, ASCE, Vol. II, Pasadena, California, pp. 600-619.

Matlock, H. and Reese, L. C. (1960). "Generalized Solutions for Laterally Loaded Piles," Proceedings, Journal of Soil Mechanics and Foundations Division, ASCE, Vol. 86, No. SM5, pp. 63-91.

McClelland, B. and Focht, J. A. (1956). "Soil Modulus for Laterally Loaded Piles," *Transactions*, ASCE, pp. 1049-1086.

McVay, M. C., Casper, R., and Shang, Te-I. (1995). "Lateral Response of Three-Row Groups in Loose to Dense Sands at 3D and 5D Pile Spacing," *Journal of Geotechnical Engineering*, ASCE, Vol. 121, No. 5, pp. 436-441.

McVay, M. C., Shang, Te-I, and Casper, R. (1996). "Centrifuge Testing of Fixed-Head Laterally Loaded Battered and Plumb Pile Groups in Sand," *Geotechnical Testing Journal*, Vol. 19, No. 1, pp. 41-50.

Meyerhof, G. G. (1976). "Bearing Capacity and Settlement of Pile Foundations," *Journal of the Geotechnical Engineering Division*, ASCE, Vol. 102, No. GT3, pp. 196-218.

Mindlin, R. D. (1936). "Force at a Point in the Interior of a Semi Infinite Solid," *Physics* 7: 195.

Mosher, R. L. (1984). "Load-Transfer Criteria for Numerical Analysis of Axially Loaded Piles in Sand, Part I: Load-Transfer Criteria," Final Report to U.S. Army Engineer Division, Lower Mississippi Valley, Vicksburg, Missouri.

Nogami, T. (1983). "Dynamic Group Effect in Axial Responses of Grouped Piles," *Journal of Geotechnical Engineering Division*, ASCE, Vol. 109, No. 2, pp. 228-243.

Nogami, T. and Konagai, K. (1988). "Time Domain Flexural Response of Dynamically Loaded Single Piles," *Journal of Engineering Mechanics*, Vol. 14, No. 9, pp. 1512-1525.

Nogami, T. and Konagai, K. (1987). "Dynamic Response of Vertically Loaded Nonlinear Pile Foundations," *Journal of the Geotechnical Engineering Division*, ASCE, Vol. 113, No. 2, pp.147-160.

Nogami, T., Otani, J., and Chen, H. L. (1992). "Nonlinear Soil-Pile Interaction Model for Dynamic Lateral Motion," *Journal of Geotechnical Engineering*, ASCE, Vol. 118, No. 1, pp.89-106.

Norris, G. M. (1987). "Foundation Stiffness Evaluation for Seismic Analysis of Highway Bridges," *Proceedings of the 23rd Engineering Geology and Soil Engineering Symposium*, pp. 375-394.

Norris, G. M and Sack, R. L. (1986). "Evaluation of the Lateral Stiffness of Pile Groups for Seismic Analysis for Highway Bridges," *Proceedings of the 22nd Engineering Geology and Soil Engineering Symposium*, pp. 323-363.

Novak, M. and Aboul-Ella, F. (1978a). "Impedance Functions of Piles in Layered Media," *Journal of Engineering Mechanics Division*, ASCE, Vol. 104, No. EM3, pp. 643-661.

Novak, M. and Aboul-Ella, F. (1978b). "Stiffness and Damping of Piles in Layered Media," *Proceedings of Specialty Conference on Earthquake Engineering and Soil Dynamics*, ASCE, Pasadena, California, pp. 704-719.

Novak, M., Nogami, T., and Aboul-Ella, F. (1978). "Dynamic Soil Reaction of Plane Strain Case," *Journal of Engineering Mechanics Division*, ASCE, Vol. 104, No. EM4, pp. 953-959.

Novak, M. and Sheta, M. (1980). "Approximate Approach to Contact Effects of Piles," in *Dynamic Response of Pile Foundations: Analysis Aspects*, Edited by M. W. O'Neill and R. Dobry, ASCE Special Technical Publication, pp. 53-79.

Ohira, A., Tazoh, T., Dewa, K., Shimizu, K., and Shimada, M. (1984). "Observations of Earthquake Response Behaviors of Foundation Piles for Road Bridge," *Proceedings of 8th World Conference on Earthquake Engineering*, San Francisco, Vol. III, pp. 577-584.

O'Neill, M. W. (1983). "Group Action in Offshore Piles," *Proceedings of Conference on Geotechnical Practice in Offshore Engineering*, ASCE, Austin, Texas, pp. 25-64.

O'Neill, M. W., Ghazzaly, O. I., and Ha, H. B. (1977). "Analysis of Three-Dimensional Pile Groups with Nonlinear Soil Response and Pile-Soil-Pile Interaction," *Proceedings of 9th Offshore Technology Conference*, Houston, Texas, Vol. II, pp. 245-256.

O'Neill, M. W., Hawkins, R. A., and Mahar, L. J. (1982). "Load Transfer Mechanisms in Piles and Pile Groups," *Journal of the Geotechnical Engineering Division*, ASCE, Vol. 108, No. 12, pp. 1605-1623.

O'Neill, M. W. and Murchison, J. M. (1983). "An Evaluation of P-Y Relationships in Sands," A report to the American Petroleum Institute (PRAC 82-41-1), University of Houston,University Park, Houston, Texas.

Pender, M. J. (1993). "Aseismic Pile Foundation Design and Analysis," *Bulletin of the New Zealand National Society for Earthquake Engineering*, Vol. 26, No. 1, pp. 49-160.

Poulos, H. G. (1968). "Analysis of Settlement of Pile Groups," *Geotechnique*, Vol. 18, pp. 449-471.

Poulos, H. G. and Davis, E. H. (1980). *Pile Foundation Analysis and Design*, John Wiley & Sons, Inc., New York.

Randolph, M. F. (1981). " Response of Flexible Piles to Lateral Loading, " *Geotechnique*, Vol. 31, No. 2, pp. 247-259.

Randolph, M. F. and Wroth, C. P. (1978). "An Analysis of Vertical Deformation of Pile Groups," *Geotechnique*, Vol. 29, No. 4, pp. 423-439.

Randolph, M. F. and Wroth, C. P. (1979). "Analysis of Deformation of Vertically Loaded Piles," *Journal of the Geotechnical Engineering Division*, ASCE, Vol. 104, No. GT12, pp. 1465-1488.

Reese, L. C. and Cox, W. R., and Koop, R. D. (1975). "Field Testing and Analysis of Laterally Loaded Piles in Stiff Clay," *Proceedings of 7th Offshore Technology Conference*, Vol. II, Houston, Texas, pp. 473-483.

Reese, L. C. and Isenhower, W. M. (1999). "Deep Foundation in the Future," in *Analysis, Design, Construction, and Testing of Deep Foundations*, Edited by J. M. Roesset, ASCE Special Technical Publication No. 88, and *Proceedings of the Offshore Technology Research Center 1999 Conference,* pp. 1-16.

Reese, L. C. and O'Neill, M. W. (1989). "Criteria for the Design of Axially Loaded Drilled Shafts," Research Report 89-11F, Center for Highway Research, the University of Texas, Austin, Texas.

Reese, L. C. and O'Neill, M. W. (1988). *Drilled Shafts: Construction Procedures and Design Methods*, U.S. Department of Transportation, Federal Highway Administration, Office of Implementation, McLean, Virginia.

Reese, L. C. and Sullivan, W. R. (1980). "Documentation of Computer Program COM624," Geotechnical Engineering Center, Department of Civil Engineering, University of Texas, Austin, Texas.

Reese, L. C. and Welch, R. C. (1975). "Lateral Loading of Deep foundations in Stiff Clay," *Journal of Geotechnical Engineering Division*, ASCE, Vol. 101, No. GT7, pp. 633-649.

Roesset, J. M. (1984). "Dynamic Stiffness of Pile Groups," *Analysis and Design of Pile Foundations*, Symposium, San Francisco, California, October 1-5, ASCE, pp. 263-286.

Roesset, J. M. (1980). "Stiffness and Damping Coefficients of Foundations," *Dynamic Response of Pile Foundations: Analytical Aspects*, Edited by M. W. O'Neill and R. Dobry, ASCE Special Technical Publication.

Rollins, K. M., Peterson, K. T., and Weaver, T., J. (1998). "Lateral Load Behavior of a Full-Scale Pile Group in Clay," A Paper Submitted to Journal of Geotechnical Engineering, ASCE, June, pp. 468-473.

Ruesta, P. F. and Townsend, F. C. (1997). "Evaluation of Laterally Loaded Pile group at Roosevelt Bridge," ASCE, *Journal of Geotechnical Engineering*, December, Vol. 123, No. 12.

Sanchez-Salinero, I. (1983). "Dynamic Stiffness of Pile Groups," Geotechnical Engineering Report GR83-5, Civil Engineering Department, University of Texas, Austin, Texas.

SAP2000 – *Integrated Finite Element Analysis and Design of Structures* (1996), Computers and Structures, Inc., Berkeley, California.

Sayed, S. M. and Bakeer, R. M. (1992). "Efficiency Formula for Pile Groups," *Journal of Geotechnical Engineering*, Vol. 118, No. 2, pp. 278-299.

Seed, H. B. and Reese, L. C. (1957). "The Action of Soft Clay Along Friction Piles," *Transactions*, ASCE, Vol. 122, pp. 731-754.

Sowers, G. F. (1979). *Introductory Soil Mechanics and Foundation Engineering*, 4th Edition, Mac-Millan Publishing Co., New York.

Stevens, J. B., Holloway, D. M., Moriwaki, Y., and Desmky, E. C. (1979). "Pile Group Response to Axial and Lateral Loading," *Proceedings of Symposium on Deep Foundation*, ASCE, Atlanta, Georgia.

Tajimi, H. (1969). "Dynamic Analysis of a Structure Embedded in an Elastic Stratum," *Proceedings of 4th World Conference on Earthquake Engineering*.

Tazoh, T., Shimizu, K. and Wakahara, T. (1988). "Seismic Observations and Analysis of Grouped Piles," *Dynamic Response of Pile Foundation-Experiment, Analysis and Observations*. ASCE Geotechnical Special Publication, No. 11, pp. 1-20.

Terzaghi, K. (1955). "Evaluation of Coefficients of Subgrade Reaction," *Geotechnique*, Vol. 5, No. 4, pp. 297-322.

Vesic, A. S. (1975). "Principles of Pile Foundation Design," Soil Mechanics Series No. 38, School of Engineering, Duke University.

Vijayvergiya, V. N., Hudson, W. R., and Reese, L. C. (1969). "Load Distribution for Drilled Shaft in Clay Shale," Research Report 89-5, University of Texas, Austin, 193p.

Wang, S., Kutter, B. L., Chacko, J. M., Wilson, D. W., Boulanger, R. W., and Abghari, A. (1998). "Nonlinear Seismic Soil-Pile-Structure Interaction," *Earthquake Spectra*, Vol. 14, No. 2, pp. 377-396.

Wen, Y. K. (1976). "Method for Random Vibration of Hysteretic Systems," *Journal of Engineering Mechanics Division*, ASCE, Vol. 102, No. EM2, pp. 249-263.

Werner, S. D., Crouse, C. B., Katafygiotis, L. and Beck, J. L. (1993). "Model Indentification and Seismic Analysis of Meloland Road Overcrossing," Report to California Department of Transportation, CA.

Wilson, E. L. (1997). "Three Dimensional Dynamic Analysis of Structures with Emphasis on Earthquake Engineering," *Computers and Structures, Inc*., Berkeley, California.